B. Pearley — 156654

E.8-10062
CR-156654

IMAGE PROCESSING SYSTEM PERFORMANCE PREDICTION AND PRODUCT QUALITY EVALUATION

Eric K. Stein and Harry B. Hammill

Calspan Corporation
P.O. Box 235
Buffalo, New York 14221

(E78-10062) IMAGE PROCESSING SYSTEM PERFORMANCE PREDICTION AND PRODUCT QUALITY EVALUATION Final Report (Calspan Corp., Buffalo, N. Y.) 302 p HC A14/MF A01 CSCL 14E G3/43

N78-17435

Unclas
00062

APRIL 1976

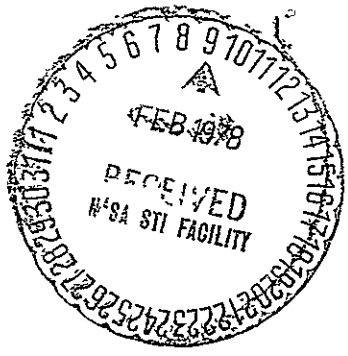

Prepared For:

GODDARD SPACE FLIGHT CENTER
GREENBELT, MARYLAND 20771

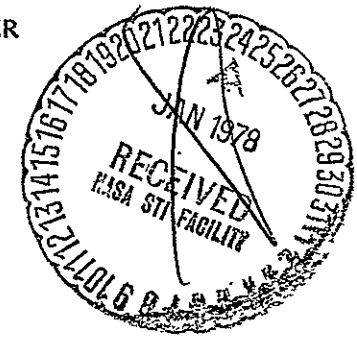

1. Report No.	2. Government Accession No.	3. Recipient's Catalog No.
ZE-5185-M-2		

4. Title and Subtitle	5. Report Date
Image Processing System Performance Prediction and Product Quality Evaluation	April 1976
	6. Performing Organization Code
7. Author(s) Eric K. Stein and Harry B. Hammill	8. Performing Organization Report No
9. Performing Organization Name and Address Calspan Corporation P. O. Box 235 Buffalo, New York 14221	10. Work Unit No.
	11. Contract or Grant No NAS5-20366
12. Sponsoring Agency Name and Address Goddard Space Flight Center Greenbelt, Maryland 20771	13. Type of Report and Period Covered Draft Final Report
	14. Sponsoring Agency Code

15. Supplementary Notes

16. Abstract

A new technique for image processing system performance prediction and product quality evaluation has been developed. It is entirely objective, quantitative, and general, and should prove useful in system design and quality control. This report describes the technique and its application to determination of quality control procedures for the Earth Resources Technology Satellite NASA Data Processing Facility.

17. Key Words (Selected by Author(s))	18. Distribution Statement
Image Quality, Estimation Theory, Computer Simulation Optical System Performance NASA/ERTS Data Processing Facility	

19. Security Classif. (of this report)	20. Security Classif. (of this page)	21. No. of Pages	22. Price*
UNCLASSIFIED	UNCLASSIFIED	293	

*For sale by the Clearinghouse for Federal Scientific and Technical Information, Springfield, Virginia 22151.

PREFACE

The work reported herein was sponsored by NASA Goddard Space Flight Center under Contract No. NAS5-20366 monitored by Mr. Bernard Peavey.

The authors are grateful to several people contributing to the study. In particular, to Mr. Robert Kinzly for many useful suggestions on various aspects of the program, to Mr. Larry Perletz for conducting the NASA/ERTS user requirements investigation and to Dr. Kenneth Piech for supplying the section on Radiometric Estimation Error and Calibration.

CONTENTS

CONTENTS (Cont.)

CONTENTS (Cont.)

LIST OF ILLUSTRATIONS

LIST OF ILLUSTRATIONS (Cont.)

LIST OF ILLUSTRATIONS (Cont.)

SECTION I
INTRODUCTION

The objective of this study was to investigate and develop techniques to characterize the quality of the products produced by an image data system in terms of measurable performance of the various system elements. The product quality measures were required to be meaningful to the user and related to unambiguous, measurable element performance descriptors. A specific objective was to investigate the requirements for quality control procedures at the Earth Resources Technology Satellite NASA Data Processing Facility (ERTS NDPF) to demonstrate the developed approach.

The fundamental problem was to establish an objective, functional measure of image quality and a means to predict that measure from accepted system element performance descriptors. Supporting tasks undertaken included familiarization with the NDPF, survey of ERTS user's "image quality" requirements and survey of currently accepted image quality evaluation techniques. It was found that adequate performance descriptors existed for the NDPF elements but that no adequate measure of image quality existed in terms of user's requirements.

The measure of image quality developed is the error introduced by the image data system into estimates of target characteristics from measurements made on output products. If the system is characterized by a sequence of operators corresponding to element performance descriptors, then the parameter estimation errors are mathematically related to the net system operator. A software program, Image Data System Simulation (IDSS), was written to implement the approach. IDSS uses computer simulation to synthesize the image data system from its element performance descriptors and computes the estimation errors for specific target parameters

The IDSS program, applied to the ERTS NDPF, can be used to analyze a large class of image processing systems, and should be useful in system design or upgrading.

In addition to NDPF quality control, the ability to monitor payload sensor performance by measurements made on NDPF output products was examined. Edge gradient spectral analyses software was written for NASA's computer as a tool for Modulation Transfer Function (MTF) measurement. The feasibility of a technique for correction of radiometric distortion due to atmospheric scattering and sensor effects based exclusively on measurements made on output products was also considered.

The next section of this report presents a summary of the background information developed at the onset of the study. It includes the results of survey of the data flow within the NDPF, ERTS imagery users' requirements, and state-of-the-art image quality evaluation techniques. Section 3 contains the mathematical bases of the approach and Section 4 describes the software written for its implementation. Section 5 identifies the elements of the NDPF and their associated performance descriptors. The results of the application of the developed technique to the NDPF are presented in Section 6. Finally, conclusions and recommendations are presented in Section 7.

SECTION 2
BACKGROUND INFORMATION

At the onset of this study a specific operational description of the NDPF and its subsystems, particularly the Bulk Processing System, had to be developed. In addition, it was necessary to form a concept of what the users of image products expect to obtain from them. Finally, a brief survey of the state-of-the-art to image evaluation was conducted. The results of these surveys provided necessary background information that is summarized in this section and presented in more detail in Appendix A.

2.1 NDPF Description

This study was limited to consideration of the NDPF video data to film product conversion process and digital products excluded. The inputs to the NDPF are video tape recordings from the ERTS payload. Although payload and telemetry link elements are external to the NDPF, the quality of the video tape input will influence the image product quality and consequently these elements were represented in the analyses.

A block diagram of the data flow within the Bulk Image Processing system is given in Figures 2-1 and 2-2. This block diagram served as a basis for system modeling. The following comments refer to the circled numbers in Figures 2-1 and 2-2. More specific data is presented in Appendix A.

The Return Beam Vidicon (RBV) (1) consists of three boresighted RCA vidicon systems in three different spectral bands. Radiometric and geometric calibration capability exists in the payload.

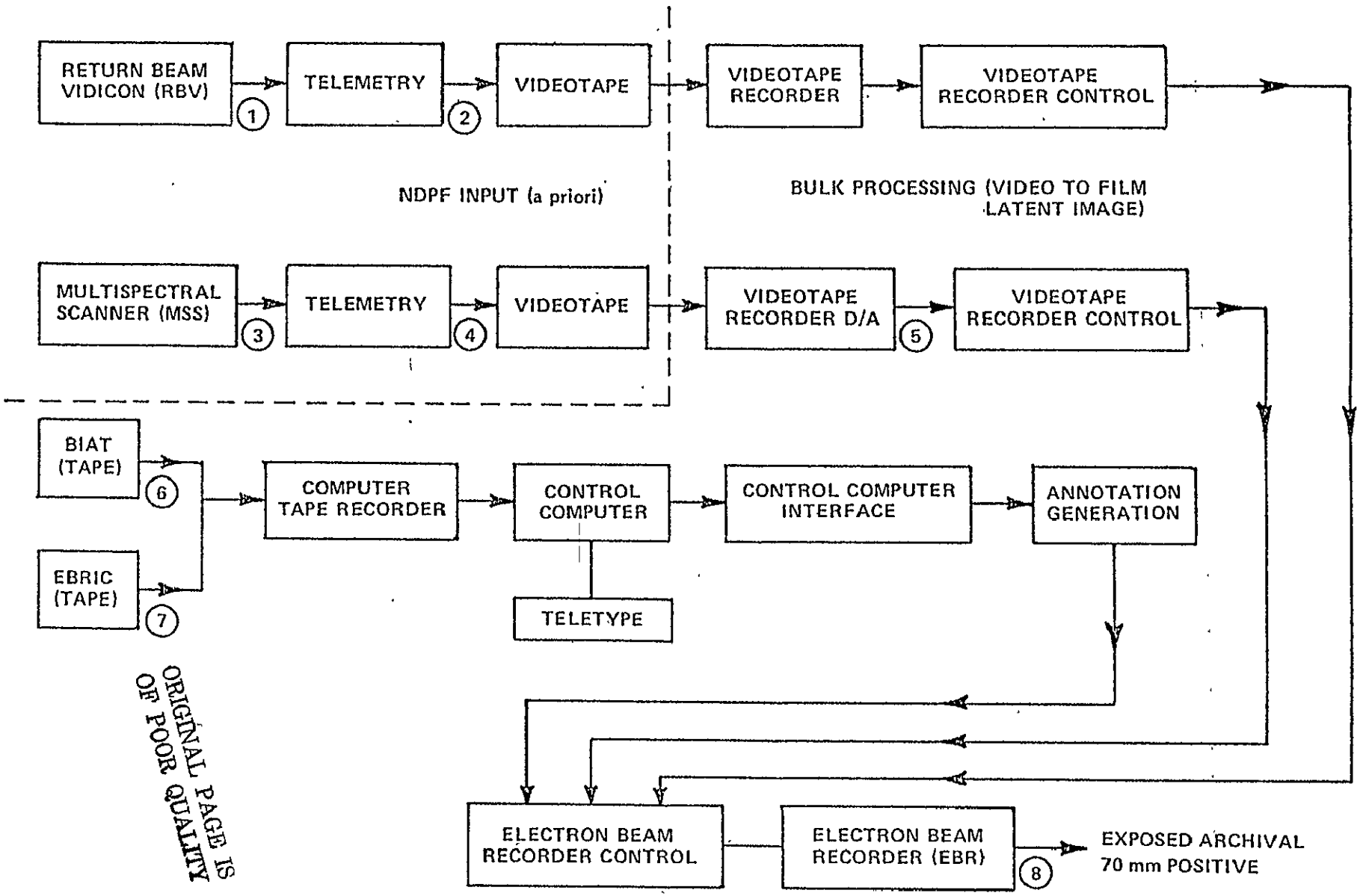

Figure 2-1 NDPF DATA FLOW BLOCK DIAGRAM (PART 1)

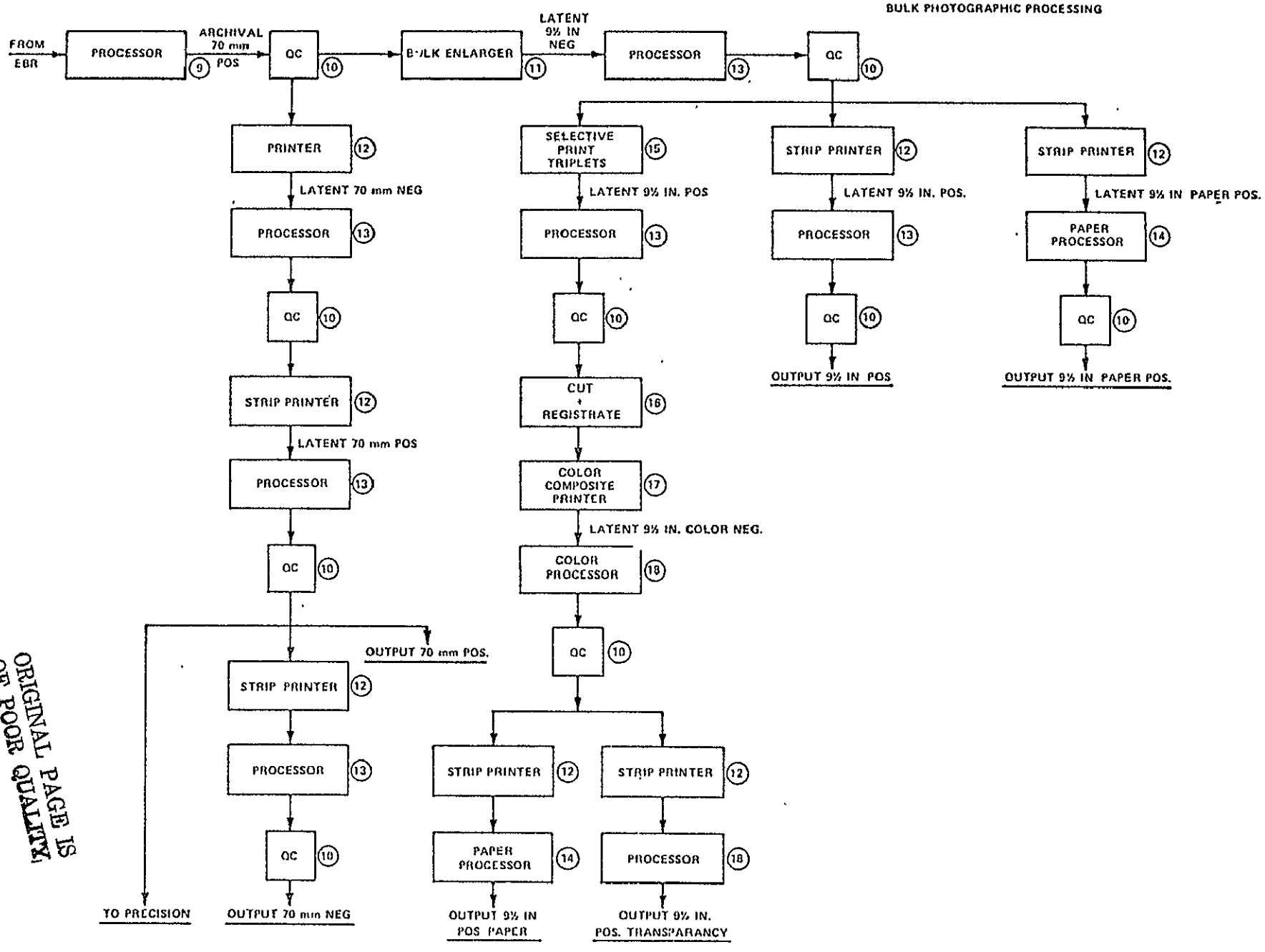

Figure 2-2 NDPF DATA FLOW BLOCK DIAGRAM (PART 2)

The RBV telemetry (2) is analog. The net frequency response of the RBV videotape record is given in Figure 2-3 (taken from Ref. 2, p. A-5).

The Hughes Multispectral Scanner (MSS) (3) has four conjugate linear detector arrays, each in one spectral band. The MSS telemetry (4) is digital. The frequency response of the MSS videotape record is given in Figure 2-4 (taken from Ref. 2, p. A-13). MSS data is D/A converted (5) in the playback operation. Radiometric corrections are applied in the digital domain before conversion.

The Electron Beam Recorder (EBR) (8) produces all archival latent images. The film type used is Kodak SO-438 (Ref. 1). A fifteen step gray scale is put on each image.

The first processor (9) is a Kodak Versamat used only for processing archival images.

The quality control blocks (QC) (10) consist of standard Kodak chemistry quality control plus the placing of a special target on the head and tail of each roll processed. The target consists of two frames: one containing a gray scale, another containing five equal, uniform density patches and a standard Air Force tri-bar target. The gray scale is read and a Hurter-Driffield (H-D) curve fit to the data points. The density values at two exposure levels are plotted and deviation from nominal values used as a processing quality criterion. The constant density is read at the five format positions to provide uniformity data. The Air Force tri-bar target allows determination of on-axis resolution. Additional information on the quality control procedures is included in Appendix A.

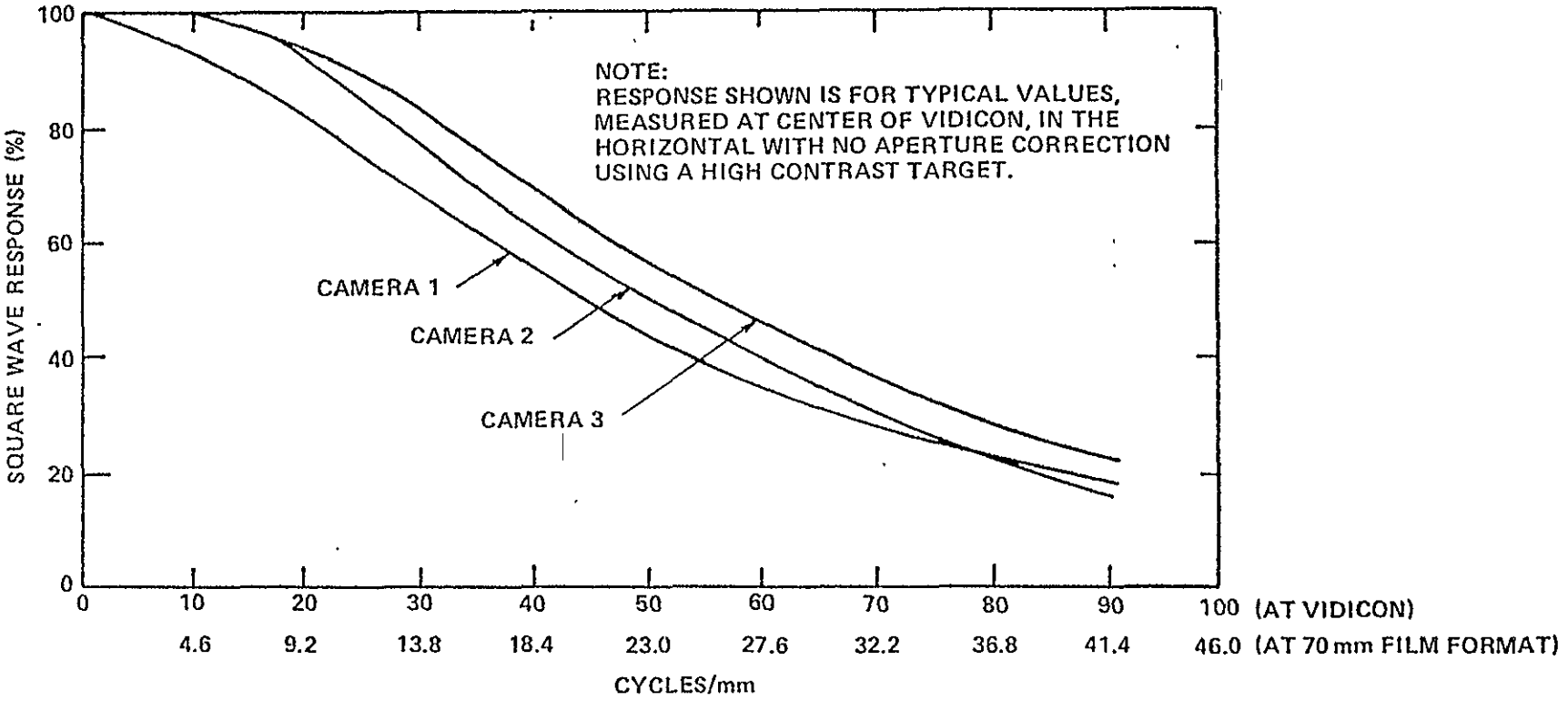

Figure 2-3 MEASURED RBV SYSTEM SQUARE WAVE RESPONSE

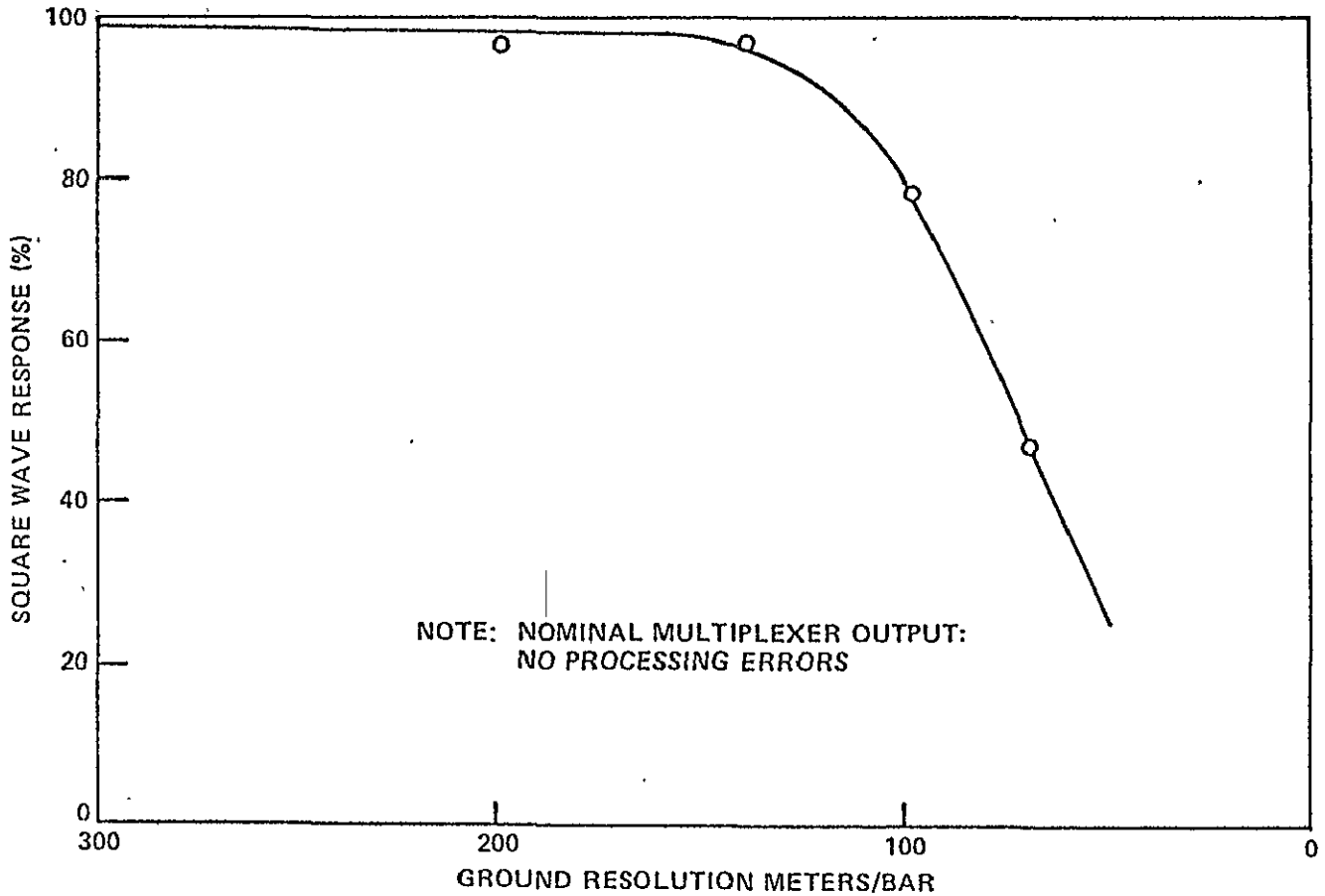

Figure 2-4 MEASURED MSS SYSTEM SQUARE WAVE RESPONSE

2.2 Users' Requirements

It is required that the image quality characterization resulting from this study contain sufficient information for users to determine the adequacy of ERTS imagery for individual needs. Users' ability to define "image quality" is not established and completeness of an image quality characterization based on users' requirements would not be expected. But a general understanding, at least, of what tasks users of ERTS imagery would like to accomplish is certainly required if the "quality" which is controlled is to have relevance.

A literature search was consequently conducted. Based on the literature sampled, no definition of "image quality" useful in accomplishing the study objectives can be drawn from the users. Surely, one might adopt the terms "radiometric fidelity", "geometric fidelity", "resolution", but these terms have different meanings to different people and are certainly not sufficiently well defined to provide a useful basis for quality control criteria. They are general terms which classify rather than specify the ability to make certain measurements on photographs.

We examined the users' tasks to determine what sort or measurements each user user was making. The results seem to span the following questions:

1. How accurately can a boundary between different transmission levels be located on a photograph?

2. How well can the radiance, size, and location of small objects be measured?

3. How well can the distance between two objects or boundaries on a photograph be measured?

4. How well does that distance represent the separation on the earth?

5. How well can the transmission of a photograph be measured?

6. How is that transmission related to radiance at the earth?

Clearly, any working definition of "image quality" adequate for the task at hand must be capable of obtaining quantitative answers to such questions and must relate those answers to measurable properties of elements of the image processing system.

2.3 System Element Performance Characterization and "Image Quality"

This section delineates the techniques commonly employed to characterize equipment performance and image quality. The purpose is to establish some concepts that will subsequently be used and to point out why some others are unsatisfactory for the study objective.

In order to ensure familiarity with the current state of the art, a literature search covering the period from 1968 to the present was undertaken.

Four overlapping categories; optical transfer function, resolution, noise, and subjective image quality, provide convenient areas for discussion.

2.3.1 Optical Transfer Function

The optical transfer function has been shown to be a useful tool to characterize the performance of many imaging devices.

The blur introduced by an optical system can be characterized by a "point spread function" $s(\vec{x})$ defined implicitly by the convolution:

$$i(\vec{x}) = o(\vec{x}) * s(\vec{x}) \tag{2-1}$$

where: $i(x)$ = image brightness, $o(\vec{x})$ = object brightness, and $\vec{x}$ = position coordinates in plane orthogonal to optical axis. (* denotes convolution).
Thus:

$$I(\vec{\nu}) = O(\vec{\nu})\,\tau(\vec{\nu}) \tag{2-2}$$

where: $I(\vec{\nu}) \rightleftharpoons i(\vec{x})$, $O(\vec{\nu}) \rightleftharpoons o(\vec{x})$, $\tau(\vec{\nu}) \rightleftharpoons s(\vec{x})$, and $\rightleftharpoons$ denotes a Fourier transform.

$\tau(\vec{\nu})$ is the optical transfer function (OTF). It is in general a two-dimensional, complex valued function. $|\tau(\vec{\nu})|$ is the modulation transfer function (MTF). It is emphasized that the OTF is <u>not</u> a measure of image quality but merely the frequency response function of a linear device and consequently a measurable property of the performance of that device.

Application of the OTF concept to photo-optical systems requires linearization of the generally non-linear development process. Generally the OTF concept is applied to the object to exposure image transfer process. Methods for measuring the OTF are discussed in Appendix A.

2.3.2 Resolution

Resolution is related to the ability to determine object characteristics especially shape from an image. A number of resolution criteria are in use.

Rayleigh's criterion assumes that the diffraction limited images of two points are just resolved if the central maximum of one lies on the first minimum of the Airy disc of the other.

The Rayleigh criterion is clearly related to the spread function and can thus be derived if the OTF is known.

A number of resolution criteria are simply defined by an observer's ability to distinguish the existence of a particular target. Such criteria depend, not only on the properties of the image, but on the properties of the detection process as well. The most common is the standard Air Force Tri-Bar target. One can obtain a "modulation detectability curve" by having a number of subjects observed tri-bars of varying spacing and contrast and plotting the detection threshold contrasts versus spatial frequency. "Resolution" is then defined as the intersection of an MTF and a modulation detectability curve. Uncontrolled variables and experience produce uncertainty in this measure of resolution. One summary measure of "image quality" that is in use is the area enclosed between the modulation detectability curve and the MTF.

The term "resolution" is sometimes applied to the ability of an optical system to "resolve" a specified object. This definition is similar to the preceding one but requires recognition as well as detection.

2.3.3 Noise

In photo-optical systems, the major noise source is the granularity of the emulsion and is expressed in the granularity constant, G.[1] The rms density fluctuation observed in scanning a uniform density area is

$$\sigma_D = \frac{G}{\sqrt{A_A}} \qquad (2\text{-}3)$$

where: A_A = area of scanning aperture

In actuality the emulsion records the continuous exposure distribution as a discrete, thin but nevertheless three-dimensional, distribution of silver particles. The photographic macro-image is a continuous intensity distribution which results from multiple scattering of photons traversing the developed emulsion. If the photographic image is observed over a very small area very close to the emulsion surface, it is not clear how the observed intensity is related to the intensity distribution which exposed the emulsion; in other words, the micro-image is not yet adequately understood. Considerable research has been performed to attempt to characterize photographic granularity.[4-6] It has been represented as both additive and multiplicative noise. Since no clearly superior model exists it is most often represented by additive white gaussian noise. We employed this approach and represented the grain noise by rms fluctuations in transmission.

For the electronic image processing system elements, an additive white gaussian noise model is theoretically as well as pragmatically acceptable.

2.3.4 Subjective Image Quality

Efforts have been made in a number of studies[7-11] to define subjective assessment of image quality in a quantitative manner.

Such techniques by definition include human variables which are not well controlled. It is not surprising that a universal subjective measure has not been accepted although correlation of subject response with measurable parameters within the limits of specific product use has been shown.

Subjective image quality efforts are directed to achieve a causal relationship between measurable system element performance properties, such as frequency response (OTF), signal-to-noise ratio, etc., and the ability of the user to make subjective judgments (usually in the form of detection/recognition decisions) on the output product. The motivation of such efforts is consistent with the objective of this study. However, the quality measures depend on the human detection process as well as the image data system. To develop quality control procedures the selected measure should depend only on the system itself. Thus, subjective image quality measures are not appropriate for the present study.

2.3.5 Conclusion

For most conceivable image processing systems, the elements' performance can be characterized by OTF's (if linear), nonlinear gains (photographic development), noise sources, or combinations of the three. Thus adequate "performance" descriptors exist. But based on the survey of the state-of-the-art of image quality evaluation, no objective technique to relate such descriptors to a quantitative measure of image quality was available.

SECTION 3

MATHEMATICAL BASES

The review of image system performance evaluation techniques indicated that descriptors of the influence of system elements on an image exist and are in common use. In particular, the performance of elements linear in intensity can be described by OTFs, the performance of elements non-linear in intensity can be described by non-linear gains, and elements which contribute noise can often be described by gaussian statistics. In general, the influence of a piece of hardware can be unambiguously described by a sequence of mathematical operators corresponding to these three measurable descriptors.

One finds no such consensus on a metric for the quality of the output product of an image processing system.

What the user of imagery does is to make observations on the output product, from which he estimates a radiant distribution (as a function of position) on the earth. But because the system is both band-limited and noisy, these estimates will necessarily be imperfect. A suitable image quality metric is therefore the error which the system introduces into estimates of ground radiant distributions. Precedent for this idea may be found in a study[12, 13] of Lunar Orbiter imagery.

In this section, it is shown that to formulate the image quality problem as one of parameter estimation yields an objective mathematical relationship between output product quality and element performance descriptors. In addition, analytic relationships required for implementation of the approach are derived.

3.1. Cramer-Rao Bound

Consider a user who wishes to measure some parameter "A", say the radiance of a wheatfield, as a function of position "x" on the earth by making observations on an NDPF output product. Let the ground object be mapped onto the photograph space as the function S (x, A). Since the system adds noise to the signal, the user will obtain a distribution of values with some standard deviation σ_A . To avoid consideration of the user's specific technique, it is assumed that he uses an optimal measurement process.

It can be shown (see Van Trees[14]) that the variance, σ_A^2, of an unbiased estimate of A made from an output signal contaminated by additive white gaussian noise is bounded by the Cramer-Rao inequality:

$$\sigma_A^2 \geq N_0 \left[\int_0^{\chi_0} \left[\frac{\partial S(\chi, A)}{\partial A} \right]^2 d\chi \right]^{-1} \qquad (3\text{-}1)$$

where N_0 = white noise power density (double-ended*) at the output and χ_0 = record length.

The user will generally be interested in estimating multiple parameters. Equation (3-1) can be generalized, for the "n" independent parameter case to:

$$\sigma_{A_i}^2 \geq N_0 \left[M^{-1} \right]_{ii} \qquad (3\text{-}2)$$

* Van Trees uses a single-ended spectrum which results in a factor of 2 in the denominator of Equation (3-1).

where the matrix M is given by:

$$M_{ij} = \int_0^{x_0} \frac{\partial S(x,\vec{A})}{\partial A_i} \quad \frac{\partial S(x,\vec{A})}{\partial A_j} \; dx \tag{3-3}$$

$\vec{A}$ is simply the vector whose components are the independent parameters: $A_1, \ldots, A_n$ used to describe the input signal.

If the noise power spectrum is not white at the system output, an inverse or "pre-whitening" filter must be included as the last system element in order to apply the bound.

The equality in the error bound represented by Equation (3-2):

(1) holds if $s(x,\vec{A})$ is linear in $\vec{A}$

(2) is approached when $s(x,\vec{A})$ is nonlinear in $\vec{A}$, but the signal-to- noise ratio becomes large.

If one can compute the set of partial derivatives $\frac{\partial S(x,\vec{A})}{\partial A_i}$ as a function of changes in $S(x,\vec{A})$ resulting from changes in the performance descriptors of elements internal to the system, one can use this relationship to predict the change in estimation error introduced. Equation (3-2) is therefore the objective relationship between "system element performance" and "image quality" required.

In order to illustrate the use of this tool, some specific examples are given:

First, consider the task of determining the boundary between two different crops and the reflectance level of each. The ground object can be represented as a three parameter "edge" target where A_1 is the radiance level of one field, A_2 the radiance level of the other, and

A_3 as the location of the boundary. One computes the sensitivities: $\frac{\partial S}{\partial A_i}$ $i = 1, 2, 3,$ determines the components of M from equation (3-3), obtains the inverse matrix M^{-1}, extracts the diagonal elements, and obtains the estimation errors on each parameter from equation (3-2).

If the user utilized an optimal measurement technique, he would obtain statistically distributed values for each parameter with standard deviation σ_{A_i} according to (3-2). If his technique is not optimal, he will do worse, but in no event will he obtain more precise results.

As a second example, consider measurement of a river. The river can be represented as a four parameter target with A_1 the radiance level of the land on both sides, A_2 the radiance of the river water, A_3 the width of the river, and A_4 the location of the river.

An example similar to "resolution" might be two bright, narrow lines on some background of radiance A_1, separated by distance A_2. The "resolution" would then be expressed by σ_{A_2} as a function of A_1 and A_2.

It can be shown that a very broad class of functions (ground objects) can be expressed as n-parameter sets. Thus, this approach can, in principle, be applied to any conceivable ground object. It is sufficient for the purposes of this effort to use simple targets with four or less parameters shown in Figure 3-1 and discussed above.

NUMBER OF PARAMETERS (TARGET IDENTIFICATION)	DESCRIPTION	SKETCH (SIGNAL VS POSITION)	POTENTIAL APPLICATION
1	CONSTANT LEVEL TARGET	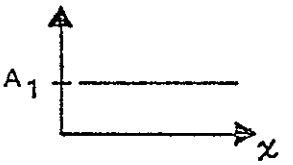	DEVELOP NOISE STATISTICS
2	DOUBLE DELTA FUNCTION TARGET	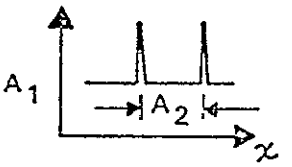	EVALUATE "RESOLUTION" AND GEOMETRIC ERROR
3	EDGE TARGET	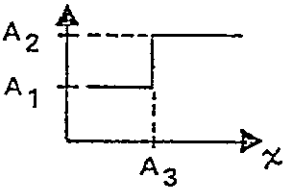	EVALUATE RADIOMETRIC AND GEOMETRIC ERROR
4	BAR TARGET	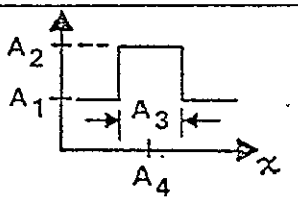	EVALUATE RADIOMETRIC AND GEOMETRIC ERROR

Figure 3-1 SELECTED TARGET CONFIGURATIONS

Note that the estimation errors are directly proportional to the white noise spectral density, N_o, the height of the double-edged noise power spectrum. Thus in the limit of a noiseless system, the object can be measured exactly regardless of the effect of the system. (It is of course implicit that the object form is a priori known in that it has been represented as a complete orthonormal set of n-parameters and that the system effects likewise are known a priori.)

In summary, a procedure has been defined for objective determination of the effect of changes in subsystem element performance on the precision to which users can make measurements of target characteristics from image products.

3.2 Dimensional Analysis

The dimensional analysis is useful in augmentation of intuitive understanding of equation (3-2) and of some of the results to be presented in Section 6.

The one-dimensional case is considered. The ground object (parameterized target) is defined by radiance as a function of position. Call the radiance unit $|R|$ and the position (distance) unit $|X|$. The autocovariance function $f'(x)$ is defined by

$$\lim_{\chi \to \infty} \frac{1}{2\chi} \int_{-\chi}^{\chi} f(x)\, f(x-x')\, dx \equiv f'(x')$$

where $f(x)$ in the image of the ground object and consequently $f'(x')$ has dimension $|R|^2$.

The double ended power spectrum:

$$N(\nu) = \int_{-\infty}^{\infty} f'(x') e^{i(2\pi\nu x')} dx' \qquad \text{where } \nu = \text{spatial frequency}$$

thus has dimension $|R|^2\,|X|$.

Therefore, $\left|N_o\right| \doteq \left|\mathcal{R}^2\right| \left|X\right|$.

Now if the input target is expressed in terms of a set of orthogonal parameters A_i, the the image is given by $f(x) = S(x, \vec{A})$ for some particular $\vec{A}$. By equation (3-2), the variances characterizing the error in estimating the components of that particular A vector are:

$$\sigma_{A_i}^2 \geq N_o \left[M^{-1}\right]_{ii} .$$

By definition

$$\left|M_{ii}\right| \equiv \left|\int_o^{x_o} \left[\frac{\partial S}{\partial A_i}\right]^2 dx\right| .$$

so that

$$\left|\left[M^{-1}\right]_{ii}\right| \doteq \frac{\left|A_i\right|^2}{\left|R\right|^2 \left|x\right|} .$$

Finally, since

$$\left|\sigma_{A_i}\right|^2 \doteq \left|N_o\right| \left|\left[M^{-1}\right]_{ii}\right|$$

substitution yields

$$\left|\sigma_{A_i}\right|^2 \doteq \left|A_i\right|^2 .$$

And the variances are seen to have the correct dimensions.

3.3 Noise Characterization

A major noise contributor in many image data systems is photographic granularity. The photographic granularity constitutes a two-dimensional noise field which, for the purpose of this study, can be characterized by a two-dimensional white noise spectral density. Transformation relationships between the two-dimensional field and a one-dimensional representation are required for two reasons:

1) Many users utilize microdensitometer traces or scans to obtain quantitative measurements from photographs. The microdensitometer record contains one-dimensional noise obtained by moving an aperture along some line over the two-dimensional photographic noise field. How do we account for the two-dimensional nature of the image and include the appropriate noise spectral density in the calculation of the Cramer-Rao bound (Eq. (3-2))?

2) Section 4 will indicate practical reasons for a one-dimensional system simulation. Such implementation requires valid characterization of the noise field in one dimension so that the simulation's results converge to the real physical situation. What magnitudes of rms noise should be added to the one-dimensional signals in simulating an image data system?

The questions are related since the measuring aperture (size and shape) will determine the magnitude of the rms noise to be added in the simulation as well as the noise content of the one-dimensional trace used to obtain quantitative measurements (parameter estimates). There are two aperture shapes which might be employed: slits and circles. Both will be treated in the discussion that follows, however, a slit aperture appears to be the more likely candidate.

3.3.1 Treatment of noise for parametric estimation from one-dimensional scans.

The procedure for establishing the variances of two-dimensional target parameters from one-dimensional scans requires knowledge of the scan noise spectrum. This, in turn, depends on the net two-dimensional spectrum as transmitted through the optical system to the point of scanning, and on the scanning aperture function.

Arguments are presented illustrating that slits are a scanning aperture compatible with both the spirit of the present study and a mathematical requirement for the validity of the variance estimator. The results for a circular aperture are included for completeness. As either the slit length becomes arbitrarily large, or the width arbitrarily small, certain simplified asymptotic behavior between the scan spectrum and the two-dimensional field spectrum emerges. We can refer to such apertures as "partially asymptotic". In the event both conditions are met (totally asymptotic slit), the following relationship occurs:

$$\Phi_s(\nu_s) = \frac{1}{\ell}\ \underline{\Phi}(\nu_s, 0) \tag{3-4}$$

where:* $\Phi_s(\nu_s)$ - scan spectrum (transmission^2-mm/cycle)

$\underline{\Phi}(\nu_s, \nu_p)$ - field spectrum (transmission^2-mm^2/cycle^2)

ℓ - length of aperture (mm)

ν_s - spatial frequency in scan direction (cycles/mm)

ν_p - spatial frequency orthogonal to ν_s (cycles/mm)

* All spectra are double-ended (i.e., $-\infty < \nu < \infty$)

The remainder of this section:

- Derives a convolution theorem having general utility to the following sections.
- Establishes the relationship between film granularity and the two-dimensional Wiener spectrum.
- Derives the relation between the scan Wiener spectrum and the field spectrum for slit and circular apertures and examines various limiting cases for the slit aperture.

3.3.1.1 A Convolution Theorem*

Consider a two-dimensional stochastic variable T(x, y) representing point transmission of a field. Allow this field to be convolved with an aperture function A to yield a new field having point transmission T_A. We write:

$$T_A(\xi,\eta) = \int_{-\infty}^{\infty}\int T(x+\xi, y+\eta)\, A(x,y)\, dx\, dy \qquad (3\text{-}5)$$

with the conditions:

$$E\{T\} = 0$$

$$\int_{-\infty}^{\infty}\int A(x,y)\, dx\, dy = 1$$

Since we shall be interested in the Wiener spectra of the two-dimensional fields, the autocovariance $[\phi_s(\alpha,\beta)]$ of T_A is computed:

$$\phi_s(\alpha,\beta) \equiv E\left\{T_A(\xi+\alpha, \eta+\beta)\, T_A(\xi,\eta)\right\} \qquad (3\text{-}6)$$

---

*An equivalent theorem in frequency space is given by O'Neill in Reference 15.

which along with Eq. (3-5) results in:

$$\phi_S(\alpha,\beta) = \int_{-\infty}^{\infty}\int\int\int\int E\left\{T(x+\xi, y+\eta)\, T(x'+\xi+\alpha, y'+\eta+\beta)\right\} A(x,y) A(x',y')\, dx\, dy\, dx'\, dy'$$

or:

$$\phi_S(\alpha,\beta) = \int_{-\infty}^{\infty}\int\int\int\int \phi(x'-x+\alpha, y'-y+\beta)\, A(x,y) A(x',y')\, dx\, dy\, dx'\, dy' \qquad (3\text{-}7)$$

where ϕ is the autocovariance of T. A change in variables $x' \to \mu$, $y' \to \nu$ according to:

$$\left.\begin{aligned} \mu &= x' - x + \alpha \\ \nu &= y' - y + \beta \end{aligned}\right\}$$

allows Eq. (3-7) to be written:

$$\phi_S(\alpha,\beta) = \int_{-\infty}^{\infty}\int \phi(\mu,\nu)\left[\int_{-\infty}^{\infty}\int A(x,y)\, A(\mu+x-\alpha, \nu+y-\beta)\, dx\, dy\right] d\mu\, d\nu \qquad (3\text{-}8)$$

The integral in brackets is the auto-"covariance"* (ϕ_A) of the aperture and we having finally:

$$\phi_S(\alpha,\beta) = \int_{-\infty}^{\infty}\int \phi(\mu+\alpha, \nu+\beta)\, \phi_A(\mu,\nu)\, d\mu\, d\nu \qquad (3\text{-}9)$$

This convolution theorem will have general utility to our analyses that follow.

3.3.1.2 Granularity and the Two-Dimensional Spectrum

The NDPF model requires the Wiener Spectrum of photographic grain as inputs at several stages.

This spectrum has already been assumed to be white thereby allowing its single degree of freedom to be evaluated in terms of the classical measure known as "granularity". Granularity is the RMS fluctuation in density (σ_D) derived from a scan of uniformly exposed film. For this purpose the scanning aperture is always large and the

* A(x, y) is, of course, not a stochastic variable.

corresponding fluctuations are small. We shall deal here with the RMS fluctuation in transmission (σ_T) rather than density, but the two are simply related.

The variance σ_T^2 of a one-dimensional scan is given by its autocovariance $\phi_S(\alpha)$ $(= \phi_S(\alpha,0))$ evaluated at zero. Thus we have through Eq. (3-9):

$$\sigma_T^2 = \phi_S(0,0) = \int_{-\infty}^{\infty}\int \phi(\mu,\nu)\ \phi_A(\mu,\nu)\ d\mu\, d\nu$$

Since the grain spectrum is white its autocovariance is written:

$$\phi(\mu,\nu) = \mathcal{N}\ \delta(\mu)\ \delta(\nu)$$

where: $\mathcal{N}$ - two-dimensional Wiener spectrum of grain (transmission^2-meter^2/cycle^2)

and the variance σ_T^2 becomes:

$$\sigma_T^2 = \mathcal{N}\ \phi_A(0,0) \qquad (3\text{-}10)$$

A uniformly transmitting aperture of area A_A is written:

$$A = \begin{cases} 1/A_A & (within\ A_A) \\ 0 & (outside\ A_A) \end{cases}$$

This yields $\phi_A(0,0) = 1/A_A$ and the value for $\mathcal{N}$ in Eq. (3-10) is established:

$$\mathcal{N} = \sigma_T^2\ A_A \qquad (3\text{-}11)$$

This is equivalent to Equation (2-3) presented earlier.

3.3.1.3 Wiener Spectra Relations

Prior to deriving the relation between one and two-dimensional spectra, it is appropriate to digress in order to present the rational for selecting slits as having special significance to the present study. We build up the logic as follows:

(1) The purpose of the present study is to determine the impact of processing parameter errors on optimum user performance and not user performance per se. To this end simple psuedo-realistic one-dimensional targets (such as edges) are sufficient to make the connection since they contain the fundamental properties of transmission level and position.

(2) In light of both (1) above and the point that the variance estimation represents optimum information extraction, the scanning aperture should not further degrade the signal. Thus, its dimension in the scan direction should be small.

(3) Generally, the lower bound of Equation (5-2) is realized only for differential departures of the parameters from their true values. The validity of this requires small noise fluctuations which in turn means a scanning aperture of large area. Since its dimension in the scan direction must be small, the other dimension must therefore be large. Since the targets are one-dimensional, no signal degradation will occur under this requirements.

We now derive an expression between the scan spectrum resulting from a slit and the two-dimensional field spectrum. First, the scan spectrum $\bar{\Phi}_s(\nu_\alpha)$ is defined as the Fourier transform of the scan autocovariance $\phi_s(\alpha)$:

$$\bar{\Phi}_s(\nu_\alpha) \equiv \int_{-\infty}^{\infty} \phi_s(\alpha, 0)\, e^{-2\pi i \nu_\alpha \alpha}\, d\alpha$$

Eliminating ϕ_s by means of Eq. (3-9) yields:

$$\bar{\Phi}_s(\nu_\alpha) = \int_{-\infty}^{\infty} \left[\iint \phi(\mu+\alpha, \nu)\, \phi_A(\mu, \nu)\, d\mu\, d\nu \right] e^{-2\pi i \nu_\alpha \alpha}\, d\alpha \qquad (3\text{-}12)$$

The field spectrum $\bar{\Phi}$ is defined by:

$$\phi(\mu, \nu) = \iint_{-\infty}^{\infty} \bar{\Phi}(\nu_\mu, \nu_\nu)\, e^{2\pi i (\nu_\mu \mu + \nu_\nu \nu)}\, d\nu_\mu\, d\nu_\nu$$

Eliminating ϕ from Eq. (3-12) allows the integration over α to be carried out in closed form:

$$\bar{\Phi}_s(\nu_\alpha) = \iint_{-\infty}^{\infty} \left[\int \bar{\Phi}(\nu_\alpha, \nu_\nu)\, e^{2\pi i (\nu_\alpha \mu + \nu_\nu \nu)}\, d\nu_\nu \right] \phi_A(\mu, \nu)\, d\mu\, d\nu \qquad (3\text{-}13)$$

The aperture autocovariance, ϕ_A , defined in Eq. (3-8) is written for a slit of width w (in the scan direction) and length l:

$$\phi_A(\mu, \nu) = \begin{cases} \frac{1}{A_A}\left(1 - \frac{1}{w}|\mu|\right)\left(1 - \frac{1}{l}|\nu|\right) = \frac{1}{A_A}\phi_\mu(\mu)\phi_\nu(\nu) & \text{(within } A_A\text{)} \\ 0 & \text{(otherwise)} \end{cases}$$

Inserting in Eq. (3-13) we have:

$$\bar{\Phi}_s(\nu_\alpha) = \frac{1}{A_A}\left[\int_{-w}^{w} \phi_\mu(\mu)\, e^{2\pi i \nu_\alpha \mu}\, d\mu \right] \int_{-\infty}^{\infty} \bar{\Phi}(\nu_\alpha, \nu_\nu) \left[\int_{-l}^{l} \phi_\nu(\nu)\, e^{2\pi i \nu_\nu \nu}\, d\nu \right] d\nu_\nu .$$

The two transforms in square brackets have solutions:

$$\left.\begin{aligned} \int_{-w}^{w} dx &= w\,\mathrm{sinc}^2(\pi \nu_\alpha w) \\ \int_{-l}^{l} dx &= l\,\mathrm{sinc}^2(\pi \nu_\nu l) \end{aligned}\right\}$$

Thus, we have the final general relationship:

$$\bar{\Phi}_s(\nu_\alpha) = \mathrm{sinc}^2(\pi \nu_\alpha w) \int_{-\infty}^{\infty} \bar{\Phi}(\nu_\alpha, \nu_\nu)\,\mathrm{sinc}^2(\pi \nu_\nu l)\, d\nu_\nu \qquad (3\text{-}14)$$

GENERAL

We now give five special cases of Eq. (3-14), all of which follow immediately. The first three are the asymptotic slits defined earlier:

$$\bar{\Phi}_s(\nu_\alpha) = \int_{-\infty}^{\infty} \bar{\Phi}(\nu_\alpha, \nu_\nu)\,\mathrm{sinc}^2(\pi l \nu_\nu)\, d\nu_\nu \qquad (3\text{-}15)$$

NARROW SLIT ($w \to 0$)

$$\bar{\Phi}_s(\nu_\alpha) = \frac{1}{l}\,\mathrm{sinc}^2(\pi w \nu_\alpha)\,\bar{\Phi}(\nu_\alpha, 0) \qquad (3\text{-}16)$$

LONG SLIT ($l \to \infty$)

$$\bar{\Phi}_s(\nu_\alpha) = \frac{1}{l}\,\bar{\Phi}(\nu_\alpha, 0) \qquad (3\text{-}17)$$

LONG AND NARROW SLIT

Finally, when both the dimensions of the slit become small or large together we have:

$$\bar{\Phi}_s(\nu_\alpha) = \int_{-\infty}^{\infty} \bar{\Phi}(\nu_\alpha, \nu_\nu)\, d\nu_\nu \qquad (3\text{-}18)$$

SMALL SLIT

$$\bar{\Phi}_s(\nu_\alpha) = \frac{N}{l}\,\mathrm{sinc}^2(\pi w \nu_\alpha). \qquad (3\text{-}19)$$

LARGE SLIT

The asymptotic form given in Eq. (3-17) is recommended since it represents optimum parameter estimation. However, formally requiring the field spectrum Φ at all frequencies can be side-stepped in those cases where the signal spectrum is severely band-limited. Under such a condition, the spectrum Φ can be taken as white over the frequency domain of the signal:

$$\Phi(\nu_\alpha, 0) \simeq \Phi(0,0) = \mathcal{N}$$

with $\mathcal{N}$ now interpreted as the net grain spectrum. Thus the scan noise spectrum is simply:

$$\Phi_s(\nu_\alpha) \equiv N_o = \frac{\mathcal{N}}{\ell} \quad . \tag{3-20}$$

Now the field spectrum $\mathcal{N}$ is given directly by Eq. (3-11), and we have:

$$N_o = \frac{\sigma_T^2 A_A}{\ell} \tag{3-21}$$

where σ_T is the composite granularity due to all contributing system elements.

An expression for the scan noise spectrum for a circular aperture was developed during an earlier study by Trabka[16], namely*

$$\Phi_s(\nu_\alpha) = \frac{4\mathcal{N}}{\pi d_o} \frac{H_1(2\pi d_o \nu_\alpha)}{(\pi d_o \nu_\alpha)^2} \tag{3-22}$$

where d_o is the diameter of the scanning aperture and Trabka's normalizing constant $k = 4/d_o$. The aperture diameter must be large enough to validate the assumption of white noise made by Trabka. Assuming that $\Phi_s(\nu_\alpha)$ varies slowly over the signal spectrum (effectively white noise) we set

$$\Phi_s(\nu_\alpha) \approx \Phi_s(o) = N_o = \frac{32}{3\pi^2} \frac{\mathcal{N}}{d_o}$$

since $H_1(2z)/z^2 \approx 8/3\pi$ for $z \ll 1$.[17] Using Eq. (3-11) for $\mathcal{N}$ we have

*The units of the independent variable have been changed from radians/mm to cycles/mm in comparison to Trabka's Equation (6).

$$N_o = \frac{32}{3\pi^2} \frac{\sigma_T^2 A_A}{d_o} = 1.08 \frac{\sigma_T^2 A_A}{d_o} \qquad (3\text{-}23)$$

which is analogus to Eq. (3-21) developed for slits. We note that both equations can also be expressed in terms of the rms density σ_o through use of the approximation

$$\sigma_T \simeq 2.3 \bar{T} \sigma_D . \qquad (3\text{-}24)$$

3.3.2 RMS Noise for One-Dimensional Simulation

If the image data system is represented by one-dimensional model we must determine an equivalent rms noise, σ_e , to be added to the signal to represent the film granularity or noise. Since we simulate at intervals, Δ , the simulated signal is band-limited by the Nyquist frequency, $\nu_N \equiv 1/2\Delta$, we should only add noise inside this bandpass. In this case

$$\sigma_e^2 = N_o(2\nu_N) = \frac{N_o}{\Delta} \qquad (3\text{-}25)$$

We can relate σ_e to Kodak measured grainularity by using Equations (3-21) or (3-23) depending upon the shape of the aperture we designate in scanning the image to obtain the one-dimensional trace. Consequently,

$$\sigma_e^2 = \begin{cases} \dfrac{\sigma_T^2 A_A}{\ell \Delta} & \text{(long and narrow slits)} \qquad (3\text{-}26a) \\ 1.08 \dfrac{\sigma_T^2 A_A}{d_o \Delta} & \text{(circles)} \qquad (3\text{-}26b) \end{cases}$$

If Kodak's published granularity values are used for σ_D , then A_A in Equations (3-26a) or (3-26b) is the area of the aperture used by Kodak in making the measurements.

SECTION 4

SOFTWARE IMPLEMENTATION

To use Equation (3-2) requires calculation of the partial derivatives $\frac{\partial S(x, \bar{A})}{\partial A_i}$. There are doubtless image data systems for which the system can be represented analytically and the derivatives of the output signal obtained directly. But for a multi-element system which contains nonlinear elements and where it is desired to arbitrarily vary the response of individual elements, an analytic approach is intractable. Consequently, a computer program was written which simulates the system in order to calculate the derivatives and the Cramer-Rao variance bound.

4.1 Image Data System Simulation (IDSS)

The primary function of the Image Data System Simulation (IDSS) is to compute the Cramer-Rao bound on the parameter estimation error introduced by a multi-element image data system composed of an arbitrary sequence of linear elements, nonlinear gains, and additive noise. A second capability of IDSS is to provide graphic display of test signals as they appear after every element of the image processing system so that the effect of individual elements can be visually assessed. A third is to determine the region of approximate linearity of the lumped-multielement system which contains individual nonlinear elements; the bounds of the "small signal" or "low contrast" linearizing approximation can be determined.

Although IDSS was developed as a tool necessary for solution of the quality control problem, application is in no way restricted to the NDPF system. The program could equally well be used in analysis of entirely photographic, electro-optic, or digital systems.

Program IDSS is written in Fortran IV for use on Calspan's IBM 370/168 computer. It requires 250K core and of the twenty three subroutines, eleven are called from the 370 system library.

What the program actually does is create a numerical isomorphism to the image processing system being studied, create test signals, propogate those signals through the simulated system, and perform the mathematical operation on the processed output signal which yield the estimation error variances.

The system simulation is one dimensional. A two dimensional simulation would involve no conceptual difficulties, but would greatly increase program size and running time. The one dimensional simulation is adequate for most conceivable purposes, but can given rise to certain subtle difficulties regarding the two dimensional photographic grain noise field which will be discussed in the second part of this section.

Input

Most image data systems can be represented by a sequence of elements whose performance is characterized by either OTF's (linear elements), nonlinear gains, and/or additive gaussian noise. The data defining the response of each element is required as input.

For the linear elements, the spread function rather than its Fourier transform, the OTF, is used for computational convenience. The spread function is of course always real valued, complex valued OTF's being manifested as asymmetrical spread functions. The effect of each linear element is thus determined by performing the convolution of its spread function with its input. The spread function defining the performance of each linear element is read as input.

The nonlinear gains encountered are typically the photographic H-D curves. A table of output density versus input density values defining each nonlinear elements H-D curve must be read as input. The input signal is converted into density space (= -log (signal)), transformed to output density by linear interpolation of the table, and converted to transmission by exponentiation ($10^{-D_{out}}$).

The noise is characterized by the standard deviation, which for the photographic granularity must be computed from Equation (3-26). A standard random number generating subroutine is used, its distribution scaled to the correct standard deviation, and the resulting white Gaussian noise added to the signal.

Any input target type can be generated that is expressible as a function of position and a set of orthogonal parameters. The number of parameters and the magnitude of each is required as input. For this study, targets with four or less parameters are adequate. Consequently, the routine that creates targets, Subroutine GEN, currently produces: 1) One parameter target - constant level A(1), 2) Two parameter target - two delta functions separated by distance A(2) on background level A(1), 3) Three parameter target - step at location A(3) between levels A(1) and A(2), or 4) Four parameter target - square pulse of width A(3) and location A(4) on background level A(1) with pulse level (height) A(2). These targets were illustrated previously in Figure 3-1.

In all computations, the signal level is represented on a scale of 0 to 1 and will henceforth be referred to as "transmission". The 0 level corresponds to zero ground radiance. The 1 level corresponds to the radiance input which yields full scale output voltage for the particular active sensor. This scale factor is defined as R_m. Therefore all standard deviations in estimation of A_i representing radiometric parameters are in units of R_m. The 0 to 1 "transmission" scale is actual photographic transmission at stages where photographs exist.

Output

The program operates in any one of three modes. In all modes of operation the values of computational parameters and the functions defining the response of each simulated system element are printed out. In mode 1 operation a table of the values and a table of errors for each of the target parameters, A(I), is printed out. The process is repeated for new system element performance data as desired.

In mode 2 operation, the noise power spectral density is computed, and N_o and the pre-whitening filter spread function are printed out. Mode 3 operation yields a plot of the target function as it appears after passing through each system element. Punched output of the processed target for auxiliary analyses (e.g., edge gradient spectral analysis) is optionally available in any mode.

Program Operation

For logical convenience, the simulation separates the system into a number of blocks each containing sequentially a spread function, non-linear gain, and additive noise. A set of control cards determine whether one, two, or all of the three possible element types are present in any particular block so that any permutation of element types is achievable. A second set of control cards determines whether data is to be changed for each element so that the program user can vary the performance of any element or any combination of elements as desired.

Mode 1

A block diagram showing the major steps in the variance calculation mode is given in Figure 4-1. Control parameters, constants, and system element performance data are first read in. Each spread function is normalized to unit area; the spread function is integrated and then divided point by point by the value of the integral. Normalization yields conservation of energy (unity gain) in the subsequent convolution operations. Values of each of the A(I) are set and a test target generated. This target is propagated through the simulated system by the correct sequence of convolution with spread functions, and alteration by non-linear gains. Additive noise elements are omitted in this mode. The resultant output signal is stored. The operation is repeated for the same target, but with each of the A(I) in turn altered by a differential increment. The partial derivatives of the output signal with respect to each A(I) are then computed by subtraction of the first stored output signal from each of the

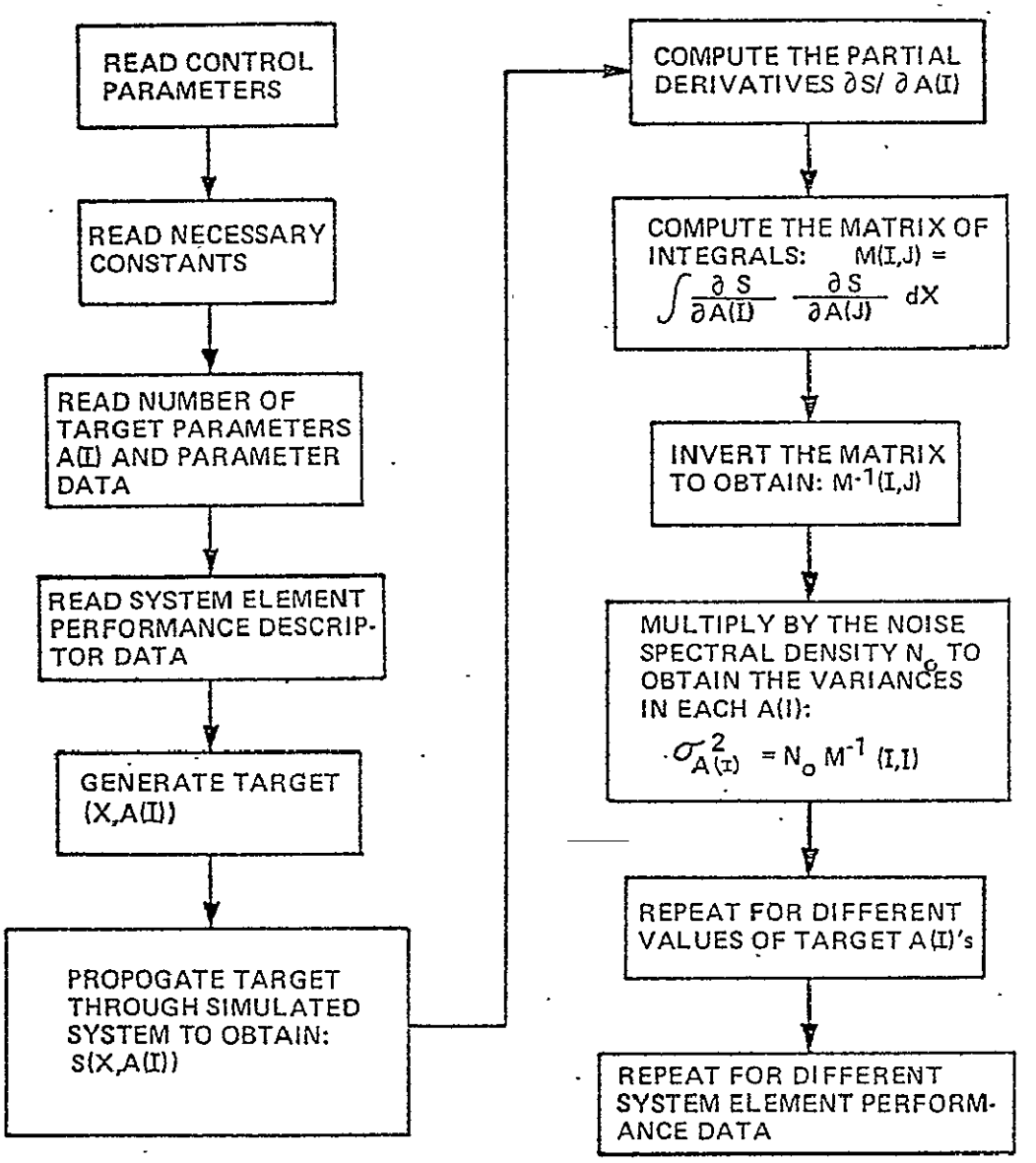

Figure 4-1 BLOCK DIAGRAM OF IDSS VARIANCE CALCULATION MODE

respective differentially altered output signals and division by the respective differential elements. The derivatives thus computed are labeled DYDA(I, X). The program next evaluates the integrals over X of DYDA(I, X) x DYDA(J, X) for I, J=1, . . . , NA where NA is the number of A(I). The matrix thus created is then inverted and diagonal elements of the inverse matrix are extracted. These elements are labeled SIG(I, I). Each is multiplied by the white noise power density, yielding new values replacing the old SIG(I, I). The quantities SIG(I, I) thus arrived at are the variances in the respective A(I).

The program then returns, assigns new values to the A(I) and repeats the computations for as many sets of A(I) values as desired.

When all target A(I) values have been exhausted, the program returns, reads new system element performance data where desired, and repeats the foregoing operations for the new simulated system. It stops when no new system element performance data remains to be read.

Mode 2

This mode is used to evaluate the noise characteristics at the output of the system. The initial data input is the same as Mode 1. A one parameter (constant level) target is generated. The target is propagated through the simulated system, in this case with the noise elements included. No differentials or matrix elements are calculated. Rather the autocovariance function of the output signal is computed and Fourier transformed to yield the power spectrum and N_o. The operation is repeated several times (the number of replications is specified as input), and the results averaged. The prewhitening filter, given by the square root of the reciprocal of the power spectrum, is computed and inverse Fourier transformed to yield the pre-whitening filter spread

function. This spread function must be used in Mode 1 operation as the last in the system simulation sequence if the power spectrum shows that the net noise is non-white. The value of N_o can also be used as input to Mode 1 for the double-ended white noise power density.

As in Mode 1, the operations are repeated for different target parameters and system element performance data as desired.

Mode 3

This mode is used to obtain plots of the target function at the output of various system elements. The initial data input is the same as Mode 1. Targets are generated and propogated through the system as in Mode 1. The signal is plotted as it appears after each system element. No operations are performed on the output signal.

As in the other two modes, the operations are repeated for different target parameters and system element performance data as desired.

User descriptions, including a listing and flowchart of IDSS program, are given in Appendix B.

SECTION 5

NDPF MODEL

The initial step in applying IDSS to an image processing system is to specify its data flow and construct a model of the system. We will illustrate this procedure using the NDPF. The data flow in the NDPF Bulk Processing or Initial Image Generating Subsystem was discussed previously in Section 2.2. In this section, the NDPF will be broken down into elements whose performance can be characterized by OTF's (frequency responses), additive gaussian noise, or non-linearities consisting of signal dependent gains. The results obtained from IDSS using this model are presented in the next section.

5.1 Element Performance Characterization

NDPF Input

The input is videotape records of telemetry from the satellite sensors. The telemetry and recording process are linear and characterized by frequency response functions (OTF's). White gaussian noise is added to the signal in transmission and recording. The RBV and MSS are linear devices characterized by OTF's and white gaussian noise.

Playback

The playback videotape recorders are linear and characterized by OTF's and white gaussian noise. The D/A conversion of MSS data and subsequent filtering is similarly characterized.

EBR Electronics

EBR Electronics are linear and characterized by an OTF and white additive gaussian noise.

EBR Preemphasis Nonlinearity

In order to obtain linearity between input radiance and archival transparency transmittance, and because of processing constraints on the EBR film, signal dependent gain is applied to the electronic input signal to the EBR.

Photographic Processors

The non-linear photographic process is defined by the Hurter-Driffield (H-D) curve which can be specified as a plot of output density as a function of input density

$$D = \log \frac{1}{T} \tag{5-1}$$

where D = density and T = transmittance. Since the linear elements of the system are linear in intensity (radiance), they are linear in T, so that the H-D curve represents a signal dependent gain. Henceforth, the relationships defining the photographic processor performance as well as that of the EBR preemphasis nonlinearity will be referred to as nonlinear gain.

Contact Printers

The physical process involved in contact printing is coupled multiple scattering within the master-duplicating film sandwich. That process yields a nonlinear image transfer in the general case, but has not been adequately studied to be useful in the present application. As part of a study[18] of the Kodak Niagara Printer, one of the authors (EKS) showed that in the limit of infintessimally thin continuous emulsions, the contact print would be the Fresnel diffraction pattern of the master. Fresnel fringes for edge targets were in fact observed by Yeadon.[18]

Diffraction phenomena result from discontinuities in the electric field. However, as edge gradients become finite and sufficiently low, the diffraction effects become less pronounced and the printing process approaches linearity. For the sensor imposed bandlimit of approximately 50 cycles/mm sufficient edge blur is expected that the linear model be valid. Should future payloads have increased OTF cutoff frequencies, this contact printer approximation must be re-examined.

In the present application, therefore, the contact printing process is considered to be a linear process with white gaussian noise (film granularity). The film MTF is lumped together with the printer OTF and referred to as a film-printer OTF.

Bulk Enlarger

The Bulk Enlarger is a linear device characterized by an OTF. That OTF is expected to vary as a function of field position, but since its magnitude at the sensor cutoff frequency ($\approx$12 cycles/mm on 9.5 in. format) should be high, field position variation can be neglected. Barring catastrophic occurrences, the enlarger's aberrations are constant, and the source of OTF variation expected in normal operation would be defocus. (Note that if the enlarger system is misaligned, there will be defocus as a function of field position, which cannot be neglected.)

The film MTF is lumped with the enlarger MTF so that the subsystem is modeled as a linear element characterized by its OTF, and additive white gaussian noise.

5.2 Model Constraints

Several constraints were imposed on the analysis of the NDPF:

1. As the RBV sensor in the current payload has been inoperative, the MSS configuration of the image processing system is emphasized.

2. The bulk processing (Initial Image Generating Subsystem) only is analyzed. Precision processing (Scene Correction Subsystem), the prime purpose of which is large scale geometric modification for mapping purposes, is not included in model manipulation.

3. Paper prints are not likely to be used quantitatively and are not considered.

4. The bulk processing is modeled only through the third generation transparency which is the prime product delivered to users for quantitative study.

5. Sensor-telemetry noise can be lumped together, and NDPF electronic element noise can be neglected.

6. Telemetry and recording apparatus can be assumed transparent (no effect on signal).

5.3 MSS Configuration Model

In terms of the subsystem element performance descriptors discussed, and under the preceding constraints, the NDPF model for processing MSS imagery is as follows:

Element	Measurable Performance Descriptor
1. Sensor	OTF
Electronics Noise	Standard deviation (gaussian, white)
2. EBR Control Electronics	OTF
3. Digital to Analog (D/A) conversion	OTF
4. Bessel Filter	OTF
5. EBR Electronics	OTF
EBR Preemphasis non-linearity	Nonlinear gain

6.	EBR (Beam)	OTF
7.	EBR (Film)	OTF
	EBR film development	Nonlinear gain (H-D)
	EBR film granularity	Standard deviation (gaussian, white)
8.	Contact printing/enlarging	OTF
	Contact printing/enlarging film development	Nonlinear gain (H-D)
	Contact printing/enlarging film granularity	Standard deviation (gaussian, white)
9.	Contact Printing	OTF
	Contact Printing film development	Nonlinear gain
	Contact Printing film granularity	Standard deviation (gaussian, white)

This model is represented by a series of 9 blocks identified above. Input values for each of the performance descriptors are presented in Section 6.1.

5.4 RBV Configuration Model

	Element	Measurable Performance Descriptor
1.	Sensor	OTF
	Electronics noise	Standard deviation (gaussian, white)
2.	EBR Control Electronics	OTF
3.	EBR Electronics	OTF
	EBR Preemphasis nonlinearity	Nonlinear gain

4-7. Same as MSS elements 6-9

5.5 Large Scale Errors

If all of the system elements introduced no degradation into the signal, the ERTS/NDPF system would only introduce a scale

change into the ERTS imagery. However, effects of payload attitude, sensor optics, and distortion internal to the NDPF result in a film plane geometry distorted compared to the ground. The NDPF was designed to correct for this mapping distortion (correction mechanisms are outlined in Appendix A.); however, some residual geometric mapping distortion error results. This error applies to measurement of distances of the order of magnitude of the frame size.

If the NDPF is described by a pseudo spread function of the entire lumped data processing system, the geometric estimation error introduced by the NDPF element performance descriptors is separable from the large scale geometric mapping distortion described above; the two error sources can be treated independently. The errors calculated assess the small scale, not the large scale geometric error.

Similarly the radiant input to the sensor would be mapped into a related radiance scale at the output product for an ideal system. However, a radiance mapping error exists over distances of the order of the frame size due to sensor and processing nonuniformities. The correction mechanisms for this error are also discussed in Appendix A, and the residual errors resulting from application of the algorithm can be calculated directly. Again, this radiometric error is separable from the parameter estimation errors of concern in this study.

5.6 Modeling Summary

The NDPF and sensors have been modeled in terms of accepted, measurable descriptors of the performance of system elements. These descriptors can be utilized as a sequence of operators to obtain system output as a function of input to the sensor. To develop or assess quality control tolerances requires determination of the effect of changes in the performance descriptors on parameter estimation errors.

SECTION 6

RESULTS

The results of application of the technique to the NDPF are presented in this section. The first part discusses the input data base identifying the specific values assigned to the descriptors (functions) which characterize the performance of each element of the NDPF model delineated previously. In the subsequent discussion, the nominal performance of the NDPF/MSS configuration is established and examined in detail. The effects of off-nominal element performance are determined. The results expected from the RBV configuration are considered by comparison to the MSS. The implications of these results on procedures for quality control of the NDPF elements are subsequently examined. Finally, a technique for calibrating ERTS imagery in order to relate transmittance to ground radiance or reflectance is illustrated.

6.1 Input Data for Element Performance

Valid quantitative definition of each spread function, nonlinear gain, and noise standard deviation are obviously required as input to IDSS. Approximate accuracy of input data is adequate to determine the influence of changes in system element performance or changes in estimation error, which is of course, the prime objective. However, accuracy of the calculated estimation errors as a measure of absolute system performance requires high confidence level input data.

Although some simple measurements of element performance were made by us, for the most part it was necessary to rely on external information sources. Sufficient confidence in the approximate accuracy stipuated is asserted; the best data found to be available was used. But it must be emphasized that the reader keep in mind that inferences of absolute system performance are affected by absolute accuracy of input data.

Input data used and the manner in which it was acquired for each system element are given below. All spread functions plotted have been normalized to unit area. The unit of length used in computations is the micrometer and distances refer to the 70 mm format. All nonlinear gains are presented as plots of input density vs output density. Noise sources, always gaussian and white, are characterized by the applicable standard deviation.

a) Payload Sensors

1. MSS - the sensor spread function was obtained by inverse Fourier transform of the MTF given in the User's Handbook.[2] No phase data were available. The curve given appears to have been fitted to only four data points. The resulting MSS spread function is plotted as Figure 6-1(a).

2. RBV - the sensor spread function was obtained by inverse Fourier transform of an "eyeball average" of the three characteristic MTF's given in the User's Handbook.[2] No phase data were available. The spread function is plotted as Figure 6-1(b).

b) Telemetry and Recording - Assumed Transparent.[1]

c) Playback Video Tape Recorder - Assumed Transparent.[1]

d) Video Tape Recorder Control Electronics - Assumed Transparent.[1]

e) EBR Control Electronics (EBR CTL) - Spread function obtained by inverse Fourier transform of MTF given in ERTM-H-81.[19] Plotted as Figure 6-1(c)

f) Digital to Analog Converter (D/A) - As in (e) above. See Figure 6-1(d).

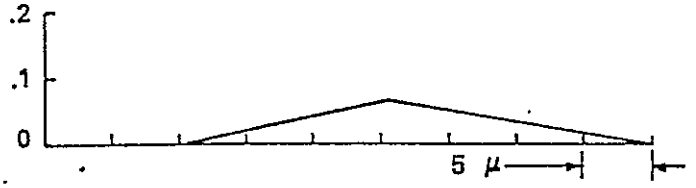

(a) MSS SPREAD FUNCTION

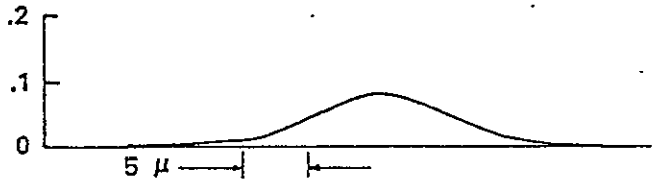

(b) RBV SPREAD FUNCTION

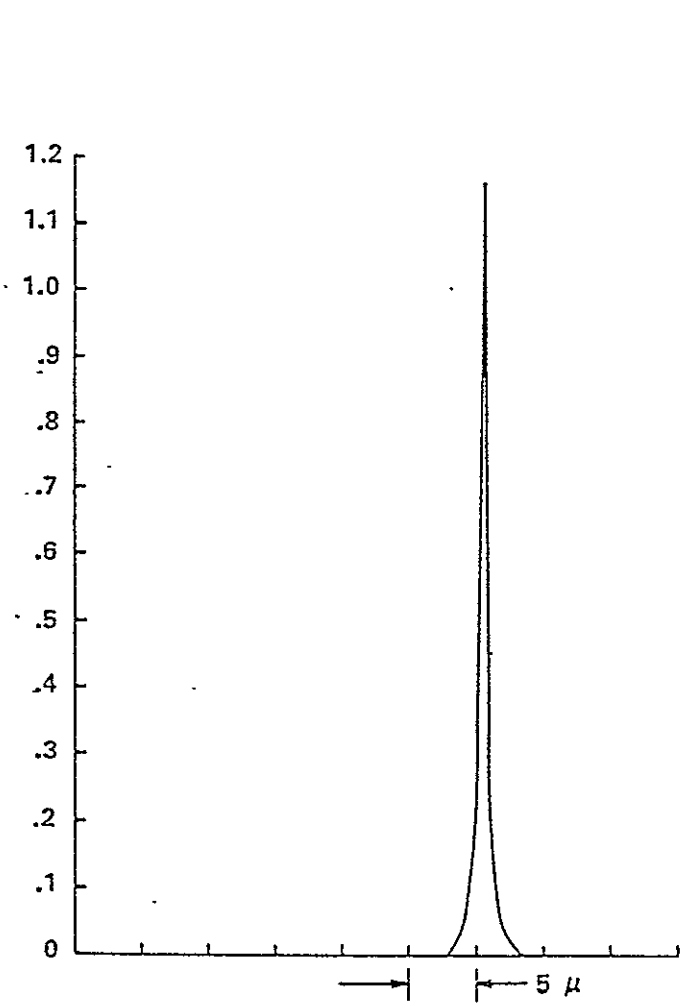

(c) EBR CTL SPREAD FUNCTION

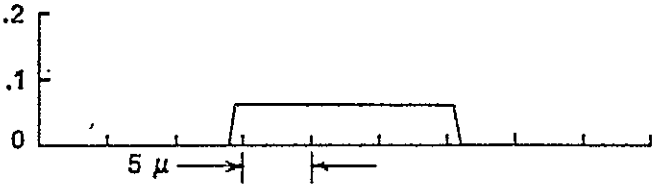

(d) D/A SPREAD FUNCTION

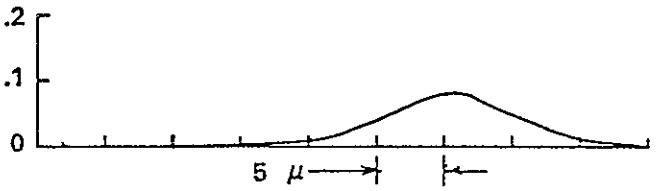

(e) BESSEL FILTER SPREAD FUNCTION

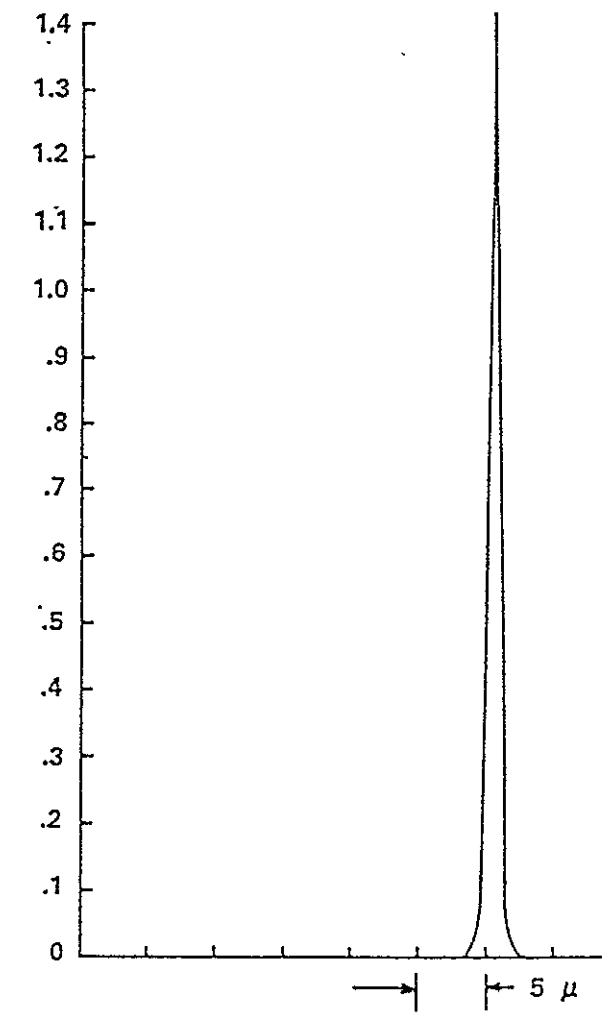

(f) EBR ELECTRONICS SPREAD FUNCTION

Figure 6-1 SPREAD FUNCTION INPUTS (PART 1)

g) Bessel Filter - As in (e) above. See Figure 6-1(e).

h) EBR Electronics - As in (e) above. See Figure 6-1(f).

i) EBR Preemphasis Nonlinearity -

Two sources of information were used.

1) User's Handbook.[2] The system is designed to obtain a net $\gamma = -1$ between log of the ground radiance and archival density. Further, the archival film is processed to $\gamma = 2$ (with "slight" deviation from linearity at end of the H-D curve, the actual shape not being given). Thus, the EBR preemphasis nonlinearity has $\gamma = \frac{1}{2}$. Mapping the 0-1 (relative) earth radiance scale onto the Handbook prescribed archival density range yields the curve shown in Figure 6-2(a).

2) Measurements - A current quality control procedure utilizes a twenty-one step gray scale at the head and tail of each roll of film processed. A sample was obtained and measured, and an archival processor H-D curve obtained. Each frame of imagery includes a fifteen step gray scale written by the EBR for radiometric calibration. The densities were read on an archival frame. The relative log radiance of the gray scale was obtained from the User's Handbook and an H-D curve for relative log ground radiance to archival density thus obtained. This curve together with the curve for archival processing alone allowed determination of the EBR preemphasis nonlinear gain plotted in Figure 6-2b.

j) EBR Beam

The EBR beam spread function was obtained from ERTM-H-81.[19] It is Gaussian in shape and plotted in Figure 6-3a.

k) Film spread functions

The film spread functions were measured from sample data. The edge of the large square in a standard Air Force tribar target currently used in quality control at the NDPF was scanned with a microdensitometer on archival, second, and third generation 70 mm

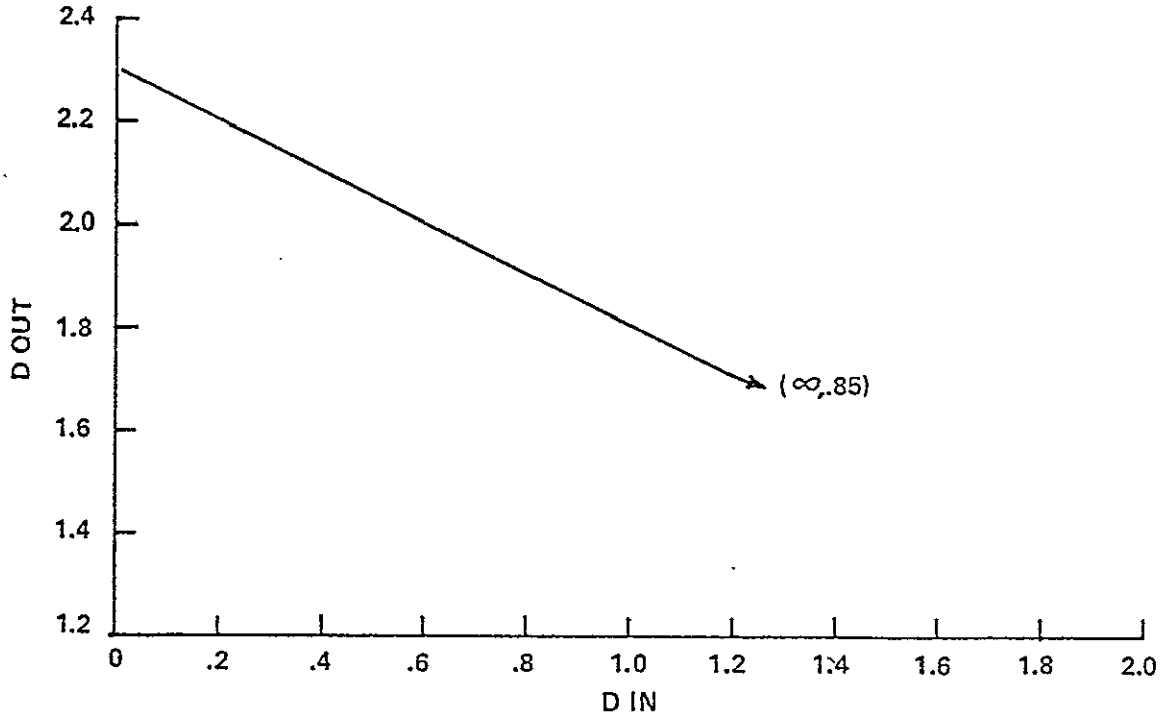

(a) EBR PREEMPHASIS NONLINEARITY (HANDBOOK)

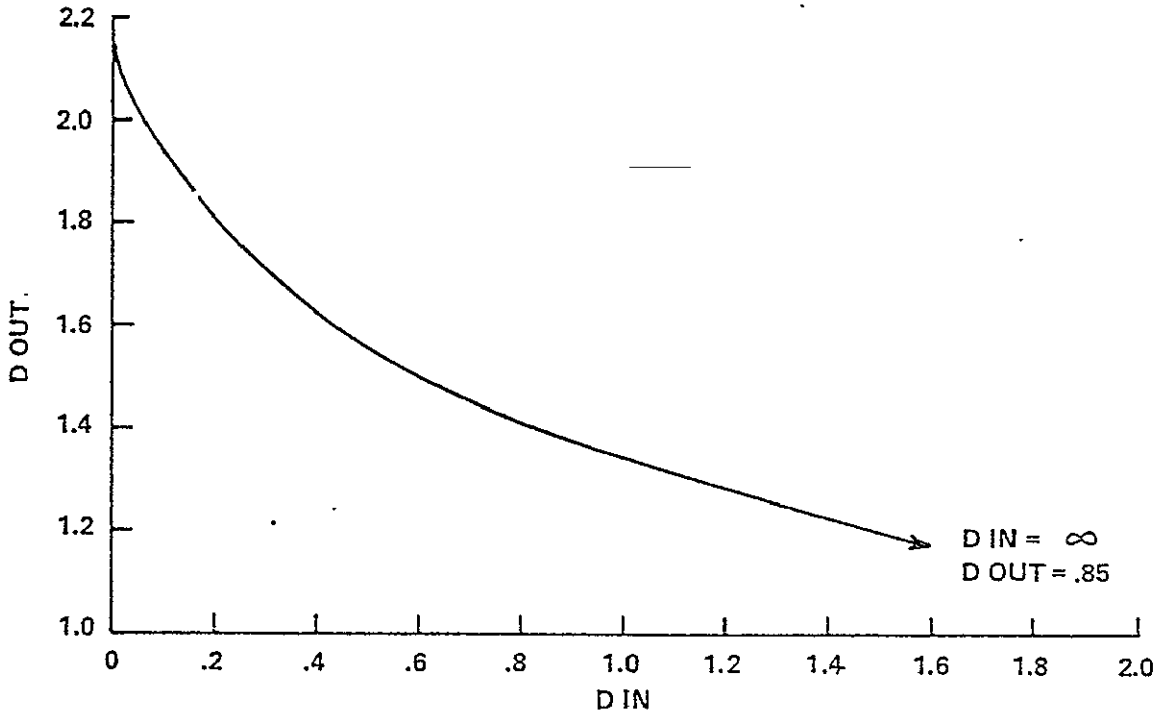

(b) EBR PREEMPHASIS NONLINEARITY (MEASURED)

Figure 6-2 EBR PRE-EMPHASIS NON-LINEAR GAIN FUNCTIONS

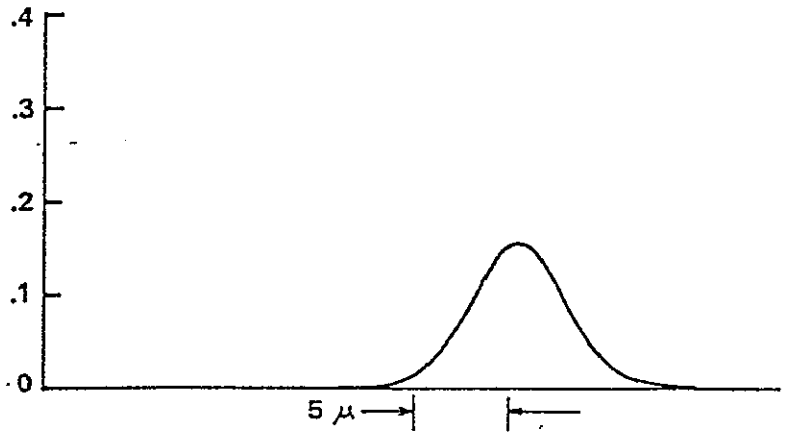

(a) EBR BEAM SPREAD FUNCTION

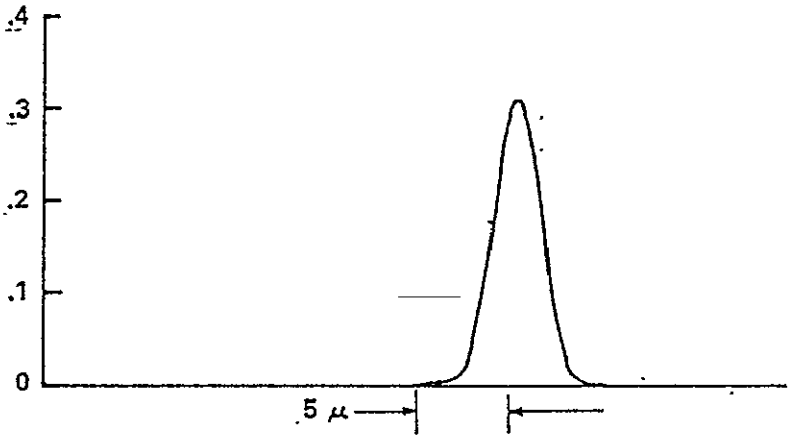

(b) FILM SPREAD FUNCTION

Figure 6-3 SPREAD FUNCTION INPUTS (PART 2)

transparencies. The edge spectra were computed by an edge gradient technique described in Appendix A. Each spectrum was divided by that of the previous generation and the resultant MTF Fourier transformed to yield the spread function of a single duplication process. The MTF's were compared to the limited section of the film MTF given in the User's Handbook[2] (Figure H-5) and found to be in agreement. It was concluded that the combined contact printer plus film MTF is approximately equal to the film MTF alone. Consequently the resulting spread function was used for both the archival film and for the second and third generation contact printer/film combinations. This spread function is plotted as Figure 6-3b. Edge ringing (Fresnel diffraction) was not observed on the samples examined which provides support for the validity of the linear contact printer model approximation.

1) Film Nonlinearities

Three approaches were used:

1. User's Handbook.[2] The design goal or nominal NDPF performance were obtained from the Handbook (Figure H-4) and are plotted in Figures 6-4 a-c for the first through third generations.

2. The twenty-one spot quality control gray scale was measured on samples of each generation. The H-D curves thus obtained are plotted in Figure 6-5 a-c for the first through third generations.

3. The fifteen level calibration gray scale was measured for each generation. The H-D curves for the second and third generation processing thus obtained are plotted as figures 6-6 a, b. This approach could not be applied to the first generation as no independent measure of the EBR preemphasis nonlinearity could be obtained and the 15 step density input to the first generation processor is unknown. The obvious disagreement between the three sets of data will be examined later.

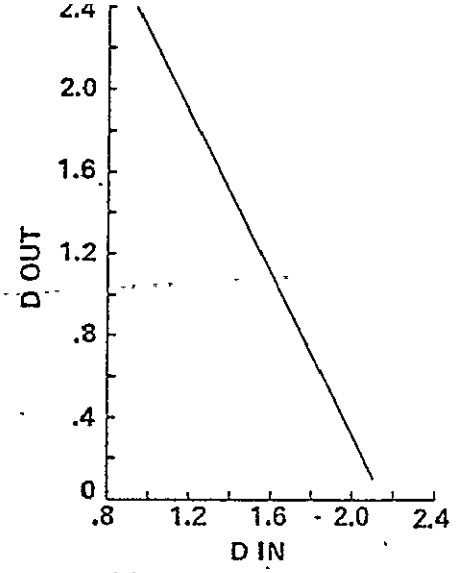

(a) FIRST GENERATION

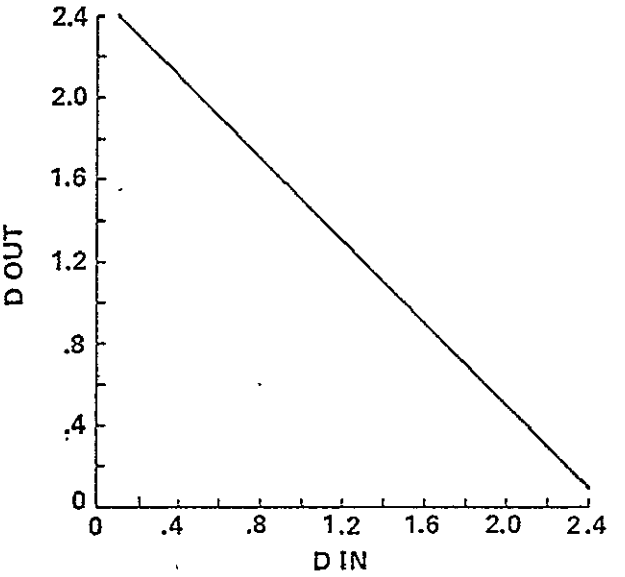

(b) SECOND GENERATION

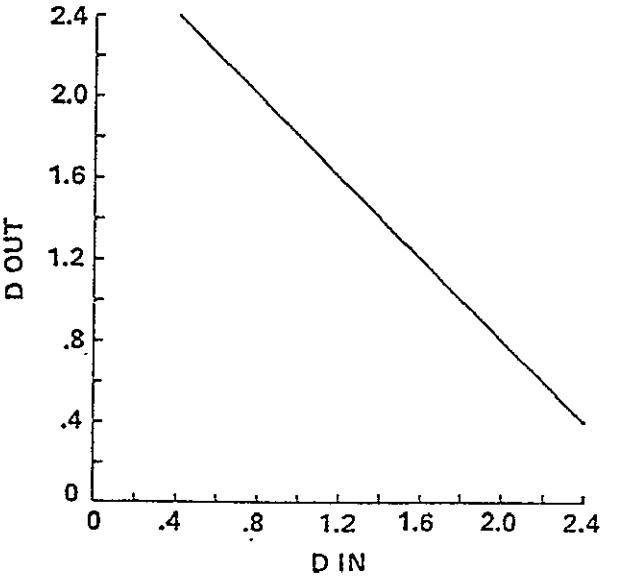

(c) THIRD GENERATION

Figure 6-4 NOMINAL FILM H-D CURVES (HANDBOOK)

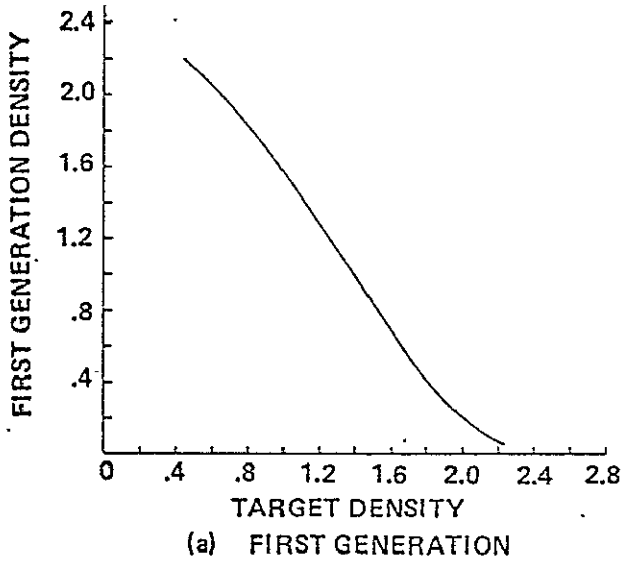

(a) FIRST GENERATION

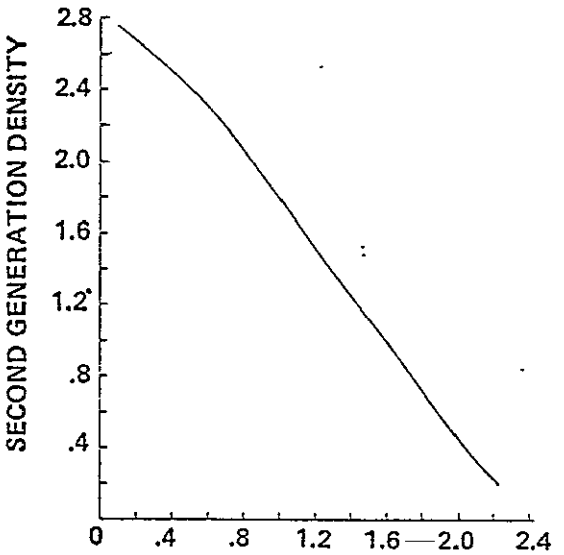

(b) SECOND GENERATION

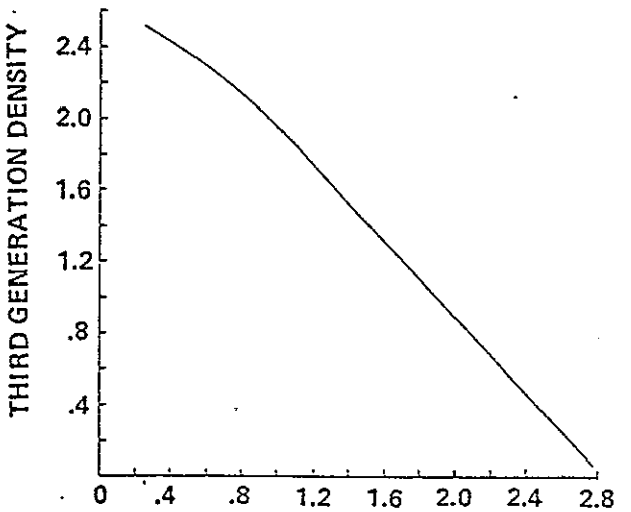

(c) THIRD GENERATION

Figure 6-5 MEASURED FILM H-D CURVES (21 STEP GREY SCALE)

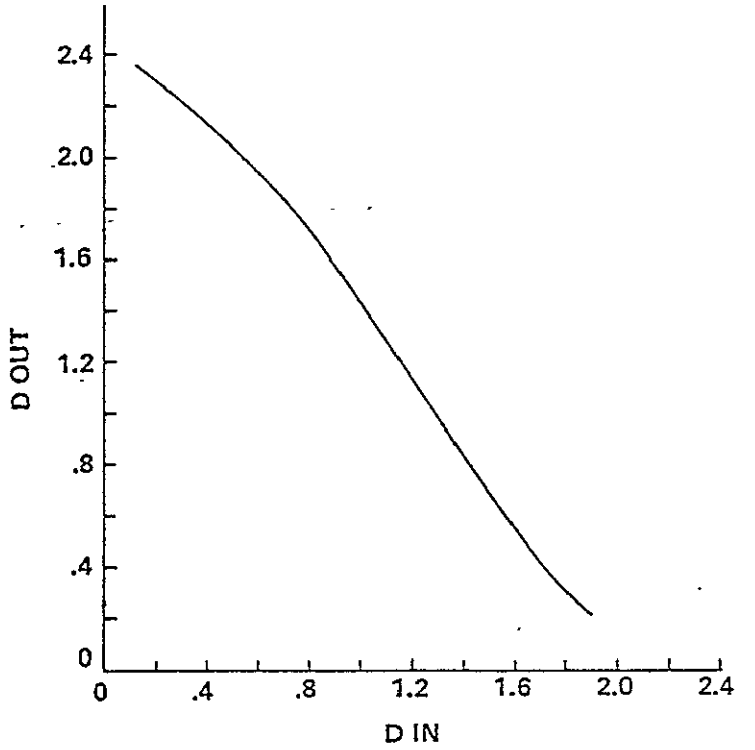

(a) SECOND GENERATION

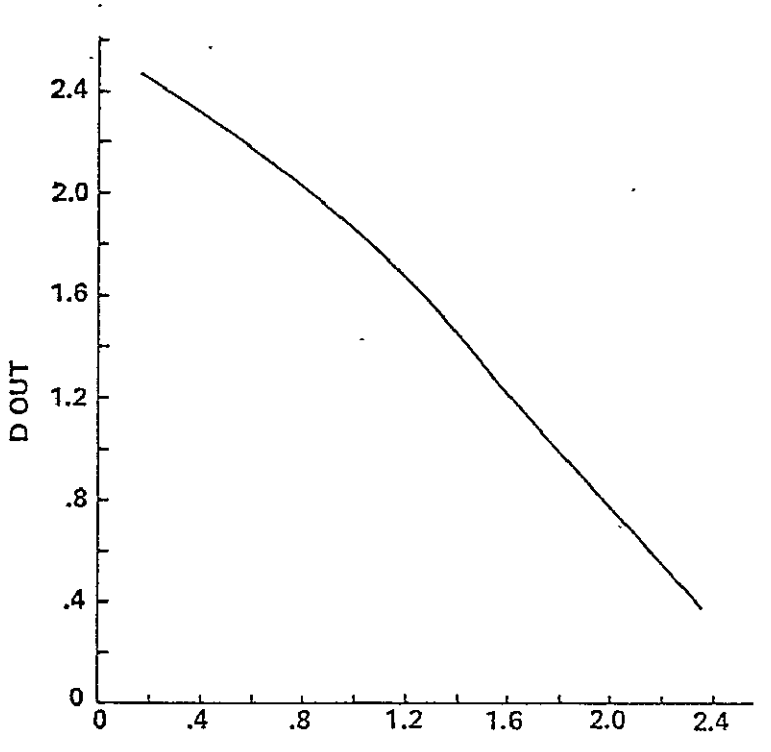

(b) THIRD GENERATION

Figure 6-6 MEASURED FILM H-D CURVES (15 STEP CALIBRATION GREY SCALE)

m) Electronic Noise

Total electronic noise at the NDPF is assumed[1] to yield electronic noise standard deviation equal to 10^{-5}. Electronic noise added by NDPF elements is neglected.[1] This noise amplitude is small compared to the photographic grain noise.

n) Film Grain Noise

The rms granularity values given in the User's Handbook[2] (Figure H-6) can be used to calculate σ_e, the rms noise fluctuation. The value of $\sigma_T^2 A_A$, presented in Figure 6-7 for either the EBR (archival) or copy film, is substituted into equation (3-26) to compute σ_e. It is recognized that some noise sources encountered may be signal-dependent; nevertheless, the perturbation technique can still yield correct results if a standard deviation corresponding to a nominal or worst case is utilized.

6.2 Nominal Performance - MSS Configuration

Referring to the MSS image processing configuration model established in Section 5.3, the operations entered in a sequence of 9 blocks in IDSS to simulate the system are:

1. Convolution with the payload spread function.
2. Convolution with the EBR Control Electronics spread function.
3. Convolution with the D/A Conversion spread function.
4. Convolution with the Bessel Filter spread function.
5. Convolution with the EBR Electronics spread function.
6. Level change by the EBR preemphasis nonlinearity.
7. Convolution with the EBR Beam spread function.
8. Convolution with the film spread function.
9. Level change by the nonlinear first generation development process (H-D curve)
10. Convolution with the film-contact printer spread function.

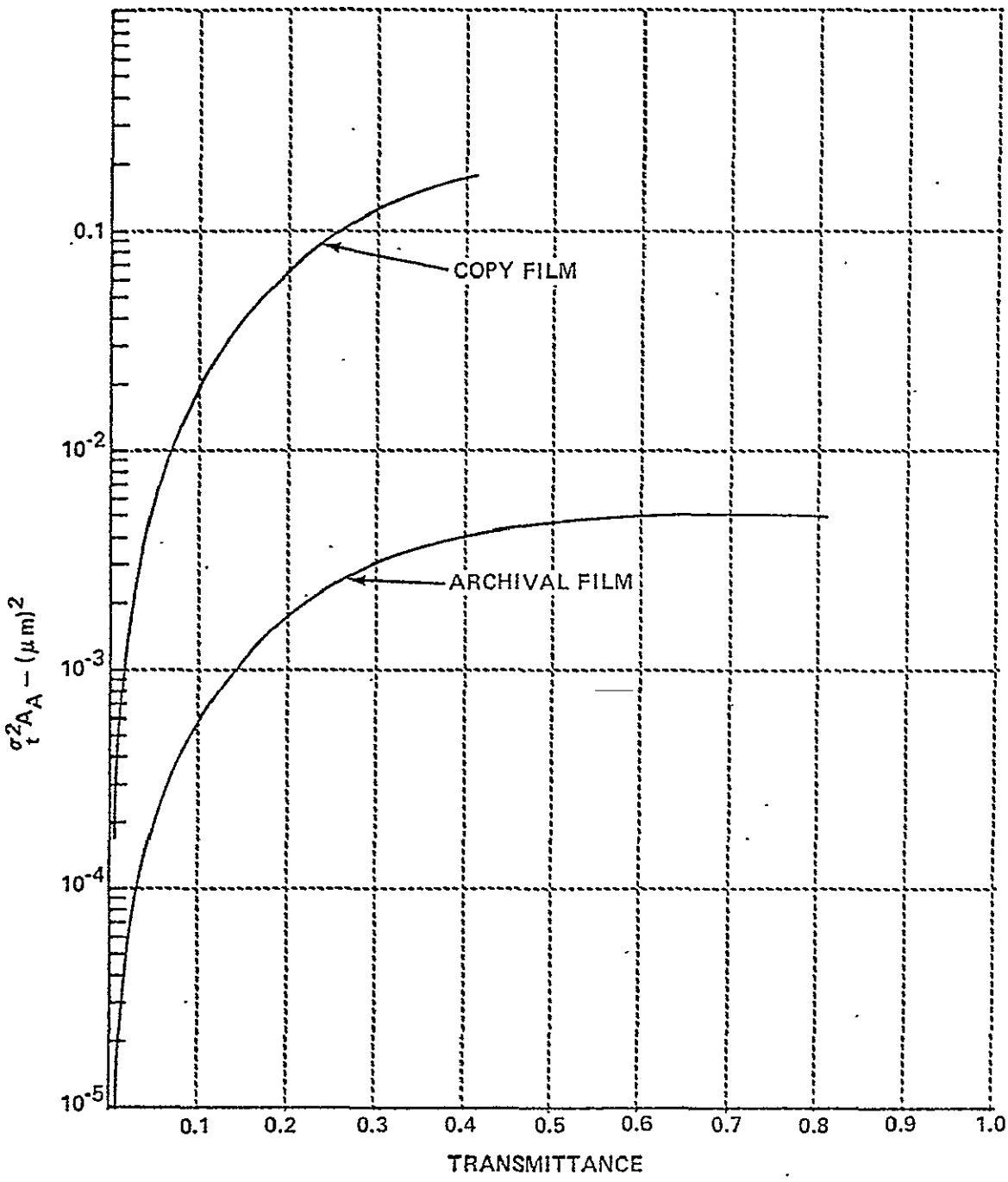

Figure 6-7 NOMINAL INPUT FOR SIMULATING GRAIN NOISE

11. Level change by the nonlinear second generation development process (H-D curve)

12. Convolution with the film-contact printer spread function.

13. Level change by the nonlinear third generation development process (H-D curve)

Operation No. 10 is replaced by convolution with the Bulk Enlarger spread function for 9.5 inch products. Distances refer to the 70 mm format unless explicitly stated otherwise.

Recalling the disparity between the User's Handbook and measured H-D curve data, a decision was required on what to accept as "nominal". Since the measured data was taken from a small sample of NDPF products, and there is no evidence confirming the data as nominal or even typical, the Handbook data were chosen. This data is, however, clearly idealized, so the measured data were also used as input and the results compared. Other sources[20] indicate that the first generation nonlinear gain or γ_1 is about 1.5 in agreement with the measured data.

In order to estimate the noise statistics the IDSS program was run in Mode 2 with nominal element performance data detailed in Section 6.1. The noise spectrum was found to be white and a pre-whitening filter spread function need not be included in subsequent computation.

To understand the noise propogation behavior in more detail, consider the last several steps in the data flow of the NDPF:

- additive noise (archival film grain)
- film-printer film spread function
- non-linear gain
- additive noise (copy film grain)

} 2nd Generation Negative

- film-printer spread function
- non-linear gain
- additive noise (copy film grain)

} 3rd Generation Positive

The input to these steps is a bandlimited, low-noise signal. Since the noise amplitude is small compared to the signal, the nonlinear gains do not modify the noise spectrum. Now the film-printer OTF cutoff frequencies are large compared to the cutoff of the signal imposed by the sensor. The first grain noise is filtered by two OTF's, the second by one, and the third not at all. Small changes in the performance of either film or printer, will consequently have negligible effect on N_o. Therefore, for the current ERTS system, N_o is independent of reasonable changes in NDPF element performance.

Another benefit is obtained from the insensitivity of N_o to NDPF system performance. From equation (3-2)

$$\sigma_{A_i}^2 \geq N_o \, (M^{-1})_{ii}$$

with the equality holding for the sufficiently high signal-to-noise ratio. The constancy of N_o for slightly off nominal element performance allows relative error comparisons, namely:

$$\frac{\sigma_i^2 \text{ (off nominal)}}{\sigma_i^2 \text{ (nominal)}} = \frac{(M^{-1})_{ii} \text{ (off nominal)}}{(M^{-1})_{ii} \text{ (nominal)}}$$

where $\sigma_i^2 \equiv \sigma_{A_i}^2$ to simplify notation. Thus the quality control problem for the current ERTS image processing system can be studied by computing only the $(M^{-1})_{ii}$ as a function of element performance. Therefore initially only the relative performance was examined. The effect of N_o was included later to relate relative performance to absolute values.

6.2.1 Edge Target Results

The three parameter "edge" target, where A_1 = one radiance level, A_2 = other radiance level, and A_3 = the position of the edge between A_1 and A_2 will be used to describe the change in image quality as a function of changes in subsystem element performance for the following reasons:

1. It is the simplest target that yields both radiometric and geometric estimation errors.

2. It corresponds to a most common user estimation task.

3. The spectrum of the output edge gradient can be used to determine system radiometric linearity.

6.2.1.1 Linearity

In order to study system linearity IDSS was used to generate the nominal MSS output for the twenty targets shown in Table 6-1.

The NDPF system output for each of these targets was subsequently used as input to an edge gradient spectrum computation program (Appendix D) and the spatial frequency response of the system thus obtained.

If a system is linear, then its frequency response is independent of input. A nonlinear system on the other hand is characterized by harmonic generation, the presence of signal at higher frequencies is observed, and the apparent frequency response is input dependent. The region over which the response of a nonlinear system is independent of input is defined as the "small signal" or quasi-linear region which is useful to those who want to approximate the nonlinear system by a linear one.

The nominal NDPF is designed such that the four cascaded nonlinearities give a net processing $\gamma = -1$ so that ground radiance should be directly proportional to third generation transmission. However, each nonlinearity generates harmonics while the OTF of the following linear element can eliminate some of those harmonics. Applying an inverse nonlinear function to the modified signal might not yield the initial input again. Therefore, the presence of the linear filters (OTF's) between the nonlinearities may cause the system to behave in a nonlinear manner even though the net γ is held equal to minus one.

TABLE 6-1. EDGE TARGET PARAMETERS

(100 μm records)

Target Designation	$\underline{A}_1$ (normalized radiance level)	$\underline{A}_2$ (normalized radiance level)	$\underline{A}_3$ (edge location)
1	.00	.0001*	50.
2	"	.2	"
3	"	.4	"
4	"	.6	"
5	"	.8	"
6	.25	.0001	"
7	"	.2	"
8	"	.4	"
9	"	.6	"
10	"	.8	"
11	.45	.0001	"
12	"	.2	"
13	"	.4	"
14	"	.6	"
15	"	.8	"
16	.65	.0001	"
17	"	.2	"
18	"	.4	"
19	"	.6	"
20	"	.8	"

(*The value .0001 was used instead of zero because the program must compute $log \frac{1}{A_2}$ in the nonlinear gain subroutine.)

The edge gradient spectra computed are shown in Figure 6-8. Note that the spectrum of all the edges except those with the very low (.0001 or .05) radiance levels are identical and that the others all contain higher modulations as frequency increases. The system thus seems to be behaving in a linear manner over a wide but bounded target radiance range. From the results obtained this range is, at least, 0.2 to 0.8 (normalized radiance).

In order to understand the cause of this result, the program was run in the signal tracing mode which yielded the plots shown in pages 214 to 233 of the data, Appendix C, corresponding to edges 1-20 respectively. Distortion of edges 1, 6, 11, 16 is obvious. Distortion can be seen in edges 2 through 5 as well, although it is less pronounced. From the plots, the distortion occurs at either the electronic preemphasis or first generation development nonlinearities. Inspection of the EBR preemphasis nonlinearity curve, Figure 6-2 shows that the linear portion of the curve extends only as high as input density $D_{in} = 1.146$ which is equivalent to a normalized input signal (transmission) of 0.07. Thus, the edges for which the system exhibits nonlinear response have at least one radiance level on the portion of the electronic preemphasis nonlinear gain curve which approaches the asymptote at $(D_{in}, D_{out}) = (\infty, .85)$. (In computation, infinity was taken as D = 1000).

As the subsequent nonlinearity H-D curves are chosen such that any input signal which lies on the linear portion of the electronic preemphasis nonlinear gain curve must also lie on the linear portion of all succeeding H-D curves, it is concluded that the system behaves in a linear manner if the signal is not clipped by the 0.07 breakpoint of the electronic preemphasis nonlinearity.

If the four H-D curves do not indeed distort spectra, the spectrum representing the linear input range in Figure 6-8 should

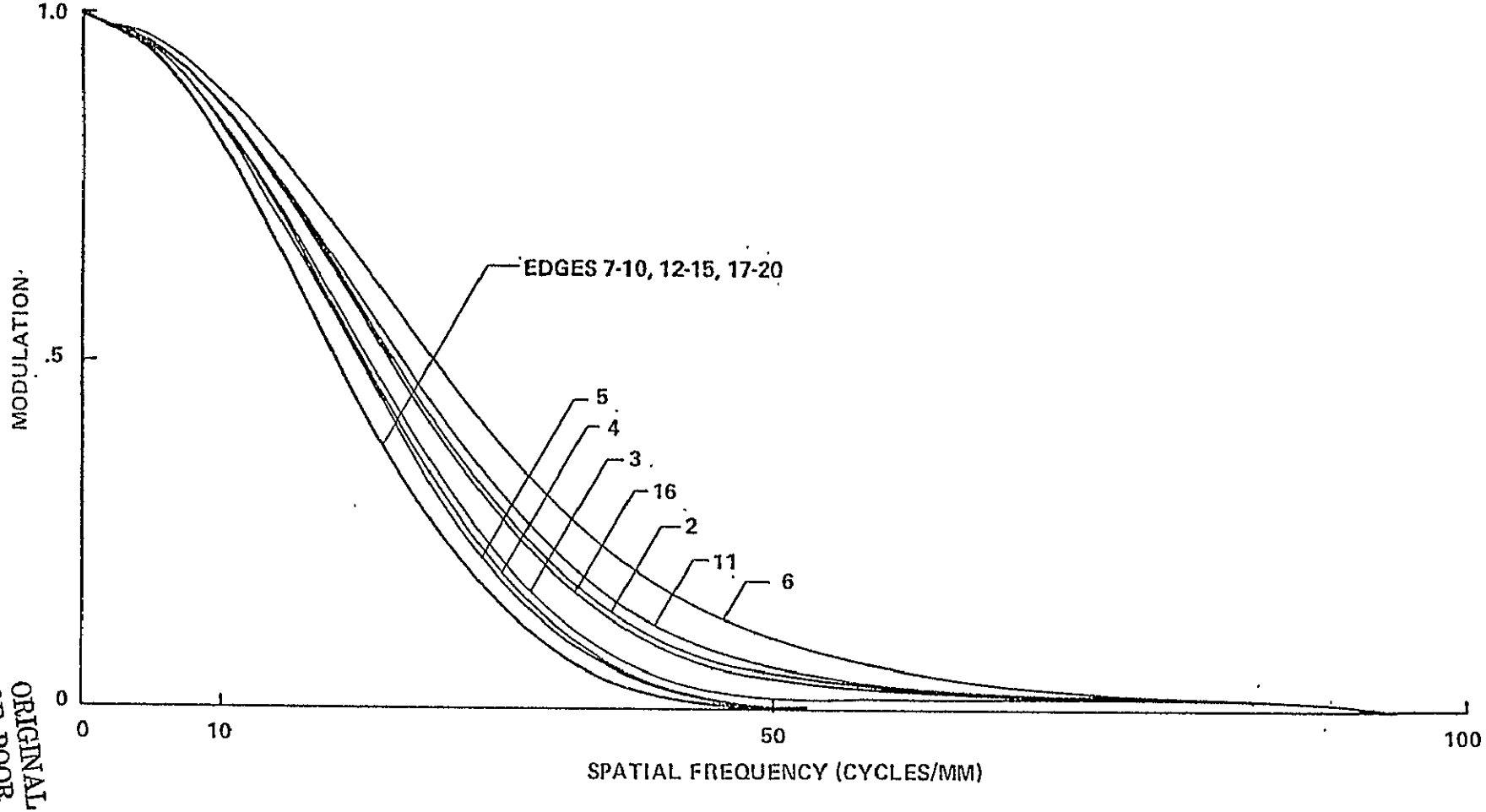

Figure 6-8 EDGE GRADIENT SPECTRA FOR NOMINAL PERFORMANCE

be matched by that obtained by the system with the nonlinearities removed (composite system OTF).

The four H-D curves were removed from the simulation model and the edges run again. The edge gradient spectra were computed as before and are plotted in Figure 6-9. The spectra for all edges are identical, equal to those in Figure 6-8, corresponding to edges 7-10, 12-15, 17-20.

It follows that the ERTS nominal system can be characterized by an end-to-end frequency response. One useful result of this conclusion is that if the NDPF is constrained to nominal performance, the OTF of the sensor in the payload can be monitored by measuring, on the output products, the edge gradient of a ground object. However, it is fallacious to ignore the nonlinear elements in computation of estimation errors as the following section shall show.

Before proceeding, it is instructive to compare the edge gradient spectra of the input to that at later stages within the NDPF. The edge targets in the quasi-linear region were generated: 1) after the MSS, 2) after D/A conversion, 3) on the archival product, and 4) on the third generation product. Edge gradient spectra were computed and are plotted in Figure 6-10. The D/A conversion is logically lumped as an integral part of the payload, even though it occurs on the ground. The NDPF processing is shown to modify the spectrum very little thus supporting the approximations made earlier in the report that were based on the signal bandlimit occurring before the addition of significant noise sources.

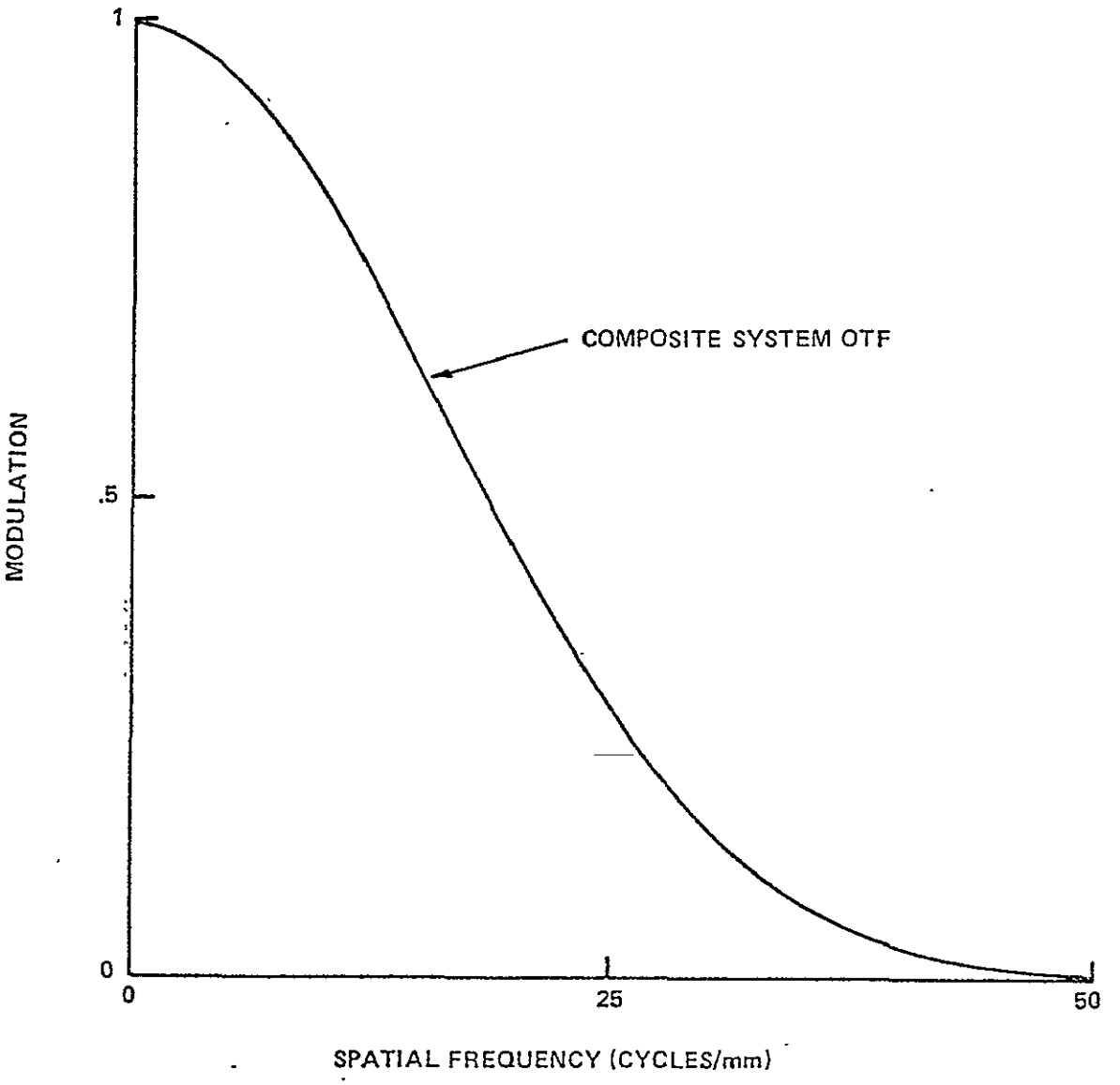

Figure 6-9 EDGE GRADIENT SPECTRA – COMPOSITE SYSTEM OTF

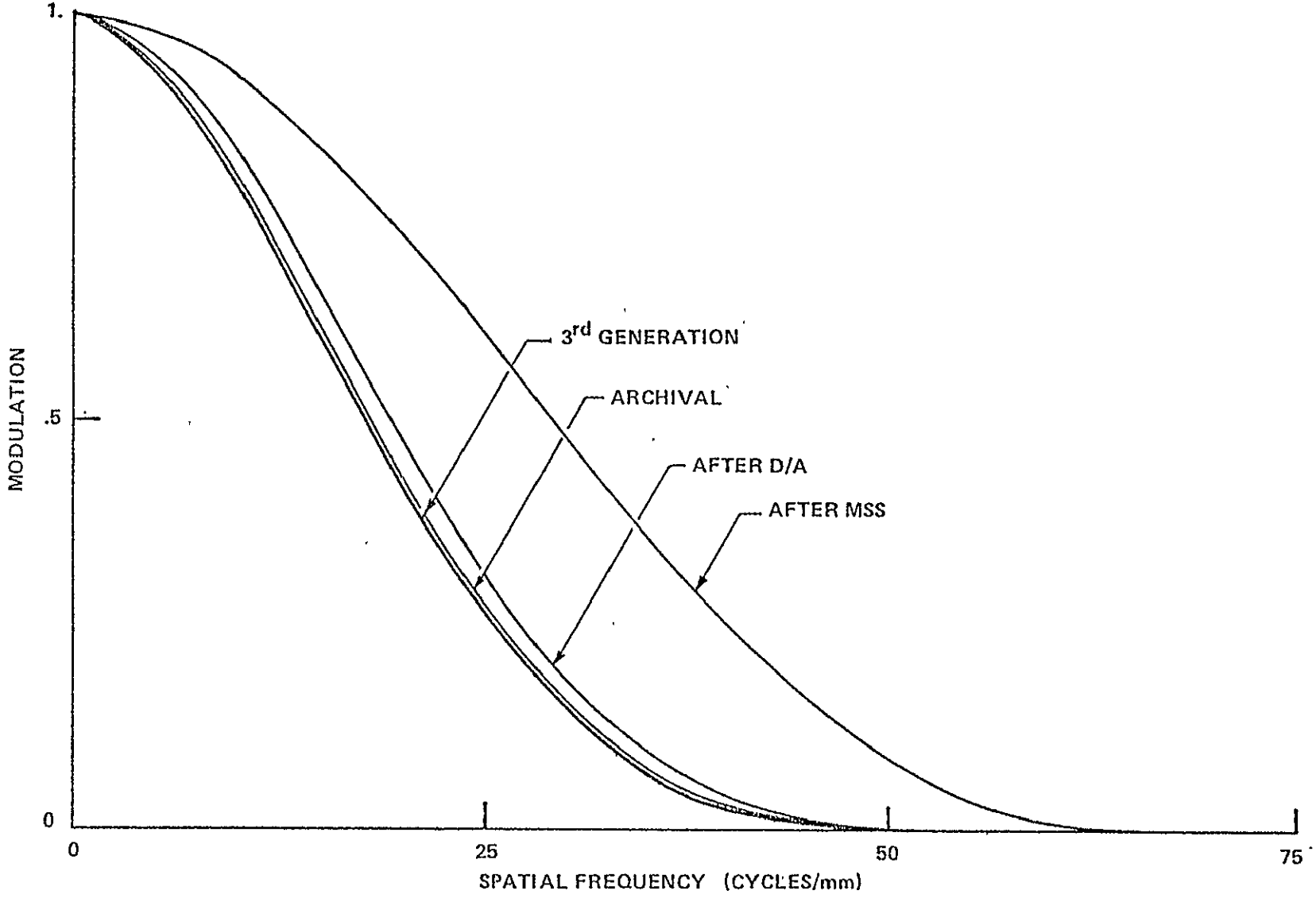

Figure 6-10 COMPARISON OF EDGE GRADIENT SPECTRA AT VARIOUS SYSTEM POINTS

6.2.1.2 Nominal Product Quality

The nominal error bounds for the estimation of the three parameter edge targets were calculated as measures of product quality. The targets outside the linear range defined in the preceding section were eliminated resulting in a new set of 12 targets having a record length = 100 micrometers, a sampling increment = 0.5 micrometers, and a distance unit = micrometer. The target set is defined in Table 6-2.

TABLE 6-2. REDUCED EDGE TARGET SET

Designation No.	A_1 (normalized radiance level)	A_2 (normalized radiance level)	A_3 (edge location)
1	.25	.2	50.
2	"	.4	"
3	"	.6	"
4	"	.8	"
5	.45	.2	"
6	"	.4	"
7	"	.6	"
8	"	.8	"
9	.65	.2	"
10	"	.4	"
11	"	.6	"
12	"	.8	"

These targets can be grouped according to the normalized radiance level difference $\Delta R/R_m = |A_1 - A_2|$ a measure of target contrast. This results in the following classification:

$\Delta R/R_m$	Designation No.
.05	1, 6, 11
.15	2, 7, 12
.25	5, 10
.35	3, 8
.45	9
.55	4

IDSS computed the matrix elements $(M^{-1})_{ii}$, i = 1, 3. $(M^{-1})_{11}$ and $(M^{-1})_{22}$, proportional to the error in estimating radiance levels, remained constant for all edges. They can be made arbitrarily small by increasing the record length--it is the change in their values as a function of subsystem element performance for a fixed record length that must be examined to evaluate quality control procedures. $(M^{-1})_{33}$, the edge location estimation component, was found to be independent of the absolute values of A_1 and A_2, but to depend on $\Delta R/R_m$ only. The results are plotted in Figure 6-11. The shape of the curve suggests the log-log plot of Figure 6-12. Note that Figure 6-12 shows the data to be exactly colinear with slope of exactly -2. Now:

$$\sigma_{A_i}^2 \sim (M^{-1})_{ii}$$ by equation (3-2)

so that the data demand:

$$\sigma_{A_3}^2 \sim \left(\frac{R_m}{\Delta R}\right)^2$$ where: $\sim$ means "is directly proportional to"

or $$\sigma_{A_3} \sim \frac{R_m}{\Delta R}$$

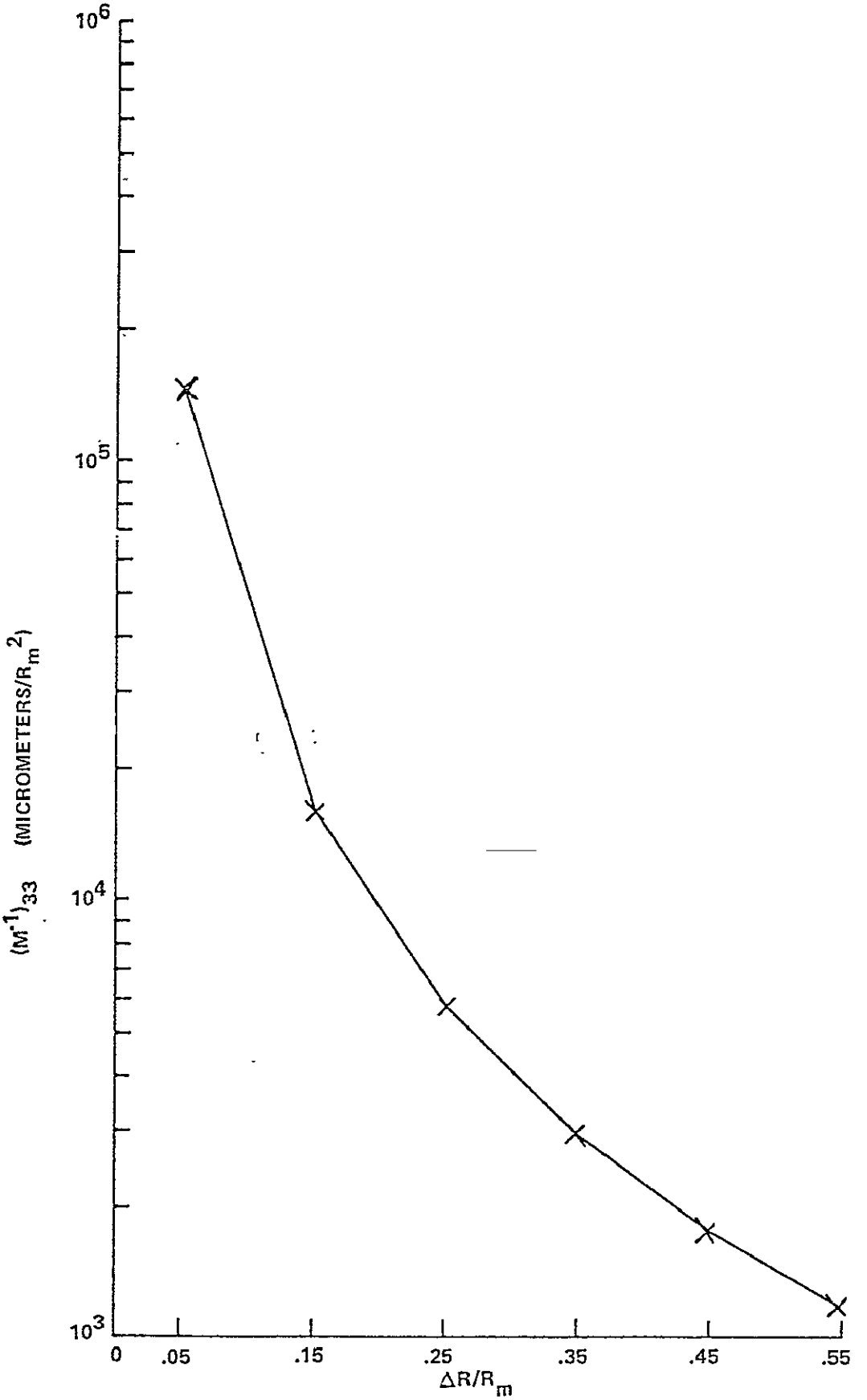

Figure 6-11 VARIATION OF EDGE POSITION ESTIMATION ERROR WITH TARGET CONTRAST (NOMINAL MSS CONFIGURATION)

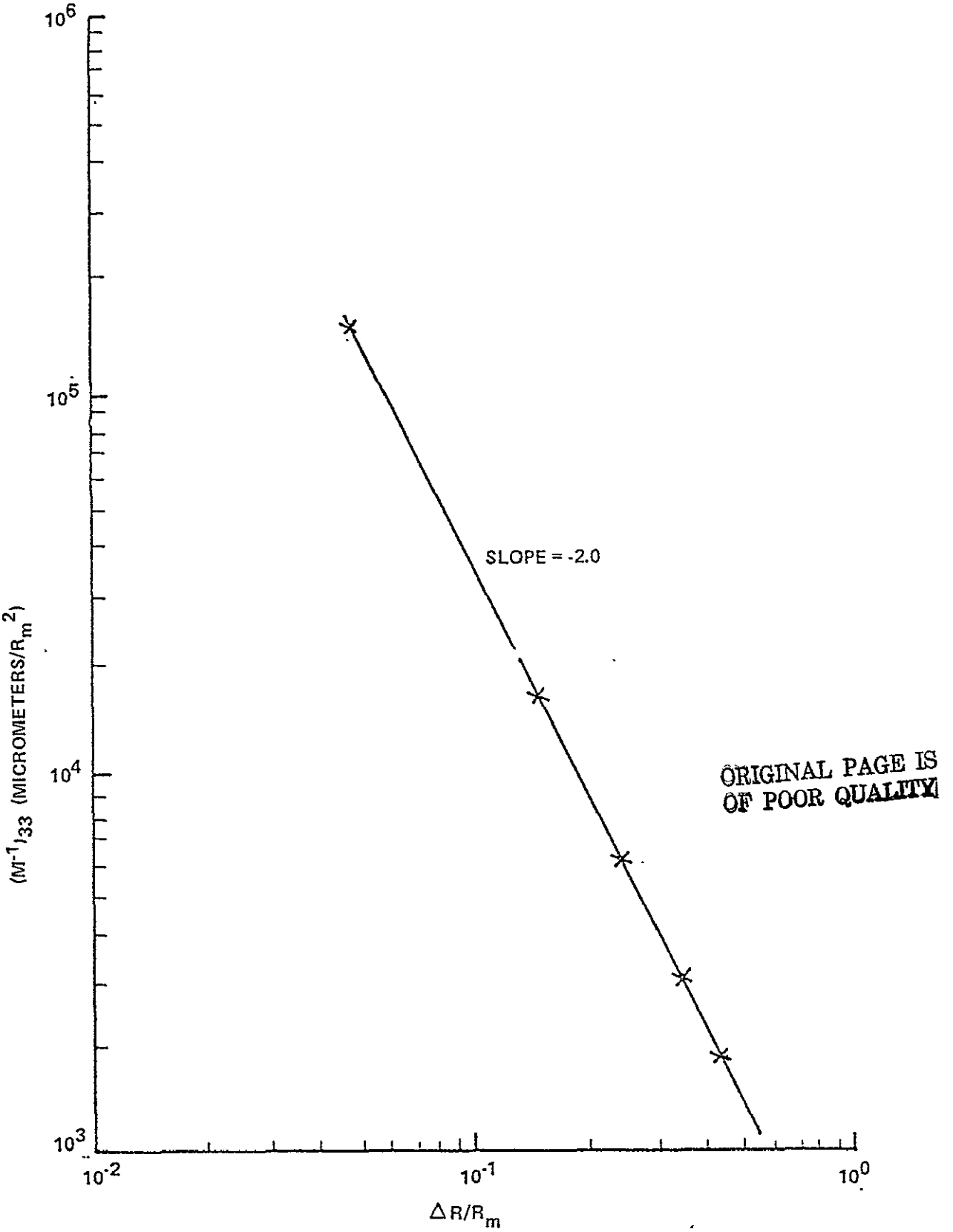

Figure 6-12 LOG-LOG PLOT OF FIGURE 6-11

This relationship is expected for a linear system and can, in fact, easily be derived from equation (3-2) analytically. It confirms that this region of input target radiance levels represents a quasi-linear performance region for the NDPF.

To determine the effect of the non-linear gains, these steps were removed from the simulated system and the set of test targets was run again. The results are plotted in Figure 6-13 and 6-14. Notice that the proportionality

$$\sigma_{A_3} \sim \frac{R_m}{\Delta R}$$

is preserved, but that the proportionality constant is roughly an order of magnitude lower. Thus we can conclude that the presence of the four nonlinear gains increases the estimation error, even though the frequency response is not distorted.

6.2.2 Square Bar Target Results

Although edge targets will be used in examining off nominal system performance, the square bar target was also considered during the nominal performance analysis as an additional descriptor. The following set of targets were generated where A_1 = background radiance level, A_2 = bar radiance level, A_3 = bar width and A_4 = bar location:

A_1 was held constant. $A_1 = 0.1$
A_2 was varied in steps of .2 between $A_2 = .15$ and $A_2 = .95$
A_3 was varied between $A_3 = 15$ and $A_3 = 105$ micrometers.
A_4 was held constant at 75 micrometers, the record midpoint.

Signal trace plots for these targets were shown in Appendix C, Pages 234 through 278. Plots of the matrix elements $(M^{-1})_{22}$, $(M^{-1})_{33}$, and $(M^{-1})_{44}$ as a function of bar width for each A_2 value are shown in Figures 6-15 through 6-17. Both the radiometric and mensuration

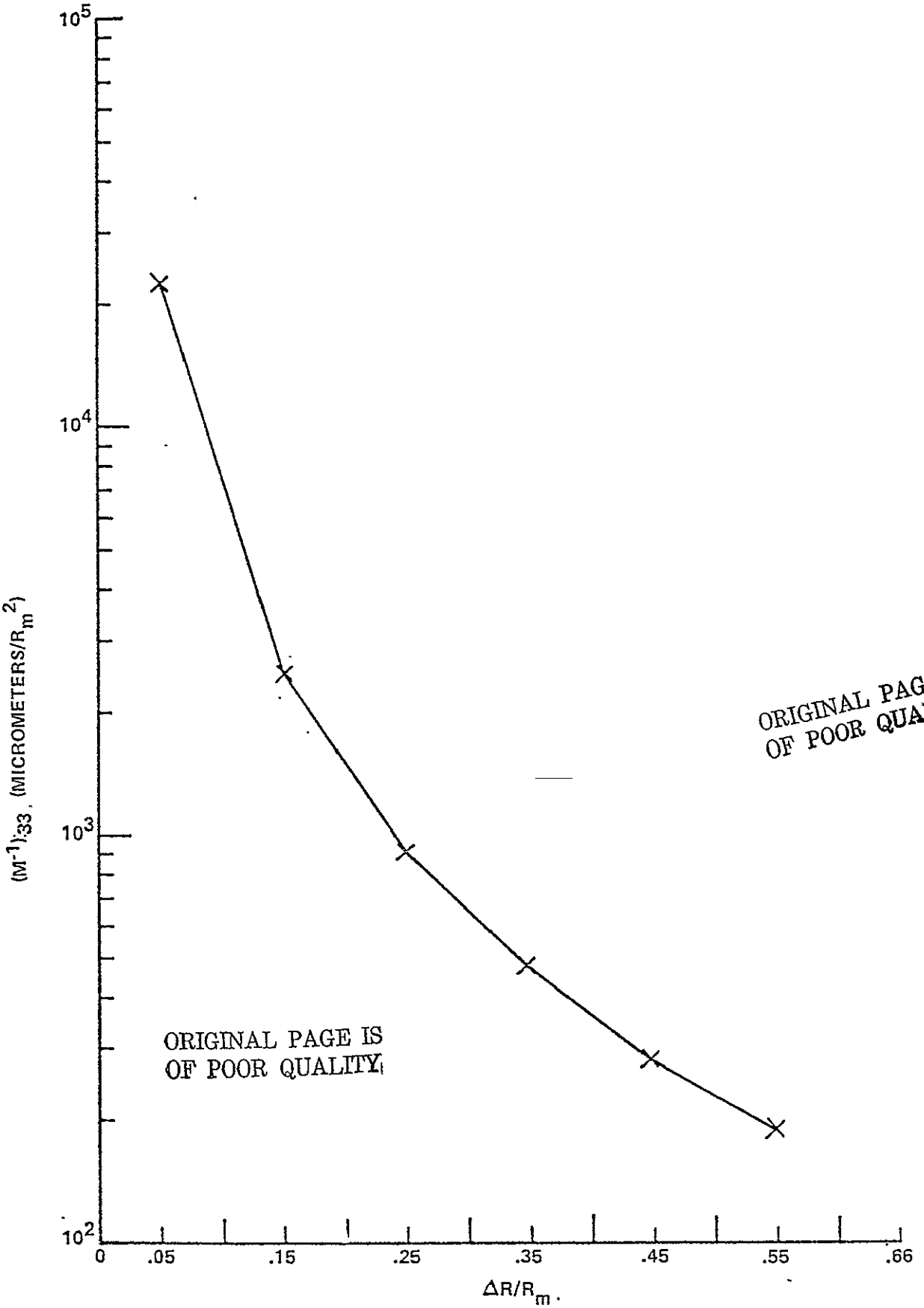

Figure 6-13 VARIATION OF EDGE POSITION ESTIMATION ERROR WITH TARGET CONTRAST (NON-LINEAR ELEMENTS REMOVED)

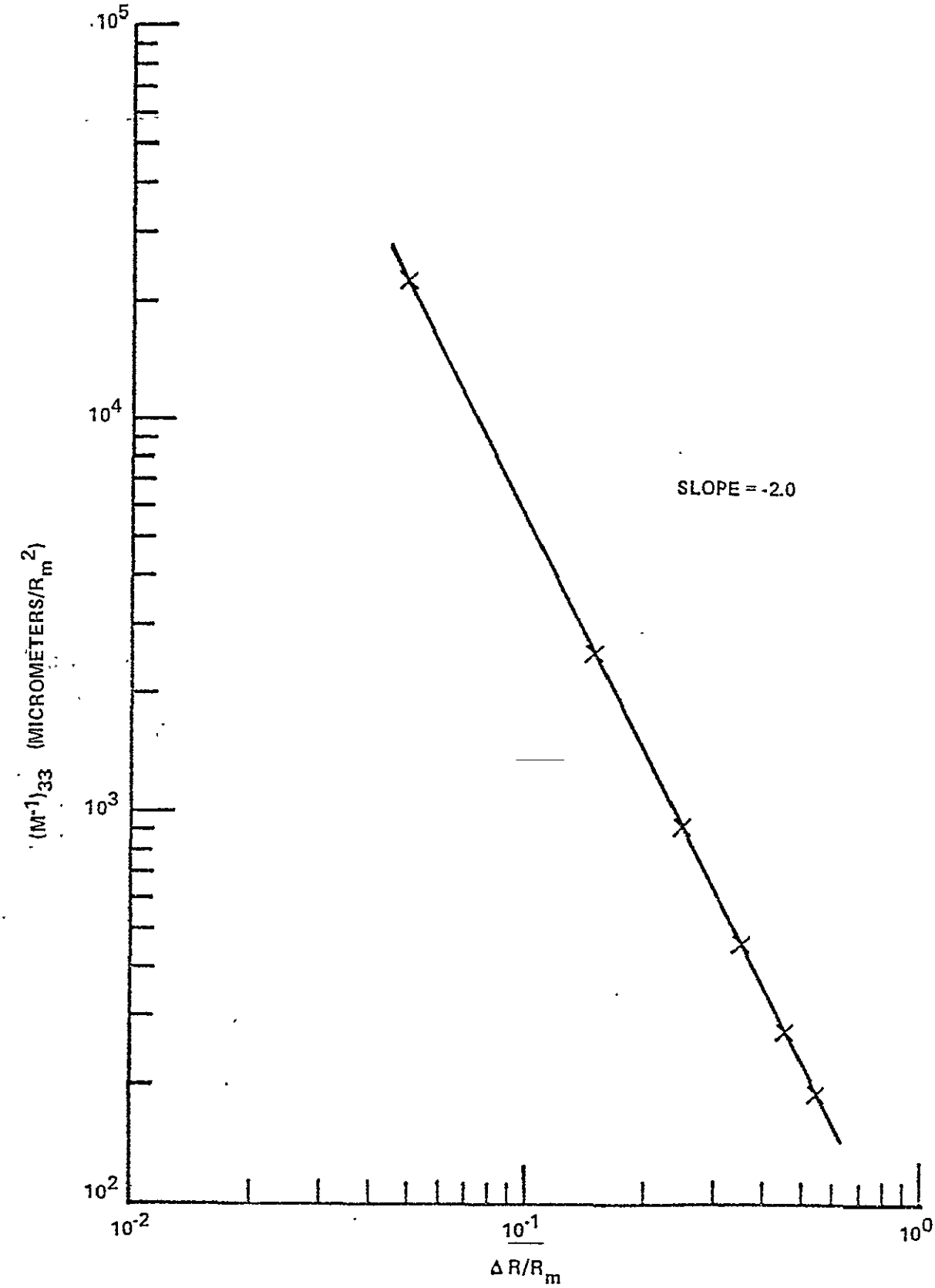

Figure 6-14 LOG-LOG PLOT OF FIGURE 6-13

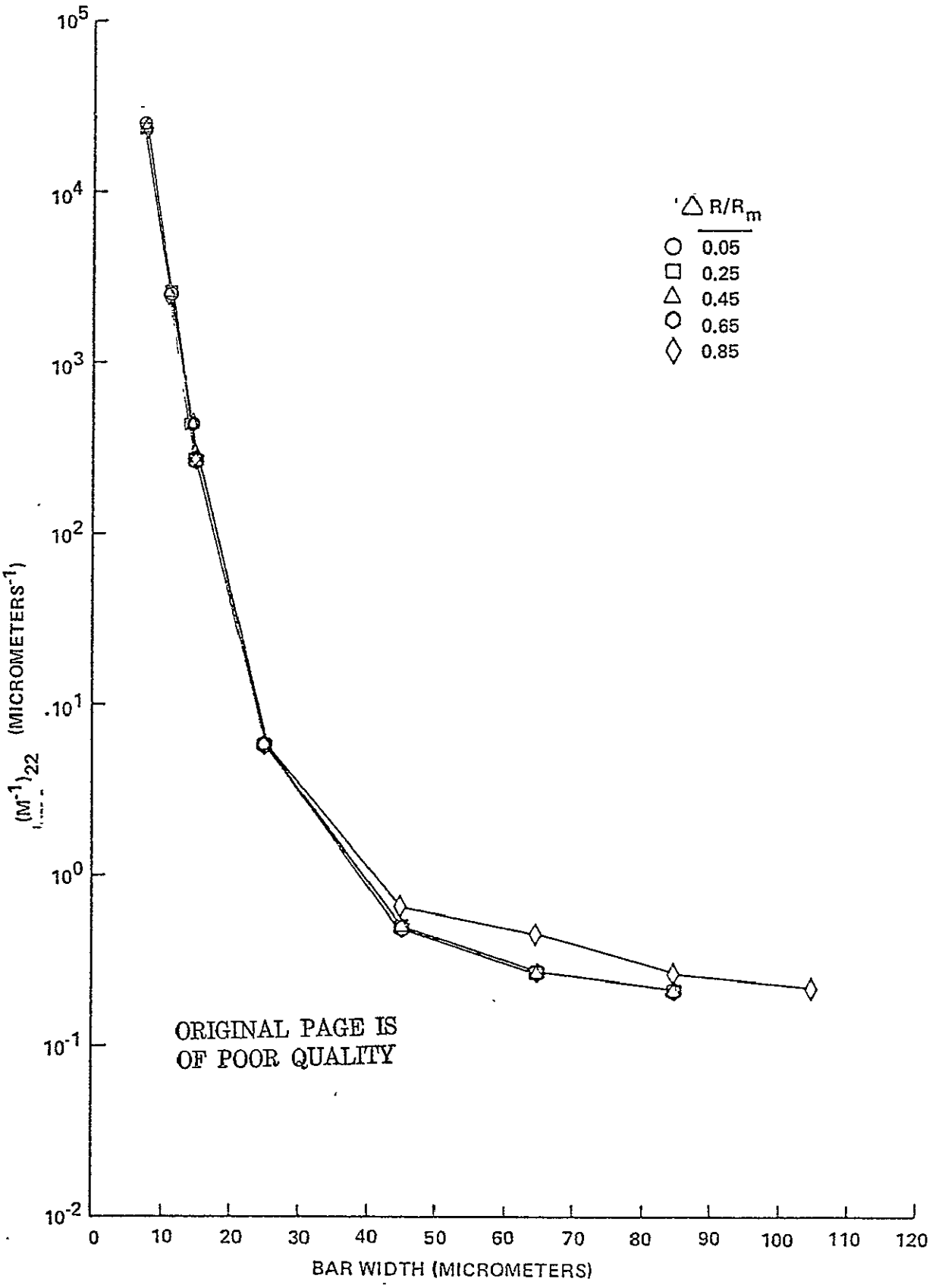

Figure 6-15 VARIATION OF BAR TARGET RADIANCE LEVEL ESTIMATION ERROR WITH TARGET WIDTH AND CONTRAST

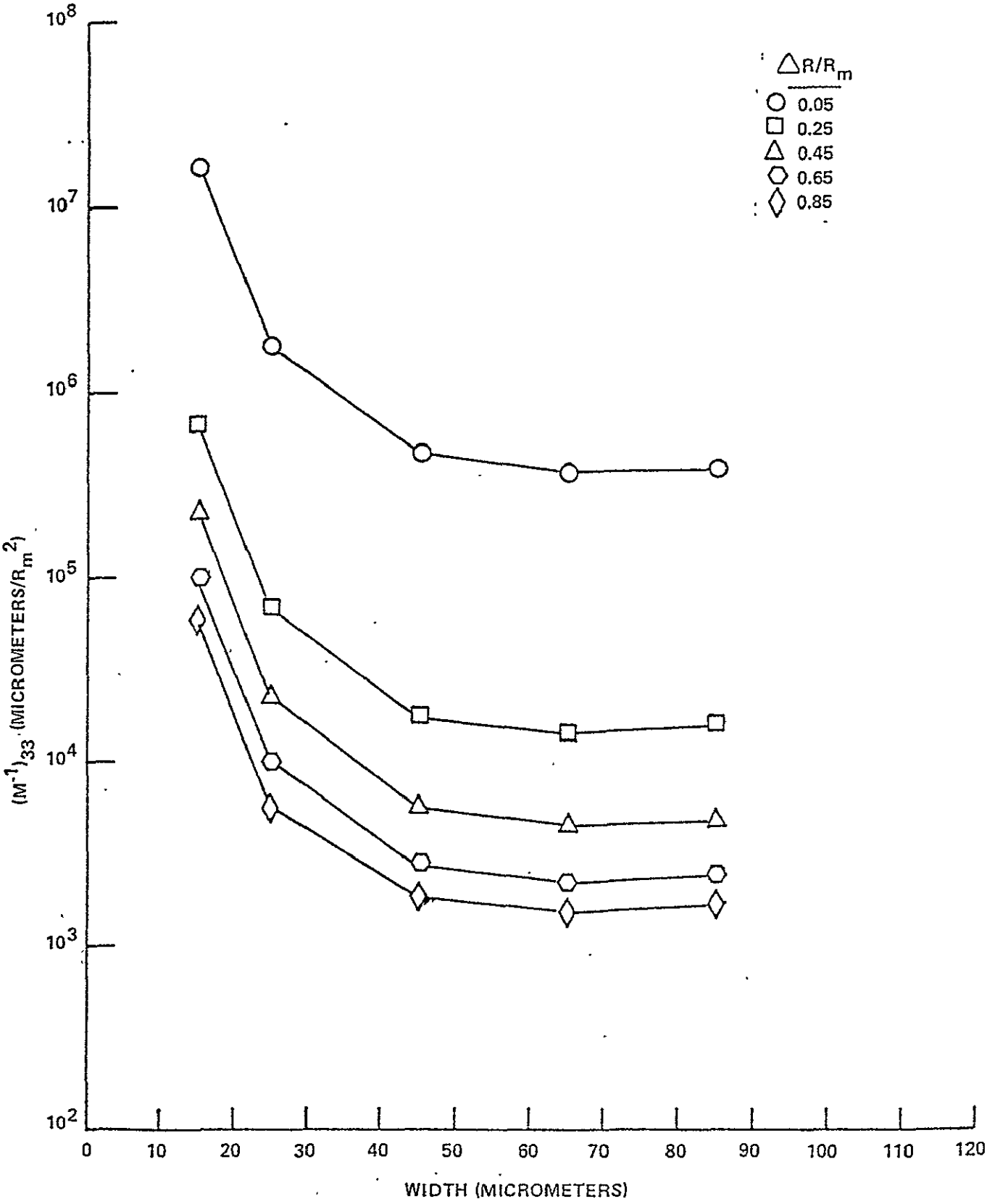

Figure 6-16 VARIATION OF BAR TARGET WIDTH ESTIMATION ERROR WITH TARGET WIDTH AND CONTRAST

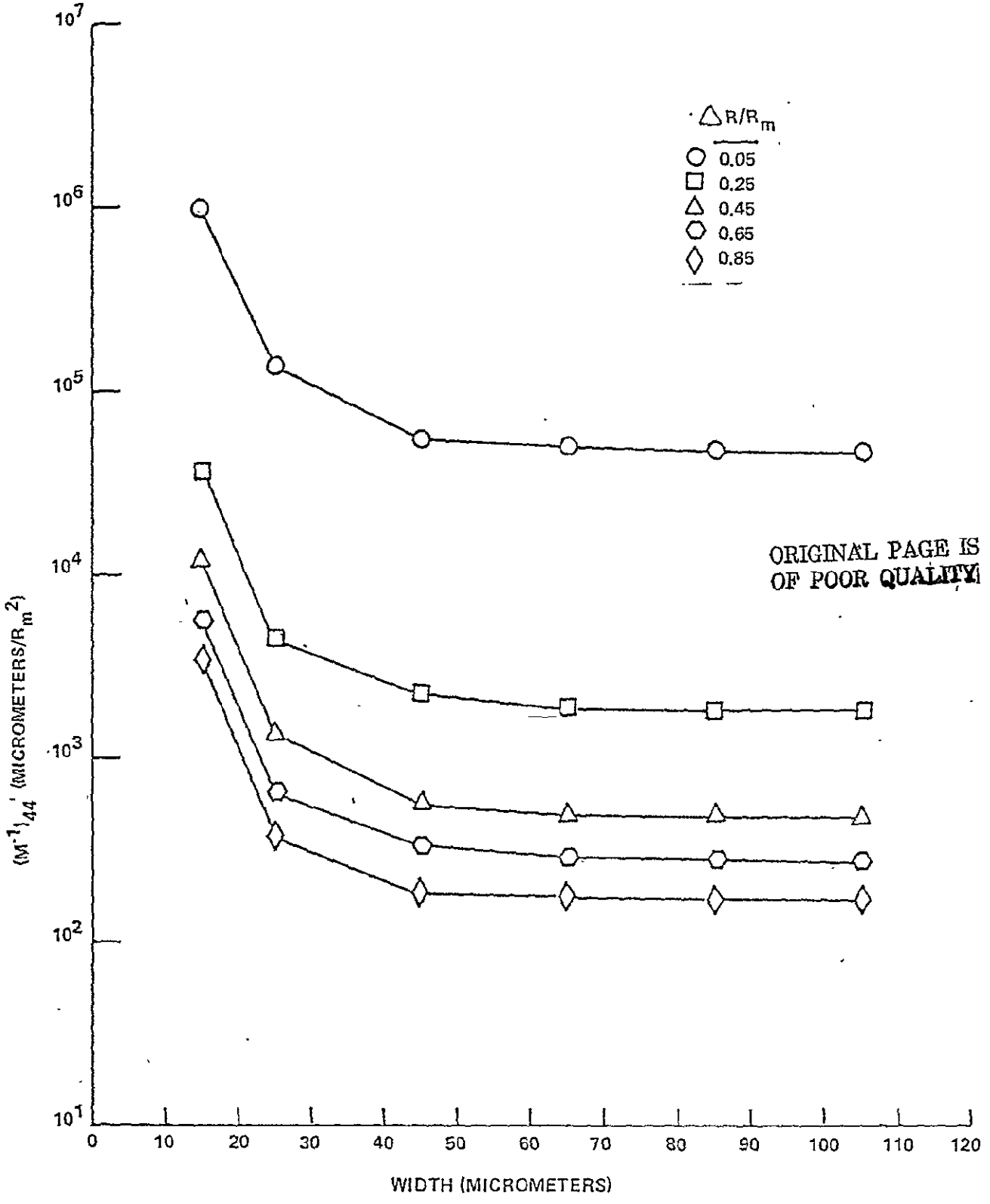

Figure 6-17 VARIATION OF BAR TARGET LOCATION ESTIMATION ERROR WITH TARGET WIDTH AND CONTRAST

accuracies represented by these relative errors begin to increase for targets less than 40 micrometers and become asympototic for targets smaller than 25 micrometers. This corresponds to ground distances of approximately 134 and 84 meters respectively. From Figure 6-15 we see that the variance in the radiometric measurement is independent of target contrast, $\Delta R/Rm$, while the variance in measurement of bar width (Figure 6-16) and location (Figure 6-17) both depend upon this contrast. If these data are presented on a plot of $\log (M^{-1})_{ii}$ versus $\log (\Delta R/Rm)$ we find that both terms have the inverse square dependence on contrast described earlier in connection with the variance in locating edges. We note that the variance in target width measurement is an order of magnitude larger than the variance of the location measurement and is about twice the variance in edge location (Figure 6-11). The later result indicates that target width measurement is equivalent to two independent edge location measurements for sufficiently wide targets.

6.2.3 Delta Function Target Results

In order to obtain an estimate of nominal system "resolution", two parameter targets consisting of two narrow bars on a constant background were used. Signal trace plots of these results are shown in Appendix C, pages 279 through 283. The two bars are no longer distinguishable at a separation of 25 micrometers which corresponds to a distance of about 84 meters on the ground in agreement with the results from the square bar targets presented above.

6.3 Effect of Off Nominal NDPF Element Performance

The effect of variation in performance of the NDPF subsystem elements is now considered for the nominal (Handbook nonlinearity data) NDPF system.

6.3.1 Electronics

The spread functions for the EBR Control Electronics and for the EBR electronics are practically delta-functions They are unlikely to vary and a great change would be required before the signal was affected. These two spread functions were therefore not varied in the sensitivity analysis.

The D/A conversion spread function is defined by the type of device used. Small variations in its shape are not likely to occur;either it works or it doesn't. The same holds for the Bessel filter. Variation in the performance of these two devices is therefore not examined here. However, both devices are related to the payload performance--if a new, higher performance sensor were used in the future, both devices would also be redesigned. In this sense, they can be considered part of the payload. The effect of higher payload performance on product quality will be examined later.

6.3.2 EBR Beam

The EBR beam can change shape due to variations in the electron optics, misalignment, contamination, etc. The effect of EBR beam width was examined. The set of test edges (see page 66) was run for EBR beam spread functions 20%, 50% and 100% wider than nominal shown in Figure 6-3a. The off nominal EBR spread functions are shown in Figure 6-18.

The effect of EBR beam width increase on σ_1^2 and σ_2^2 is shown in Figure 6-19a. The effect on σ_3^2 is shown in Figure 6-19 b. The graphs represent the data for all twelve test edges; the variation among the targets is shown by the vertical bar.

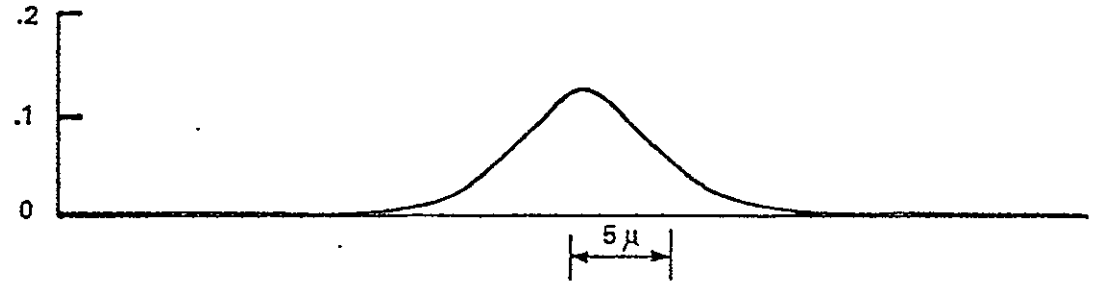

20% OFF NOMINAL

(a)

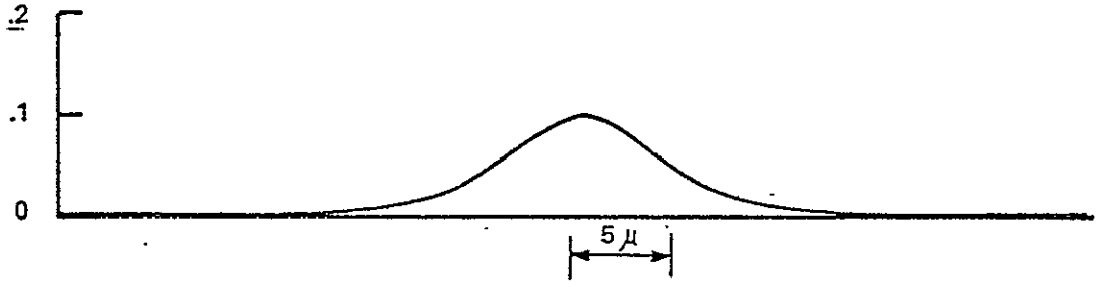

50% OFF NOMINAL

(b)

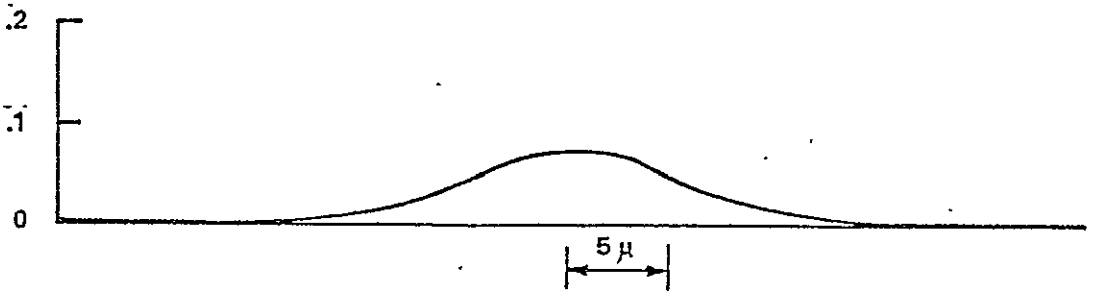

100% OFF NOMINAL

(c)

Figure 6-18 OFF NOMINAL EBR BEAM SPREAD FUNCTIONS

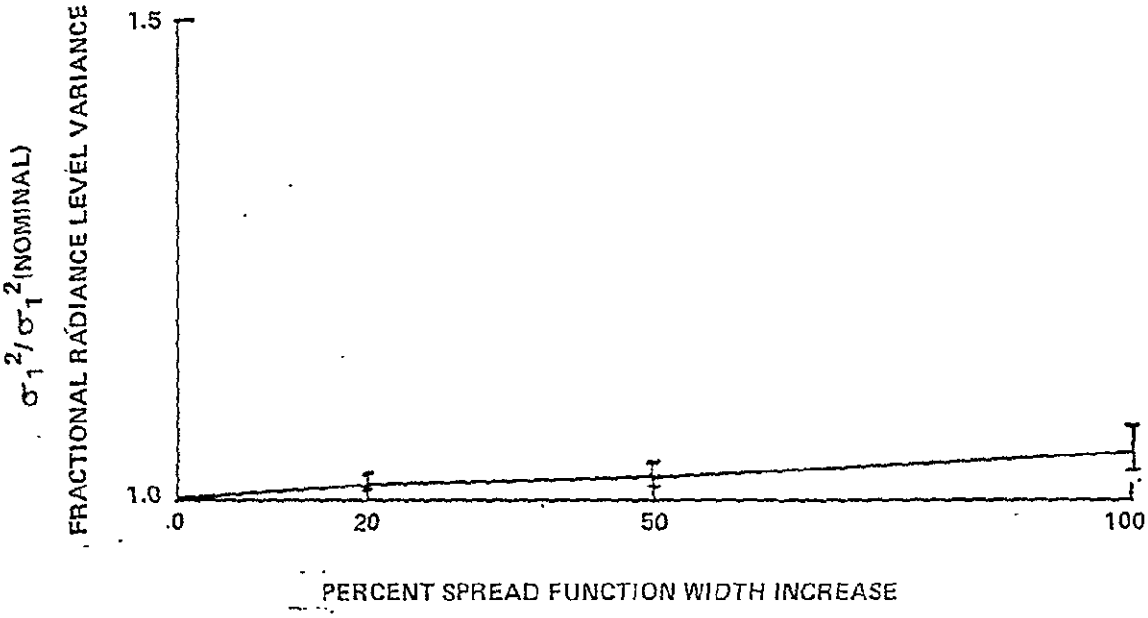

(a)

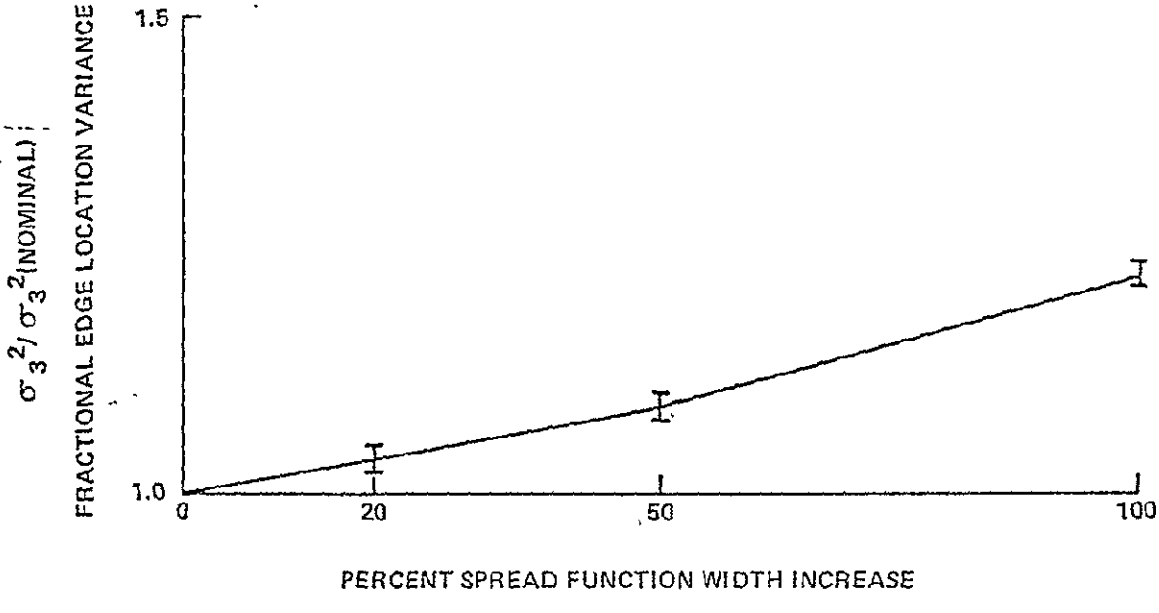

(b)

Figure 6-19 EFFECT OF EBR BEAM SPREAD FUNCTION INCREASE ON LOCATION AND RADIOMETRIC ERROR

The variation in σ_3^2 is the largest. However, the standard deviation in edge location estimation for a 100% EBR beam width increase is only ten percent larger than the nominal value. This insensitivity indicates that abberrations causing assymetry of the beams and also minor beam misalignment need not be monitored.. The monitoring procedure need only be capable of detecting gross changes in the beam width or alternatively in the EBR OTF.

6.3.3 Film-Printer Spread Functions

The sensitivity of the estimation errors to changes in the film-printer spread functions was next examined. The edge target set was propagated through the system for 20%, 50% and 100% increase in each of the three film stages (archival film, second or third generation printer-film). Figure 6-20 shows plots of the three off nominal film or film-printer spread functions. The effects on the estimation errors were identical regardless of which of the three elements were degraded. The results for all twelve edges are shown in Figure 6-21 a and b. The estimation errors have very low sensitivity to the film element's performance.

The performance of the three film/film-printer system elements were next all made off nominal at once in the 20%, 50% and 100% amounts. The results for the twelve test edges are shown in Figure 6-22a and b. The critical position estimation error parameter, σ_3^2 exhibits only a 20% increase over the nominal value when all three spread functions at once are 100% too wide. A 20% increase in the variance of course corresponds to only a 10% increase in the standard deviation σ_3.

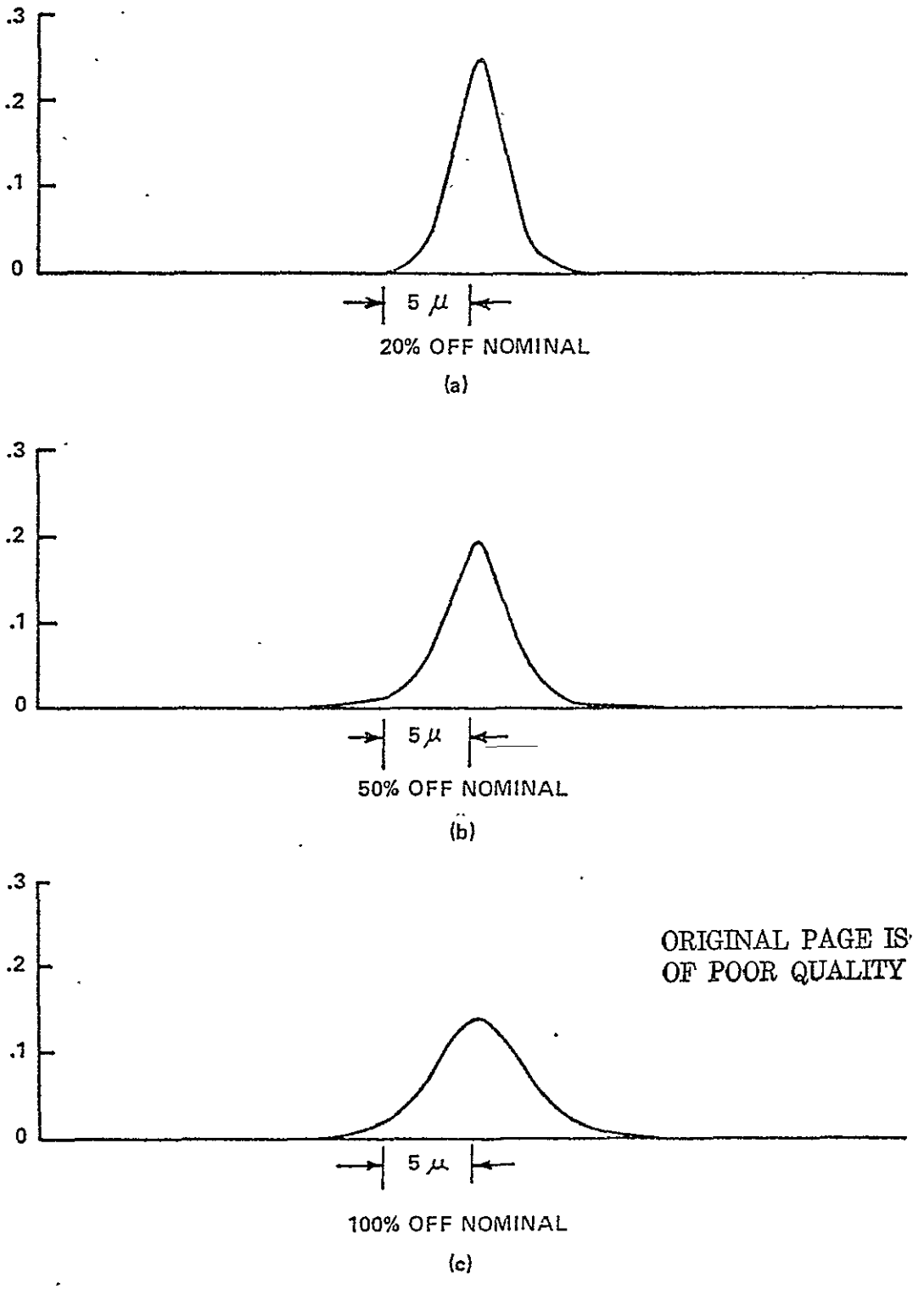

Figure 6-20 OFF NOMINAL FILM/FILM-PRINTER SPREAD FUNCTIONS

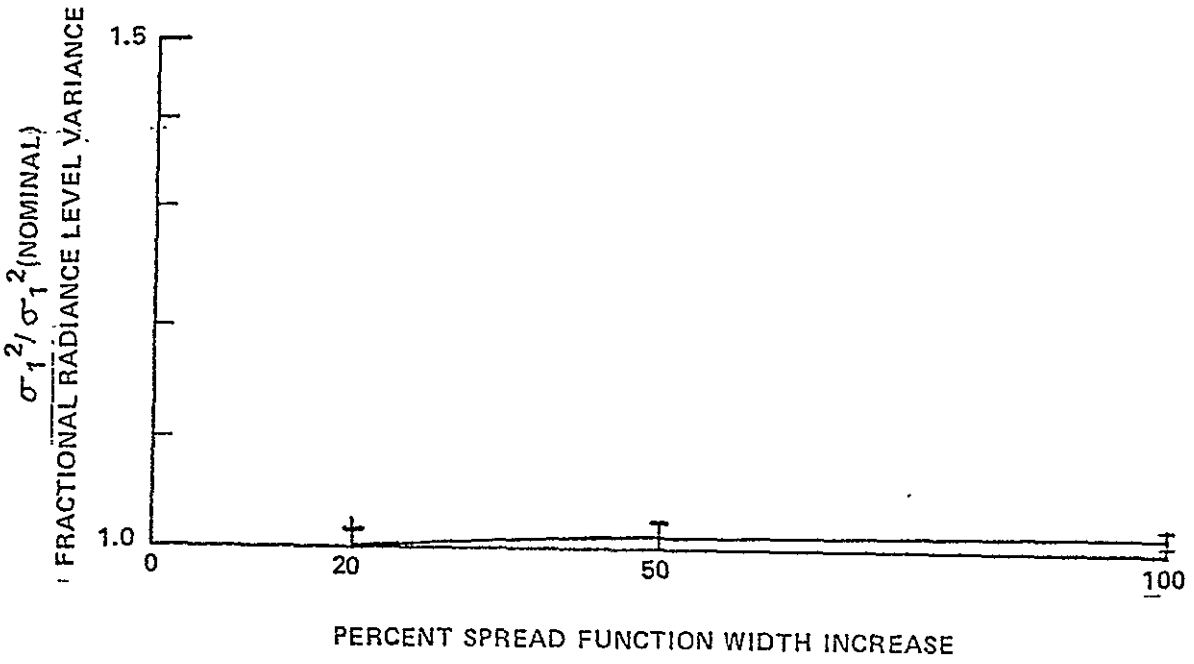

(a)

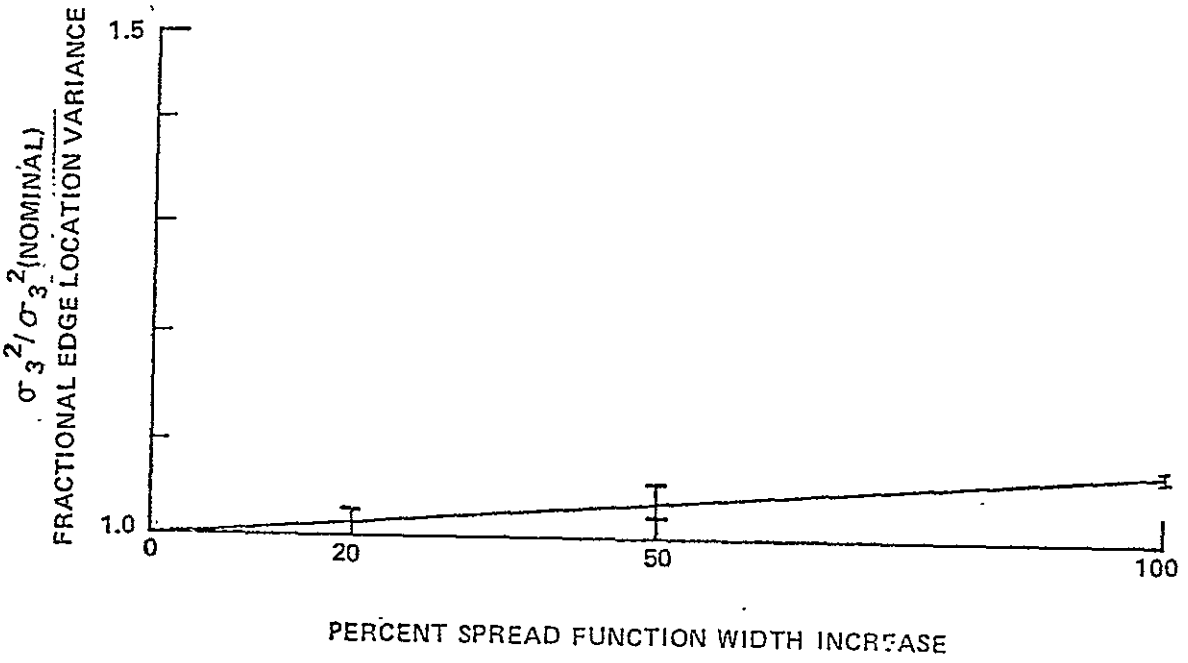

(b)

Figure 6-21 EFFECT OF ONE OFF NOMINAL FILM OR FILM-PRINTER SPREAD FUNCTION ON ESTIMATION ERRORS

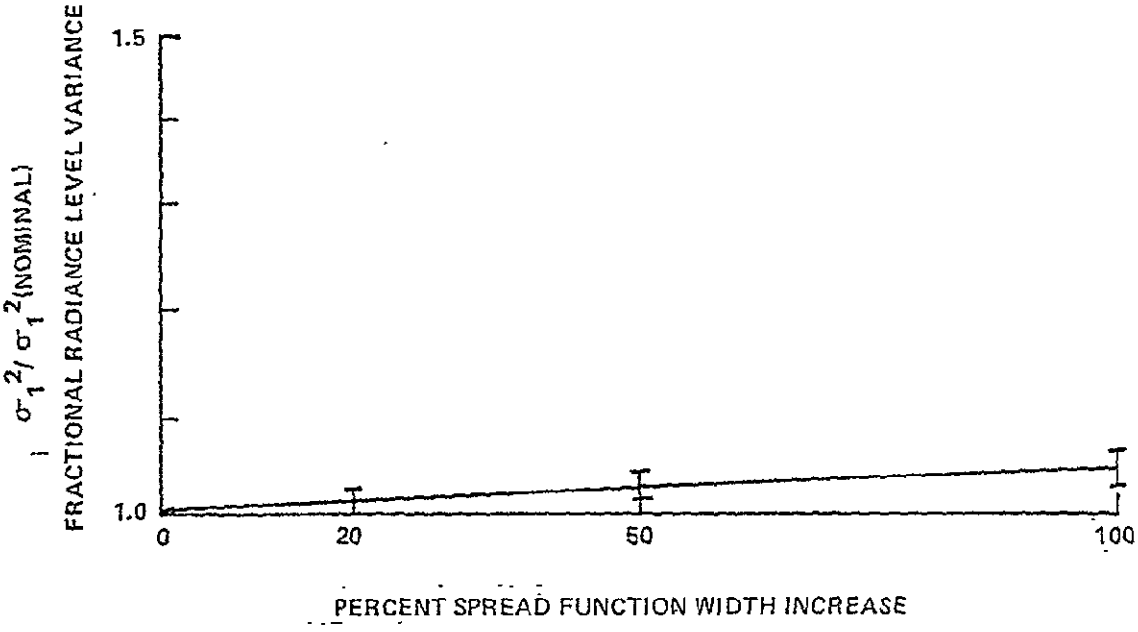

(a)

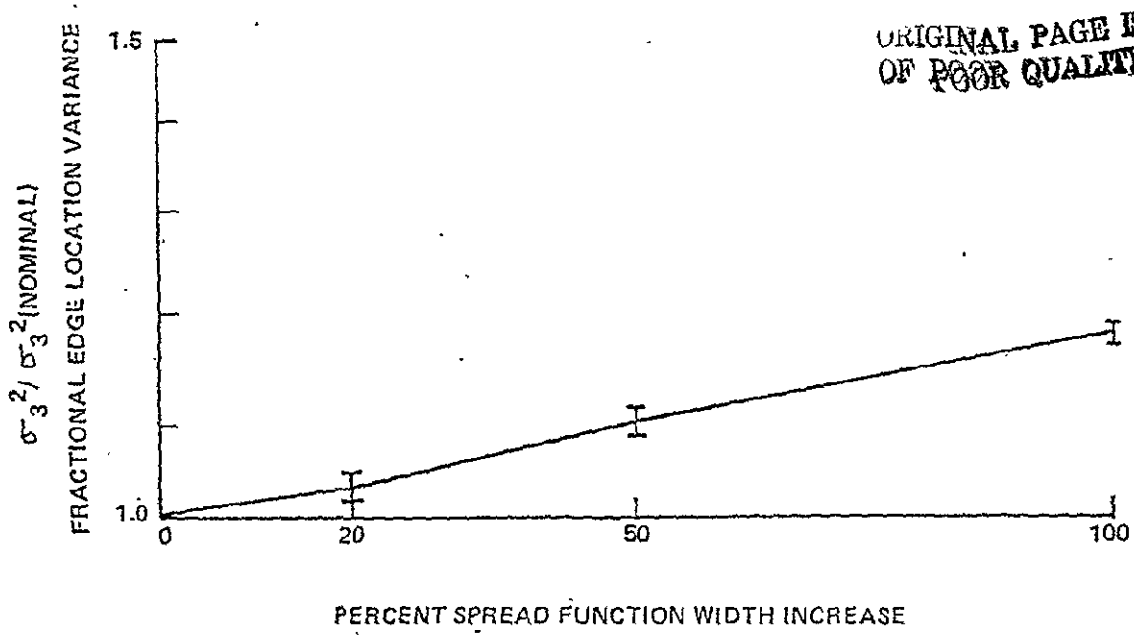

(b)

Figure 6-22 EFFECT OF HAVING ALL FILM OR FILM-PRINTER SPREAD FUNCTIONS SIMULTANEOUSLY OFF NOMINAL IN EQUAL AMOUNTS

6.3.4 EBR and Film/Film-Printer Spread Functions Off Nominal Simultaneously

The film and film-printer spread functions were considered in combination with a 20% off nominal EBR spread function. The 20% value was chosen simply because it is quite gross and would be easy to detect but nonetheless not so gross a degradation as to be totally unlikely to occur. The results of the computation for 20%, 50% and 100% width increase of a single film-printer spread function are shown in Figure 6-23. Comparison of these data with the preceding shows little difference. Thus to hold a reasonably coarse tolerance an EBR performance does not preclude the even coarser tolerances indicated for the film/film-printer spread functions.

6.3.5 Film Development - H-D Curve

The following target edges were generated in the computations discussed in this subsection.

Designation No.	A_1 (normalized radiance level)	A_2 (normalized radiance level)	A_3 (edge location)
1	.25	.2	50.
2	"	.8	"
3	.65	.2	"
4	"	.8	"

$\Delta R/R_m$	Designation No.
.05	1
.15	4
.45	3
.55	2

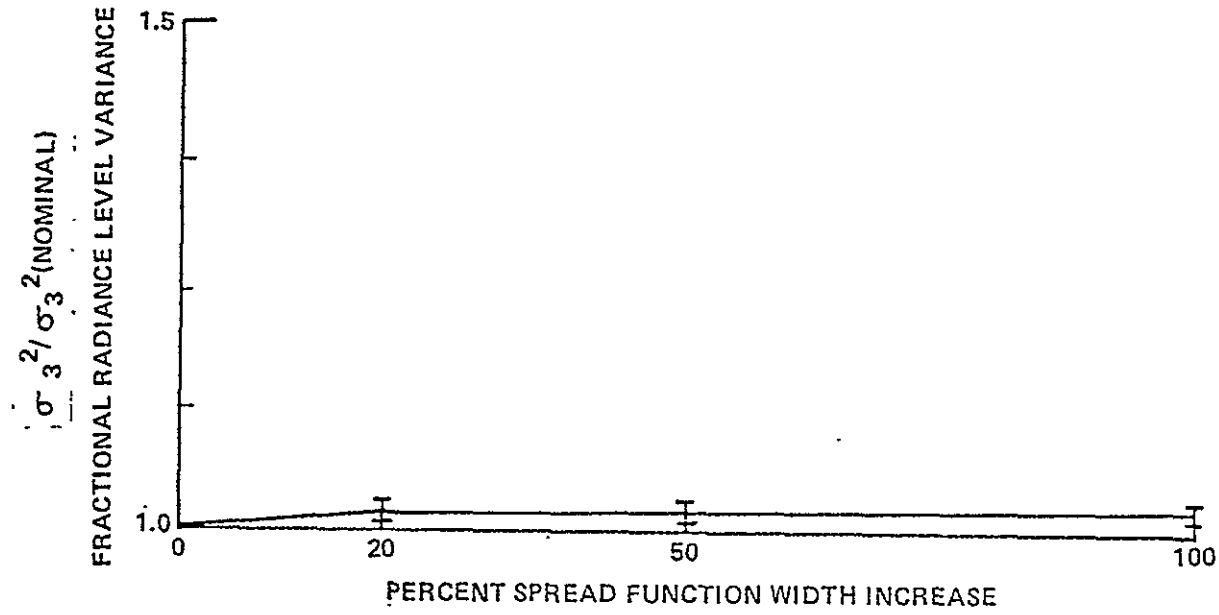

(a)

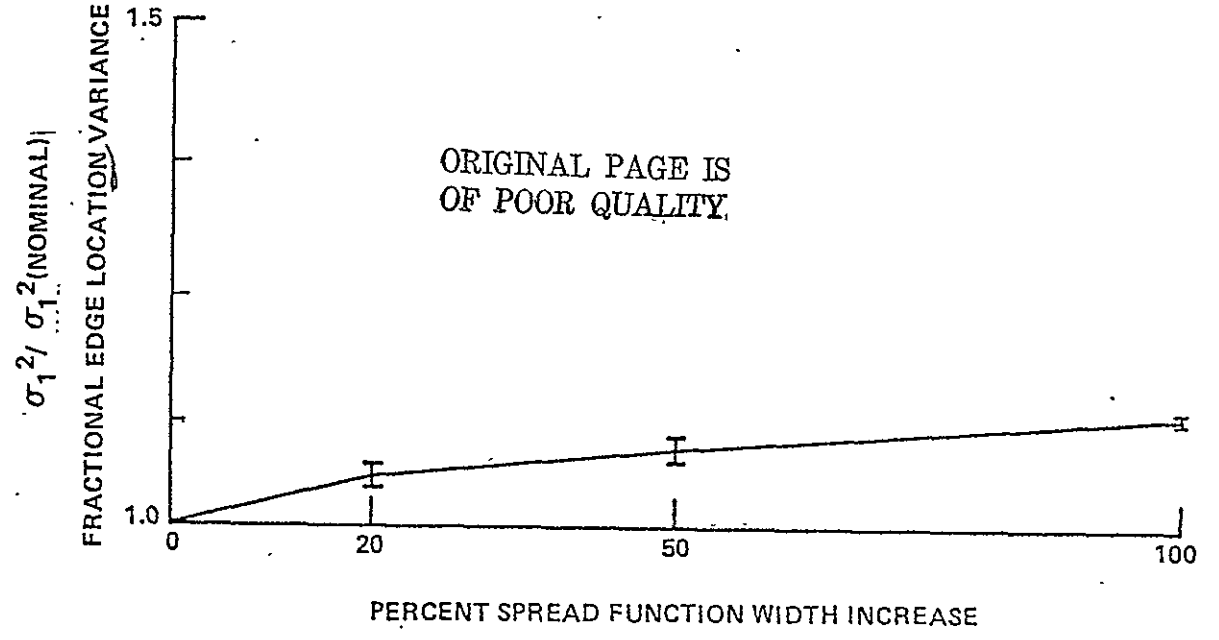

(b)

Figure 6-23 EFFECT OF HAVING EBR 20% OFF NOMINAL AND ONE FILM-PRINTER OFF NOMINAL SIMULTANEOUSLY

The processing γ of each development process was varied and the change in variances computed.

First Generation

The set of H-D curves used is shown in Figure 6-24. Nominally $\gamma_1 = 2.0$. Computations were performed for off nominal $\gamma_1 = 1.8, 1.9, 2.1$ and 2.2. The results are shown in Figure 6-25. Note: 1) The very large sensitivity to γ compared to the preceding spread function results.

2) The difference in sensitivity of each target edge to the processing changes. The system begins to exhibit nonlinear response for small departures from nominal γ.

3) Edges 2 and 4 which both have $A_2 = .8$ have rapidly increasing estimation errors for $\gamma_1 > 2.1$. The increased γ_1 evidently causes saturation and clipping at this radiance level.

4) Increasing γ_1 actually decreases the estimation error to some extent before the catastrophic increase for the high radiance level targets occurs.

Second Generation

Nominal second generation processing is to $\gamma_2 = 1.0$. Computations were performed for $\gamma_2 = .8, .9, 1.1$, and 1.2. Results are shown in Figure 6-26. Sensitivities are very high for all targets. From the σ_1^2 sensitivities, it is clear that the high radiance values are being forced into saturation and are clipping. Consideration of the σ_3^2 sensitivities indicates that the only target with relative insensitivity to γ_2 is target number one with normalized radiance values .25 and .2. Target number four which has the highest radiance level is most sensitive to an increase in γ_2. The graphs show that it is critical to hold this processing element as close to the nominal value as possible.

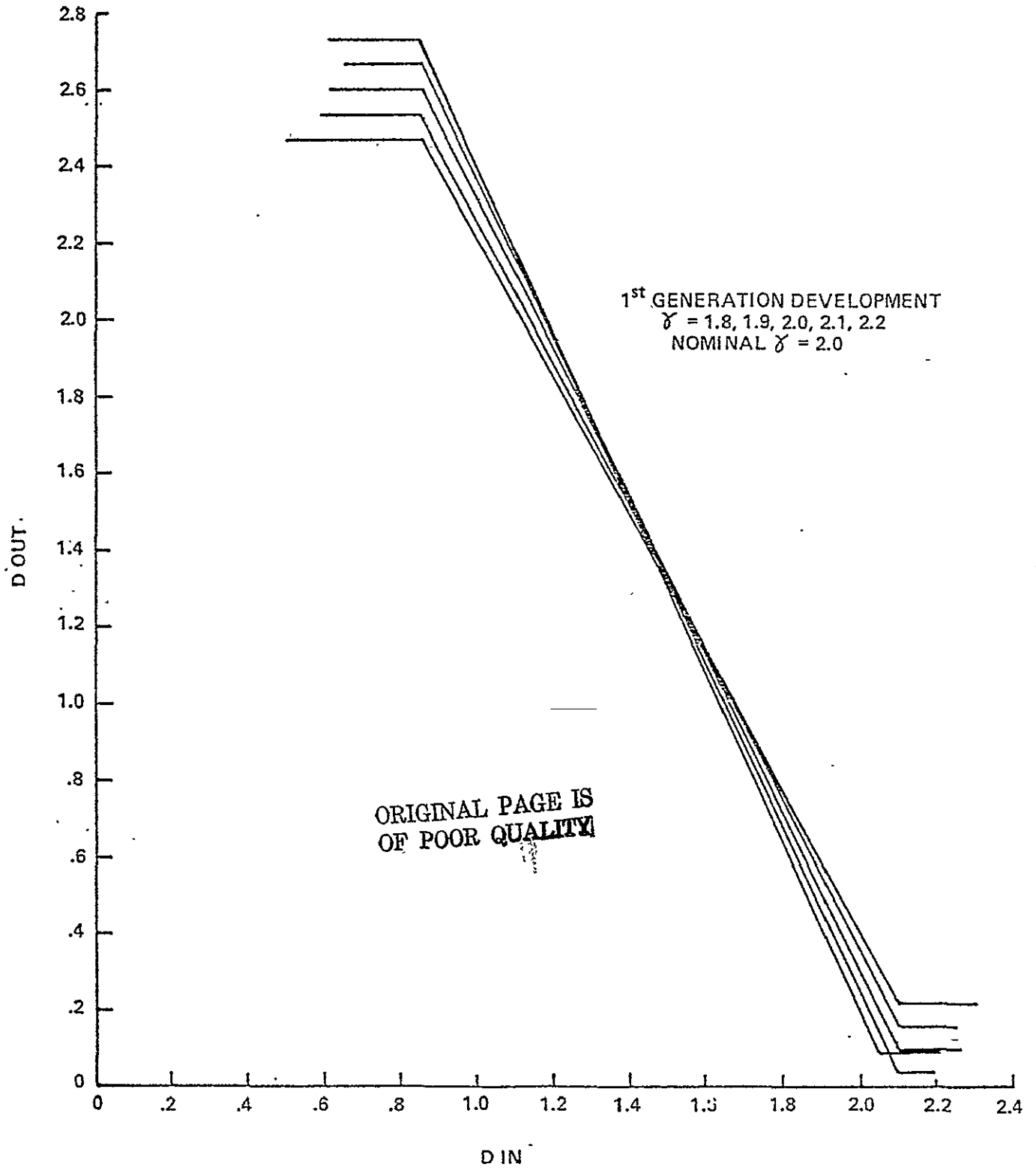

Figure 6-24 FIRST GENERATION H-D CURVES

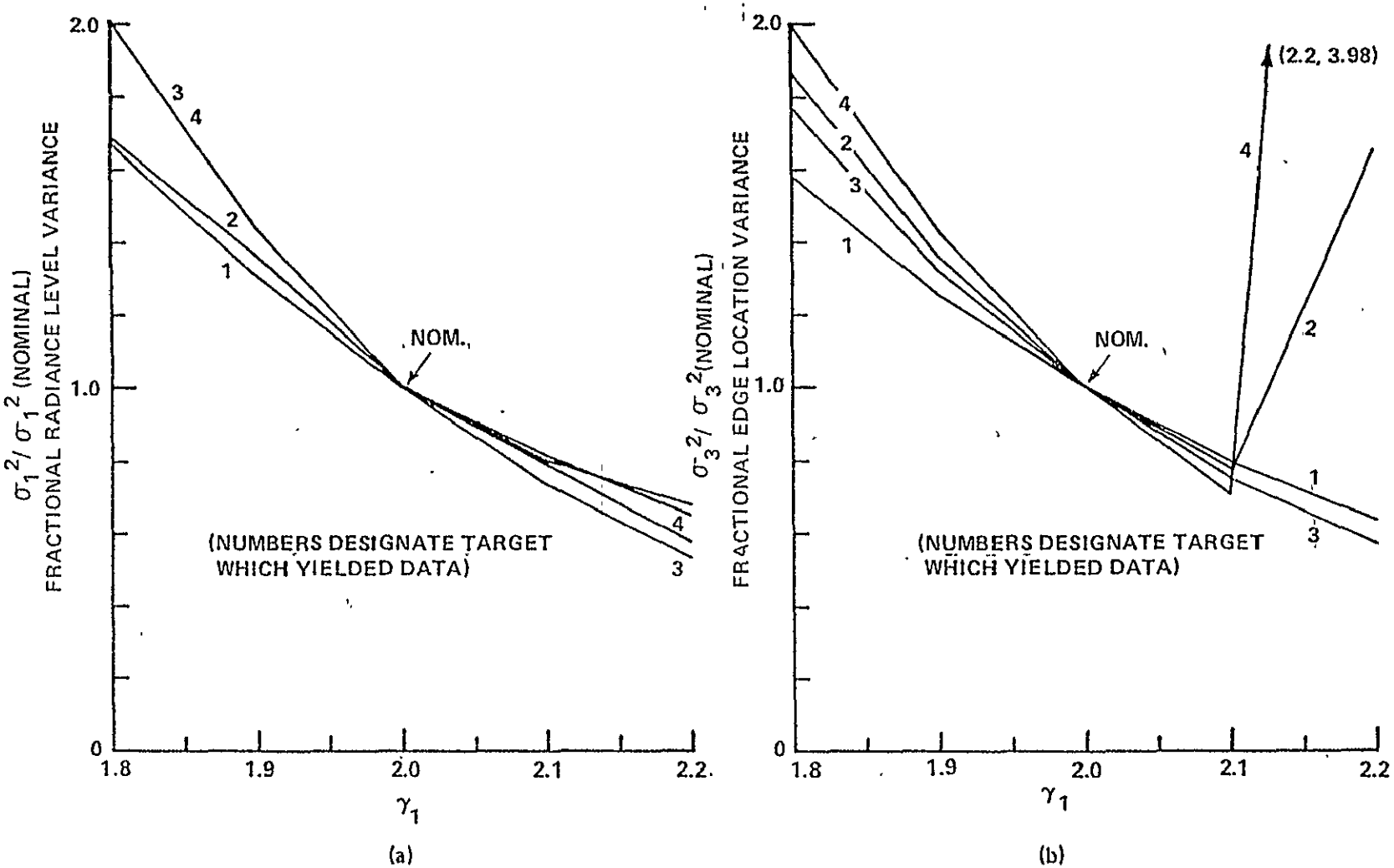

Figure 6-25 EFFECT OF OFF NOMINAL FIRST GENERATION PROCESSING γ

C-2

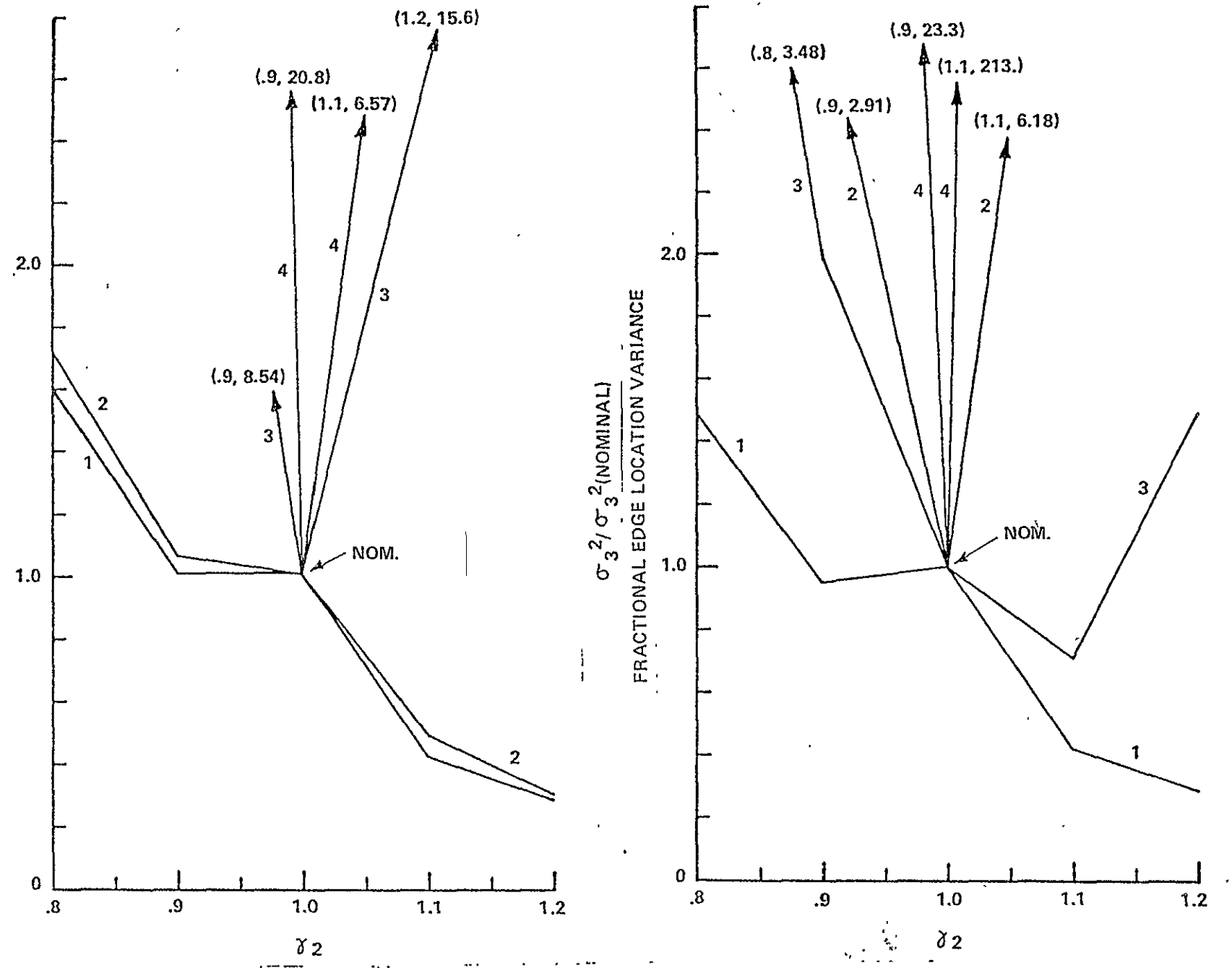

Figure 6-26 EFFECT OF SECOND GENERATION PROCESSING γ

Third Generation

Nominal third generation processing is to $\gamma_3 = 1.0$. Computations were performed for $\gamma_3 = .8, .9, 1.1$ and 1.2. Results are shown in Figure 6-27. Sensitivities are very high for all targets as noted for the second generation processing.

6.3.6 Measured Nonlinearity Data

The simulation was run using the H-D curves measured from NDPF samples discussed in Section 6.1 and the set of twelve edges defined in Table 6-2. Using the data obtained from the fifteen step calibration grey scale on an actual frame of imagery yielded the plot of edge position estimation error shown in Figures 6-28 and 6-29. Note that the data points lie quite close to the nominal results. The spread of estimation errors at each $\Delta R/R_m$ value indicates that the system is not linear - the estimation error depends on the absolute A_1, A_2 values as well as $|A_1 - A_2|$. There is no evidence that the frames examined are typical NDPF products.

The twenty-one step quality control grey scale H-D data was also used. For this data, the system exhibited extreme nonlinearity which resulted in severe clipping. Figure 6-30 is a plot of edge position estimation error versus $\Delta R/R_m$. It is included to dramatize the effect processing control can have on the image quality. As the 21 step grey scale data are inconsistent with both the Handbook (nominal) and the measured 15 step grey scale data, it is likely not typical of NDPF performance.

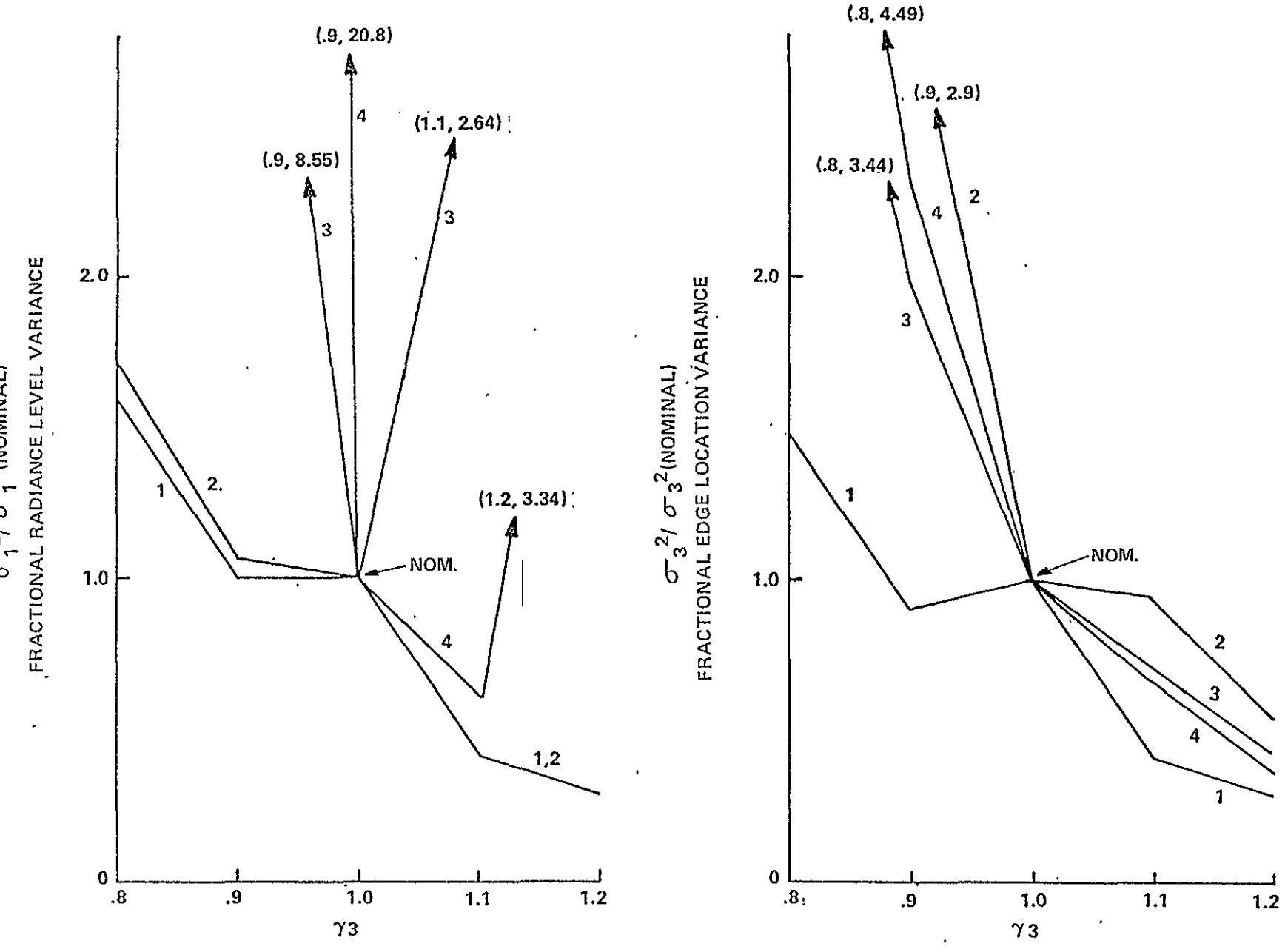

Figure 6-27 EFFECT OF THIRD GENERATION PROCESSING γ

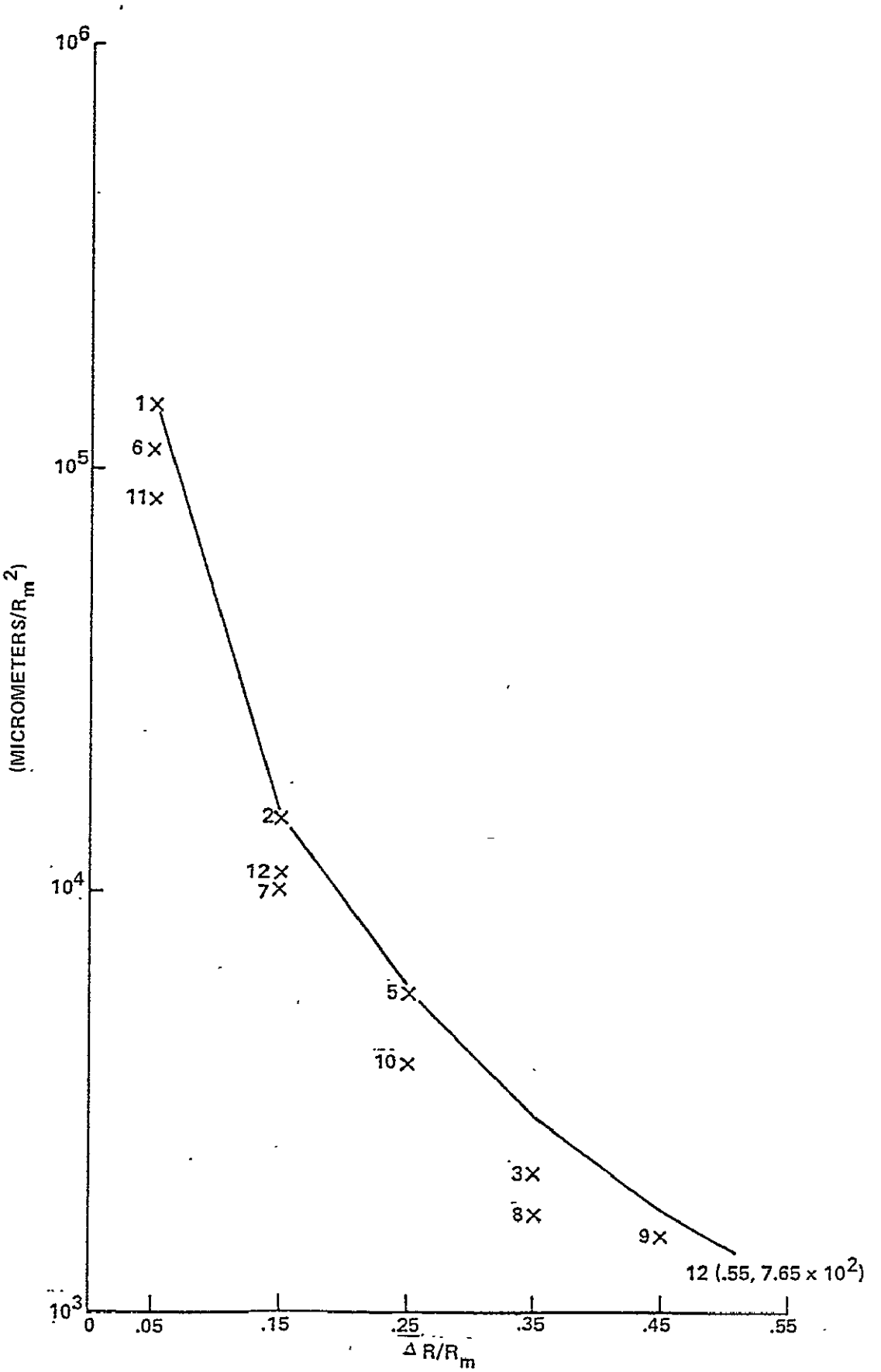

Figure 6-28 VARIATION OF EDGE POSITION ESTIMATION ERROR WITH EDGE CONTRAST-MEASURED (15 STEP) NONLINEARITY DATA

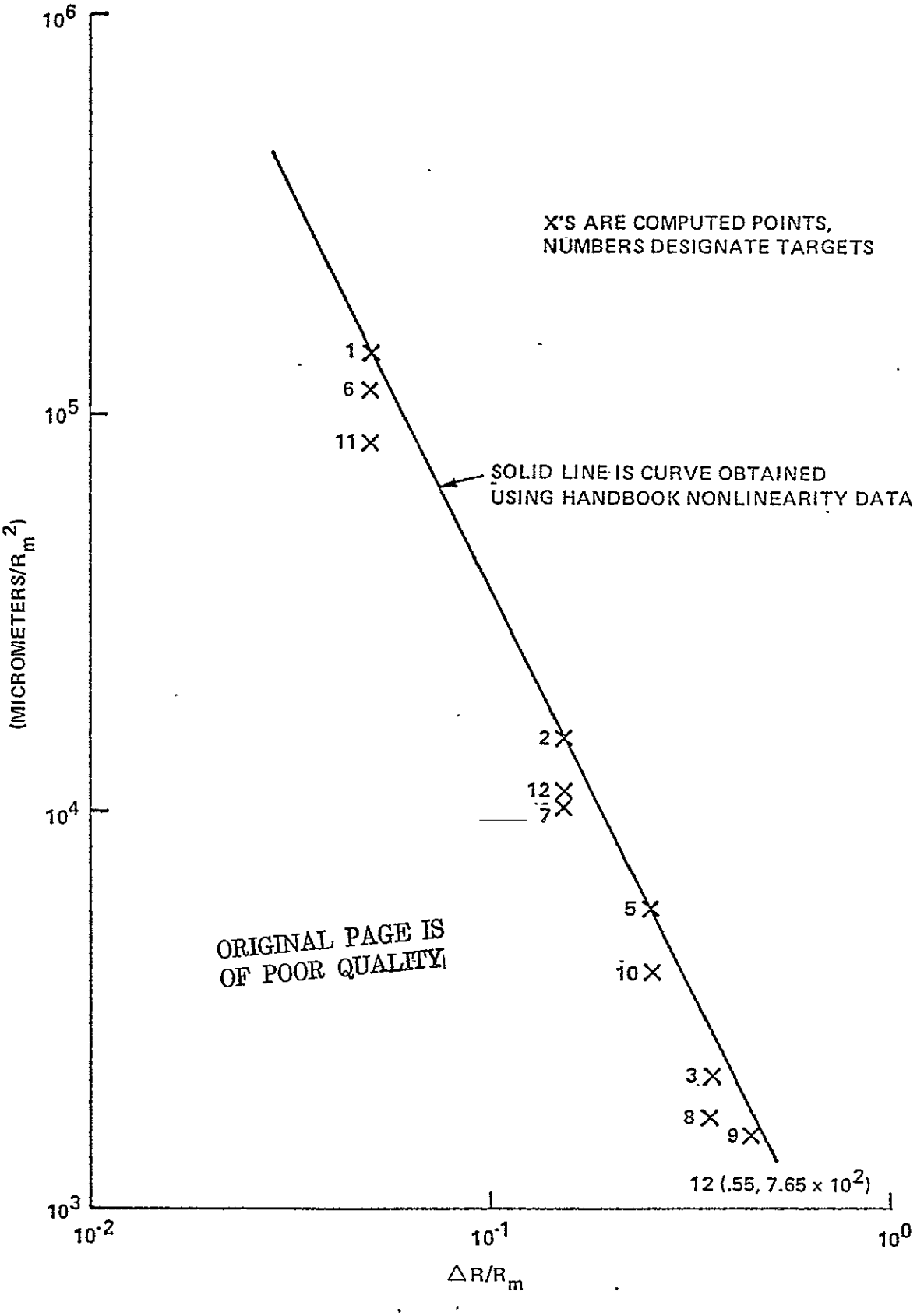

Figure 6-29 LOG-LOG PLOT OF FIGURE 6-28

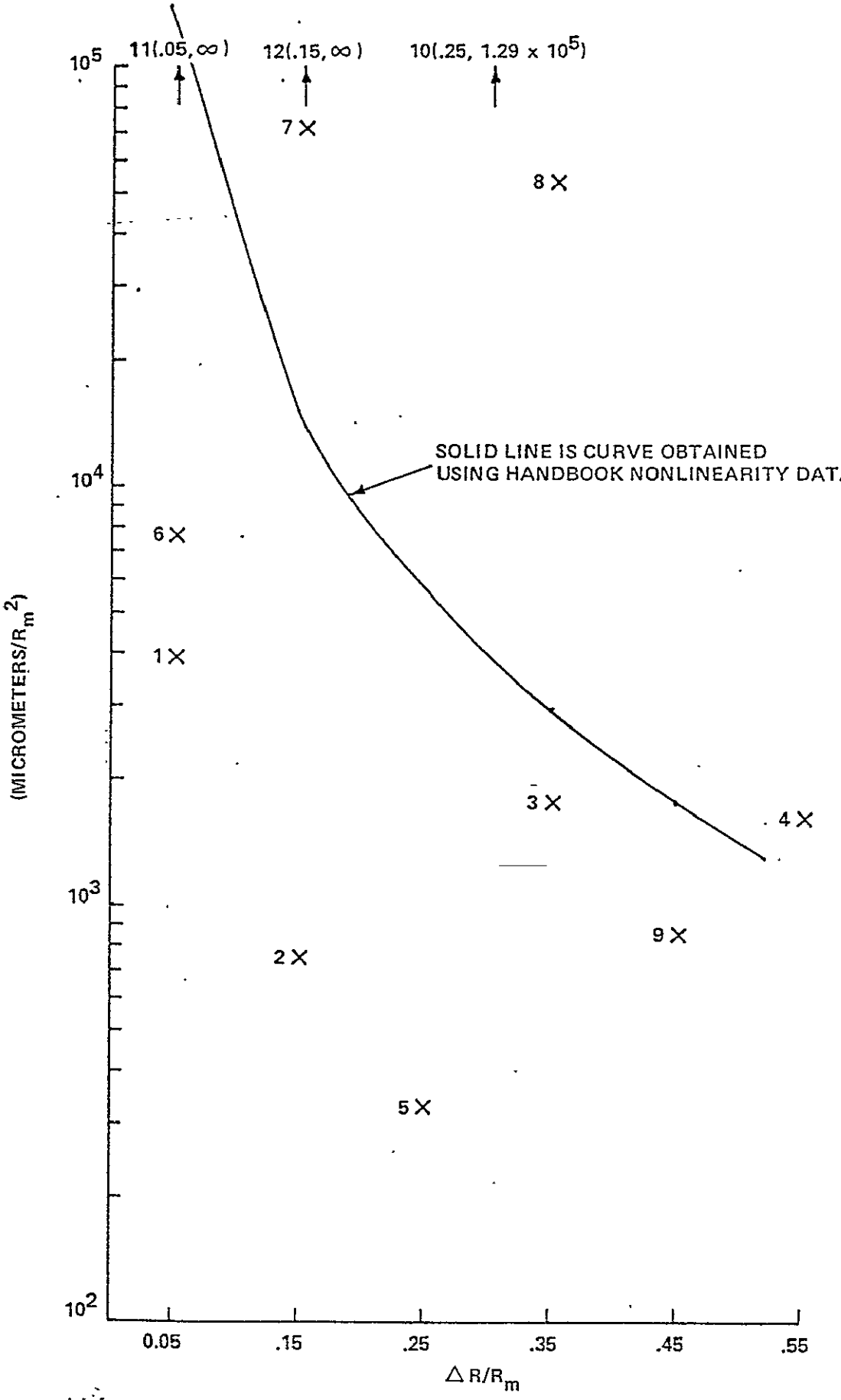

Figure 6-30 VARIATION OF EDGE POSITION ESTIMATION ERROR WITH EDGE CONTRAST- MEASURED NONLINEARITY DATA (21 SPOTS)

6.4 RBV Output Product Quality

Since the RBV sensor has been inoperable during the ERTS-A mission, the RBV configuration NDPF performance was not as thoroughly examined as for the MSS. Referring back to Figure 6-1, we see that the RBV spread function is somewhat worse than the MSS spread function. However, when the D/A conversion and Bessel filter operations are added to the MSS sensor performance, the RBV input signal, which is analog to begin with, has somewhat better frequency content than the MSS input signal. Consequently, the estimation errors for the RBV products would be slightly smaller than those for the MSS presented above. In addition, the sensitivity of the estimation errors to changes in the EBR and film-printer spread function would be somewhat greater. But since these sensitivities are so low and the difference between the RBV and MSS analog inputs so small, repetition of the computations for the RBV was not required. It is concluded that quality control procedures adequate for the MSS products are adequate for the RBV products as well.

6.5 Effect of Better Sensor Performance

It was desired by NASA to obtain an estimate on the improvement in image quality that might be obtained with better sensor performance (Figure 6-31). It is emphasized that use of a better payload would require reexamination of two approximations valid for the current system:

1. The assumption that N_o remains constant with small changes in subsystem element performance becomes invalid when the processing element spread functions are not narrow compared to the sensor spread function.

2. The linearity of the contact printing process is questionable for imagery with higher cutoff frequency than that imposed by current sensors.

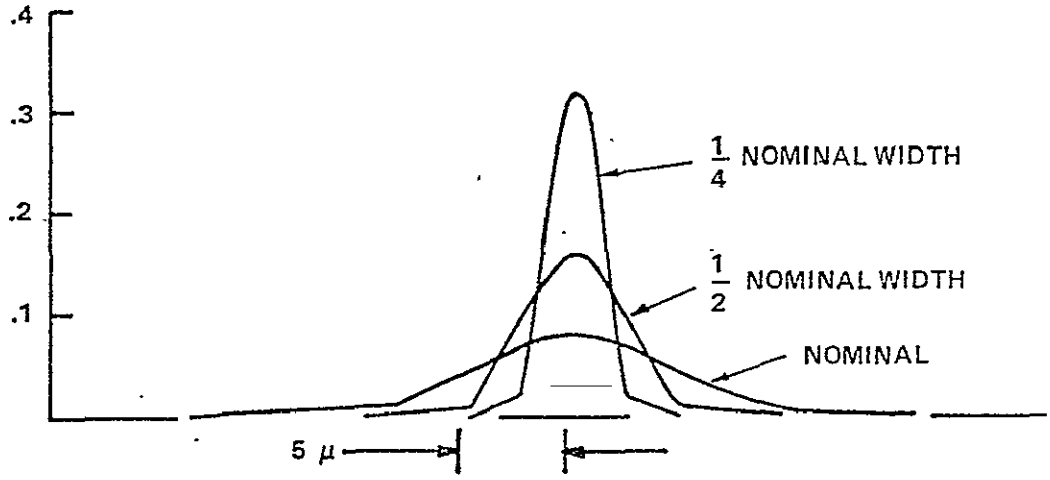

Figure 6-31 HYPOTHETICAL IMPROVED SENSOR SPREAD FUNCTIONS

If the assumptions were to remain valid, and the sensor performance were improved by factors of two and four, the edge position estimation errors would improve as shown in Figure 6-32. The RBV spread function was used to obtain these data in order to avoid having to change the D/A converter and Bessel filter spread functions together with the MSS sensor. Clearly doubling the sensor "resolution" does not reduce the variance by a factor of two.

We believe that the first assumption could be invalid for the improved cases considered. However, the technique is still valid: the N_o term would simply have to be computed as a function of element performance as well, which involves slightly more time, but involves no conceptual difficulties. If the payload spread function becomes close to processing element spread function sizes, it may be necessary to use a two dimensional simulation in order to correctly determine the effect of element performance on the two dimensional noise field.

Should the contact printer linearity become invalid, a better mathematical model for that physical process than currently exists will have to be found.

6.6 Absolute Performance

To relate the relative measurements considered thus far to absolute estimation errors requires determination of N_o. A reliable estimate of the sensor noise level was not available, and, consequently, the following "absolute" performance calculations are for illustration only. It is clear from Section 3.3 that N_o depends on the aperture used in the measurements. The long, narrow slit approximation will be used here for illustration. For the current ERTS system, this approximation applies to slits narrower than seven micrometers.

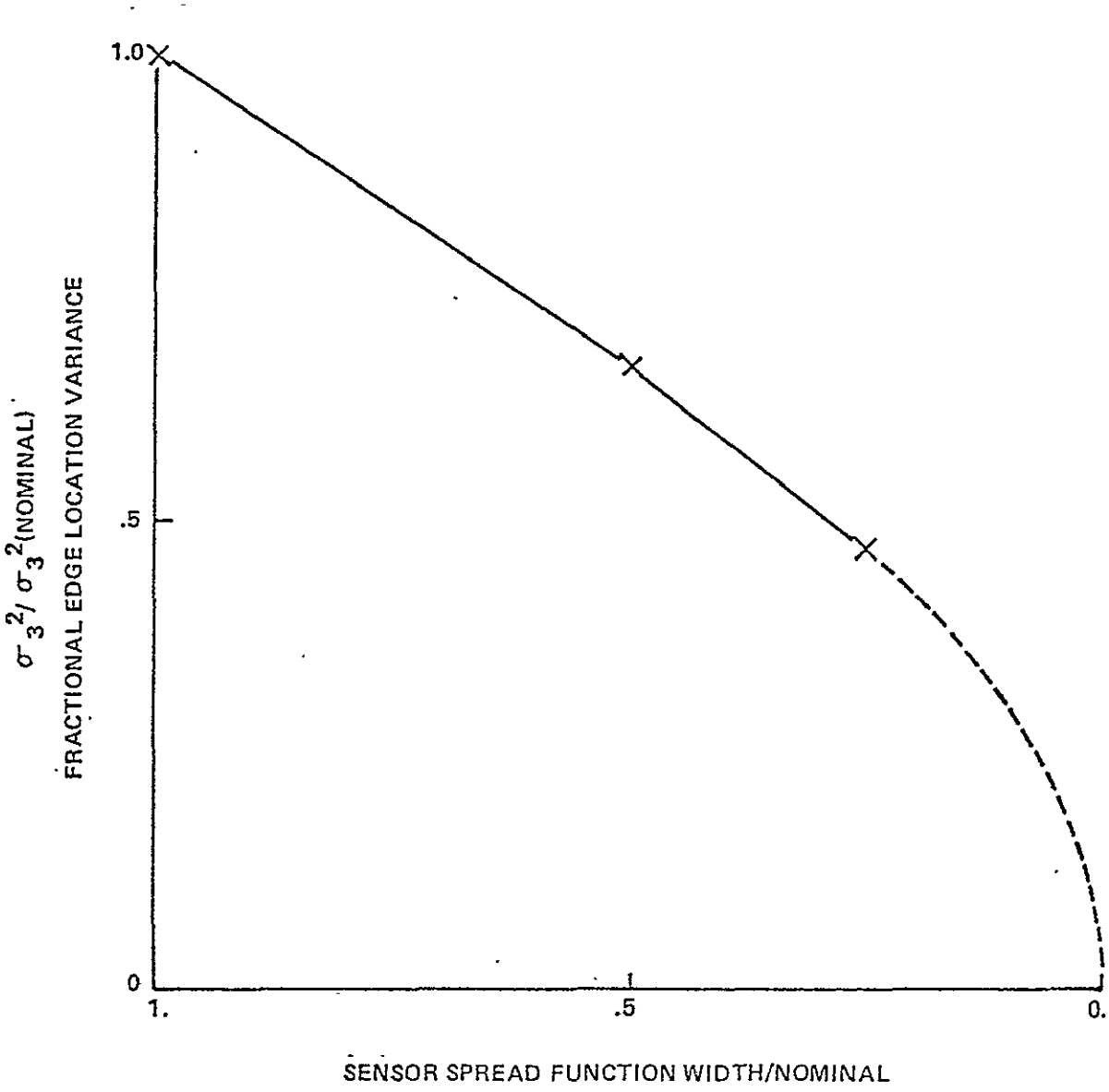

Figure 6-32 HYPOTHETICAL EFFECT OF IMPROVED SENSOR PERFORMANCE ON EDGE POSITION ESTIMATION

The values for $\sigma_T^2 A_A$ presented earlier in Figure 6-7 for the "copy film" were substituted into Equation 3-21 to compute N_o for slit lengths of 30, 150 and 300 micrometers. This corresponds to targets about 100, 500 and 1000 meters long on the ground. The resulting N_o values are shown in Figure 6-33. These data were combined with the results for the bar target radiance level (Figure 6-15) and bar width (Figure 6-16) using Equation 3-2 to obtain the absolute percentage errors for the three lowest contrast targets. The high contrast targets were excluded to permit the use of an N_o value at the average signal level (transmittance) of the target and avoid the dependence of the noise upon signal level. The resulting percentage errors are shown in Figure 6-34 as a function of the width of the target in meters on the ground for a target 500 meters long. Both the radiance and width estimation errors decreases rapidly with increasing target width as would be expected. The independence of M_{22}^{-1} on target contrast, $\Delta R/Rm$, combined with the increase of noise power with radiance or transmittance cause the percentage error in radiance estimation to increase rather than decrease with contrast or radiance level. The width estimation error, on the other hand, decreases with increasing contrast. The reader is reminded that these error estimates assume optimal data use and that their accuracy depends directly upon the accuracy of the system element performance descriptors used as input to the IDSS Program.

6.7 Geometric Mapping Error

The positional estimation errors calculated apply to local measurements. For measurements across the frame format, geometric mapping error must be added. No new work was done in this study to assess the magnitude of this error. Residual errors remaining after application of correction algorithms currently employed by the NDPF are summarized in Appendix A.

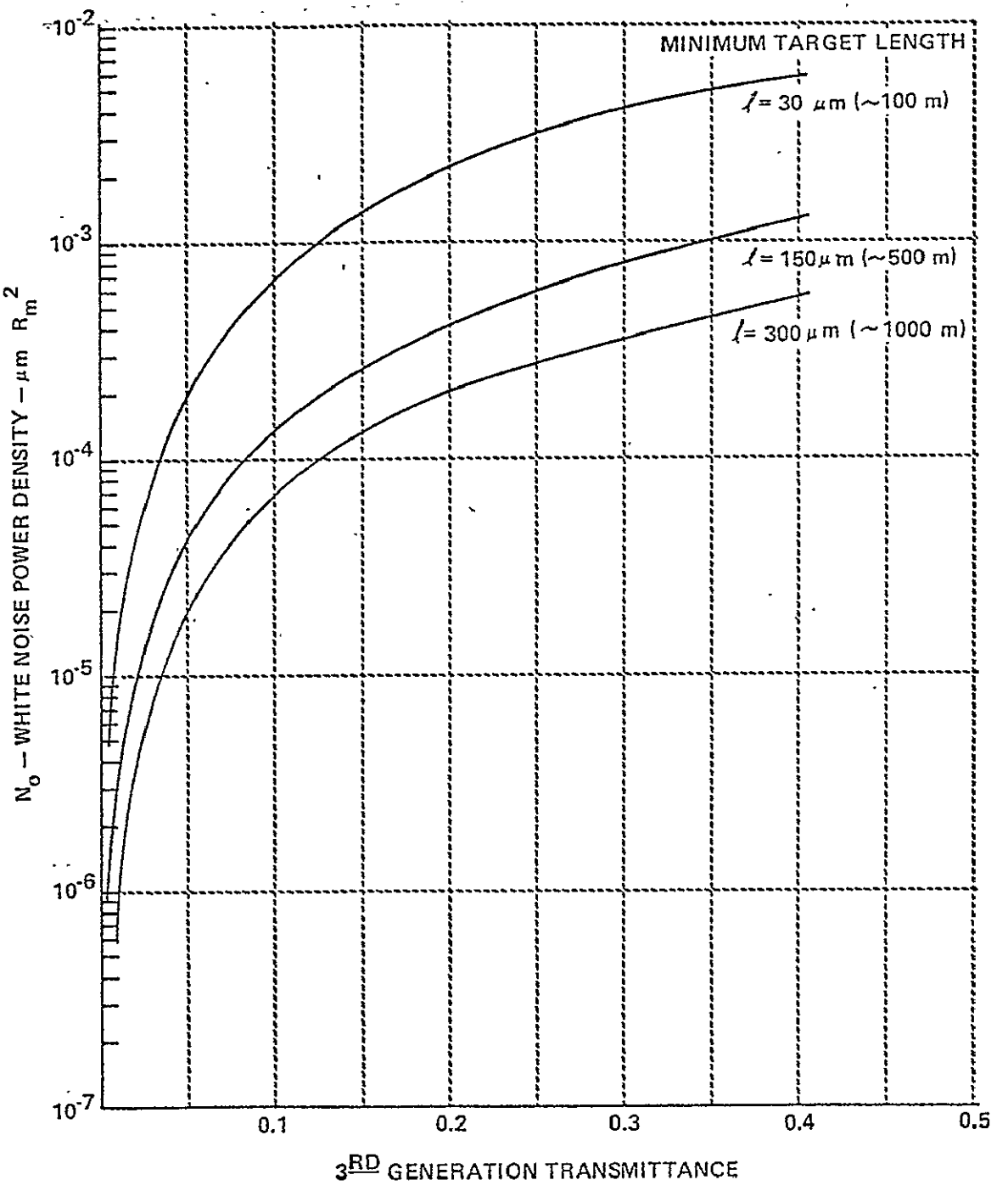

Figure 6-33 NOMINAL WHITE NOISE POWER DENSITY

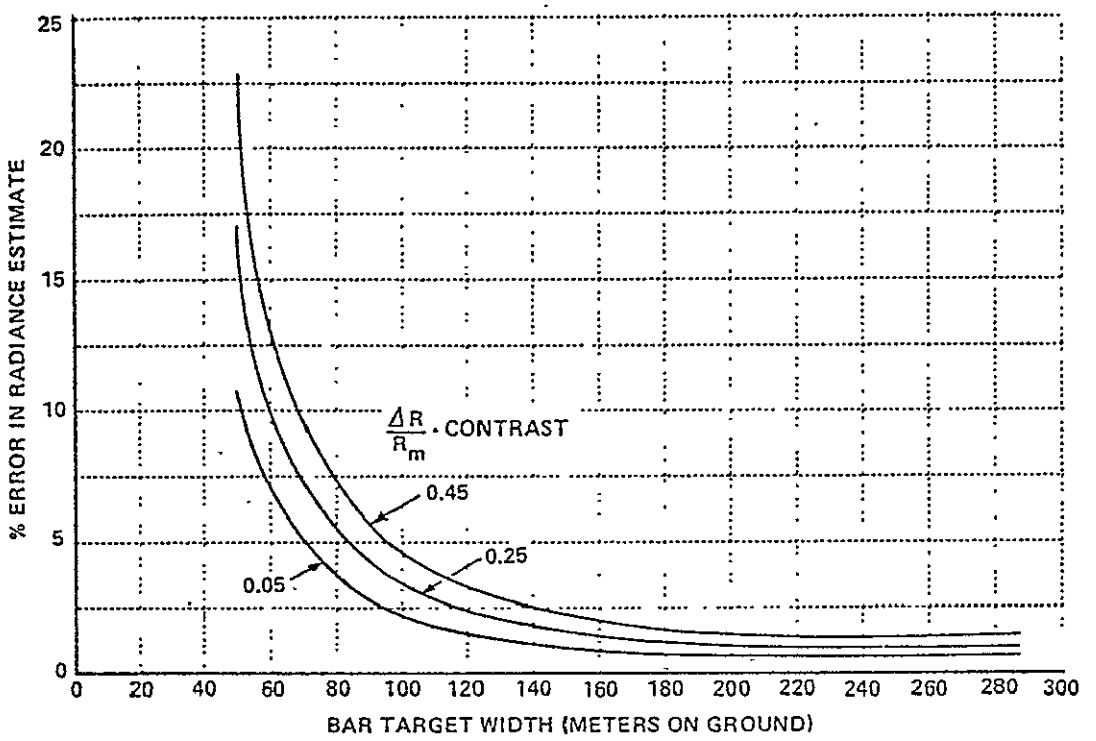

(a) RADIANCE ESTIMATION ERROR

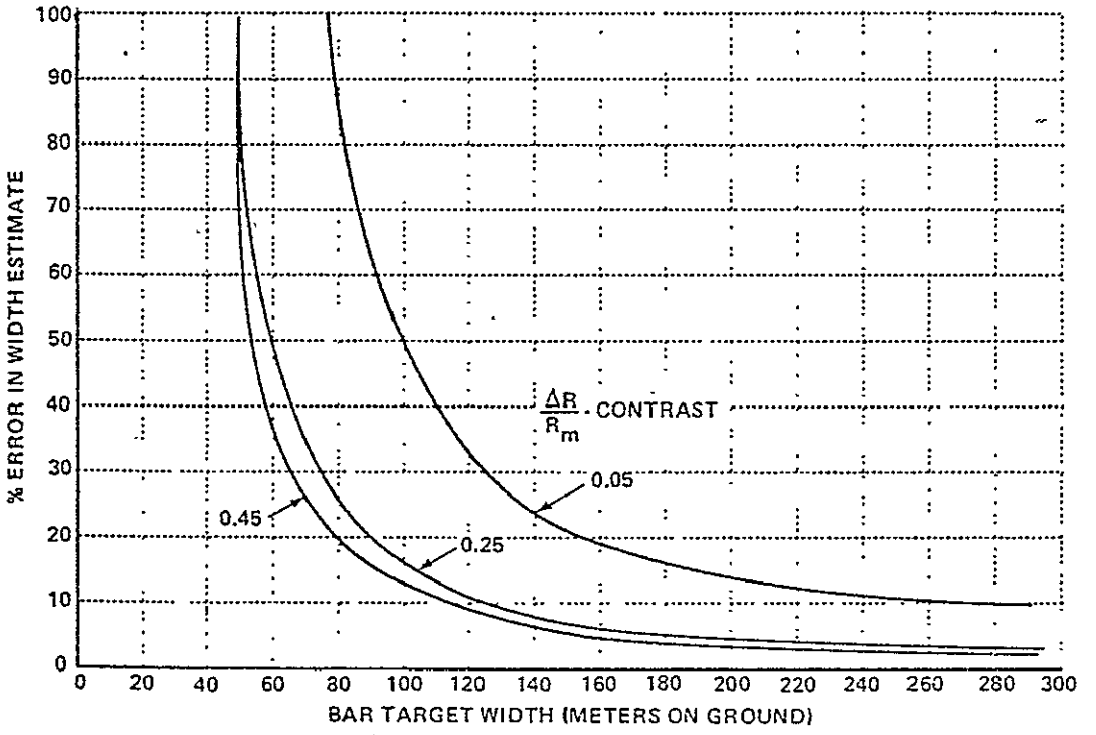

(b) WIDTH ESTIMATION ERROR

Figure 6-34 TYPICAL VALUES FOR PERCENTAGE ERROR IN TARGET WIDTH AND RADIANCE MEASUREMENT FOR A RECTANGULAR TARGET 500 METERS IN LENGTH

6.8 Radiometric Estimation Error and Calibration

The radiance estimation errors calculated yield only the local error and must be added to the large scale error. Algorithms for correction of non-uniform sensor sensitivity are currently used in the NDPF. They are summarized in Appendix A along with the residual errors.

To determine the target radiance level users must relate output product transmission to ground radiance by removing the effects of the atmosphere and contamination of sensor optics. For the past several years we have been developing techniques to calibrate the transmittance of aerial photographs in terms of ground reflectance.[21-23] We examined the application of these techniques to some typical ERTS imagery and found that they might be successfully applied.

The calibration techniques use analyses of scene shadow areas to establish the relationship between sensor irradiance and ground reflectance.* Very briefly, a linear relationship exists between the radiance just inside and outside a shadow. The parameters of this relationship are related to the component of radiance due to atmospheric scattering or flare and to the ratio of sunlight to skylight irradiance. Thus, the relationship between sensor irradiance and scene radiance or reflectance can be established by measuring sunlight and shadow radiance for a set of shadows and determining the parameters of the fit to the data set. The shadow calibration techniques require no atmospheric modeling (and consequent model parameter measurement); rather, the calibration proceeds entirely from the sensor record of shadow elements within the scene to determine the atmospheric component of radiance.

As a result, a calibrated sensor record is obtained in which sensor response is directly proportional to scene reflectance. Absolute calibration requires knowledge of only one element in the scene,

*U.S. Patent 3,849,006.

similar to laboratory use of a MgO standard or its equivalent. It should be noted that the calibration process can be automated so that data tapes are immediately corrected for the effects.

Our previous analyses have been at sufficiently large image scales that shadows from buildings and boulders could be utilized. The scale and resolution of ERTS imagery preclude use of such shadows; however, we have found that shadows on terrain with large relief and certain cloud shadows can be used to calibrate ERTS imagery successfully.

The first step in the calibration procedure is to reduce the measured film densities or sensor voltages to relative exposure or radiance by means of a D-log E or instrument response curve. Analyses then proceed from these relative exposure values. It is important to note that it is not necessary to have a relationship between sensor response and absolute exposure. All analyses can proceed from a relative exposure relationship; hence, the problems currently existing with the MSS mirrors (contamination) have no effect on the calibration process.

The resultant exposures are dependent upon meteorological conditions, altitude of measurement and illumination conditions such as proportion of sunlight to skylight and the amount of "airlight" (the contribution to exposure by illumination scattered to the sensor by the atmosphere beneath the satellite). These effects are depicted in Figure 6-35.

All of these effects can be approximately coupled into three parameters for a given spectral band: α, α', and β. The parameter α is proportional to atmospheric transmittance and total (sunlight + skylight) irradiance; α' is proportional to atmospheric transmittance and skylight irradiance; and β is proportional to the amount of air light in the scene. The exposure in sunlight, E, for an object with reflectance R is

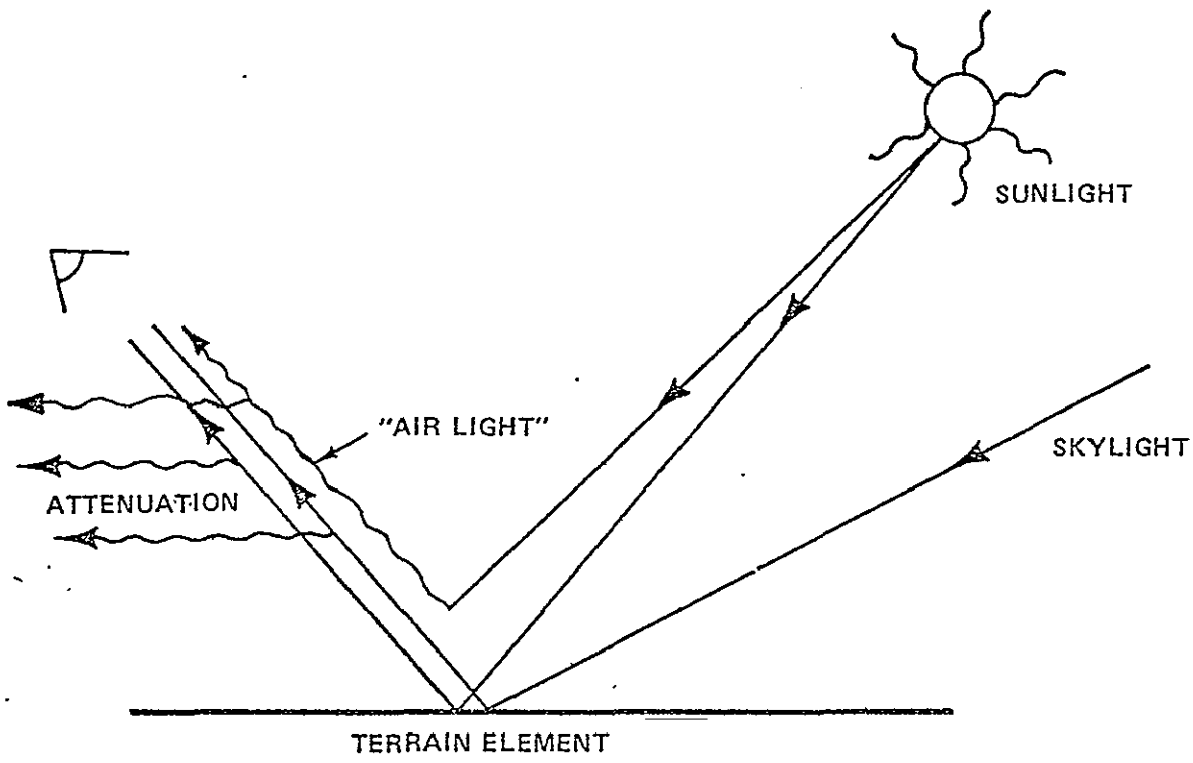

Figure 6-35 ATMOSPHERIC AND ILLUMINATION EFFECTS INVOLVED IN ESTABLISHING EXPOSURE OF A TERRAIN ELEMENT

$$E = \alpha R + \beta \ , \qquad (6\text{-}1)$$

while the exposure of the same object in shadow, E', is

$$E' = \alpha' R + \beta \qquad (6\text{-}2)$$

Measurements of terrain reflectance thus requires knowledge of α , α' and β in each sensor spectral band. These parameters can be determined in a straightforward manner using a shadow calibration procedure called the Scene color Standard (SCS) technique.

Calibration is accomplished by densitometry of the illumination discontinuities at shadow edges.[21] It is convenient to write $\alpha = \delta + \alpha'$ with δ a term proportional to solar irradiance only. The discontinuity measured at shadow edges on two different terrain elements then determines β and δ / α' as follows.

In the sunlight just outside a shadow the exposure, E, is

$$E = (\delta + \alpha') R + \beta \qquad (6\text{-}3)$$

The R is the terrain reflectance. Just inside the shadow the exposure E' is given by Eq. (6-2). Eqs. (6-2) and (6-3) yield

$$E = (1 + \frac{\delta}{\alpha}) E' - \beta \frac{\delta}{\alpha'} \qquad (6\text{-}4)$$

Eq. (6-4) is a linear relationship between E and E' with slope $(1 + \frac{\delta}{\alpha'})$ and intercept $-\beta \frac{\delta}{\alpha'}$. Two similarly oriented shadows determine the slope and intercept, and hence β and $\frac{\delta}{\alpha'}$. In practice a number of shadows are analyzed, and a least squares fit is made to the data.

The atmospheric conditions have now been determined. One aspect remains -- that of establishing an absolute level of reflectance, akin to laboratory use of a MgO standard or its equivalent. A tar or sheet asphalt scene element in sunlight (roadway, roof) is usually used to establish the value of α and complete the calibration.

These elements are used as: (1) their reflectances are spectrally flat; (2) their reflectance remains constant to good approximation over the year; and (3) their reflectance can be easily estimated or measured. Other objects more appropriate for a particular image can, of course, be used.

The SCS technique was applied to several frames of ERTS-A imagery. An example of calibration using terrain shadows is given in Part a of Figure 6-36, a print of Band 6 (IR) ERTS MSS image of Antarctica taken 14 February 1973. Some typical shadows used for calibration are depicted by arrows on the figure. About twelve shadows were used in the calibration, although easily fifty shadows could be found and so utilized. The reflectance of the snow was established at 70% and used as the standard in this case.

Figure 6-37 displays the linear fit to sunlight and shadow exposures for the Antarctica scene. The parameters beta and illumination ratio show that the atmospheric component of radiance at the satellite is equivalent to a 7% scene reflector, and that the ratio of sunlight to skylight irradiance is 3.2. Equivalent atmospheric flare of 7% means that a perfectly black object (zero reflectance) would appear to be a 7% reflector, a true 5% reflector would appear as a 12% reflector, etc.

The snow covered areas in the scene are regions of 70% reflectance. Even for these bright areas, 10% of the scene radiance is due to atmospheric flare. The rocky peaks are measured from the ERTS image to have a 17% reflectance so that over 40% of the apparent radiance is due to atmospheric flare. ERTS investigators using the multispectral characteristics of scene objects clearly must take great care to remove the effects of atmospheric flare from their data before analyses.

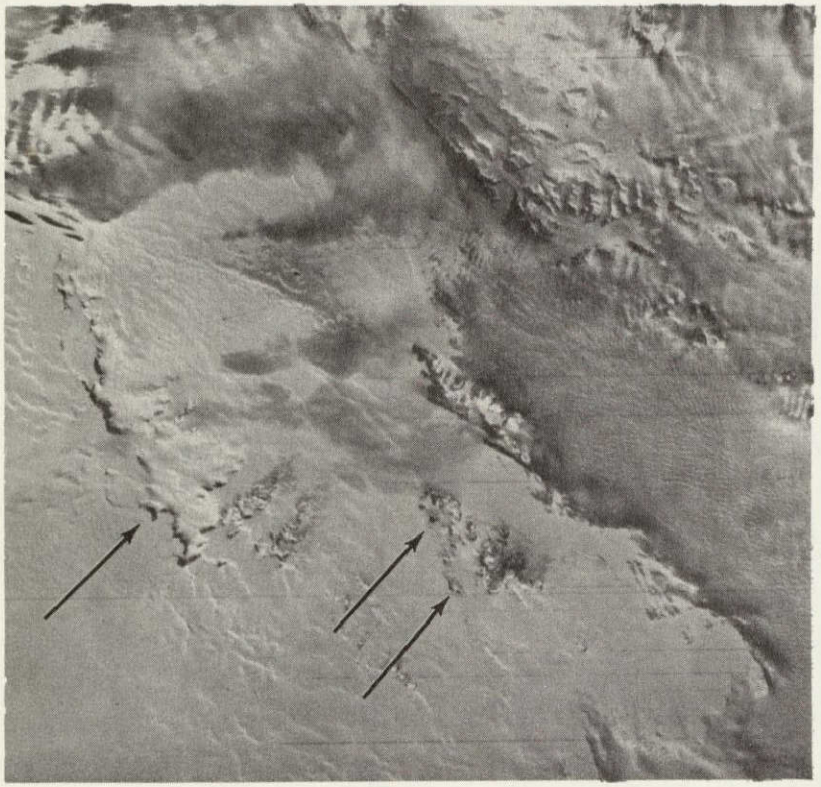

(a) BAND 6 - ANTARTICA
(TERRAIN SHADOWS)

(b) BAND 6 - LAKE ONTARIO
(CLOUD SHADOWS)

Figure 6-36 ERTS MSS IMAGERY USED TO DEMONSTRATE RADIOMETRIC CALIBRATION

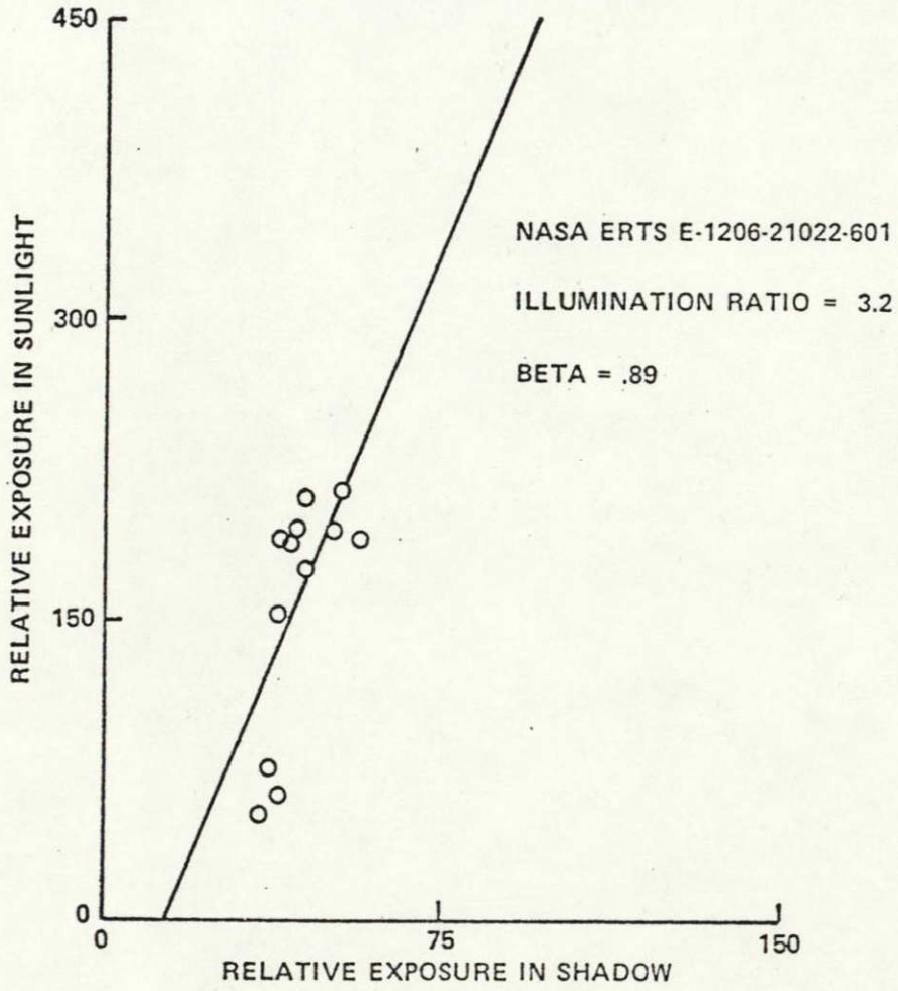

Figure 6-37 RELATIONSHIP BETWEEN SENSOR RADIANCE IN SUN AND SHADOW FOR BAND 6 OF ANTARTICA SCENE

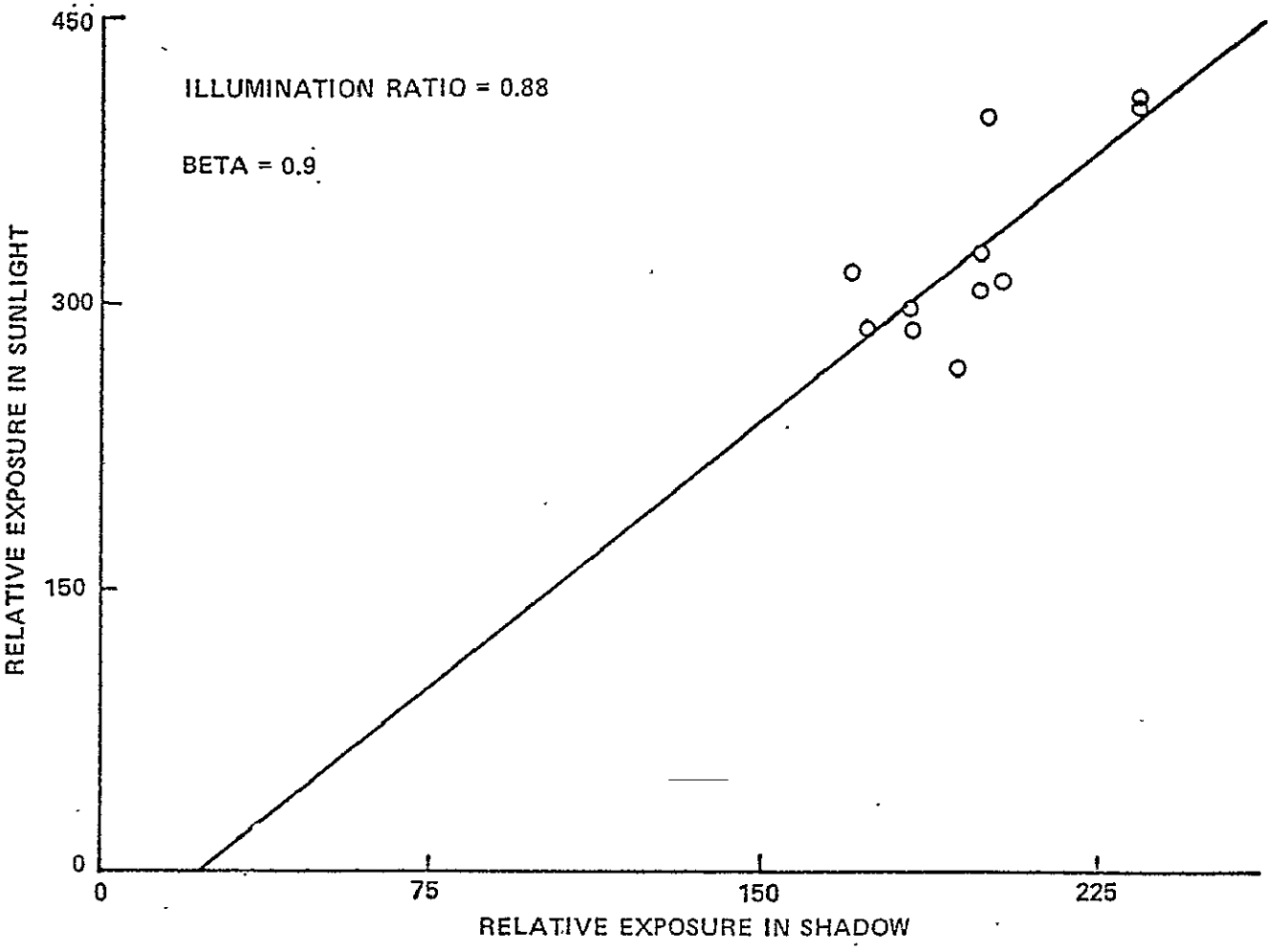

Figure 6-38 RELATIONSHIP BETWEEN SENSOR RADIANCE IN SUN AND SHADOW FOR BAND 4 OF LAKE ONTARIO SCENE

SECTION 7

CONCLUSIONS AND RECOMMENDATIONS

In order to predict image data system performance and evaluate product quality a new technique was developed, implemented and demonstrated using the NASA Data Processing Facility (NDPF). The technique has wide potential application, not only in quality control, but in system design and performance prediction.

Quality was defined as the limiting accuracy in estimating information from an output product in terms of the Cramer-Rao error bound. An Image Data System Simulation (IDSS) software program was written to compute this error bound in terms of accepted system element performance descriptors. The development and implementation of this technique are major results of the study. Insights into quality control requirements for the NDPF are also among the significant results.

7.1 NDPF Quality Control Requirements

As a result of the application of the IDSS program to the NDPF requirements for quality control were reviewed. These requirements are discussed below in terms of OTF monitoring and photographic processing control

7.1.1 OTF Monitoring

The sensitivities of estimation errors to changes in spread function widths have been shown to be quite small. Changes of fifty percent are possibly tolerable, changes of twenty percent are certainly tolerable. Since the increase in spread function width is manifested in frequency space as an equal fractional decrease in OTF cutoff frequency, rough methods for detecting changes in cutoff frequency are adequate. Resolution targets, accepting the variability inherent in the human element, can be used and are recommended because of the speed of diagnosis and relatively simple operator task involved.

In addition, an edge gradient spectrum computation program has been written (Appendix D) and can be used in diagnosis. Edge target signals can be generated electronically and used as input to the EBR. These targets can be measured on an output (3rd generation) product to define the quasi-linear region of signal input as demonstrated in Section 6.2. Under nominal conditions the NDPF is linear over a signal range at least from 0.2 to 0.8 normalized radiance. Measurements of these targets on intermediate products will permit the assessment of the frequency degradation for each stage.

If the system is constrained to nominal (Handbook) performance, the edge gradient procedure can also be applied to traces of ground objects to yield the overall system frequency response. When the system behaves linearly, changes in the sensor OTF can thus be remotely monitored.

Most of the spatial frequency or resolution degradation occurs prior to production of the archival copy, i.e. at the spacecraft sensors. Improvement in sensor OTF will produce an improvement in product quality. With improved sensor performance, the need to monitor system OTF will become more significant.

7.1.2 Photographic Processing Control

The simulation results showed the estimation errors to be highly sensitive to changes in H-D curve γ. Deviations of less than 10% in γ decreased product "quality" by a factor of two. The shape of the individual processing element H-D curves must therefore be as tightly controlled as is possible. Current quality control procedures measure the H-D curves and routinely perform a polynominal fit to the measured data. However, the entire curve is not observed, rather the values of only certain selected points are checked.

It is recommended that the complete curve be monitored. A graphics output could be attached to the computer which currently performs the polynomial fit, or if that is not feasible, a programmable desk calculator with graphic output could be substituted for the computer in this application. In any event, the results show that it is essential that the entire H-D curve be constrained to remain within tight bounds if the loss in quality and departure from linearity is to be avoided.

It would also be useful to monitor composite γ; that is, to plot third generation density against the log of the EBR input signal. Measurements could be made on the fifteen step calibration grey scale. The composite γ should, of course, equal minus one, and the shape of the curve should be very nearly a straight line over the input signal range. Since the input signal that generates the grey scale does not change with time, it would only be necessary to measure third generation density. Plotting and mathematical processing could easily be accomplished with a programmable desk calculator equipped with a plotter attachment.

7.2 Potential Radiometric Calibration Procedure

Output product transmission cannot be related to ground reflectance correctly unless atmospheric and payload optics contamination scattering effects can be compensated. The SCS technique described in Section 6.8 could be applied, either by the user, or perhaps at the NDPF to obtain relative reflectance values from transmission measurements. A reflectance standard on the ground would be required to relate the relative scale thus obtained to absolute values. The precision with which this technique can be applied to ERTS imagery has not been fully established, and additional empirical work would be required before an estimate of the error in ground reflectance can be given.

7.3 Comments on User "Optimality"

The variances given by the Cramer-Rao bound as applied to the ERTS NDPF quality control problem characterize the estimation error that would be obtained by using an optimal information extraction procedure. It is likely that the errors actually obtained by most users will not be as small as these.

The term "optimal" has been used in a strict communication theoretical sense. That the user's equipment is working properly, he uses the calibration grey scale properly, etc. is taken for granted. It is implicit that the user has a priori knowledge of the type of object he intends to observe and that he has knowledge of the system performance, and noise spectrum. Unless his detection technique makes use of this knowledge, the estimation errors predicted by the Cramer-Rao bound will not be achieved.

7.4 NDPF Nominal Product Quality

The IDSS program was used to evaluate the nominal quality of the NDPF 3rd generation imagery, a primary ERTS product. The quality assessment summarized here depends on the absolute accuracy of the data base supplied as hypothesis by NASA. Although we cannot stipulate the accuracy of that data, we state the product quality deduced for completeness. Quality was measured in terms of the limiting errors in estimating target apparent radiance, size and location. The percentage error in both the metric and radiometric measurements exhibited the expected variation with target size showing a rapid increase for widths less than 120 meters. For widths greater than 120 meters the target size measurement errors varied from 2% to 30% and target apparent radiance measurement errors from 0.5% to 3.5% depending upon target size and contrast. The radiometric accuracy due to large scale effects (e.g. EBR non-uniformity, printer shading, film sensitivity variations, etc.) is

stated to be 5% in the Data Users Handbook. Thus the ability to measure the transmittance of the photographic product and knowledge of the transmittance to apparent radiance calibration curve have about the same magnitude errors. For the larger targets the imprecise knowledge of the calibration curve could limit the radiometric accuracy if the user employs near "optimum" measurement techniques.

7.5 Recommendations

As a result of this study the following recommendations are made.

(1) More complete monitoring of the NDPF film processing functions should be developed.

(2) The use of the shadow-sunlight measurement technique for radiometrically calibrating ERTS imagery should be studied to establish its utility and accuracy.

(3) Application of the technique developed under this study to other image data system design/analysis problems ought to be considered.

REFERENCES

1. NDPF Familiarization Technical Conference, September 12, 13, 1972; Personal communication with B. Peavey (Contract Technical Monitor, NASA Goddard SFC), R. Johnson (Bendix Corp.), T. Rossi (General Electric Corp.).

2. "NASA Earth Resources Technology Satellite Data Users Handbook," General Electric, Dept. 71-SD-4249 (1972).

3. The paragraph in which reference 3 appeared has been subsequently deleted.

4. Hamilton, J.F., Lawton, W.H. and Trabka, E.A. "Some Spatial and Temporal Point Processes in Photographic Science" in Stochastic Point Processes: Statistical Analysis, Theory and Applications, P.A.W. Lewis, Editor (Wiley, New York, 1972), pp 817-867.

5. Lawton, W., Trabka, E.A. and Wilder, D.R., "Crowd Emulsions: Granularity Theory for Multilayers", J. Opt. Soc. Am., Vol. 62, pp. 659-667, May 1972.

6. Castro, P.E., Kemperman, J.H.B., and Trabka, E.A. "Alternating Renewal Model of Granularity" J. Opt. Soc. Am. Vol. 63, pp. 820-825, July 1973.

7. Mazurowski, M.J., Hammill, H.B., Snider, G.H., "A Study of Image Quality Evaluation," Cornell Aeronautical Laboratory, Inc., November 1963.

8. Granger, E.M. and Cupery, K.N., "An Optical Merit Function (SQF), which Correlates with Subjective Image Judgments," Photographic Science and Engineering, Volume 16, Number 3, May-June 1972.

9. Scott, F., "The Search for a Summary Measure of Image Quality--A Progress Report," Photographic Science and Engineering, Volume 12, Number 3, May-June 1968.

10. Jones, R.A., "Investigation of Image Simulation Procedures," Photographic Science and Engineering, Volume 13, Number 1, January-February 1969.

11. Barnard, T.W., "Image Evaluation by Means of Target Recognition," Photographic Science and Engineering, Volume 16, Number 2, March-April 1972.

12. Kinzly, R.E., Mazurowski, M.J., "Project Slope - A Study of Lunar Orbiter Photographic Evaluation Techniques, Implementation and Accuracy," Cornell Aeronautical Laboratory, Inc., April 1967.

13. Kinzly, R.E., Mazurowski, M.J. and Holladay, T.M., "Image Evaluation and Its Application to Lunar Orbiter," Applied Optics, Volume 7, Number 8, August 1968, pp. 1577.

14. Van Trees, H., "Detection, Estimation and Modulation Theory - Part I," Wiley (1968).

15. O'Neill, E., Introduction to Statistical Optics, Addison-Wesley Publishing Co., 1963.

16. Trabka, E.A., "Wiener Spectrum of Scans Obtained from an Isotropic Two-Dimensional Random Field," J. Opt. Soc. Am. Vol. 55, Number 2, February 1965, pp. 203.

17. Jankc, E. and Ende F., Tables of Functions, Dover Publications, 1945, 4th Ed., p. 211.

18. Yeadon, E.C., Jones, R.A., "Advanced Contact Printing Final Report," Tech. Report AFAL-TR-69-254 (1969).

19. ERTM-H-81, "Bulk Processing Modulation Transfer Function".

20. Shaffner, R.M., "The Earth Resources Technology Satellite Photographic Facility Quality Control Program", Image Technology, Volume 15, Number 3 and 4, April/July 1973, p. 19-23.

21. Piech, K.R., and Walker, J.E., "Aerial Color Analyses of Water Quality," Journal of the Surveying and Mapping Division, ASCE, Volume 97, No. SU2, November 1971, pp. 185-197.

22. Piech, K.R., and Walker, J.E., "Thematic Mapping of Flooded Acreage," Photogrammetric Engineering, Volume 38, November 1972, pp. 1081-1090.

23. Piech, K.R., "International Field Year on the Great Lakes: Optical Properties of Lake Ontario Waters," Calspan Corporation Report No. KS-5108-M-1, November 1972.

BIBLIOGRAPHY

General

Born, M., Wolf, E., "Principles of Optics," Pergamon Press, 1964.

Goodman, J. W., "Introduction to Fourier Optics, McGraw-Hill, 1968.

Klemperer, O., "Electron Optics," Cambridge University Press, 1953.

Mees, C. E. K., James, T. H., "The Theory of the Photographic Process," MacMillan Co., 1966.

Van Trees, H. L., "Detection, Estimation, and Modulation Theory," John Wiley and Sons, Inc., 1968.

Users Requirements

Anderson, J. R., "Land-Use Classification Schemes," Photogrammetric Engineering, 1971.

Anuta, P. E., "Spatial Registration of Multispectral and Multitemporal Digital Imagery Using Fast Fourier Transform Techniques," IEEE Transactions on Geoscience Electronics, Vol. GE-8, No. 4, October 1970.

Barnes, J. C., Chang, D. T., and Willand, J. H., "Image Enhancement Techniques for Improving Sea-Ice Depiction in Satellite Infrared Data," Journal of Geophysical Research, Vol. 77, No. 3, January 20, 1972.

Belcher, D. J., "Potential Benefits to be Derived from Applications of Remote Sensing or Agricultural, Forest, and Range Resources," Center for Aerial Photographic Studies, Cornell University, Ithaca, New York, December 1967.

Bodechtel, J. and Kritikos, G., "Quantitative Image Enhancement of Photographic and Non-Photographic Data for Earth Resources," Seventh International Symposium on Remote Sensing of Environment, Vol. 1, May 1971.

Braunwarth, C. A., Tuttle, J. C., and Eifert, C. R., "Operational Capabilities of a Manned Space Station for Earth Resources Observation," AIAA 9th Aerospace Sciences Meeting, New York, New York, January 25-27, 1971, AIAA Paper No. 71-75.

Colvocoresses, A. P., "ERTS-A Satellite Imagery," Photogrammetric Engineering, Vol. 36, June 1970.

"Ecological Surveys from Space," National Aeronautics and Space Administration, Washington, D. C. 1970.

Estes, J. E., and Golomb, B., "Oil Spills: Method for Measuring Their Extent on the Sea Surface," Science, Vol. 169, August 14, 1970.

Egan, W. G., and Hair, M. E., "Automated Delineation of Wetlands in Photographic Remote Sensing," Seventh International Symposium on Remote Sensing of the Environment, Vol. III, May 1971.

"EREP User's Handbook," National Aeronautics and Space Administration, March 1971.

Eyre, A. E., "High-Altitude Color Photos," Photogrammetric Engineering, Vol. 37, November 1971.

Fischer, W. A., "Projected Uses of Observations of the Earth from Space--The Eros Program of the Department of the Interior," AIAA Earth Resources Observations and Information Systems Meeting, Annapolis, Maryland, March 2-4, 1970, AIAA Paper No. 70-332.

Haas, I. S., "ERTS Remote Sensor Data Processing - The Key to a Space Application," AIAA Space Systems Meeting, Denver, Colorado, July 19-20, 1971, AIAA Paper No. 71-839.

Hall, D. J., Endlich, R. M., Wolf, D. E., and Brain, A. E., "Objective Methods for Registering Landmarks and Determining Cloud Motions from Satellite Data," Proc. 2-D Signal Processing Conf. IEEE, October 1971.

Harmon, L. D. and Knowlton, K. C., "Picture Processing by Computer," Science, Volume 164, Number 3875, April 1969.

Hart, E. and Gutlove, N., "Earth Resources National Data Processing Center: Why, What, When, How Much?" AIAA Earth Resources Observations and Information Systems Meeting, Annapolis, Maryland, March 2-4, 1970, AIAA Paper No. 70-324.

Hieronymus, W. S., "Resource Satellite Effort Spurred," Aviation Week and Space Technology, November 17, 1969.

Houseman, E. E., "Remote Sensors--A New Data Source for Agricultural Statistics," AIAA Earth Resources Observations and Information Systems Meeting, Annapolis, Maryland, March 2-4, 1970, AIAA Paper No. 70-312.

Katz, A. H., "Let Aircraft Make Earth-resource Surveys," Astronautics and Aeronautics, June 1969.

Kawamura, J. G., "Automatic Recognition of Changes in Urban Development from Aerial Photographs," IEEE Transaction on Systems, Man, and Cybernetics, Vol. SMC-1, No. 3 July 1971.

Kracht, J. B., and Howard, W. A., "Applications of Remote Sensing Aerial Photography, and Instrumented Imagery Interpretation to Urban Area Studies," Council of Planning Librarians Exchange Bibliography, December 1970.

Klass, P. J., "Data System to Serve Variety of Users," Aviation Week and Space Technology, July 31, 1972.

Krumpe, P. F., Deselm, H. R., and Amundsen, C. C., "The Delineation of Forest Cover and Site Parameters by Multiband Remote Sensing," Proc. of Society of American Photogrammetry, 1971.

"Land Use Classification with Simulated Satellite Photography," U. S. Department of Agriculture, Washington, D. C., April 1971, Agriculture Information Bulletin No. 352.

Layton, J. P., "Proceedings of the Princeton University Conference on Aerospace Methods for Revealing and Evaluating Earth's Resources," The Princeton University Conference, Princeton, N. J., June 1970.

Lent, J. D. and Nichols, J. D., "Machine-Aided Photo Interpretation Techniques for Vegetation Analysis," Vol. 7, No. 11 Presented as Paper 70-308 at the AIAA Earth Resources Observations and Information Systems Meeting, Annapolis, Maryland, March 2-4, 1970.

Lindgren, D. T., "Dwelling Unit Estimation with Color-IR Photos," Photogrammetric Engineering, Vol. 37, April, 1971.

Lowman, P. D. Jr., "Geologic Orbital Photography: Experience from the Gemini Program," Photogrammetria, V. 24, p. 77-106, 1969.

Lowman, P. D. Jr., "Apollo 9 Multispectral Photography: Geologic Analysis," Goddard Space Flight Center, September 1969.

Lowman, P. D. Jr., and Tiedemann, H. A., "Terrain Photography from Gemini Spacecraft: Final Geologic Report," Goddard Space Flight Center, January 1971.

Mallon, H. J., "Experimental Applications of Multispectral Data to Natural Resource Inventory and Survey," Seventh International Symposium on Remote Sensing of Environment, Vol. II, May 1971.

Miroshnikov, M. M., Karizhenskiy, Ye Ya, Shilin, B. V., and Gusev, N. A., "Theory and Experiment--Thermal Infrared Imaging in Aerial Surveys of Natural Resources," Soviet J. of Optical Technology Vol. 38, No. 3, March 1971.

Munday, J. C., Jr., MacIntyre, W. G., and Penney, M. E., "Oil Slick Studies using Photographic and Multispectral Scanner Data," Seventh International Symposium on Remote Sensing of Environment, Vol. II, May 1971.

Musgrove, R. G., "Photometry for Interpretation," Photogrammetric Engineering, Vol. 37, October 1969.

Nunnally, N. R., "Remote Sensing for Land-Use Studies," Photogrammetric Engineering, Vol. 36, May 1970.

Robinove, C. J., "Future Applications of Earth Resource Surveys from Space," AIAA Earth Resources Observations and Information Systems Meeting, Annapolis, Maryland, March 2-4, 1970, AIAA Paper No. 70-302.

Sapp, C. D., "Applications of Space and High Altitude Photography to Interior Department Functions," Proc. of American Society of Photogrammetry, 1971.

"Second Annual Earth Resources Aircraft Program Status Review," National Aeronautics and Space Administration, Volume I, Geology and Geography, September 16-18, 1969.

"Second Annual Earth Resources Aircraft Program Status Review," National Aeronautics and Space Administration, Volume III, Hydrology and Oceanography, September 16-18, 1969.

"Second Annual Earth Resources Aircraft Program Status Review," National Aeronautics and Space Administration, Volume II, Agriculture/Forestry, and Sensor Studies, September 16-18, 1969.

"Second International Geoscience Electronics Symposium -- Digest of Technical Papers," IEEE, Washington, D. C. April 14-17, 1970.

Smith, E. A., and Phillips, D. R., "Automated Cloud Tracking using Precisely Aligned Digital ATS Pictures," Proc. 2-D Digital Signal Processing Conf., IEEE, October 1971.

Smith, J. T., Jr., "Oil Slick Remote Sensing," Photogrammetric Engineering, Vol. 37, December 1971.

Strickland, Z., "Experiments Have Global Scope," Aviation Week and Space Technology, July 31, 1972.

Su, M. Y., and Krause, F. R., "Automatic Processing of Multispectral Observations," AIAA Integrated Information Systems Conference, Palo Alto, California, February 17-19, 1971, AIAA Paper No. 71-234.

Tomlinson, R. F., "Geographical Data Handling," International Geographical Union Commission on Geographical Data Sensing and Processing (No No.), Vol. 1 and 2, 1972.

Tueller, P. T., and Lorain, G., "Environmental Analysis of the Lake Tahoe Basin from Small Scale Multispectral Imagery," Seventh International Symposium on Remote Sensing of Environment, Vol. I, May 1971.

Vette, J. I., and Karlow, N., "Data Management at the National Space Science Data Center," AIAA Earth Resources Observations and Information Systems Meeting, Annapolis, Maryland, March 2-4, 1970, AIAA Paper No. 70-320.

Walsh, D., "Space Oceanography," U. S. Naval Institute Proc., February 1969.

Welch, R., "Analysis of Image Definition," Photogrammetric Engineering, Vol. 37, December 1969.

Wobber, F. J., "The ERTS Program," Photographic Applications in Science, Technology and Medicine, November 1972.

Yost, E., and Wenderoth, S., "Remote Sensing of Coastal Waters Using Multispectral Photographic Techniques," Long Island University, 1 January 1970, Technical Report SERG-TR-10.

Image Analysis and Modelling

Arguello, R. and Sellner, H., "Optimal Processing Bandwidth for Optical Transfer-Function Compensation," Photographic Science and Engineering, Volume 15, Number 4, July-August 1971.

Ausfresser, H. D., Johnson, A. C. and Kowalski, R. A., "Computer Correction of Distortion in ATS-SSCC Photographs," Bulletin American Meteorological Society, Vol. 50, No. 2, February 1969.

Baker, A. and Korff, D., "Fourier Analysis and Nonlinear Optical Systems," Applied Optics, Vol. 8, No. 3, March 1969.

Becherer, R. J., and Parrent, G. B. Jr., "Nonlinearity in Optical Imaging Systems," Journal of the Optical Society of America, Volume 57, Number 12, December 1967.

Berg, W. F., "The Photographic Emulsion Layer as a Three-Dimensional Recording Medium," Applied Optics, Vol. 8, No. 12, December 1969.

Bloss, W. H., Lohnert, G. H., and Schneider, R. T., "Photoelectric Restoring System for Images Degraded by Atmospheric Turbulence," Electronics Letters, Vol. 4, No. 14, July 1968.

Braga-Illa, A., "Resolution and Frequency Response in Secondary Emission Devices," IEEE Transactions on Electron Devices, Vol. ED-14, No. 12, December 1967.

Carroll, J. P. and Cupery, K.N., "Objective Measurement of Resolution in Film Images," Applied Optics, Vol. 10, No. 10, October 1971.

Chambers, R. P. and Courtney-Pratt, J. S., "Experiments on the Detection of Visual Signals in Noise Using Computer-Generated Signals," Photographic Science and Engineering, Volume 13, Number 6, November-December 1969.

Colvocoresses, A. P. "Image Resolutions for ERTS, SKYLAB, and GEMINI/APOLLO," Photogrammetric Engineering, 1972.

Diamantides, N. D., "Correlation Measure of Contrast for Map Matching," Journal of the Optical Society of America, Vol. 58, Number 7, July 1968.

Dilworth, D. C., "Fast MTF Calculation in the Presence of Diffraction," Applied Optics, Vol. 11, No. 5, May 1972.

Ericson, R. H. and Marchant, J. C., "RMS Granularity of Monodisperse Photographic Emulsions," Photographic Science and Engineering, Volume 16, Number 4, July-August 1972.

Foreman, J. W. Jr., Hunt, G. H., and Lawson, E. K., "Images of Truncated One-Dimensional Periodic Bar Targets in Aberration-Limited Optical Systems," Applied Optics, Vol. 10, No. 1, January 1971.

Gaven, J. V., Jr. and Tavitian, J., "The Informative Value of Sampled Images as a Function of the Number of Gray Levels Used in Encoding the Images," Photographic Science and Engineering, Volume 14, Number 1, January-February 1970.

Gaven, J. V., Jr., Tavitian, J., and Hollanda, P. A., "Relative Effects of Gaussian and Poisson Noise on Subjective Image Quality," Applied Optics, Vol. 10, No. 9, September 1971.

Ghosh, S. K., "Deformations of Space Photos," Photogrammetric Engineering, 1972.

Gilmore, H. F., "Factors Influencing the Growth of Small Photographic Images," Journal of the Optical Society of America, Volume 58, Number 10, October 1968.

Goddard, M. C. and Gendron, R. G., "An MTF Meter for Film," Photographic Science and Engineering, Volume 13, Number 3, May-June 1969.

Gogolev, Y. A., "Orientation Erros in Panoramic Aerial Photographs and their Influence on the Resolving Power of Photographic Systems," Society Journal of Optical Technology, Vol. 34, No. 4, July-August, 1967.

Goede, W. F., "Performance Differences Between Cathode-Ray Tubes and DOT Matrix Displays."

Goodman, J. W., Miles, R. B., and Kimball, R. B., "Comparative Noise Performance of Photographic Emulsions in Holographic and Conventional Imagery," Journal of the Optical Society of America, Volume 58, Number 5, May 1968.

Helstron, C. W., "Resolvability of Objects from the Standpoint of Statistical Parameter Estimation," Journal of the Optical Society of America, Volume 60, Number 5, May 1970.

Higgins, G. C., "Methods for Analyzing the Photographic System, Including the Effects of Nonlinearity and Spatial Frequency Response," Photographic Science and Engineering, Volume 15, Number 2, March-April 1971.

Hollanda, P. A., Scott, F., and Harabedian, A., "The Informative Value of Sampled Images as a Function of the Number of Scans Per Scene Object and the Signal-to-Noise Ratio," Photographic Science and Engineering, Volume 14, Number 6, November-December, 1970.

Hugnagel, R. E., "Significance of the Phase of Optical Transfer Functions," Journal of the Optical Society of America, Volume 58, Number 11, November 1968.

Jansson, P. A., "Least-Squares Polynomial Filtering of Images by Convolution," Journal of the Optical Society of America, Volume 62, Number 2, February 1972.

Johnson, C. B., "A Method for Characterizing Electro-Optical Device Modulation Transfer Functions," Photographic Science and Engineering, Volume 14, Number 6, November-December 1970.

Jones, R. A., and Kelly, J. T., "Reliability of Image Evaluation Techniques," Applied Optics, Vol. 8, No. 5, May 1969.

Kornfeld, G. H. and Lawson, W. R., "Visual-Perception Models," Journal of the Optical Society of America, Volume 61, Number 6, June 1971.

Kumar, G. R. V., "Measurement of Optical Transfer Function by its Moments," Journal of the Optical Society of America, Volume 58, Number 10, October 1968.

Lamberts, R. L., "Optical-Path Variation in a Photographic Emulsion," Journal of the Optical Society of America, Volume 60, Number 10, October 1970.

Lauroesch, T. J., Fulmer, G. G., Edinger, J. R., Keene, G. T., and Kerwirk, T. F., "Threshold Modulation Curves for Photographic Films," Applied Optics, Vol. 9, No. 4, April 1970.

Levi, L., "Detector Response and Perfect-Lens-MTF in Polychromatic Light," Applied Optics, Vol. 8, No. 3, March 1969.

Limansky, I., "A New Resolution Chart for Imaging Systems," The Electronic Engineer, June 1968.

Macmillan, R. S. and Young, G. O., "Optimization of Information-Processing Optical Systems by Transcorrelation-Function Maximization," Journal of the Optical Society of America, Volume 58, Number 3, March 1968.

Nelson, C. N., "Prediction of Densities in Fine Detail in Photographic Images," Photographic Science and Engineering, Volume 15, Number 1, January-February 1971.

Nelson, C. N., "Photographic System as a Communication Channel," Applied Optics, Vol. 11, No. 1, January 1972.

Pollehn, H. and Roehring, H., "Effect of Noise on the Modulation Transfer Function of the Visual Channel," Journal of the Optical Society of America, Volume 60, Number 6, June 1970.

Pryor, P., "The Performance of Imaging Sensors Aloft," Astronautics and Aeronautics, September 1971.

Rabedeau, M. E., "Effect of Truncation of Line-Spread and Edge-Response Functions on the Computed Optical Transfer Function," Journal of the Optical Society of America, Volume 59, Number 10, October 1969.

Rindfleisch, T. C., Dunne, J. A., Frieden, H. J., Stromberg, W. D., and Ruiz, R. M., "Digital Processing of the Mariner 6 and 7 Pictures," Journal of Geophysical Research, Vol. 76, No. 2, January 10, 1971.

Rino, C. L., "Bandlimited Image Restoration By Linear Mean-Square Estimation," Journal of the Optical Society of America, Volume 59, Number 5, May 1969.

Rosenblum, L., "Image Quality in Aerial Photography," Optical Spectra, January-February, 1968.

Rushforth, C. K. and Harris, R. W., "Restoration, Resolution, and Noise," Journal of the Optical Society of America, Volume 58, Number 4, April 1968.

Scott, F., Hollanda, P. A., and Harabedian, A., "The Informative Value of Sampled Images as a Function of the Number of Scans per Scene Object," Photographic Science and Engineering, Volume 14, Number 1, January-February 1970.

Seats, P., "The Cathode-Ray Tube--A Review of Current Technology and Future Trends," IEEE Transactions on Electron Devices, Vol. ED-18, No. 9, September 1971.

Shaw, R., "Multilevel Grains and the Ideal Photographic Detector," Photographic Science and Engineering, Volume 16, Number 3, May-June 1972.

Shepp, A. and Kammerer, W., "Increased-Detectivity by Low Gamma Processing," Photographic Science and Engineering, Volume 14, Number 5, September-October 1970.

Singh, K. and Chopra, K. N., "Modulation of a General Periodic Object with Triangular Waveform by a Narrow Rectangular Aperture with Amplitude Filters," Applied Optics, Vol. 8, No. 8, August 1969.

Swerling, P., "Parameter Estimation Accuracy Formulas," IEEE Trans. on Information Theory, Vol. IT-10, October 1964.

Tokarski, J. M. J., "The Effect on the Hologram Record of a Nonlinear Relationship Between Amplitude Transmission and Exposure," Applied Optics, Vol. 7, No. 5, May 1968.

Toraldo, G., "Degrees of Freedom of an Image," Journal of the Optical Society of America, Volume 59, Number 7, July 1969.

Wasielewski, J. E., "Optical Filter Analysis as a Function of Nonoptimum Noise Conditions," Applied Optics, Vol. 10, No. 11, November 1971.

Wassle, H. and Heinrich, F., "Untersuchungen Zum Helligkeitskontrast," Vision Research.

Williams, R., "A Re-examination of Resolution Prediction from Lens MTF's and Emulsion Thresholds," Photographic Science and Engineering, Volume 13, Number 5, September-October 1969.

Wray, J. D., "Quantitative Analytic Composite Photography," The Astronomical Journal, Volume 75, Number 3, April 1970.

Yu, F. T. S., "Markov Photographic Noise," Journal of the Optical Society of America, Volume 59, Number 3, March 1969.

APPENDIX A
BACKGROUND INFORMATION

To provide background information for this study a number of surveys were performed at its onset. These included a detailed survey of the NASA Data Processing Facility (NDPF) operations to identify the image data flow, radiometric and geometric correction procedures, element performance specifications and quality control procedures. A survey of the state-of-the-art in image quality analysis and evaluation was made to identify potential measures of product quality and element performance descriptors. Finally a review of users' requirements for product quality was made. The information obtained form these surveys is contained in this appendix and summarized in the main body of this report.

A.1 NDPF DESCRIPTION

The information on NDPF operations was obtained from on-site visits, discussions with NASA personnel, NASA furnished documentation and the Data Users Handbook.

A.1.1 SUBSYSTEM ELEMENTS AND DATA FLOW

The initial task undertaken was identification of the NDPF subsystem elements and data flow. The only information source available initially was the NASA ERTS Data User's Handbook.[1] Subsequently, a conference[2] was held at Goddard SFC for the purpose of obtaining fundamental information for the study. In addition to the verbal information, copies of a number of NASA documents[3-24] and Bendix Corp. technical memos[25-34] were obtained. The information contained in some of these documents was not necessarily current. The User's Handbook[1] on the other hand is kept up to date; consequently, that documents plus verbal information received at the technical conference served as the major quantitative information source during the first phase of this study. However, some of the data contained in the Handbook is clearly idealized. The data were ultimately supplemented by measurements from ERTS data products.

Note: Superscript numbers refer to the References in Section A.4.

PRECEDING PAGE BLANK NOT FILMED

This survey was explicitly limited to consideration of the NDPF video to photographic output product conversion process. NDPF digital output products were excluded. The input to the NDPF is video tape recordings of telemetry from the ERTS payload. Payload and telemetry link elements are external to the NDPF. However, characterization of the video tape input will be found to enter the analysis of the NDPF per se and is given a priori.

A block diagram of the NDPF data flow is given in Figures A-1 to A-3. This block diagram served as a basis for system modeling. The following comments refer to the circled numbers in Figures A-1 to A-3.

The Return Beam Vidicon (RBV) (1) consists of three boresighted RCA vidicon systems in three different spectral bands. Radiometric and geometric calibration capability exists in the payload.

Radiometric Calibration Images (RCI's) consisting of white, gray, and black constant field illumination are taken before and after each sequence of exposures (10-15 minute period). These images are processed in the NDPF as if they were real scenes and consequently yield a radiance map that can be fed back into the system for updating the radiometric correction. Currently, the NDPF assumes that the camera radiometric response is slowly varying, hence the feedback or updating is applied to the processing of subsequent ground image sets, not to processing of the set corresponding in time to the particular calibration images.

Geometric correction is provided by analysis of a reseau fixed at each of the vidicon faceplates. The reseaus allow correction for geometric optical distortion and boresight errors. A record is being kept of individual camera relative position and distortion.

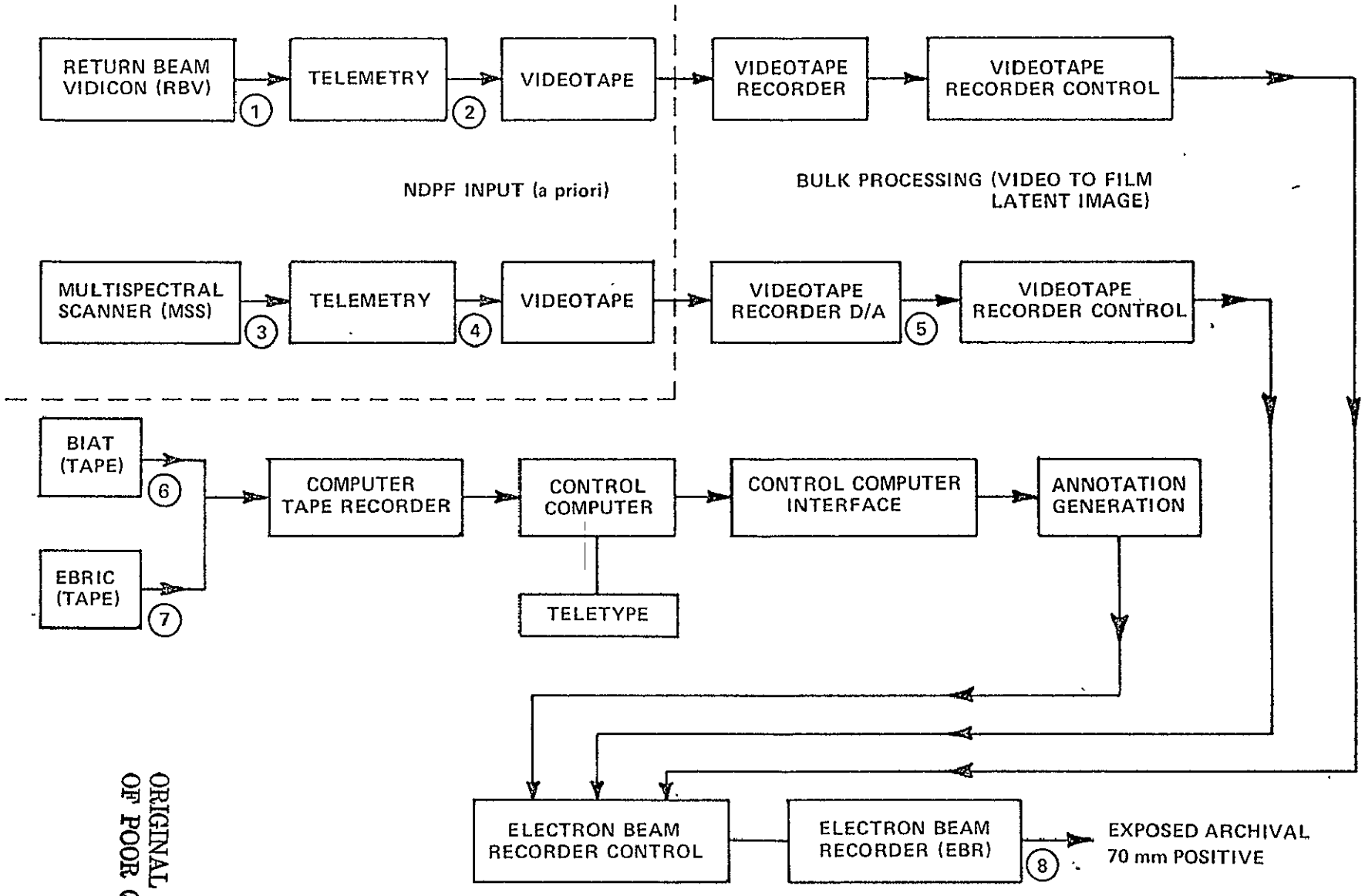

Figure A-1 NDPF DATA FLOW BLOCK DIAGRAM (PART 1)

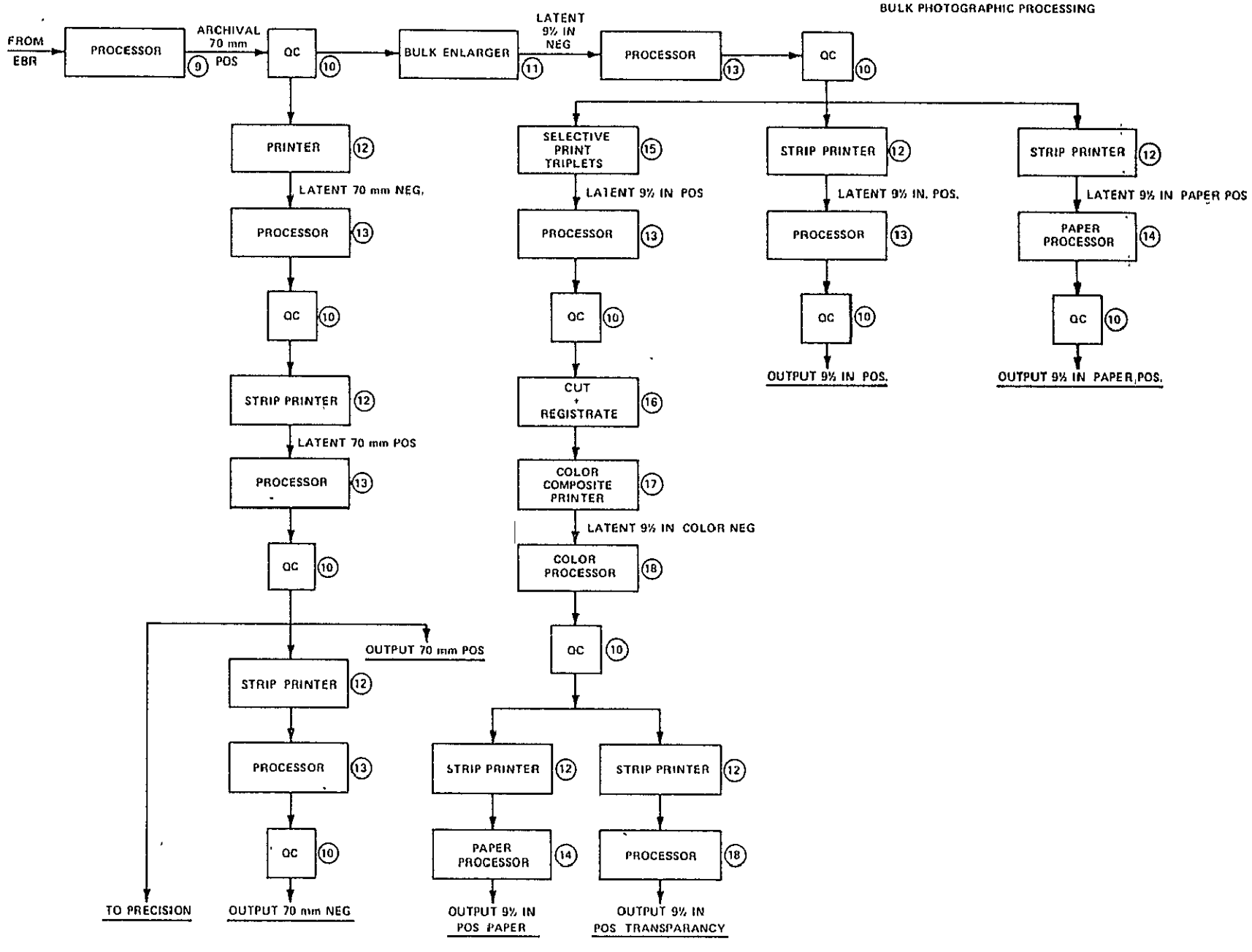

Figure A-2 NDPF DATA FLOW BLOCK DIAGRAM (PART 2)

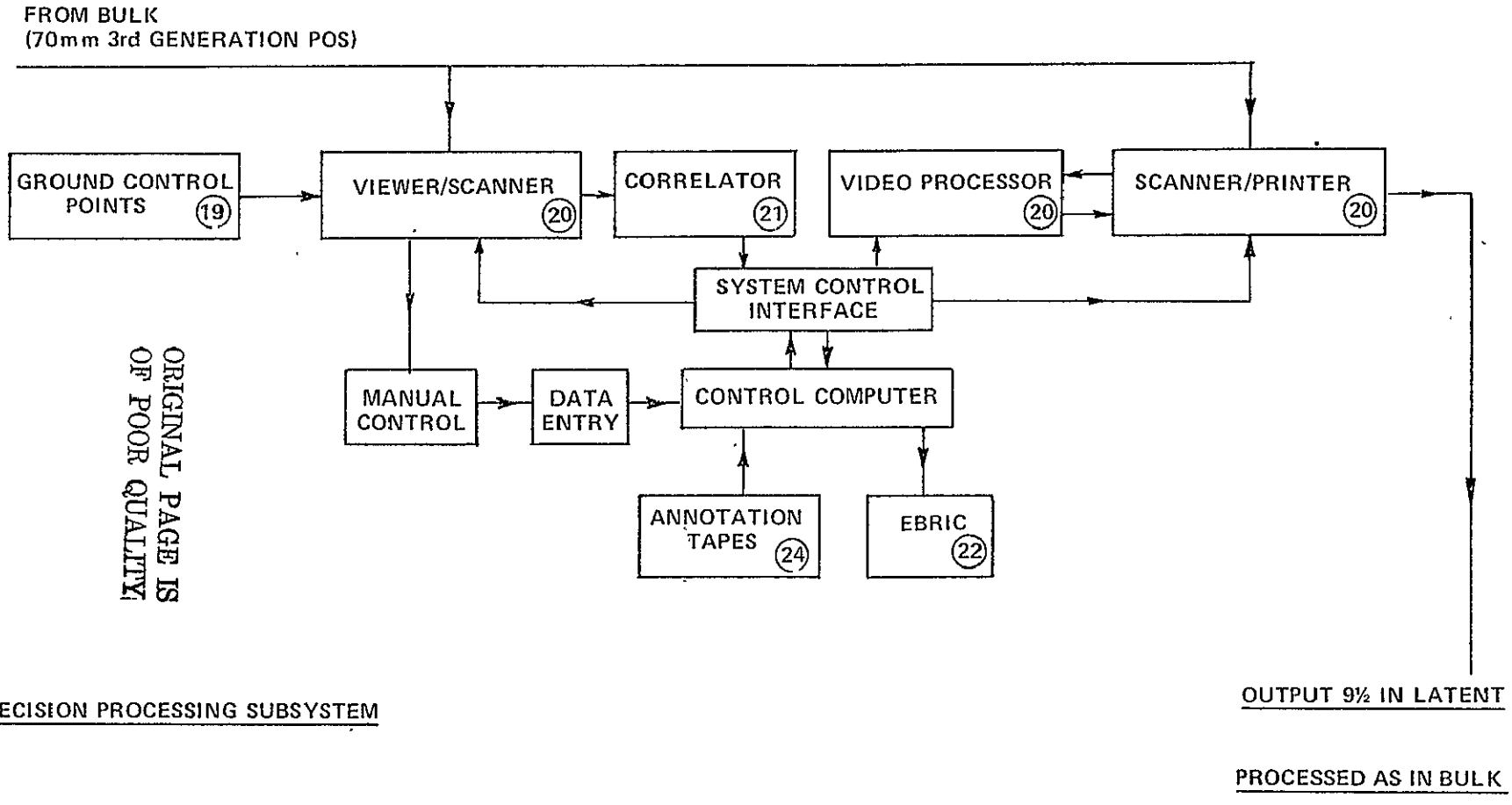

Figure A-3 NDPF DATA FLOW BLOCK DIAGRAM (PART 3)

The RBV telemetry (2) is analog with 3.5 mHz bandwidth. The signal to noise ratio on the videotape record is 12-13 db (Ref. 2). The three channels are exposed simultaneously, but broadcast sequentially. The band limit of the RBV videotape record is given in Figure A-4 (Ref. 1, p. A-5).

The Hughes Multispectral Scanner (MSS) (3) has four conjugate linear detector arrays, each in one spectral band. No geometric distortion is introduced by the instrument between the individual bands (registration), however a mapping error can be introduced. Two procedures take place in the payload for the purpose of radiometric calibration; a lamp provides a linear intensity wedge, and a pinhole image of the sun is passed over the array. The MSS telemetry (4) is digital with 16 MHz bandwidth. The error rate on the videotape is $1/10^5$ (Ref. 2). The band limit of the MSS videotape record is given in Figure A-5 (Ref. 1 p. A-13). MSS data is D/A converted (5) in the playback operation. Radiometric corrections are applied in the digital domain before conversion.

The Bulk Image Annotation Tape (BIAT) (6) generates tick marks, denotes the scene, and provides input for geometric correction for payload attitude. Attitude data are provided for nine points north to south across each frame. The frame format is divided by a nine by nine grid, and attitude correction is linear over each sector (only translation and rotation operations line by line within each sector). Attitude correction is the only geometric correction applied to MSS data. Attitude correction for RBV data is only part of the total geometric correction.

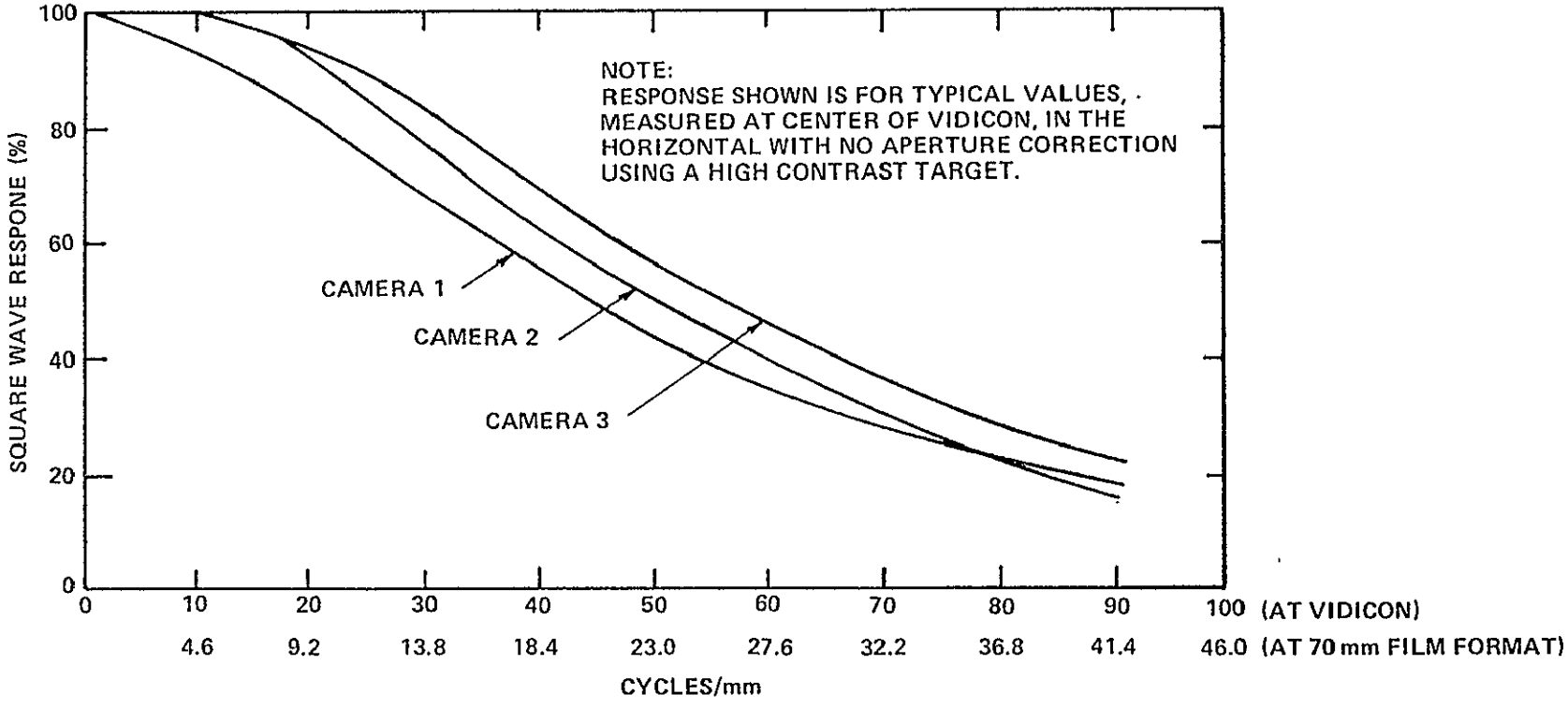

Figure A-4 MEASURED RBV SYSTEM SQUARE WAVE RESPONSE

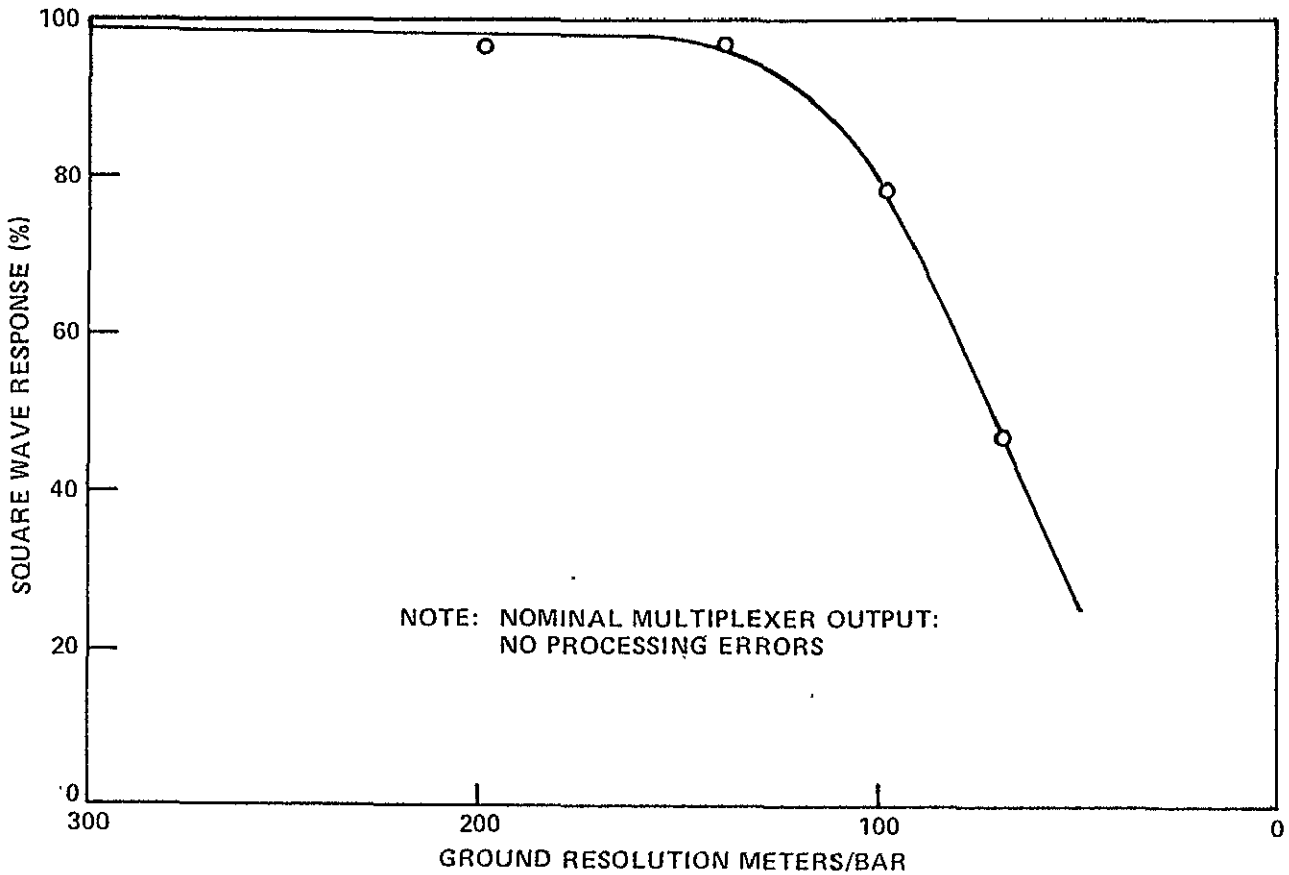

Figure A-5 MEASURED MSS SYSTEM SQUARE WAVE RESPONSE

The Electron Beam Recorder Image Correction (EBRIC) tape (7), provides input for radiometric and geometric correction of RBV imagery.

Radiometric correction data are derived from the Radiometric Calibration Images (RCIs) described in the comments on the RBV. The Bulk processed RCIs are taken to the Precision Processing Subsystem where EBRIC radiometric correction tapes are generated. These EBRIC tapes are subsequently applied to new Bulk imagery.

Geometric correction results from checking the reproduced reseaus in Precision. Comparison of the actual reseau coordinates with a priori knowledge results in generation of geometric correction coefficients for the EBRIC tape.

The only effect EBRIC tapes have on MSS imagery is correction for errors internal to the NDPF.

The Electron Beam Recorder (EBR) (8) produces all archival latent images. The film type used is Kodak SO-438 (Ref. 2). A fifteen step gray scale is put on each image.

The first processor (9) is a Kodak Versamat used only for processing archival images.

The quality control blocks (QC) (10) consist of standard Kodak chemistry quality control plus the placing of a special target on the head and tail of each roll processed. The target consists of a gray scale,

five equal constant density patches over the format, and a standard Air Force bar target in the frame center. The gray scale is read and a Hurter-Driffield (H-D) curve fit to the data points. The density values at two exposure levels are plotted and deviation from nominal values used as a processing quality criterion. The constant density is read at the five format positions to provide uniformity data. The Air Force tri-bar target allows determination of on axis resolution.

The Bulk Enlarger (11) is a modified Miller-Halzwarth

The Strip Printers (12) are Kodak Colorado printers.

The processors (13) are Kodak Versamats and the paper processor (14) is likewise a standard Kodak device.

The selective printing process (15) is a hand operation. Three Mark III printers are employed.

Registration (16) of color composites is accomplished by punching holes in the black and white transparencies and fitting these holes on locating pegs in the spectial Bendix Color Composite Printer (17). Registration accuracy is one pixel.

The color processing is done in a Kodak 1811 Versamat (18).

Ground control points (19) are provided by film chips cut from a contact print of a master plate.

The Viewer/Scanner, Video Processor, and Scanner Printer (20) are analog devices. The Viewer/Scanner image is digitized and the correlation (21) and fit takes place in the digital domain. The Precision Processing Subsystem generates either precision images or EBRIC tapes. No radiometric correction is performed on products in precision. The system is expected to meet geometric specifications but not radiometric specifications (due to the optical transfer functions of the various devices). Accuracy within each precision processed frame is two hundred feet with respect to ground control points. Absolute ground location accuracy is not specified.

The annotation tapes (24) provide tick marks and annotation for Universal Transverse Mercator (UTM) projection.

Input to precision results from cutting out selected second generation negatives, pasting them to a plastic sheet, and contact printing to produce a third generation positive.

The photographic processing subsystems have a .03ΔD capability (ΔD = photographic density error) but this precision inhibits throughput. Processing to $\gamma = -1$ is sought for the system as a whole (including the EBR as well). All film (except in the EBR) is Kodak SO-467. Chemistry is Kodak 641 or 2420.

A.1.2 BULK PRODUCT GEOMETRIC AND RADIOMETRIC CORRECTIONS

The ERTS Data Users Handbook (Ref. 1) discusses system performance including output product geometric and radiometric accuracy. Two types of geometric accuracy are quantified; mapping accuracy and spatial registration accuracy. The error sources are classified into three categories; errors external to the sensor, internal sensor errors and processing errors. Table A-1 summarizes the external and internal errors for both the RBV and MSS sensors. These

TABLE A-1 GEOMETRIC ERROR SOURCES

ERROR	rms magnitude (meters)	
	RBV	MSS
External Internal	723 1355	710 26
Net-NDPF Input	1536	710
Bulk Product-Mapping	766	743
Bulk Product-Registration	336	159

combine to yield the net error in the input signal to the NDPF. During the input video-to-film conversion corrections are applied to reduce the resulting error in the bulk image products. These corrections are partially negated by degradations introduced by the NDPF. In addition, the NDPF does not attempt to correct for all of the input error sources; specifically external sources including exposure time spacecraft ephemeris and altitude errors are not corrected. Figure A-6 presents schematics of the image correction procedures for both the RBV and MSS sensors. The net mapping and registration rms errors in the bulk film products after correction are also included in Table A-1.

RBV radiometric calibration is accomplished through the EBRIC tape which contains the EBR beam adjustment information. These data are derived from two sources: 1) the pre-flight RBV radiance mapping and 2) the on-board erase lamps which produce in-flight Radiometric Calibration Images (RCI's). The radiometric error in bulk processed RBV imagery is 9% of full scale sensor voltage. The equivalent error in radiance varies with level because RBV voltage is not linearly proportional to apparent radiance.

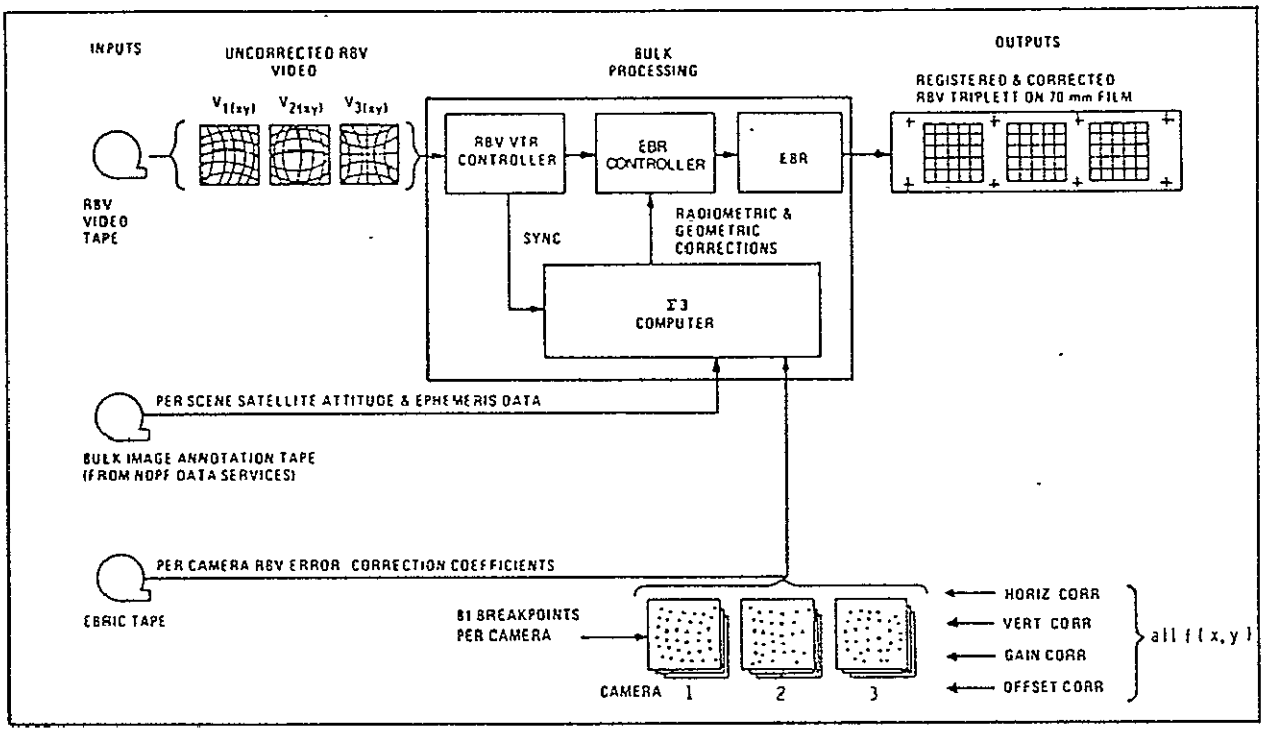

RBV

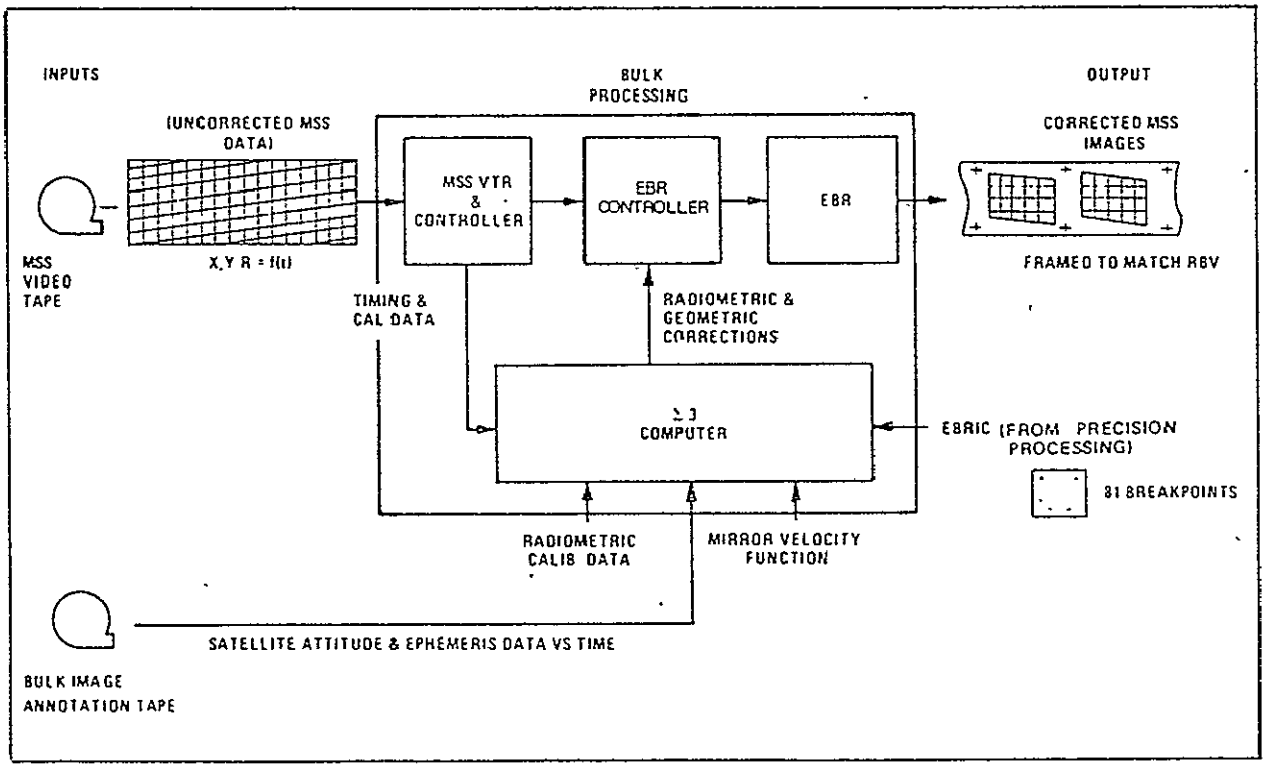

MSS

Figure A-6 BULK PROCESSING IMAGE CORRECTION SCHEMATIC

MSS radiometric calibration is accomplished through an internal radiance source and sun scans. The in-flight internal calibration data are obtained every MSS scan and it is used to obtain the optimum linear relationship between radiance in and voltage out for each detector. The internal calibration source was initially measured on the ground. Long term drift in the absolute radiance calibration is corrected through periodic sun scans. The MSS radiometric error in bulk processed MSS imagery is 5% of full scale sensor count or apparent radiance.

A.2 SURVEY OF GENERAL USERS' REQUIREMENTS

That the image quality characterization resulting from this study contain sufficient information for users to determine the adequacy of ERTS imagery for individual needs is a necessary condition. Users' ability to define "image quality" is not established and completeness of an image quality characterization based on users requirements would not be expected. But a general understanding, at least, of what tasks users of ERTS imagery would like to accomplish is certainly required if the "quality" which is controlled is to have relevance.

A literature search was consequently conducted. A large variety of journal articles and symposium proceedings were sampled to survey aerial and satellite imagery users' activities and needs. (Those not referenced in the text are included in the bibliography.) In many instances the user's requirements were stated or implied only in general terms. Other cases provided specific, but qualitative, definitions of image quality parameters. Finally, a few authors stated specific, quantitative, image quality requirements.

It should be noted that some of the papers concern aerial remote sensing, with its inherent capability for image resolution superior to that of ERTS imagery; thus they cannot be directly applied to

ERTS data user requirements. They do, however, provide additional background on the use of remote sensing in the field discussed.

The surveyed articles were grouped into broad classes: land use studies, vegetation and crop studies, geology and geography, oceanography and hydrology, and oil pollution surveys. User requirements as deduced from the articles listed in the bibliography will be discussed class by class.

A.2.1 Land Use Studies

More articles on land use surveys were available than on any of the other topics. In addition, this class of articles contained some of the most specific and quantitative statements of user image quality requirements. In one article[35] concerning a study performed to determine the effects of various environments on the levels and types of information retrieved from orbital-acquired (Gemini and Apollo) imagery, the authors employed a technique of placing an artificial grid of resolution cells over the image and then counting the number of image elements in that cell. They concluded that for land use mapping the minimum resolution requirement is that at least 50% of the cells contain only one element. In terms of ground resolved distance (GRD) they stated:

Level of interpretation	GRD
General identification of terrain	300 ft.
Precise identification	15 ft.
Description	5 ft.

Another study with a similar purpose[36] discussed space photographs simulated by artifically reducing the resolution of aerial photographs by various degrees. The photos were then subjected to human photo-

interpretation. The results indicated that simulated ERTS data (GRD of 250 ft.) contain sufficient information to allow an interpreter to discriminate among woody vegetation, grassland and water bodies. For more detailed information such as species identification of the woody vegetation, the imagery must have a ground resolved distance of 50 feet which is beyond current ERTS capability. A third study[37] supports the above results with its own conclusion that ERTS is most useful for broad land use mapping in regions such as the Great Plains which is dominated by large blocks of natural categories. Additional articles in this area discuss high resolution aerial imagery or land use classification schemes.

A.2.2 Geology and Geography

Another area for potential ERTS data users is that of geology and geography. An example of a remote sensing project where both the radiance and size of a small object is required in given by Vincent and Thomson[38]. Silicate concentration in rocks is estimated to within 14% using a technique that relies on the SiO_2 concentration dependence of the shape of the emissivity spectrum of silicate rocks. Radiometric fidelity of 1μ in wavelength is required. A resolution cell of less than 100 ft. is preferred, but the authors feel this requirement can be reduced through the use of visible and near IR sensors. Another paper[39] compares aerial and space-acquired (Gemini IV) imagery for use in geological mapping. The authors concluded that the space photography identification performance was good, but not equal to that of aerial photography because of reduced resolution on the space photographs.

A.2.3 Oceanography and Hydrology

Stevenson[40] gives a list of specific qualitative image derived parameters as well as some quantitative estimates of the desired precision in these parameters. Cited as of interest to oceanographers are: ocean color, sea-surface roughness, sea-surface temperature, slope of the ocean surface and of significant waves, atmospheric profiles of temperature, moisture and CO_2 and lunar magnitude of tide producing forces. Estimates of accuracy required in image quality are 100Å in wavlength; 1°C in temperatures; spatial resolutions of $10km^2$ for islands, coasts, and current boundaries, $500km^2$ for open oceans, $25km^2$ for ocean surface patterns, 5m for wave heights, and 100m for surface features and required repetition intervals of 24 hrs. near coasts, 5 days in the open ocean.

Hydrological data goals as given by Bock[41] were stated in broad terms as: study of the hydrological cycle; ice and snow, saline, water pollution mapping; and coastal surveys.

A.2.4 Oil Pollution Surveys

Another field for potential users of ERTS data is oil pollution monitoring. Several articles have implications for the relevance of ERTS data to this field. Wobber[42] suggest satellite coverage for use in monitoring open sea slicks, major coastal spills, and highly probable spill areas (pipelines, ports). Aerial coverage, however, is preferred for its speed and flexibility in covering a sudden oil spill. In addition, this and other articles place the useful region of the EM spectrum for oil pollution monitoring at visible blue to ultra-violet. Thermal infrared can also be useful if ground truth data are available.

A.2.5 Crops and Vegetation Monitoring

Crop disease surveys and vegetation mapping are another area where use of aerial remote sensing makes it a candidate for an ERTS data user. Philpotts[43] discuss crop disease patterns revealed by moderate scale color IR photos.

A.2.6 Summary

Based on the literature sampled, no definition of "image quality" useful in accomplishing the study objectives can be drawn from the users. Surely, one might adopt the terms "radiometric fidelity", "geometric fidelity", "resolution", but these terms have different meanings to different people and are certainly not sufficiently well defined to provide a useful basis for quality control criteria. They are general terms which classify rather than specify the ability to make certain measurements on photographs.

One can look at the users' tasks just described once again however, and ask exactly what sort of measurements is each user making. The following seem to span the tasks:

1. How accurately can a boundary between different transmission levels be located on a photograph?
2. How well can the radiance, size, and location of small objects be measured?
3. How well can the separation between two objects or boundaries on a photograph be measured?
4. How well does that separation represent the separation on the earth?
5. How well can the transmission of a photograph be measured?

6. How is that transmission related to radiance at the earth?

Clearly, any working definition of "image quality" adequate for the task at hand must be capable of obtaining quantitative answers to such questions and must relate those answers to measurable properties of elements of the NDPF.

A.3 SYSTEM ELEMENT PERFORMANCE CHARACTERIZATION AND "IMAGE QUALITY"

This section is to delineate techniques commonly employed to characterize image processing system element performance and to predict the quality of the images produced. The purpose is to establish some concepts that will subsequently be used and to point out why some others are unsatisfactory for the study objective.

In order to ensure familiarity with the current state of the art, a literature search covering the period 1968 - date was undertaken. This section reflects the content of the resulting bibliography.

Four overlapping categories, optical transfer function, resolution, noise, and subjective image quality, provide convenient headings for discussion.

A.3.1 Optical Transfer Function

The optical transfer function has been shown to be a useful tool to characterize the performance of many image processing devices. Some techniques for its measurement are pointed out in this section.

The blur introduced by an optical system linear in intensity can be characterized by a "point spread function" $s(\vec{x})$ defined implicitly by the convolution:

$$i(\vec{x}) = o(\vec{x}) * s(\vec{x}) \tag{A-1}$$

where: $i(\vec{x})$ = image brightness, $o(\vec{x})$ = object brightness, and $\vec{x}$ = position coordinates in plane orthogonal to optical axis. ($*$ denotes convolution).

Thus:

$$I(\vec{\nu}) = O(\vec{\nu})\,\tau(\vec{\nu}) \tag{A-2}$$

where: $I(\vec{\nu}) \rightleftharpoons i(\vec{x})$, $O(\vec{\nu}) \rightleftharpoons o(\vec{x})$, $\tau(\vec{\nu}) \rightleftharpoons s(\vec{x})$, and $\rightleftharpoons$ denotes a Fourier transform.

$|\tau(\vec{\nu})|$ is the optical transfer function (OTF). It is in general a two-dimensional, complex valued function. $|\tau(\vec{\nu})|$ is the modulation transfer function (MTF). It is emphasized that the OTF is not a measure of image quality but merely the frequency response function of a linear device and consequently a measurable property of the performance of that device.

Application of the OTF concept to photo-optical systems requires linearization of the generally non-linear development process. Generally the OTF concept is applied to the object to exposure image transfer process.

Methods of measurement of the OTF of photo-optical systems are well-documented in the literature.[44-47] Such measurement obviously requires use of object targets with known Fourier spectra. The three most commonly employed are considered here in brief.

1) Sine Wave Targets - Sine wave targets consist of objects whose brightness varies sinusoidally with distance (Figure A-7). The targets are photographed, image transmission is measured and transmission values are converted to exposure space through the Hurter-Driffield (H-D) curve. The ratio of the exposure contrast to the target contrast is the value of the MTF at the target spatial frequency. The phase component of the OTF cannot be measured unless a method of measuring the displacement of the image sine wave peaks from the optic axis (or other convenient datum) is provided.

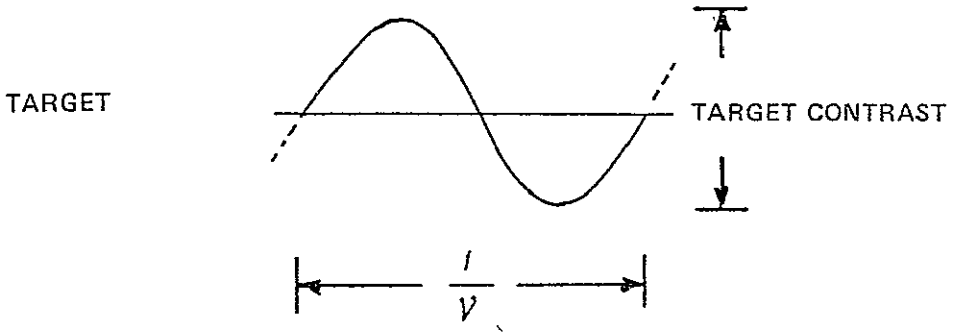

$$|\tau(\nu)| = \frac{\text{IMAGE CONTRAST}}{\text{TARGET CONTRAST}}$$

Figure A-7 SINE WAVE TARGETS

2) Square Wave Targets - Square wave targets consist of objects whose brightness consists of a periodic discontinuous variation between brightness levels (Figure A-8a). When the widths of the two levels are the same, the targets can be used in the same manner as sine waves. The "square wave modulation" obtained is not the OTF. A relationship between square wave modulation and the modulus of the OTF is:[48]

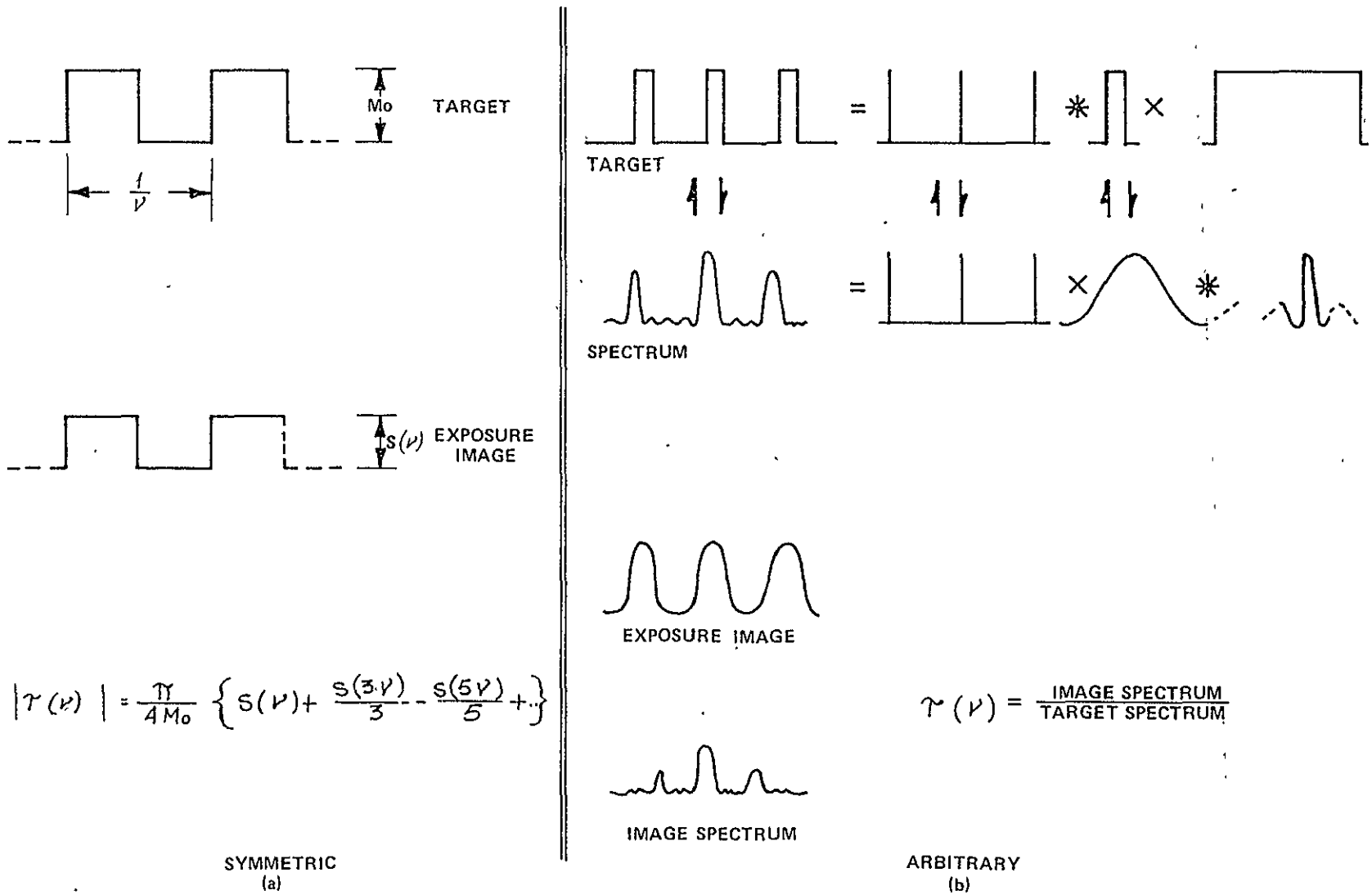

Figure A-8 SQUARE WAVE TARGETS

$$\left|T(\nu)\right| = \frac{\pi}{M_o}\left\{S(\nu) + \frac{S(3\nu)}{3} - \frac{S(5\nu)}{5} + \cdots\right\} \qquad (A-3)$$

where M_o is the target contrast and $S(\nu)$ is the image square wave contrast.

Another use of square wave targets results from observing that a target consisting of a finite number of square bars of arbitrary width and spacing can be represented by an infinite periodic array of Dirac δ functions convolved with a square pulse equal to the bar width and multiplied by a square pulse equal to the target width (Figure A-8b). The target spectrum is consequently given by an infinite periodic array of δ functions convolved with the Sinc $(\frac{\sin \pi \nu x}{\pi \nu x})$ function corresponding to the target width and multiplied by the Sinc function corresponding to the bar width. The photographic image can be scanned with a microdensitometer, converted through the H-D curve to exposure space and Fourier transformed. The ratio of the calculated exposure image spectrum to the known target spectrum is the OTF.

3) Edge Targets - Knife edge targets consist of a step function in object brightness (Figure A-9). Since the derivative of a step function is a δ function, the spectrum of the target gradient is a constant. Consequently, the OTF is given by the Fourier transform of the derivative of the exposure image of an edge obtained by scanning the photograph with a microdensitometer and using the H-D curve for conversion to exposure space. Edge targets have found wide acceptance because they are easy to produce, analysis is straightforward, and they have the additional attractive property of often being found in natural aerial photographic scenery.

It should be noted that the targets discussed all yield one-dimensional transfer functions.

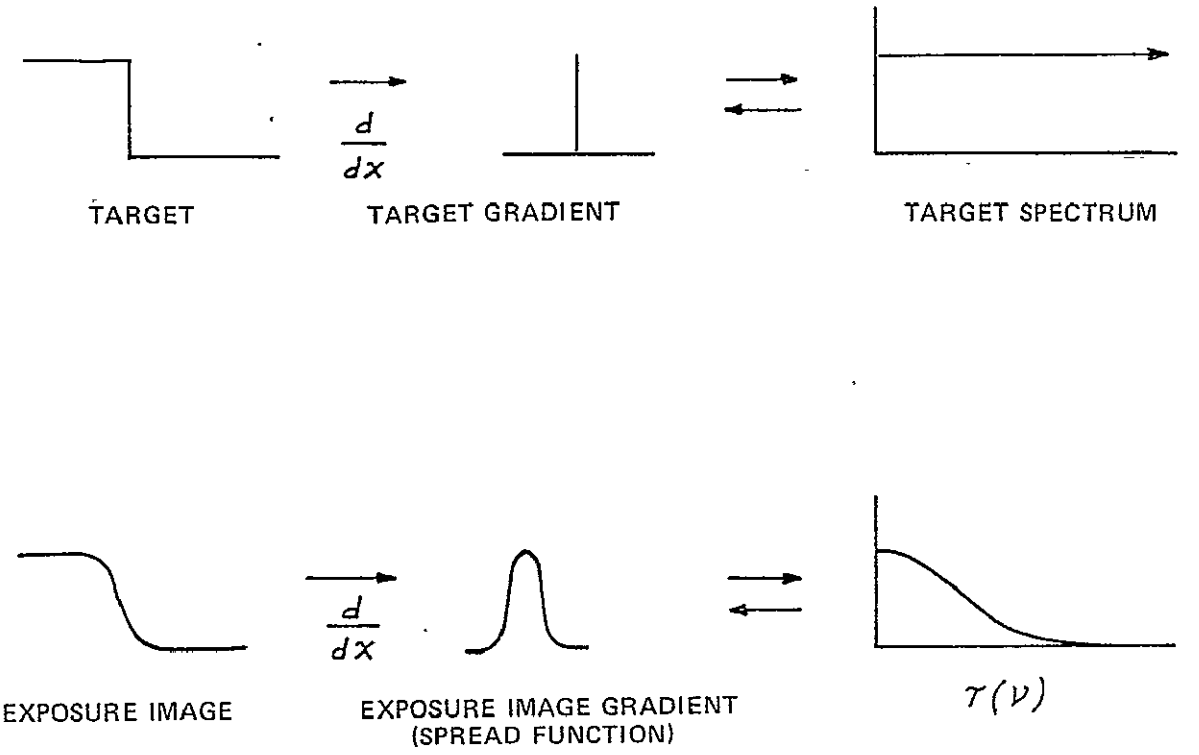

Figure A-9 EDGE TARGETS

The accuracy of OTF measurement in photo-optical systems is related to system photographic (grain) noise. Four independent studies of the relationship of noise to OTF accuracy are referenced.[44, 49-51] All concern delination of proper filtering techniques to minimize the uncertainty introduced by grain noise. The work of Kinzly and Mazurowski[44] deserves special mention since, in addition to application of the technique suggested by Blackman[49], it develops a promising adaptive filtering technique. All four references have primary application to edge gradient techniques. In consideration of optimum methods for reducing error due to noisy data, the obvious should not be overlooked: since the measurement techniques are one-dimensional, noise in the data can be reduced by increasing the length of target and scanning (slit) aperture in the direction orthogonal to the scan.

Two image quality assessment parameters based on the OTF are the Strehl definition and Shade's equivalent passband. The Strehl definition is the ratio of the volume enclosed by the measured MTF to the volume enclosed by the diffraction limited MTF. Shade's equivalent passband is the volume enclosed by $|T(\vec{\nu})|^2$. Roetling, et al.[52] have shown that Shade's equivalent passband is equivalent to acutance (mean square edge density gradient) and is consequently useful as an expression of detail rendition as perceived by a human observer.

A.3.2 Resolution

Resolution is the ability to distinguish between two adjacent objects in an image. A number of resolution criteria are in use.

Rayleigh's criterion is that the diffraction limited images of two points are just resolved if the central maximum of one lies on the first minimum of the Airy disc of the other. Thus, Rayleigh's criterion can be expressed:

$$R = \frac{0.61\lambda}{NA} \qquad \text{where: } \lambda = \text{wavelength}, \ NA = \text{numerical aperture} \tag{A-4}$$

A perceptible dip exists between point images separated by Rayleigh's criterion. The dip disappears at

$$R = \frac{0.5\lambda}{NA} \tag{A-5}$$

which is Sparrow's criterion.

Both the Rayleigh and Sparrow criteria are clearly related to the spread function and can thus be derived if the OTF is known.

A number of resolution criteria are simply defined by an observer's ability to distinguish the existence of a particular target. Such criteria depend not only on the properties of the image but on the properties of the detection process as well. The most common is the standard Air Force Tri-Bar target. One can obtain a "modulation detectability curve" by having a number of subjects observe tribars of varying spacing and contrast and plotting the statistical detection threshold contrasts versus spatial frequency. "Resolution" can then be defined as the intersection of an MTF and a modulation detectability curve. Uncontrolled variables and experience produce uncertainty in this measure of resolution. One summary measure of "image quality" that is in use is the area enclosed between the modulation detectability curve and the MTF.

The term "resolution" is sometimes applied to the ability of an optical system to "resolve" a specified object. This definition is similar to the preceding one but requires recognition as well as detection.

The concept "resolution" can be more precisely expressed as estimation error as a function of object properties and imaging system performance. In this case we eliminate the subjective detection process in order to obtain increased predictive validity.

A.3.3 Noise

In photo-optical systems, the major noise source is the granularity of the emulsion and is expressed in the granularity constant, G. The rms density fluctuation observed in scanning a uniform density area is

$$\sigma_g = \frac{G}{\sqrt{A}} \qquad \text{where: } A = \text{area of scanning aperture} \qquad (A\text{-}6)$$

In actuality the emulsion records the continuous exposure distribution as a discrete, thin but nevertheless three-dimensional, distribution of silver particles. The photographic macro-image is a continuous intensity distribution which results from multiple scattering of photons traversing the developed emulsion. If the photographic image is observed over a very small area very close to the emulsion surface, it is not clear how the observed intensity is related to the intensity distribution which exposed the emulsion; in other words, the micro-image is not yet adequately understood.

The approach usually followed is to model a micro-image scan as a continuous signal to which white gaussian noise has been added. Although a model postulating a photographic micro-image to be the result of a continuous signal having modulated a white noise "carrier" might be somewhat closer to the actual physics, the standard signal plus noise model is adopted for this study. It is emphasized that this approach is taken not in support of the standard model but simply because to establish a better model exceeds the study scope.

For the electronic image processing system elements, an additive white gaussian noise model is theoretically as well as pragmatically acceptable.

A.3.4 Subjective Image Quality

Efforts have been made in a number of studies [50, 53-56] to define subjective assessment of image quality in a quantitative manner. Such techniques by definition include human variables which are not well defined. It is not surprising that a universal subjective measure has not been accepted although correlation of subject response with measurable parameters within the limits of specific photographic product uses has been shown.

Subjective image quality efforts are directed to achieving a causal relationship between measurable system element performance properties: frequency response (OTF), signal-to-noise ratio, and the ability of the user to make subjective judgments (usually in the form of detection/recognition decisions) on the output product. The motivation of such efforts is consistent with the objective of this study. However, the estimation error is the result not only of an estimation error introduced by the image processing system but also of an error introduced by that subject's own detection process. There is no way to separate the two unless an independent value for either can be obtained.

To determine quality control procedures for the NDPF requires determination of the estimation error due to the system itself. Thus, subjective image quality measures are useless unless a valid model of the human subject "receiver" properties and a statement of its optimality were to be available. As this model is not established, subjective techniques necessarily lack the predictive validity required for this study's purposes.

It should be recalled that some of the performance measures previously point out: resolution, MTFA, etc. are subjective.

A.4 REFERENCES

1. "NASA Earth Resources Technology Satellite Data Users Handbook," General Electric, Dept. 71-SD-4249 (1972)

2. NDPF Familiarization Technical Conference, September 12, 13, 1972; Personal communication with B. Peavey (Contract Technical Monitor, NASA Goddard SFC), R. Johnson (Bendix Corp.), T. Rossi (General Electric Corp.)

3. FAM-71-SD-5208, "Operation and Maintenance Manual-Image Processing System Familiarization"

4. OM-71-SD-5206, "Operation and Maintenance Manual-Bulk Processing Subsystem, Vol. I"

5. OM-71-SD-5207, "Operation and Maintenance Manual-Precision Processing Subsystem, Vol. I"

6. SVS-7854, "Specification for the Data Services Laboratory of the NDPF"

7. SVS-7854, "Preliminary Specification for the Data Services Laboratory of the NDPF"

8. SVS-7756, "Performance and Design Requirements for the ERTS Ground Data Handling System"

9. SVS-7758, "Performance and Design Requirements for the ERTS NDPF Segment"

10. ES-0092-2, "Performance Specification - Return Beam Video Processor and Sync Separator Unit"

11. ERTS-2300-C, "Specification for the Image Data Processing Subsystem of the Ground Data Handling System of the ERTS"

12. ETM-510B-A, "ERTS Specification Change Notice"

13. ETM-510B-A, "ERTS Specification Change Notice"

14. ETM-510B-A, "Design and Performance Specification for ERTS High-Resolution Film Recorder"

15. ES-0172, "Electron Beam Recorder Controller"

16. ERTS-2001, "Bulk Processing Subsystem Performance Specification"

17. ES-0012, "Multispectral Scanner Video Tape Recorder/Reproducer Controller"

18. ERTS-2002, "Multispectral Scanner Video Tape Recorder/Reproducer"

19. 2A00-1904, "MSS CAL Wedge Word Selection"

20. 2A00-1917, "MSS Sun Calibration Approach and Software Requirements"

21. "QC Line Test Imagery Definitions"

22. 1H05-007 Rev "A", "MSS CAL Wedge Weighting Coefficients - Pre T/V Test"

23. "MSS Spectral Band Offsets for Bulk Geometric Corrections"

24. "Geometric Image Correction Algorithms for the Bulk Processing Subsystem"

25. ERTM-H-43, "Geometric Image Correction Algorithms for the Bulk Processing Subsystem"

26. ERTM-H-51, "Maximum Allowable Attitude and Altitude Errors (MSS Video-to-Film Conversion Mode)"

27. ERTM-H-78, "Radiometric Image Correction Algorithms for the Bulk Processing Subsystem"

28. ERTM-H-81, "Bulk Processing Modulation Transfer Function"

29. ERTM-H-85, "Film Gamma Compensator Analysis"

30. ERTM-H-66, "Revision A (MSS Radiometric Correction Algorithms)"

31. ERTM-H-194, "Preliminary Radiometric Calibration (RVFC)"

32. ERTM-H-197, "RBV Radiometric Correction Test"

33. ERTM-H-200, "MSS Radiometric Correction Test"

34. ERTM-H-201, "MSS Framing--RBV Aperture Compensation and Gamma Compensation"

35. Ratzlaff, J. R., "The Factor of Resolution in Land Use Studies from Orbital-Acquired Imagery," Proc. of American Society of Photogrammetry, 1971.

36. Lauer, D. T., and Thaman, R. R., "Information Content of Simulated Space Photographs as a Function of Various Levels of Image Resolution," Seventh International Symposium on Remote Sensing of Environment, Vol. II, May 1971.

37. Simonett, D.S., and Coiner, J. C., "Susceptibility of Environments to Low Resolution Imaging for Land-Use Mapping," Seventh International Symposium on Remote Sensing of Environment, Vol. 1, May 1971.

38. Vincent, R. K., and Thomson, F. J., "Discrimination of Basic Silicate Rocks by Recognition Maps Processed from Aerial Infrared Data," Seventh International Symposium on Remote Sensing of Environment, Vol. I, May 1971.

39. van der Meer Mohr, H. E. C., and Krishnanunni, "Evaluation of Hyperaltitude Photography for Geological Mapping," Seventh International Symposium on Remote Sensing of the Environment, Vol. III, May 1971.

40. Stevenson, R. E., "Oceanographic Data Requirements for the Development of an Operational Satellite System," Princeton U. Conf. Aerospace Methods Revealing and Evaluating Earth's Resources, Princeton, NJ, 1970.

41. Bock, P., "Space Acquired Data: Hydrological Requirements," Proc. Princeton U. Conf. on Aerospace Methods for Revealing and Evaluating Earth's Resources, Princeton, NJ, 1970.

42. Wobber, F. J., "Imaging Techniques for Oil Pollution Survey Purposes," Photographic Applications in Science, Technology and Medicine, July 1971.

43. Philpotts, L. E., "IR Color for Crop Disease Identification," Photogrammetric Engineering, Vol. 35, November 1969.

44. Kinzly, R. E., Mazurowski, M. J., "Project Slope - A Study of Lunar Orbiter Photographic Evaluation Techniques, Implementation and Accuracy," Cornell Aeronautical Laboratory, Inc., April 1967.

45. SPIE, Seminar-in-Depth: Modulation Transfer Function, SPIE Seminar Proceedings, Volume 13, SPIE, 1969.

46. Attaya, W. L., Brock, G. C., et. al., "Study of Image Evaluation Techniques," AFAL No. AFAL-TR-66-343, November 1966.

47. Scott, R. M., Offner, A., Hufnagel, R. E., Scott, F., Rosenau, M. D., Preston, K., "The Practical Application of Modulation Transfer Functions," Photographic Science and Engineering, Vol. 9, No. 4, July-August 1965.

48. Coltman, J. W., "The Specification of Imaging Properties by Response to a Sine Wave Input," J. Opt. Soc. Am., Vol. 44, No. 6, June 1954, p. 468.

49. Blackman, E. S., "Effects of Noise on the Determination of Photographic System Modulation Transfer Functions," Photographic Science and Engineering, Volume 12, Number 5, September-October 1968.

50. Mazurowski, M. J., Hammill, H. B., Snider, G. H., "A Study of Image Quality Evaluation," Cornell Aeronautical Laboratory, Inc., November 1963.

51. Jones, R. A., and Yeadon, E. C., "Determination of the Spread Function from Noisy Edge Scans," Photographic Science and Engineering, volume 13, Number 4, July-August 1968.

52. Roetling, P.G., Trabka, E.A., and Kinzly, R.E., "Theoretical Prediction of Image Quality," Journal of the Optical Society of America, volume 58, Number 3, March 1968.

53. Hammill, H.B., Snider, G.H., Trabka, E.A., "A Study of Photographic Signal to Noise Ratio," Cornell Aeronautical Laboratory, Inc., December 1964.

54. Granger, E.M. and Cupery, K.N., "An Optical Merit Function (SQF), which Correlates with Subjective Image Judgments," Photographic Science and Engineering, Volume 16, Number 3, May-June 1972.

55. Scott, F., "The Search for a Summary Measure of Image Quality--A Progress Report," Photographic Science and Engineering, Volume 12, Number 3, May-June 1968.

56. Jones, R.A., "Investigation of Image Simulation Procedures," Photographic Science and Engineering, Volume 13, Number 1, January-February 1969.

APPENDIX B

IDSS PROGRAM: LIST AND FLOWCHART

FORTRAN MODULE (LIST)

CARD NO	****	CONTENTS	****
1	C	--E.K. STEIN 3/73	
2	C		
3	C		
4	C	THIS PROGRAM SIMULATES IMAGE PROCESSING SYSTEMS FOR THE PURPOSE OF	
5	C	CALCULATION OF VARIANCES IN PARAMETER ESTIMATION FROM MEASUREMENTS	
6	C	MADE ON OUTPUT PRODUCTS AS A FUNCTION OF SUBSYSTEM ELEMENT	
7	C	PERFORMANCE. ANY SYSTEM WHICH CAN BE REPRESENTED BY AN ARBITRARY	
8	C	SEQUENCE OF LINEAR ELEMENTS,NONLINEAR GAINS,AND ADDITIVE NOISE CAN	
9	C	BE SIMULATED. INPUT TARGETS GENERATED HAVE THE FORM: Y=F(X,A(I))	
10	C	WHERE THE A(I) ARE TARGET PARAMETERS AND X=DISTANCE (CURRENTLY	
11	C	X.LE.4). THE CRAMER-RAO BOUNDS ON THE VARIANCES OF THE A(I)	
12	C	ESTIMATES ARE CALCULATED.	
13	C		
14	C		
15	C	THE PROGRAM OPERATES IN ONE OF THREE MODES	
16	C	MODE=1 IMPLIES CALCULATION OF VARIANCES	
17	C	MODE=2 IMPLIES CALCULATION OF NOISE SPECTRAL DENSITY AND PRE-WHITENING	
18	C	FILTER SPREAD FUNCTION	
19	C	MODE=3 IMPLIES TARGET IS PLOTTED AFTER EACH SYSTEM ELEMENT	
20	C	UNITS: THE UNITS OF THE CALCUALATED VARIANCES= THE UNITS OF THE	
21	C	RESPECTIVE A(I) SQUARED	
22	C		
23	C	DEFINITIONS	
24	C	NPUNCH.NE.0 YIELDS OUTPUT TARGET PUNCHED ON CARDS	
25	C	MONTE=NUMBER OF REPETITIONS FOR NOISE POWER SPECTRUM CALCULATION	
26	C	WNPD=WHITE NOISE POWER SPECTRAL DENSITY	
27	C	IREFO=RANDOM NUMBER GENERATOR SEED	
28	C	NA=NUMBER OF A'S OF INPUT TARGET	
29	C	DIFA=DECIMAL FRACTIONAL CHANGE IN EACH A FOR PARTIAL DIFFERENTIAL	
30	C	COMPUTATION	
31	C	IF ANY A(I) REPRESENTS POSITION, THEN DIFA.MUST BE CHOSEN SUCH THAT:	
32	C	DIFA*A(I)/DELTX = INTEGER	
33	C	N(I)=NUMBER OF VALUES OF A(I)	
34	C	DA(I)=INCREMENT IN VALUE OF A(I) INCREASE	
35	C	A(I)=INITIAL VALUE OF A(I)	
36	C	CHOOSE A(3),A(4) EQUAL TO INTEGER MULTIPLES OF DELTX	
37	C	NX=NUMBER OF POINTS IN TARGET GENERATED (CURRENTLY NX.LE.2001	
38	C	DELTX=DISTANCE BETWEEN POINTS IN X DIRECTION	
39	C	NBLOCK=NUMBER OF SYSTEM BLOCKS --ONE SYSTEM BLOCK=LINEAR ELEMENT,	
40	C	NONLINEAR ELEMENT,ADDITIVE NOISE (CURRENTLY NBLOCK.LE.20)	
41	C	OP(I,J)=0 IMPLIES SYSTEM ELEMENT TYPE J BYPASSED IN I'TH	
42	C	SYSTEM BLOCK	
43	C	J=1 REFERS TO LINEAR ELEMENT	
44	C	J=2 REFERS TO NONLINEAR ELEMENT	
45	C	J=3 REFERS TO ADDITIVE NOISE	
46	C	NRUN=NUMBER OF SYSTEM BLOCK PERFORMANCE CONFIGURATIONS	
47	C	ICONTIRUN,I)=0 IMPLIES NO CHANGE IN SFCN DATA FOR I'TH BLOCK	
48	C	ILEVIIRUN,I)=0 IMPLIES NO CHANGE IN NONLINEARITY FOR I'TH BLOCK	
49	C	INOISIIRUN,I)=0 IMPLIES NO CHANGE IN NOISE FOR I'TH BLOCK	
50	C	NS=NUMBER OF POINTS IN SFCN	
51	C	SFCN=SPREAD FUNCTION OF PARICULAR SYSTEM BLOCK	
52	C	SET THE NUMBER OF POINTS IN EACH SFCN=NX	
53	C	THE X INCREMENT OF SFCN MUST ALSO EQUAL DELTX	
54	C	NO(I)=NUMBER OF POINTS IN H-D CURVE FOR BLOCK I	

```
CARD NO  ****                    CONTENTS                    ****
   55        C     DIN(I,J)=INPUT DENSITY VALUES FOR H-D CURVE OF BLOCK I
   56        C     DOUT(I,J)=OUTPUT DENSITY VALUES FOR DIN(I,J)
   57        C     SIGMA=STD. DEVIATION OF NOISE
   58              DIMENSION N(4),DA(4),A(4),B(4),Y(16),B(4),YH(200)
   59              COMMON NA,NX,NBLOCK,I5,IRUN,IB,DIFA,DELTX,OP(20,3),ICON(20,20),ILE
   60             1V(20,20),INOIS(20,20),A(4),OP(4),Y(20,999),DYDA(4,999),SIG(4,4),SF
   61             2CN(20,200),SIGMA(20),MODE,ERR,CLEV(20,4),MONTE,
   62             3DIN(20,30),DOUT(20,30),ND(20),NS
   63          201 CONTINUE
   64              WRITE(6,2013)
   65        C     INITIALIZE CONSTANTS AND CONTROL INDICES
   66              READ(5,1001,END=200)MODE
   67              READ(5,1001)NPUNCH
   68              READ(5,1001)MONTE
   69              READ(5,1011)NNPD
   70              GO TO (21,22,23),MODE
   71           21 WRITE(6,2014)MODE
   72              GO TO 24
   73           22 WRITE(6,2015)MODE
   74              GO TO 24
   75           23 WRITE(6,2016)MODE
   76           24 CONTINUE
   77              WRITE(6,2011)
   78              READ(5,1010) IREFG
   79              CALL GANURG(IREFG)
   80              READ(5,1001)NA,DIFA
   81              D=1.+DIFA
   82              READ(5,1001)NX,DELTX
   83              WRITE(6,2000)NA,DIFA,NX,DELTX
   84              WRITE(6,2001)IREFG
   85              READ(5,1004)NBLOCK,NRUN
   86              WRITE(6,2012)
   87              DO 13 I=1,NA
   88              READ(5,1002) N(I),DA(I),A(I)
   89              WRITE(6,2017)N(I),DA(I),A(I)
   90              B(I)=A(I)
   91           13 CONTINUE
   92              NI=N(1)
   93              IF(NA.GE.2) N2=N(2)
   94              IF(NA.GE.3) N3=N(3)
   95              IF(NA.GE.4) N4=N(4)
   96              DO 14 I=1,NBLOCK
   97           14 READ(5,1004)(OP(I,J),J=1,3)
   98              DO 15 I=1,NRUN
   99              READ(5,1006)((ICON(I,J),J=1,NBLOCK)
  100              READ(5,1006)((ILEV(I,J),J=1,NBLOCK)
  101              READ(5,1006)((INOIS(I,J),J=1,NBLOCK)
  102           15 CONTINUE
  103              C=SQRT(4./(3.*DELTX))/.4343
  104              READ(5,1001) NS
  105              DO 99 IRUN=1,NRUN
  106              WRITE(6,2002)IRUN
  107              WRITE(6,2003)
  108        C     SET SYSTEM ELEMENT PERFORMANCE PARAMETERS/FUNCTIONS
  109              NNS=N3-1
  110              DO 20 I=1,NBLOCK
```

ORIGINAL PAGE IS
OF POOR QUALITY

CARD NO	**** CONTENTS ****
111	IF(ICON(IRUN,I).EQ.0) GO TO 103
112	READ(5,1003) (SFCN(I,J),J=1,NS)
113	C NORMALIZE SFCN
114	S=(SFCN(I,1)+SFCN(I,NS))/2.
115	DO 50 J=2,NNS
116	50 S=S+SFCN(I,J)
117	S=S*DELTX
118	DO 51 J=1,NS
119	51 SFCN(I,J)=SFCN(I,J)/S
120	WRITE(6,2004)I
121	WRITE(6,2005)(SFCN(I,J),J=1,NS)
122	103 CONTINUE
123	IF(ILEV(IRUN,I).EQ.0) GO TO 105
124	READ(5,1002)ND(I)
125	NDD=ND(I)
126	READ(5,1003)(DIN(I,J),J=1,NDD)
127	READ(5,1003)(DOUT(I,J),J=1,NDD)
128	WRITE(6,2018)I
129	WRITE(6,2020)(DIN(I,J),J=1,NDD)
130	WRITE(6,2019)(DOUT(I,J),J=1,NDD)
131	2018 FORMAT(1HO,'BLOCK',I4,2X,'NONLINEAR LEVEL TRANSFER CURVE')
132	2019 FORMAT(1H ,'DOUT',20F6.3)
133	2020 FORMAT(1H ,'DIN',20F6.3)
134	105 CONTINUE
135	IF(INOIS(IRUN,I).EQ.0) GO TO 107
136	READ(5,1003)SIGMA(I),DIA
137	SIGMA(I)=SIGMA(I)*C*SQRT(DIA)
138	WRITE(6,2007)I,SIGMA(I)
139	107 CONTINUE
140	20 CONTINUE
141	C SET VALUES OF THE A(I)
142	IF(NODE.EQ.1) WRITE(6,2010)
143	DO 1 I1=1,N1
144	A(I)=B(I)+(I1-1)*DA(1)
145	IF(NA.EQ.1) GO TO 10
146	DO 2 I2=1,N2
147	A(2)=B(2)+(I2-1)*DA(2)
148	IF(NA.EQ.2) GO TO 10
149	DO 3 I3=1,N3
150	A(3)=B(3)+(I3-1)*DA(3)
151	IF(NA.EQ.3) GO TO 10
152	DO 4 I4=1,N4
153	A(4)=B(4)+(I4-1)*DA(4)
154	10 CONTINUE
155	DO 11 I=1,NA
156	11 AP(I)=A(I)
157	IF(NODE.NE.1) I5=1
158	IF(NODE.NE.1) GO TO 6
159	C COMPUTE DIFFERENTIAL INPUT FOR EACH A(I)
160	NN=NA+1
161	DO 5 I5=1,NN
162	GO TO (6,7,8,9,12),I5
163	12 CONTINUE
164	AP(3)=A(3)
165	AP(4)=D*AP(4)
166	GO TO 6

```
CARD NO  ****                    CONTENTS                    ****
   167          9 CONTINUE
   168            AP(2)=A(2)
   169            AP(3)=D*AP(3)
   170            GO TO 6
   171          8 CONTINUE
   172            AP(1)=A(1)
   173            AP(2)=D*AP(2)
   174            GO TO 6
   175          7 CONTINUE
   176            AP(1)=D*AP(1)
   177          6 CONTINUE
   178      C     GENERATE TARGET AND PROPOGATE THROUGH SIMULATED SYSTEM
   179            CALL GEN
   180            IF(MODE.NE.2) GO TO 64
   181            DO 67 MO=2,MONTE
   182            DO 67 MM=1,MX
   183         67 Y(MO,MM)=Y(1,MM)
   184            M=0
   185         60 CONTINUE
   186            M=M+1
   187            IS=M
   188         64 CONTINUE
   189            CALL SYSTEM(INPUT,CH)
   190            IF(MODE.EQ.1) GO TO 5
   191            IF(MODE.EQ.3) GO TO 4
   192            IF(M.NE.MONTE) GO TO 60
   193            DO 66 IS=1,MONTE
   194         66 CALL POSPEC
   195            GO TO 4
   196          5 CONTINUE
   197      C     COMPUTE PARTIAL DERIVATIVES WRT, THE A(I)
   198            CALL DIF
   199      C     COMPUTE INTEGRAL OVER X OF EACH PRODUCT COMBINATION OF PARTIAL
   200      C      DERIVATIVES WRT, THE A(I) TAKEN TWO AT A TIME
   201            CALL INT
   202            IF(IERR.NE.0) GO TO 4
   203      C     INVERT MATRIX OF INTEGRALS
   204      C     WRITE MATRIX INTO VECTOR FOR INPUT ACCEPTABLE TO MINV (SSP)
   205            K=0
   206            DO 40 J=1,NA
   207            DO 40 I=1,NA
   208            K=K+1
   209         40 V(K)=SIG(I,J)
   210            CALL MINV(V,NA,DET,L,M)
   211      C     EXTRACT DIAGONAL ELEMENTS FROM VECTOR STORED INVERSE MATRIX
   212            K=1
   213            DO 41 I=1,NA
   214            SIG(I,I)=V(K)
   215            SIG(I,I)=SIG(I,I)*HMPO
   216         41 K=K+NA+1
   217            WRITE(6,2008)(A(I),I=1,NA)
   218            WRITE(6,2009)(SIG(I,I),I=1,NA)
   219          4 CONTINUE
   220          3 CONTINUE
   221          2 CONTINUE
   222          1 CONTINUE
```

```
CARD NO      ****                    CONTENTS                    ****
  223          99 CONTINUE
  224        1001 FORMAT(I4,F8.3)
  225        1002 FORMAT(I4,2F10.4)
  226        1003 FORMAT(10F8.3)
  227        1004 FORMAT(3I4)
  228        1006 FORMAT(40I2)
  229        1010 FORMAT(I9)
  230        1011 FORMAT(F10.3)
  231        2000 FORMAT(1HO,'NA=',I2,2X,'DIFA=',F6.3,4X,'NX=',I4,2X,'DELTX=',F6.3)
  232        2001 FORMAT(1H ,'IREFC=',I9)
  233        2002 FORMAT(1H1,'IRUN=',I4)
  234        2003 FORMAT(1HO,'NEW SYSTEM ELEMENT PERFORMANCE DATA')
  235        2004 FORMAT(1HO,'BLOCK',I4,2X,'SFCN')
  236        2005 FORMAT(1H ,10F8.3)
  237        2006 FORMAT(1HO,'BLOCK',I4,2X,'CLEV1=',F6.3,2X,'CLEV2=',F6.3,2X,'CLEV3=
  238            1',F6.3,2X,'CLEV4=',F6.3)
  239        2007 FORMAT(1HO,'BLOCK',I4,2X,'SIGMA=',F6.3)
  240        2008 FORMAT(1H ,4E10.3)
  241        2009 FORMAT(1H+,40X,4E10.3)
  242        2010 FORMAT(//3X,'A(1)',6X,'A(2)',6X,'A(3)',6X,'A(4)',5X,'SIG(1)',4X,'S
  243            IG(2)',4X,'SIG(3)',4X,'SIG(4)')
  244        2011 FORMAT(1HO,'CONSTANTS')
  245        2012 FORMAT(1HO,'N(I)',5X,'DA(I)',5X,'A(I)')
  246        2013 FORMAT(1H1,'PROGRAM SIPS')
  247        2014 FORMAT(1HO,'MODE',I2,2X,'CALCULATION OF VARIANCES')
  248        2015 FORMAT(1HO,'MODE',I2,2X,'CALCULATION OF NOISE SPECTRAL DENSITY AND
  249            1 PRE-WHITENING FILTER SPREAD FUNCTION')
  250        2016 FORMAT(1HO,'MODE',I2,2X,'TRACE PLOT OF TARGET PROPOGATED THROUGH S
  251            IMULATED SYSTEM')
  252        2017 FORMAT(1H ,I4,2F10.3)
  253             GO TO 201
  254         200 CALL EFPLOT
  255             STOP
  256             END
  257             SUBROUTINE GEN
  258           C THIS SUBROUTINE GENERATES ONE OF FOUR POSSIBLE TARGETS
  259           C   NA=1 IMPLIES CONSTANT LEVEL OF A(1)
  260           C   NA=2 IMPLIES TWO DELTA FCNS ON BACKGROUND LEVEL A(1) SEPERATED BY
  261           C      DISTANCE A(2)
  262           C   NA=3 IMPLIES STEP AT A(3) BETWEEN LEVELS A(1) AND A(2)
  263           C   NA=4 IMPLIES BAR OF LEVEL A(2) ON BACKGROUND OF LEVEL A(1) WITH
  264           C      WIDTH A(3) AND CENTER POSITION A(4)
  265             COMMON NA,NX,NBLOCK,I5,IRUN,IB,DIFA,DELTX,OP(20,3),ICON(20,20),ILE
  266            1V(20,20),IND(5(20,20),A(4),AP(4),Y(20,999),DYDA(4,999),SIG(4,4),SF
  267            2CN(20,200),SIGMA(20),MODE,IERR,CLEV(20,4),MONTE,
  268            3DIN(20,30),DOUT(20,30),ND(20),NS
  269             GO TO (301,302,303,304),NA
  270         301 CONTINUE
  271             DO 306 IX=1,NX
  272             Y(15,IX)=AP(1)
  273         306 CONTINUE
  274             GO TO 300
  275         302 CONTINUE
  276             NXX=AP(2)/DELTX+.5
  277             NXX=(NX-NXX)/2
  278             DO 312 IX=1,IX
```

CARD NO **** CONTENTS ****

```
      312 Y(I5,IX)=AP(1)
          Y(I5,NXX)=1.
          IX=NX-NXX
          Y(I5,IX)=1.
          GO TO 300
      303 CONTINUE
          NXX=AP(3)/DELTX+0.5
          DO 305 IX=1,NXX
          Y(I5,IX)=AP(1)
      305 CONTINUE
          NXX=NXX+1
          DO 308 IX=NXX,NX
          Y(I5,IX)=AP(2)
      308 CONTINUE
          GO TO 300
      304 CONTINUE
          NXX=AP(3)/DELTX+0.5
          NXXX=AP(4)/DELTX+0.5
          N2=NXX/2
          DO 309 IX=1,NX
          Y(I5,IX)=AP(1)
      309 CONTINUE
          NXXX=NXXX-N2
          NXX=NXXX+NXX
          DO 310 IX=NXXX,NXX
          Y(I5,IX)=AP(2)
      310 CONTINUE
      300 CONTINUE
          RETURN
          END
          SUBROUTINE SYSTEM(I,PUNCH)
C         THIS SUBROUTINE PROPOGATES TARGET THROUGH SIMULATED SYSTEM
          COMMON NA,NX,NBLOCK,I5,IRUN,IB,DIFA,DELTX,OP(20,3),ICON(20,20),ILE
         1Y(20,20),INOIS(20,20),A(4),AP(4),Y(20,999),DYDA(4,999),SIG(4,4),SF
         2CN(20,200),SIGMA(20),MODE,CERR,CLEY(20,4),MONTE,
         3DIN(20,30),DOUT(20,30),ND(20),NS
          IF(MODE.NE.3) GO TO 110
          IS=0
          CALL FNLPPP(IS)
          IS=1
      110 CONTINUE
          DO 101 I=1,NBLOCK
          IB=I
          IF(OP(I,1).EQ.0) GO TO 104
          CALL CON
          IF(MODE.NE.3) GO TO 104
          CALL FNLPPP(IS)
      104 CONTINUE
          IF(OP(I,2).EQ.0) GO TO 106
          CALL YLEV
          IF(MODE.NE.3) GO TO 106
          CALL FNLPPP(IS)
      106 CONTINUE
          IF(OP(I,3).EQ.0) GO TO 108
          CALL YNOISE
          IF(MODE.NE.3) GO TO 108
```

```
CARD NO  ****                    CONTENTS                    ****
  335          CALL PNLPPP(15)
  336        108 CONTINUE
  337        101 CONTINUE
  338            IF(INPUNCH.NE.0).AND.(I5.EQ.1))WRITE(7,3000)(Y(I5,IX),IX=1,NX)
  339       3000 FORMAT(10F8.5)
  340            RETURN
  341            END
  342            SUBROUTINE CON
  343            AUTHOR- M.J.MAZUROWSKI
  344            DIMENSION CF(999)
  345            COMMON NA,NX,NBLOCK,I5,IRUN,IB,DIFA,DELTX,OP(20,3),ICON(20,20),ILE
  346           1V(20,20),INOIS(20,20),A(4),AP(4),Y(20,999),DYDA(4,999),SIG(4,4),SF
  347           2CN(20,200),SIGMA(20),MODE,IERR,CLEV(20,4),MONTE,
  348           3DIN(20,30),DOUT(20,30),ND(20),NS
  349            N=NS/2
  350            DO 700 I=1,NX
  351            CF(I)=0
  352            DO 700 J=1,NS
  353            K=N+I-J
  354            IF(K.LT.1) K=1
  355            IF(K.GT.NX) K=NX
  356        700 CF(I)=CF(I)+SFCN(IB,JJ)*Y(I5,K)
  357            DO 701 I=1,NX
  358        701 Y(I5,I)=CF(I)*DELTX
  359            RETURN
  360            END
  361            SUBROUTINE YLEV
  362        C   THIS SUBROUTINE MODIFIES THE SIGNAL BY A PHOTOGRAPHIC HURTER-
  363        C      DRIFFIELD (H-D) CURVE
  364            COMMON NA,NX,NBLOCK,I5,IRUN,IB,DIFA,DELTX,OP(20,3),ICON(20,20),ILE
  365           1V(20,20),INOIS(20,20),A(4),AP(4),Y(20,999),DYDA(4,999),SIG(4,4),SF
  366           2CN(20,200),SIGMA(20),MODE,IERR,CLEV(20,4),MONTE,
  367           3DIN(20,30),DOUT(20,30),ND(20),NS
  368            I=IB
  369            K=ND(I)
  370            DMAX=DIN(I,K)
  371            DMIN=DIN(I,1)
  372            DO 900 IX=1,NX
  373            DY=-ALOG10(Y(I5,IX))
  374            IF(DY.GE.DMAX) DY=DMAX
  375            IF(DY.LE.DMIN) DY=DMIN
  376            J=2
  377        902 IF(DY.LE.DIN(I,JJ)) GO TO 901
  378            J=J+1
  379            GO TO 902
  380        901 CONTINUE
  381            JJ=J-1
  382            DS=(DY-DIN(I,JJ))/(DIN(I,J)-DIN(I,JJ))
  383            DY=DOUT(I,JJ)+DS*(DOUT(I,J)-DOUT(I,JJ))
  384        900 Y(I5,IX)=10.**(-DY)
  385            RETURN
  386            END
  387            SUBROUTINE YNOISE
  388            COMMON NA,NX,NBLOCK,I5,IRUN,IB,DIFA,DELTX,OP(20,3),ICON(20,20),ILE
  389           1V(20,20),INOIS(20,20),A(4),AP(4),Y(20,999),DYDA(4,999),SIG(4,4),SF
  390           2CN(20,200),SIGMA(20),MODE,IERR,CLEV(20,4),MONTE,
```

```
CARD NO  ****  CONTENTS
  391          1DIN(20,30),DOUT(20,30),ND(20),NS
  392           I=IB
  393           DO 601 IX=1,NX
  394           Y(IS,IX)=Y(IS,IX)*(1.+SIGMA(I)*GRN(0))
  395         601 CONTINUE
  396           RETURN
  397           END
  398           SUBROUTINE DIF
  399           COMMON NA,NX,NBLOCK,IS,IRUN,IB,DIFA,DELTX,OP(20,3),ICON(20,20),ILE
  400          1V(20,20),IND(S(20,20),A(4),AP(4),Y(20,999),DYDA(4,999),SIG(4,4),SF
  401          1CN(20,2000),SIGMA(20),MODE,IERR,CLEV(20,4),MONTE,
  402          1DIN(20,30),DOUT(20,30),ND(20),NS
  403           DO 201 J=1,NA
  404           DA=DIFA*A(J)
  405           DO 202 IX=1,NX
  406           DYDA(J,IX)=(Y(J+1,IX)-Y(1,IX))/DA
  407         202 CONTINUE
  408         201 CONTINUE
  409           RETURN
  410           END
  411           SUBROUTINE INT
  412         C
  413         C     SUBROUTINE INT PERFORMS TRAPEZOIDAL INTEGRATION OVER X OF EACH
  414         C     PRODUCT COMBINATION OF PARTIAL DERIVATIVES MAT. THE A(I)
  415         C      TAKEN TWO AT A TIME
  416         C
  417           COMMON NA,NX,NBLOCK,IS,IRUN,IB,DIFA,DELTX,OP(20,3),ICON(20,20),ILE
  418          1V(20,20),IND(S(20,20),A(4),AP(4),Y(20,999),DYDA(4,999),SIG(4,4),SF
  419          1CN(20,2000),SIGMA(20),MODE,IERR,CLEV(20,4),MONTE,
  420          1DIN(20,30),DOUT(20,30),ND(20),NS
  421           IERR=0
  422           DO 401 I=1,NA
  423           DO 402 J=1,NA
  424           DSIG=DYDA(I,J)*DYDA(J,J)+DYDA(1,NX)*DYDA(J,NX)
  425           DSIG=DSIG/2.
  426           NXX=NX-1
  427           DO 403 IX=2,NXX
  428           DSIG=DSIG+DYDA(J,IX)*DYDA(I,IX)
  429         403 CONTINUE
  430           SIG(I,J)=DSIG*DELTX
  431           SIG(J,I)=SIG(I,J)
  432           IF(SIG(I,J).NE.0.) GO TO 402
  433           WRITE(6,2008)(A(II),II=1,NA)
  434           WRITE(6,4000)I,J
  435           IERR=1
  436           RETURN
  437         402 CONTINUE
  438         401 CONTINUE
  439        2008 FORMAT(1H ,4E10.3)
  440        4000 FORMAT(1H+,40X,'SIG(',I2,I2,')=0, CALCULATION TERMINATED')
  441           RETURN
  442           END
  443           SUBROUTINE FNLPFP(IS)
  444         C     AUTHOR- N.J.MAZUROWSKI
  445           DIMENSION XP(999),YP(999)
  446           COMMON NA,NX,NBLOCK,IS,IRUN,IB,DIFA,DELTX,OP(20,3),ICON(20,20),ILE
```

CARD NO	**** CONTENTS ****
447	IV(20,20),TNOIS(20,20),A(4),AP(4),Y(20,999),DYDA(4,999),SIG(4,4),SF
448	ICN(20,200),SIGMA(20),MODE,IERR,CLEY(20,4),MONTE,
449	IDIN(20,30),DOUT(20,30),ND(20),NS
450	IF(IS.NE.0) GO TO 10
451	5 KNT=0
452	CALL PLOT(0.,0.,0)
453	T=7.0
454	DO 6 I=1,3
455	T=T-2.6
456	CALL NGRID(0.5,T,10.,2.5,0.2,0.25,0)
457	6 CALL NGRID(0.5,T,10.,2.5,2.,2.5,1)
458	10 KNT=KNT+1
459	IF(KNT.GT.15) GO TO 5
460	XOR=8.5-2*MOD(KNT-1,5)
461	YOR=7.7-2.6*MOD((KNT-1)/5,3)
462	CALL PLOT(XOR,YOR,-3)
463	DO 15 I=1,NX
464	YP(I)=2*Y(15,I)
465	15 XP(I)=2.5*(1.0-T)/NX
466	CALL LINE(YP,XP,NX,1)
467	CALL PLOT(-XOR,-YOR,-3)
468	RETURN
469	END
470	SUBROUTINE POSPEC
471	C AUTHOR- N.J.MAZUROWSKI
472	C THIS SUBROUTINE CALCULATES THE PRE-WHITENING FILTER AND THE NOISE
473	C SPECTRAL DENSITY
474	DIMENSION F(200),PS(110),PHI(50),ACF(110),ACFA(220),PSA(110)
475	COMMON NA,NX,NBLOCK,IS,IRUN,IB,DIFA,DELTX,OP(20,3),ICON(20,20),ILE
476	IV(20,20),TNOIS(20,20),A(4),AP(4),Y(20,999),DYDA(4,999),SIG(4,4),SF
477	ICN(20,200),SIGMA(20),MODE,IERR,CLEY(20,4),MONTE,
478	IDIN(20,30),DOUT(20,30),ND(20),NS
479	IF(IS.NE.1) GO TO 5
480	WRITE(6,2020)MONTE
481	2020 FORMAT(1H0,'MONTE=',I4)
482	CALL CLEAR(F(1),PSA(110))
483	NNP0=0.0
484	SS=0.0
485	5 DX=DELTX
486	AV=0.0
487	DO 10 I=1,NX
488	F(I)=Y(IS,I)
489	10 AV=AV+F(I)
490	AV=AV/NX
491	NF=0.1*NX
492	NN=2*NF-1
493	DO 30 J=1,NF
494	NJ=NX-J+1
495	SUM=0.0
496	DO 20 I=1,NJ
497	IJ=I+J-1
498	20 SUM=SUM+(F(I)-AV)*(F(IJ)-AV)
499	30 ACF(J)=SUM/NJ
500	ACFA(NF)=ACF(1)
501	DO 40 I=2,NF
502	ID=NF-I+1

```
CARD NO  ****                    CONTENTS                    ****
  503        IU=NF+I-1
  504        FAC=(COS(1.5708*(I-1)/NF))**2
  505        ACFA(IU)=ACF(I)*FAC
  506     40 ACFA(I0)=ACF(I)*FAC
  507        CALL FOURTR (ACFA,NN,DX,PS,PH,DF,NM,0)
  508        FC=1./PS(1)
  509        SUM=0.
  510        DO 50 I=1,NH
  511        PS(I)=FC*PS(I)
  512        PSA(I)=PSA(I)+PS(I)
  513     50 SUM=SUM+PS(I)
  514        SUM=DF*(SUM-.5)
  515        SS=SS+ACF(1)
  516        WNPD=WNPD+ACF(1)/12.+SUM
  517        IF(IS.NE.MONTE) RETURN
  518        DO 510 I=1,NH
  519    510 PS(I)=PSA(I)/MONTE
  520        WNPD=WNPD/MONTE
  521        SS=SS/MONTE
  522        WRITE(6,2017)
  523        WRITE(6,2005)(PS(I),I=1,NH)
  524        WRITE(6,2018)WNPD,SS
  525        WRITE(7,1011)WNPD
  526        DO 51 I=1,NH
  527     51 PS(I)=1./SQRT(PS(I))
  528        CALL CLEAR (PH(1),PH(NH))
  529        CALL FORINV (PS,PH,NH,DF,F,NF,DN,0)
  530        FC=1./F(NF/2)
  531        DO 52 I=1,NF
  532     52 F(I)=FC*F(I)
  533        WRITE(6,2019)
  534        WRITE(6,1003)(F(I),I=1,NF)
  535        WRITE(7,1003)(F(I),I=1,NF)
  536  1003 FORMAT(10F8.3)
  537  1011 FORMAT(F10.3)
  538  2005 FORMAT(1H ,10F8.5)
  539  2017 FORMAT(1HO,'NORMALIZED POWER SPECTRUM')
  540  2018 FORMAT(1HO,'WNPD=',E16.5,2X,'SIGMA SQUARED=',E16.5)
  541  2019 FORMAT(1HO,'PRE-WHITENING SPREAD FUNCTION')
  542        RETURN
  543        END
  544        SUBROUTINE FOURIR(DATA,NDATA,DX,TAU,PHI,DELTAU,NHARM,IOPT)
  545     C  AUTHOR- M.J.MAZUROWSKI
  546        DIMENSION DATA(1),TAU(1),PHI(1),F(1950),G(1950),A(1950),B(1950),
  547       * VCOS(576),VSIN(576)
  548        IF(NDATA/2.EQ.(NDATA+1)/2)  GO TO 8
  549        NDATA=NDATA+1
  550        DATA(NDATA)=DATA(NDATA-1)
  551     8  NHARM=NDATA/2
  552        F(1) = DATA(NHARM)
  553        G(1) = 0.0
  554        F(NHARM+1) = DATA(NDATA)
  555        G(NHARM+1) = 0.0
  556        DO 1  I=2,NHARM
  557        NHP = NHARM+I-1
  558        NHM = NHARM-I+1
```

ORIGINAL PAGE IS OF POOR QUALITY

CARD NO **** CONTENTS ****

```
      F(I) = DATA(NHP1+ DATA(NHM1
    1 G(I) = DATA(NHP1- DATA(NHM1
      HNO = NHARM1
      SUM0 = 0.0
      NHP1 = NHARM+1
      DO 2  I=1,NHP1
    2 SUM0 = SUM0 + F(I)
      A(1) = SUM0/HNO
      NHCS = (NHARM+3)/2
      DO 3  K=1,NHCS
      VCOS(K)=COS(3.14159*(K-1)/HNO)
    3 VSIN(K)=SIN(3.14159*(K-1)/HNO)
      B(NHP1) = 0.0
      B(1) = 0.0
      DO 5  I=2,NHARM
      SUM1 = 0.0
      SUM2 = 0.0
      DO 4  J=1,NHP1
      MD  =(I-1)*(J-1)/(2*HNHARM)
      L = (I-1)*(J-1)-2* MD*NHARM
      NSIGN = 2*L /NHARM +1
      GO TO (31,32,33,34),NSIGN
   31 SUM1 = SUM1+F(J)*VCOS(L+1)
      SUM2 = SUM2+G(J)*VSIN(L+1)
      GO TO 4
   32 L = NHARM-L
      SUM1 = SUM1-F(J)*VCOS(L+1)
      SUM2 = SUM2+G(J)*VSIN(L+1)
      GO TO 4
   33 L = L-NHARM
      SUM1 = SUM1-F(J)*VCOS(L+1)
      SUM2 = SUM2-G(J)*VSIN(L+1)
      GO TO 4
   34 L = 2*NHARM-L
      SUM1 = SUM1+F(J)*VCOS(L+1)
      SUM2 = SUM2-G(J)*VSIN(L+1)
    4 CONTINUE
      A(I) = SUM1/HNO
      B(I) = SUM2/HNO
    5 CONTINUE
      SUM3 = 0.0
      DO 6  K=1,NHP1
    6 SUM3 = SUM3+F(K)*(-1.)**(K-1)
      A(NHP1) = SUM3/(2.*HNO)
      DELNU = 1./(FLOAT(NDATA- )*DX)
      IF(INOPT.EQ.1) GO TO 60
      DO 7  M=1,NHP1
      TAU(M) = 0.5*SQRT(A(M)**2+B(M)**2)
      IF(B(M).EQ.0.) GO TO 61
   60 PHI(M) = ATAN2(B(M),A(M))+3.1415927*(1.-SIGN(1.,B(M)))
      GO TO 7
   61 PHI(M)=(1.-SIGN(1.,A(M)))*3.1415927/2.
    7 CONTINUE
      RETURN
   80 DO 85 M=1,NHP1
      TAU(M)=A(M)
```

CARD NO **** CONTENTS ****

```
      65 PHI(N)=B(M)
         RETURN
         END
         SUBROUTINE FORINV(TAU,PHI,NHARM,DELNU,FUNC,NFUN,DELF,KLIP)
         AUTHOR- M.J.MAZUROWSKI.
         DIMENSION TAU(500),PHI(500),FUNC(1000),A(500),B(500),VCOS(255),
        *VSIN(255),SIGF(50)
         NHP1 = NHARM +1
         HNO = NHARM
         IF(KLIP.EQ.0) GO TO 41
         DO 1 I=2,NHP1
         FI = I-1
       1 SIGF(I)=SIN(3.141593*FI/HNO)/(3.141593*FI/HNO).
         SIGF(1)=1.0
         DO 4 I=1,NHP1
         A(I) = 2.*TAU(I)*COS(ABS(PHI(I)))*SIGF(I)
       4 B(I) = 2.*TAU(I)*SIN(PHI(I))*SIGF(I)
         GO TO 43
      41 DO 42 I=1,NHP1
         A(I) = 2.*TAU(I)*COS(ABS(PHI(I)))
      42 B(I) = 2.*TAU(I)*SIN(PHI(I))
      43 A(1) = A(1)/2.0
         NFUN = 2*NHARM
         DELF=1.0/(2.0*HNO*DELNU)
         NHCS=NHARM/2 +1
         DO 5 IT = 1,NHCS
         FIT = IT-1
         VCOS(IT) = COS(3.141593 *FIT/HNO)
       5 VSIN(IT)=SIN(3.141593 *FIT/HNO)
         DO 10 N = 1,NFUN
         SUM = 0.0
         NN = -NHARM +N
         NNA = IABS(NN)
         DO 8 NH=1,NHP1
         NNH=NNA*(NH-1)
         MG = NNH/(2*NHARM)
         L = (ABS(NNH-2*MG*NHARM))
         KSIGN = 2*L/NHARM+1
         SN = ISIGN(1,NN)
         GO TO (51,52,53,54),KSIGN
      51 SUM = SUM+A(NH)*VCOS(L+1)+B(NH)*   SN    *VSIN(L+1)
         GO TO 8
      52 L = NHARM-L
         SUM = SUM -A(NH)*VCOS(L+1)+B(NH)*   SN    *VSIN(L+1)
         GO TO 8
      53 L = L - NHARM
         SUM = SUM -A(NH)*VCOS(L+1)-B(NH)*   SN    *VSIN(L+1)
         GO TO 8
      54 L = 2*NHARM -L
         SUM = SUM+A(NH)*VCOS(L+1)-B(NH)*   SN    *VSIN(L+1)
       8 CONTINUE
      10 FUNC(N) = SUM
         RETURN
         END
```

ORIGINAL PAGE IS
OF POOR QUALITY

CARD ID PAGE/BOX NAME REFERENCES (SOURCE SEQUENCE NO. AND PAGE/BOX)

FORTRAN MODULE

CHART TITLE - INTRODUCTORY COMMENTS

CHART TITLE - PROCEDURES

CARD ID	PAGE/BOX	NAME	REFERENCES (SOURCE SEQUENCE NO. AND PAGE/BOX)					
(0000208)	8.08		(0000209)	8.10				
(0000209)	8.09	40						
(0000214)	8.15		(0000216)	8.17				
(0000216)	8.16	41						
(0000219)	8.22	4	(0000191)	7.21	(0000195)	7.26	(0000202)	8.04
(0000220)	8.23	3						
(0000221)	8.24	2						
(0000222)	8.25	1						
(0000223)	8.26	99						

CHART TITLE - NON-PROCEDURAL STATEMENTS

CHART TITLE - SUBROUTINE GEN

(0000258)	10.01	GEN	(0000179)	7.08-X				
(0000270)	10.02	301	(0000269)	10.01				
(0000272)	10.04		(0000273)	10.05				
(0000273)	10.05	306						
(0000275)	10.06	302	(0000269)	10.01				
(0000279)	10.09	312						
(0000279)	10.09		(0000279)	10.10				
(0000284)	10.12	303	(0000269)	10.01				
(0000287)	10.15		(0000288)	10.16				
(0000288)	10.16	305						
(0000291)	10.19		(0000292)	10.20				
(0000292)	10.20	308						
(0000294)	10.21	304	(0000269)	10.01				
(0000299)	10.24		(0000300)	10.25				
(0000300)	10.25	309						
(0000304)	10.28		(0000305)	10.29				
(0000305)	10.29	310						
(0000306)	10.30	300	(0000274)	10.05	(0000283)	10.11	(0000293)	10.20

CHART TITLE - NON-PROCEDURAL STATEMENTS

CHART TITLE - SUBROUTINE SYSTEM(1/PUNCH)

(0000310)	12.01	SYSTEM	(0000169)	7.19-X				
(0000319)	12.05	110	(0000315)	12.01				
(0000321)	12.07		(0000337)	12.24				
(0000326)	12.13	104	(0000322)	12.08	(0000324)	12.11		
(0000331)	12.18	106	(0000327)	12.14	(0000329)	12.16		
(0000336)	12.23	108	(0000332)	12.19	(0000334)	12.21		
(0000337)	12.24	101						
(0000340)	12.28		(0000338)	12.25				

CHART TITLE - NON-PROCEDURAL STATEMENTS

CHART TITLE - SUBROUTINE CON

(0000343)	14.01	CON	(0000323)	12.09-X				
(0000351)	14.03		(0000356)	14.12				
(0000353)	14.05		(0000356)	14.11				
(0000355)	14.08		(0000354)	14.00				
(0000356)	14.10	709						
(0000356)	14.10		(0000355)	14.08				

CARD ID PAGE/BOX NAME REFERENCES (SOURCE SEQUENCE NO. AND PAGE/BOX)

(0003581 14.14 701
(0003581 14.14 (0003581 14.15

CHART TITLE - NON-PROCEDURAL STATEMENTS

CHART TITLE - SUBROUTINE YLEV

(0003621 16.01 YLEV (0003281 12.15-X
(0003731 16.03 (0003611 16.14
(0003751 16.06 (0003741 16.04
(0003761 16.08 (0003751 16.06
(0003771 16.09 902 (0003791 16.10
(0003801 16.11 901 (0003771 16.09
(0003841 16.13 900

CHART TITLE - NON-PROCEDURAL STATEMENTS

CHART TITLE - SUBROUTINE YNOISE

(0003921 18.01 YNOISE (0003331 12.20-X
(0003941 18.03 (0003951 18.04
(0003951 18.04 001

CHART TITLE - NON-PROCEDURAL STATEMENTS

CHART TITLE - SUBROUTINE DIF

(0004031 20.01 DIF (0001981 8.02-X
(0004041 20.02 (0004081 20.06
(0004061 20.04 (0004071 20.05
(0004071 20.05 202
(0004081 20.06 201

CHART TITLE - NON-PROCEDURAL STATEMENTS

CHART TITLE - SUBROUTINE INT

(0004131 22.01 INT (0002011 8.03-X
(0004231 22.03 (0004361 22.17
(0004241 22.04 (0004371 22.16
(0004281 22.06 (0004291 22.07
(0004291 22.07 403
(0004371 22.16 402 (0004321 22.09
(0004381 22.17 401

CHART TITLE - NON-PROCEDURAL STATEMENTS

CHART TITLE - SUBROUTINE FNLPPP(IS)

(0004441 24.01 FNLPPP (0003171 12.03-X (0003251 12.12-X (0003301 12.17-X (0003351 12.22-X
(0004511 24.02 5 (0004591 24.12
(0004551 24.06 (0004571 24.09
(0004571 24.08 6
(0004581 24.11 10 (0004501 24.01
(0004641 24.16 (0004651 24.18
(0004651 24.17 15

CARD ID PAGE/BOX NAME REFERENCES (SOURCE SEQUENCE NO. AND PAGE/BOX)

CHART TITLE - NON-PROCEDURAL STATEMENTS

CHART TITLE - SUBROUTINE POSPEC

(0000471)	26.01	POSPEC	(0000194)	7.24-X	
(0000485)	26.06	5	(0000479)	26.01	
(0000488)	26.08		(0000489)	26.10	
(0000489)	26.09	10			
(0000494)	26.13		(0000499)	26.19	
(0000497)	26.15		(0000498)	26.17	
(0000498)	26.16	20			
(0000499)	26.18	30			
(0000502)	26.22		(0000506)	26.24	
(0000506)	26.23	40			
(0000511)	26.28		(0000513)	26.30	
(0000513)	26.29	50			
(0000518)	27.01		(0000517)	26.32	
(0000519)	27.02	510			
(0000519)	27.02		(0000519)	27.03	
(0000527)	27.13	51			
(0000527)	27.13		(0000527)	27.14	
(0000532)	27.19	52			
(0000532)	27.19		(0000532)	27.20	

CHART TITLE - NON-PROCEDURAL STATEMENTS

CHART TITLE - SUBROUTINE FOURTR(DATA,NDATA,DX,TAU,PHI,DELNU,NHARM,NOPT)

(0000545)	29.01	FOURTR	(0000507)	26.25-X				
(0000551)	29.03	8	(0000548)	29.01				
(0000557)	29.06		(0000560)	29.09				
(0000560)	29.07	1						
(0000565)	29.11	2						
(0000565)	29.11		(0000565)	29.12				
(0000569)	29.15		(0000570)	29.17				
(0000570)	29.16	3						
(0000574)	29.20		(0000596)	30.04				
(0000577)	29.22		(0000595)	30.02				
(0000581)	29.24	31	(0000580)	29.23				
(0000584)	29.25	32	(0000580)	29.23				
(0000588)	29.26	33	(0000580)	29.23				
(0000592)	30.01	34	(0000580)	29.23				
(0000595)	30.02	4	(0000583)	29.24	(0000587)	29.25	(0000591)	29.26
(0000598)	30.04	5						
(0000601)	30.07	6						
(0000601)	30.07		(0000601)	30.08				
(0000606)	30.12		(0000611)	30.21				
(0000608)	30.14	60						
(0000613)	30.15	80	(0000604)	30.10				
(0000614)	30.16		(0000615)	30.18				
(0000615)	30.17	85						
(0000610)	30.20	61	(0000607)	30.13				
(0000611)	30.21	7	(0000609)	30.14				

CHART TITLE - NON-PROCEDURAL STATEMENTS

CARD ID PAGE/BOX NAME REFERENCES (SOURCE SEQUENCE NO. AND PAGE/BOX)

CHART TITLE - SUBROUTINE FORINV(TAU,PHI,NHARM,DELNU,FUNC,NFUN,DELF,KLIP)

CHART TITLE - NON-PROCEDURAL STATEMENTS

LOCATION		DIAGNOSTIC
CARD ID	PAGE/BOX	
(0000254)	3.11	UNDEFINED - 'EFPLOT' EXTERNAL REFERENCE
(0000079)	3.25	UNDEFINED - 'GRNORG' EXTERNAL REFERENCE
(0000210)	8.12	UNDEFINED - 'MINV' EXTERNAL REFERENCE
(0000452)	24.03	UNDEFINED - 'PLOT' EXTERNAL REFERENCE
(0000456)	24.07	UNDEFINED - 'NGRID' EXTERNAL REFERENCE
(0000457)	24.08	UNDEFINED - 'NGRID' EXTERNAL REFERENCE
(0000462)	24.14	UNDEFINED - 'PLOT' EXTERNAL REFERENCE
(0000466)	24.19	UNDEFINED - 'LINE' EXTERNAL REFERENCE
(0000467)	24.21	UNDEFINED - 'PLOT' EXTERNAL REFERENCE
(0000482)	26.04	UNDEFINED - 'CLEAR' EXTERNAL REFERENCE
(0000528)	27.15	UNDEFINED - 'CLEAR' EXTERNAL REFERENCE

CHART TITLE - INTRODUCTORY COMMENTS

THIS PROGRAM SIMULATES IMAGE PROCESSING SYSTEMS FOR THE PURPOSE OF CALCULATION OF VARIANCES IN PARAMETER ESTIMATION FROM MEASUREMENTS MADE ON OUTPUT PRODUCTS AS A FUNCTION OF SUBSYSTEM ELEMENT PERFORMANCE. ANY SYSTEM WHICH CAN BE REPRESENTED BY AN ARBITRARY SEQUENCE OF LINEAR-ELEMENTS, NONLINEAR GAINS, AND ADDITIVE NOISE CAN BE SIMULATED. INPUT TARGETS GENERATED HAVE THE FORM: Y=F(X,A(I)) WHERE THE A(I) ARE TARGET PARAMETERS AND X=DISTANCE (CURRENTLY I.E.4). THE CRAMER-RAO BOUNDS ON THE VARIANCES OF THE A(I) ESTIMATES ARE CALCULATED.

THE PROGRAM OPERATES IN ONE OF THREE MODES
MODE=1 IMPLIES CALCULATION OF VARIANCES
MODE=2 IMPLIES CALCULATION OF NOISE SPECTRAL DENSITY AND PRE-WH FILTER SPREAD FUNCTION
MODE=3 IMPLIES TARGET IS PLOTTED AFTER EACH SYSTEM ELEMENT
UNITS: THE UNITS OF THE CALCUALATED VARIANCES= THE UNITS OF THE RESPECTIVE A(I) SQUARED

DEFINITIONS
NPUNCH.NE.0 YIELDS OUTPUT TARGET PUNCHED ON CARDS
NONTE=NUMBER OF REPETITIONS FOR NOISE POWER SPECTRUM CALCULATION
WNPD=WHITE NOISE POWER SPECTRAL DENSITY
IREFS=RANDOM NUMBER GENERATOR SEED
NA=NUMBER OF A'S OF INPUT TARGET
DIFA=DECIMAL FRACTIONAL CHANGE IN EACH A FOR PARTIAL DIFFERENTIAL COMPUTATION
IF ANY A(I) REPRESENTS POSITION, THEN DIFA MUST BE CHOSEN SUCH THA
DIFA*A(I)/DELTX = INTEGER
N(I)=NUMBER OF VALUES OF A(I)
DA(I)=INCREMENT IN VALUE OF A(I) INCREASE
A(I)=INITIAL VALUE OF A(I)
CHOOSE A(3),A(4) EQUAL TO INTEGER MULTIPLES OF DELTX
NX=NUMBER OF POINTS IN TARGET GENERATED (CURRENTLY NX.LE.200)
DELTX=DISTANCE BETWEEN POINTS IN X DIRECTION
NBLOCK=NUMBER OF SYSTEM BLOCKS --ONE SYSTEM BLOCK=LINEAR ELEMENT, NONLINEAR ELEMENT, ADDITIVE NOISE (CURRENTLY NBLOCK.LE.20)
OP(I,J)=0 IMPLIES SYSTEM ELEMENT TYPE J BYPASSED IN I'TH SYSTEM BLOCK
J=1 REFERS TO LINEAR ELEMENT
J=2 REFERS TO NONLINEAR ELEMENT
J=3 REFERS TO ADDITIVE NOISE
NRUN=NUMBER OF SYSTEM BLOCK PERFORMANCE CONFIGURATIONS
ICONTRUN,I)=0 IMPLIES NO CHANGE IN SPCN DATA FOR I'TH BLOCK

CHART TITLE - INTRODUCTORY COMMENTS

ILEVEL(RUN,I)=0 IMPLIES NO CHANGE IN NONLINEARITY FOR I'TH BLOCK
INOISE(RUN,I)=0 IMPLIES NO CHANGE IN NOISE FOR I'TH BLOCK
NS=NUMBER OF POINTS IN SFCN
SFCN=SPREAD FUNCTION OF PARTICULAR SYSTEM BLOCK
SET THE NUMBER OF POINTS IN EACH SFCN=NX
THE X INCREMENT OF SFCN MUST ALSO EQUAL DELTX
ND(I)=NUMBER OF POINTS IN H-D CURVE FOR BLOCK I
DIN(I,J)=INPUT DENSITY VALUES FOR H-D CURVE OF BLOCK I
DOUT(I,J)=OUTPUT DENSITY VALUES FOR DIN(I,J)
SIGMA=STD. DEVIATION OF NOISE

CHART TITLE - PROCEDURES

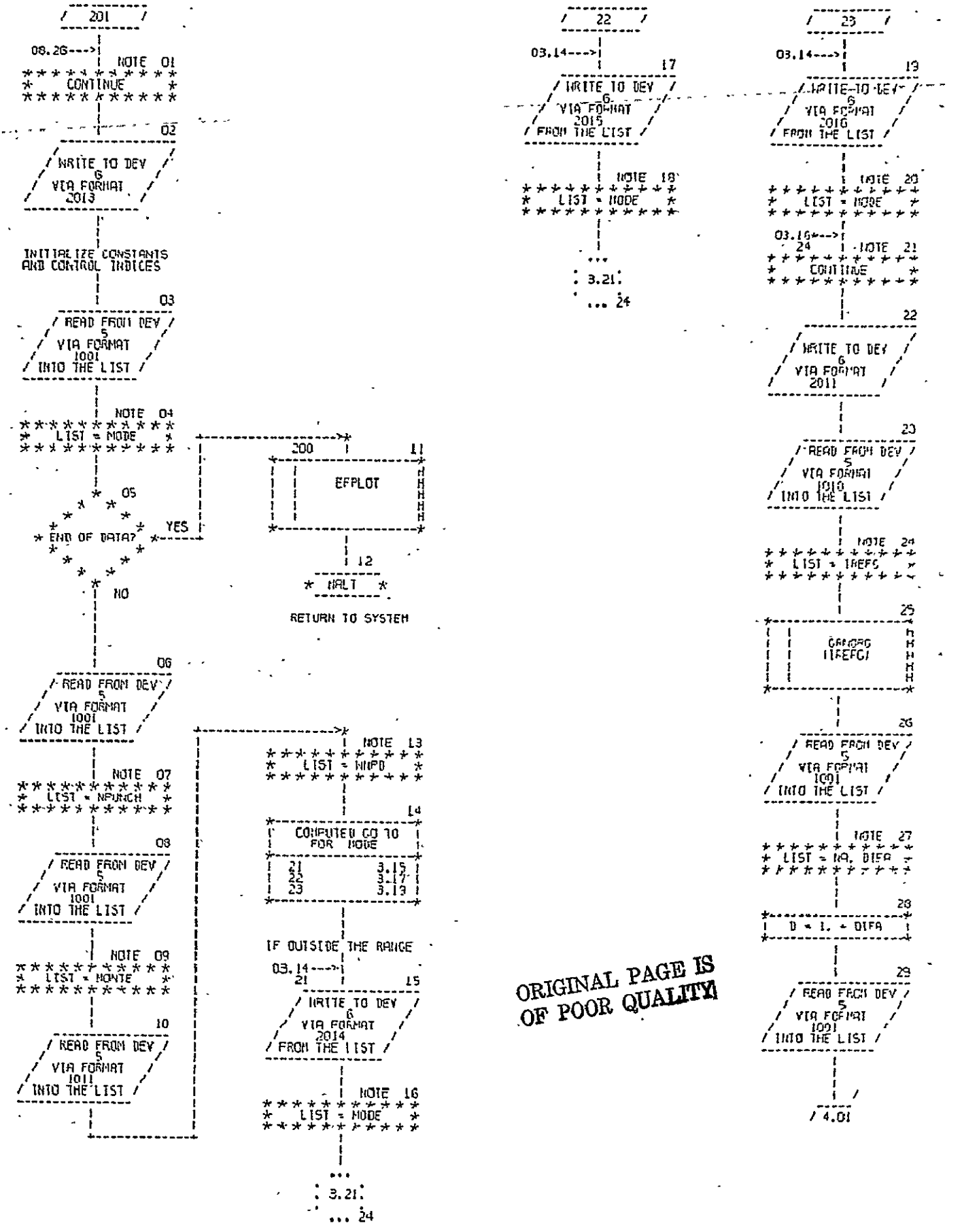

CHART TITLE - PROCEDURES

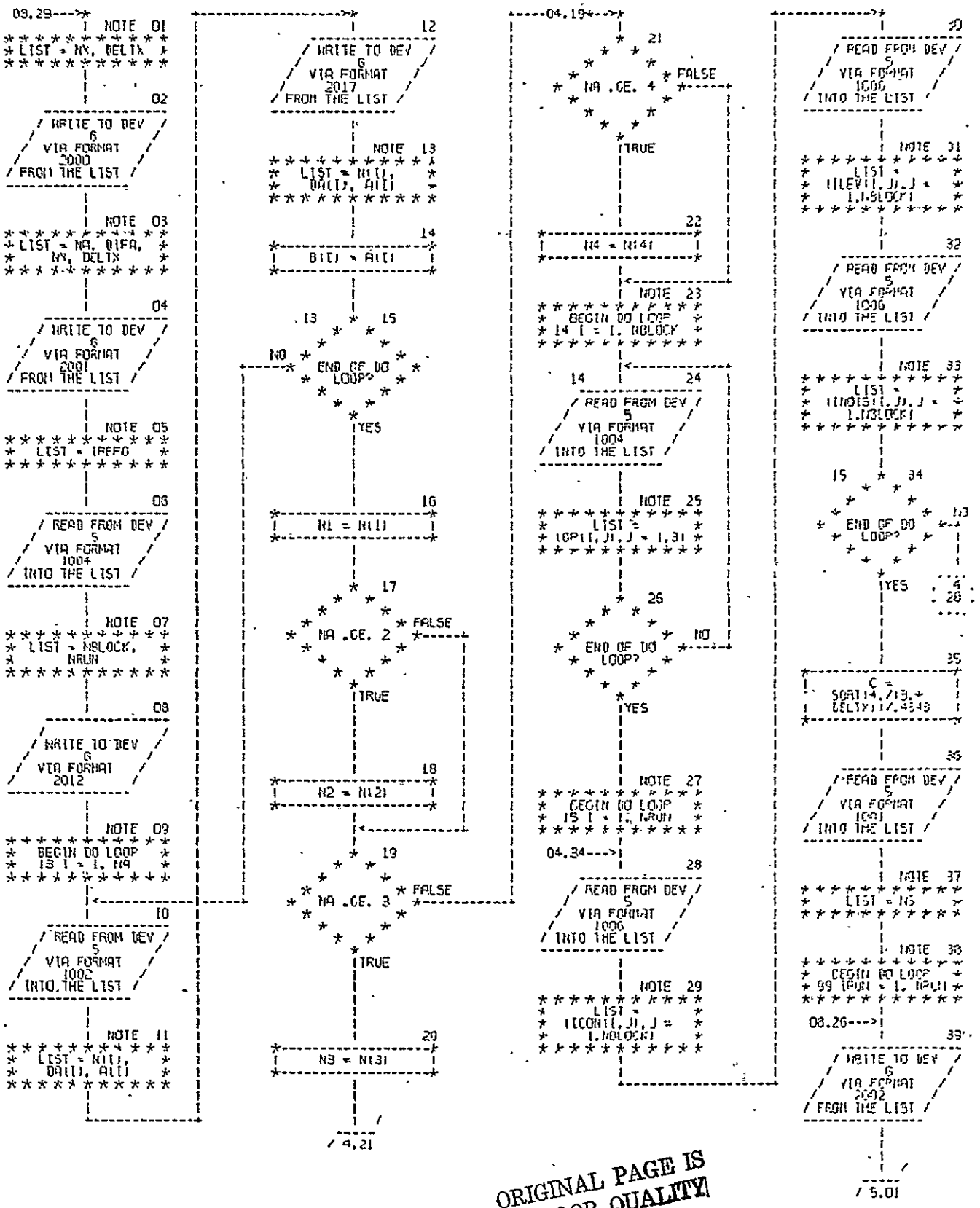

ORIGINAL PAGE IS OF POOR QUALITY

CHART TITLE - PROCEDURES

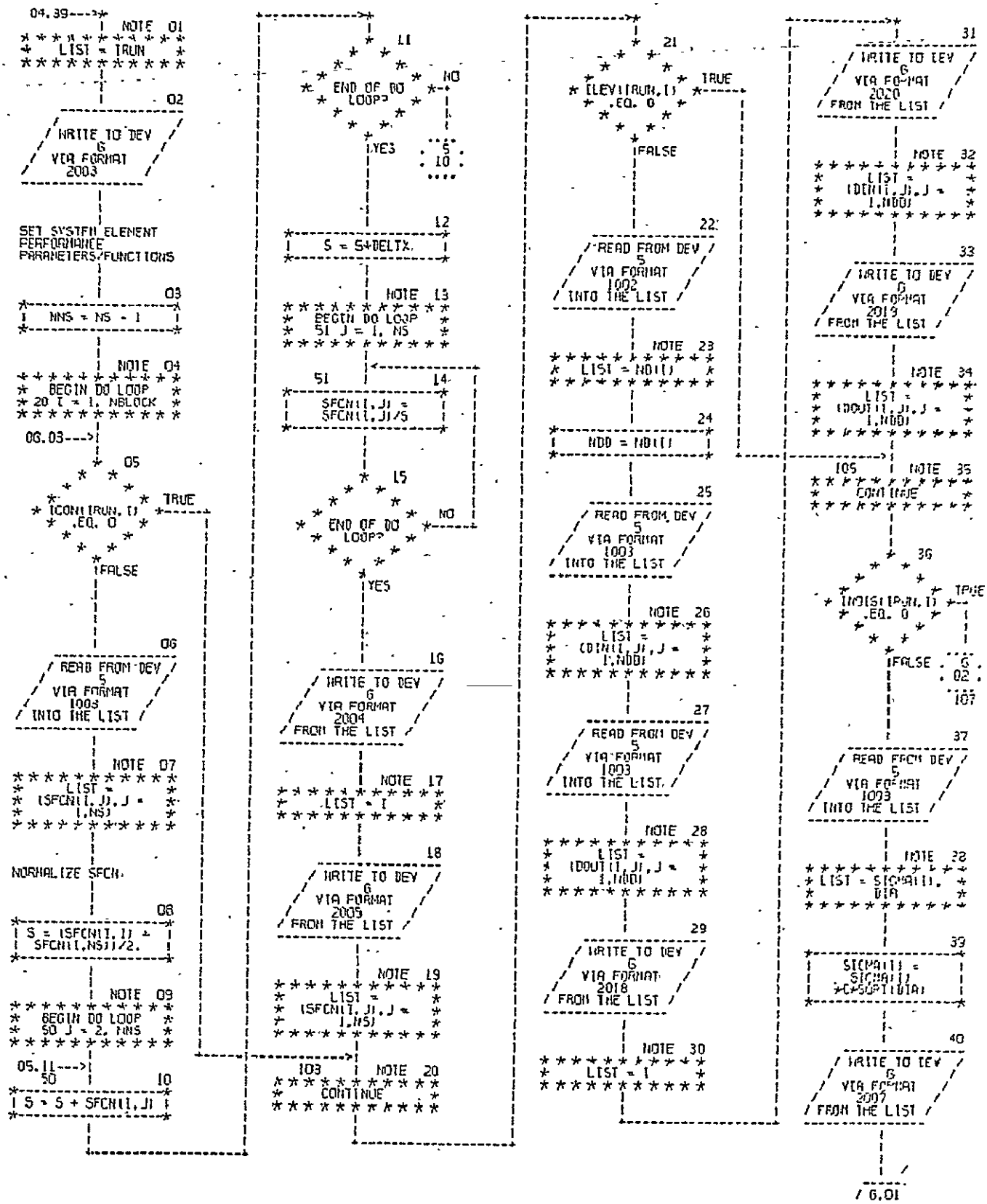

CHART TITLE - PROCEBURES

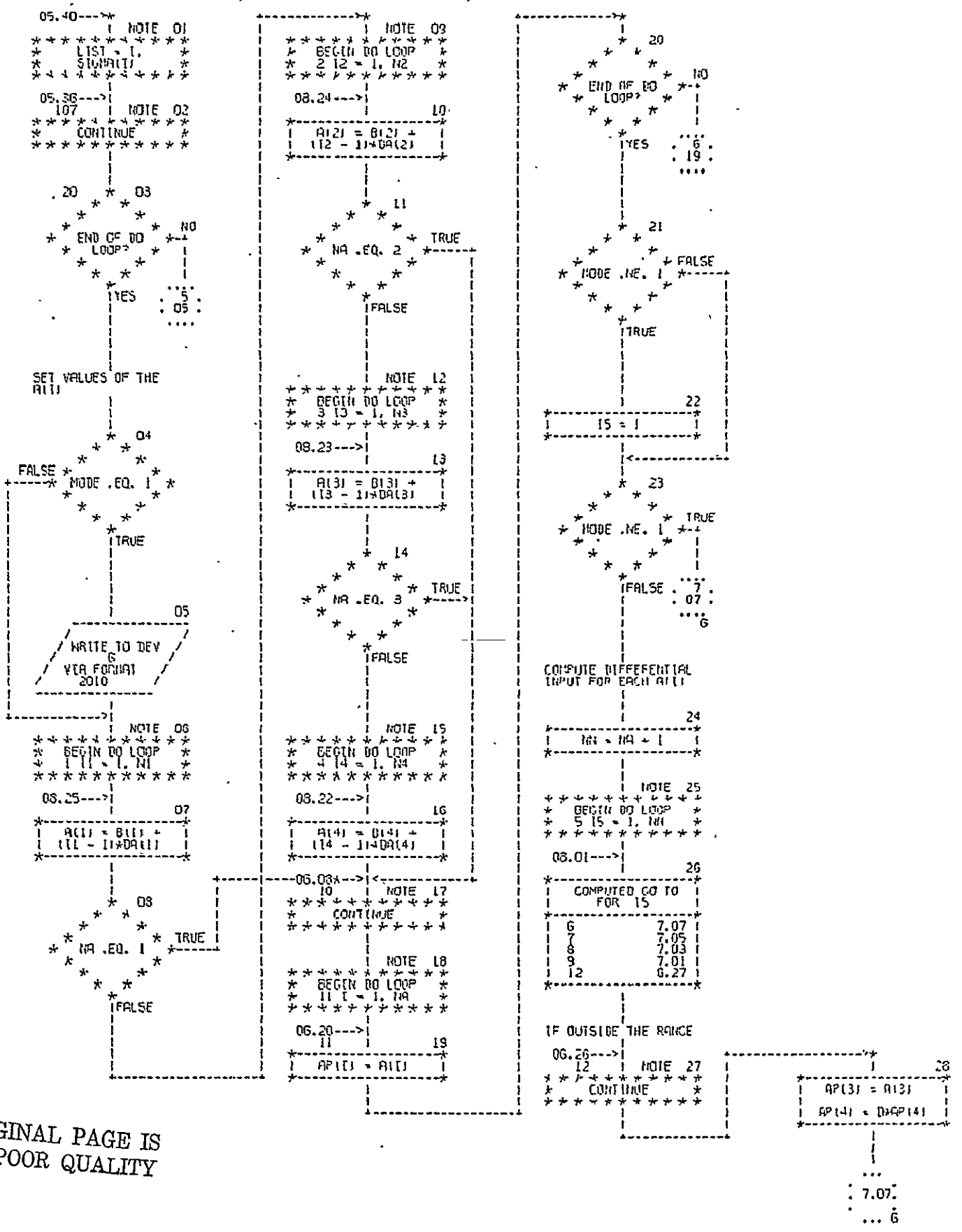

ORIGINAL PAGE IS
OF POOR QUALITY

CHART TITLE - PROCEDURES

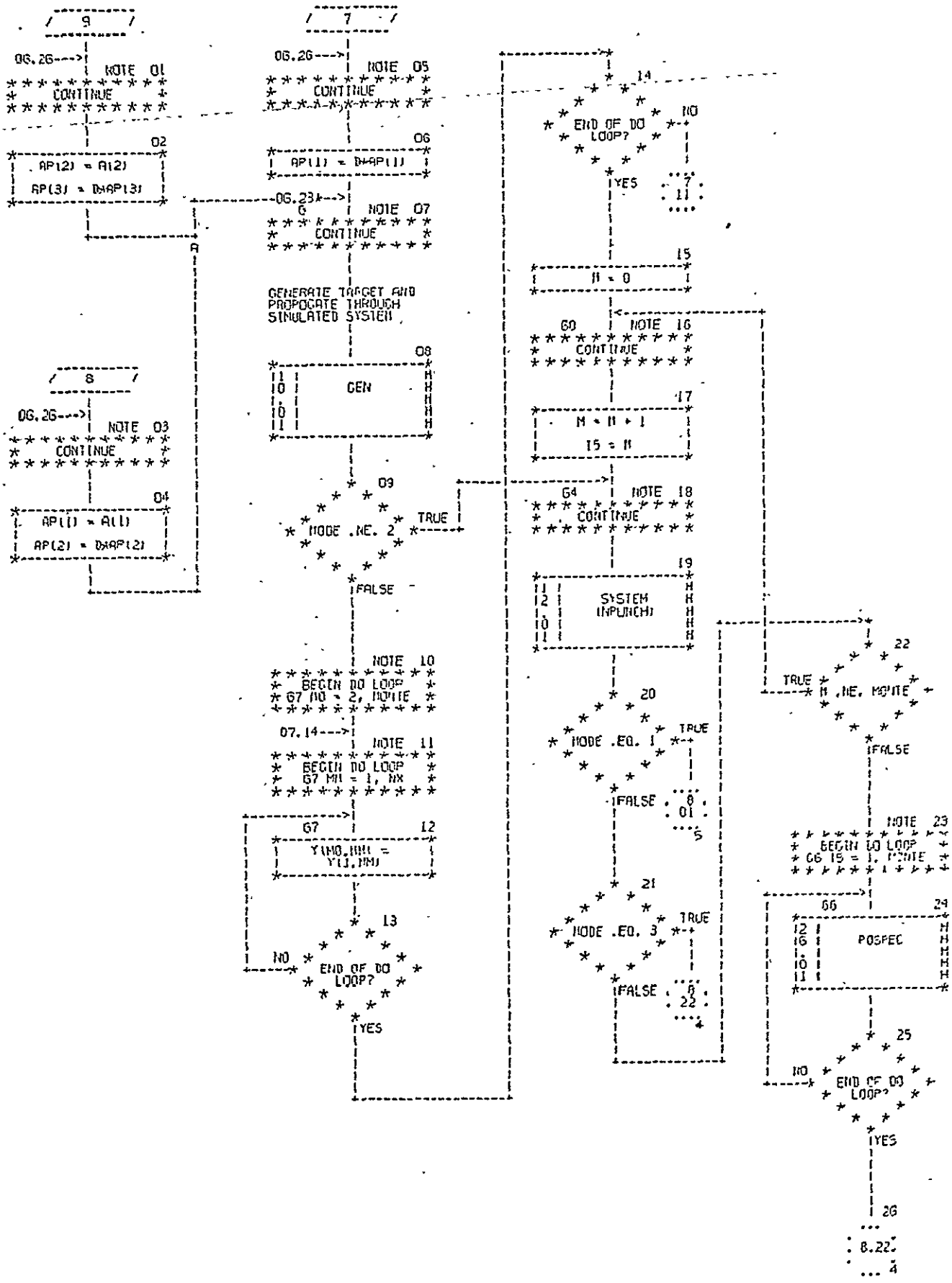

CHART TITLE - PROCEDURES

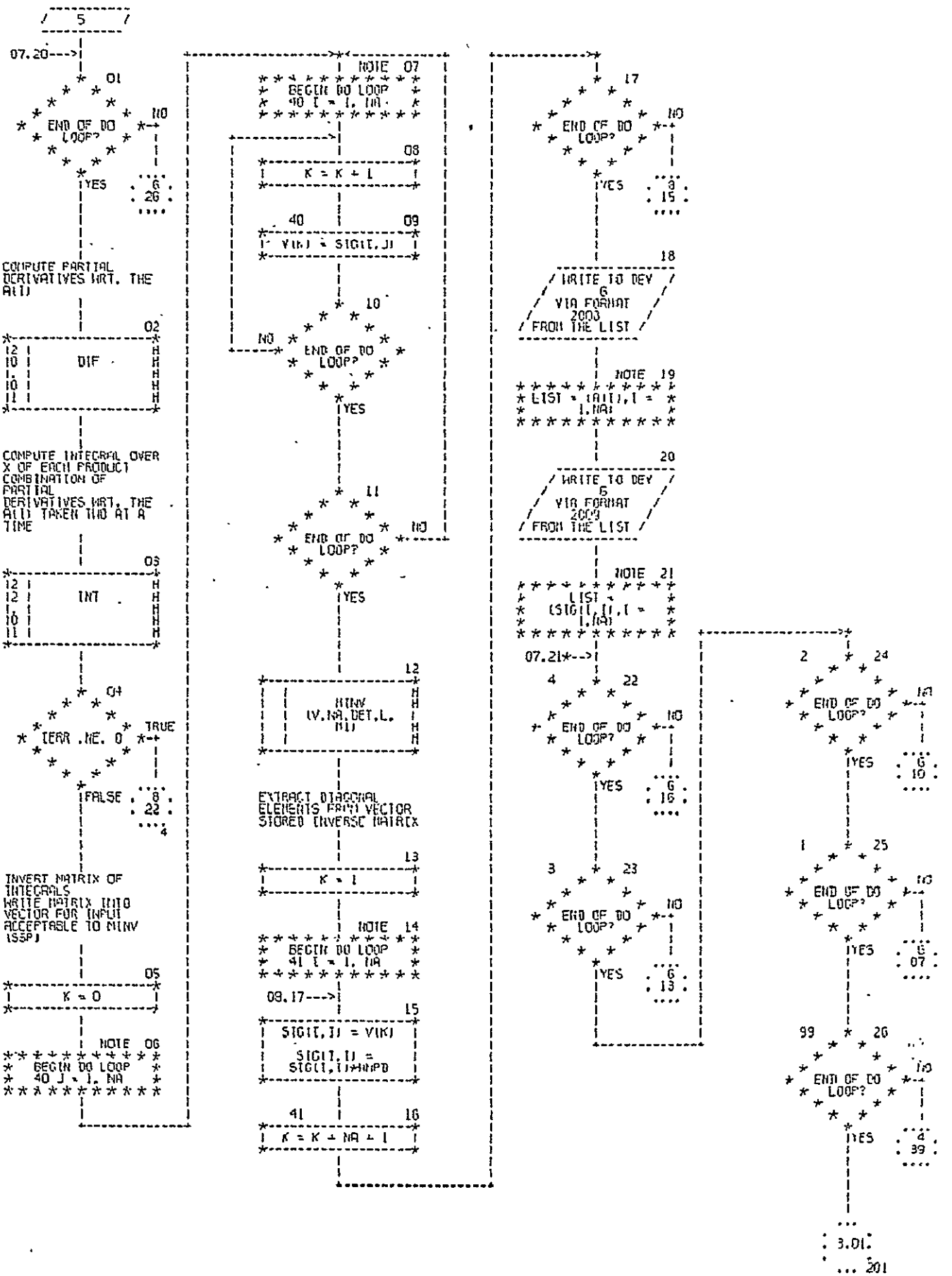

CHART TITLE - NON-PROCEDURAL STATEMENTS

```
      DIMENSION N(4),DA(4),L(4),NI(4),V(16),B(4),YH(200)
      COMMON NA,NX,NBLOCK,IS,IRUN,IB,DIFA,DELTX,OP(20,3),ICON(20,20),ILE
     V(20,20),INOIS(20,20),A(4),AP(4),Y(20,999),DYDQ(4,999),SIG(4,4),SF
     CN(20,200),SIGNA(20),MODE,IERR,CLEV(20,4),MONTE,
     DIN(20,30),DOUT(20,30),ND(20),NS
2018  FORMAT(1H0,'BLOCK',I4,2X,'NONLINEAR LEVEL TRANSFER CURVE')
2019  FORMAT(1H ,'DOUT',20F6.3)
2020  FORMAT(1H ,'DIN',20F6.3)
1001  FORMAT(I4,F8.3)
1002  FORMAT(I4,2F10.4)
1003  FORMAT(10F8.3)
1004  FORMAT(3I4)
1006  FORMAT(40I2)
1010  FORMAT(I9)
1011  FORMAT(F10.3)
2000  FORMAT(1H0,'NA=',I2,2X,'DIFA=',F6.3,4X,'NX=',I4,2X,'DELTX=',F6.3)
2001  FORMAT(1H ,'IREFG=',I9)
2002  FORMAT(1H1,'IRUN=',I4)
2003  FORMAT(1H0,'NEW SYSTEM ELEMENT PERFORMANCE DATA')
2004  FORMAT(1H0,'BLOCK',I4,2X,'SFCN')
2005  FORMAT(1H ,10F8.3)
2006  FORMAT(1H0,'BLOCK',I4,3X,'CLEV1=',F6.3,2X,'CLEV2=',F6.3,2X,'CLEV3=
     ',F6.3,2X,'CLEV4=',F6.3)
2007  FORMAT(1H0,'BLOCK',I4,2X,'SIGNA=',F6.3)
2008  FORMAT(1H ,4E10.3)
2009  FORMAT(1H+,40X,4E10.3)
2010  FORMAT(//3X,'A(1)',6X,'A(2)',6X,'A(3)',6X,'A(4)',5X,'SIG(1)',4X,'S
     IG(2)',4X,'SIG(3)',4X,'SIG(4)')
2011  FORMAT(1H0,'CONSTANTS')
2012  FORMAT(1H0,'N(I)',5X,'DA(I)',5X,'A(I)')
2013  FORMAT(1H1,'PROGRAM STPS')
2014  FORMAT(1H0,'MODE',I2,2X,'CALCULATION OF VARIANCES')
2015  FORMAT(1H0,'MODE',I2,2X,'CALCULATION OF NOISE SPECTRAL DENSITY AND
      PRE-WHITENING FILTER SPREAD FUNCTION')
2016  FORMAT(1H0,'MODE',I2,2X,'TRACE PLOT OF TARGET PROPOGATED THROUGH S
     IMULATED SYSTEM')
2017  FORMAT(1H ,I4,2F10.3)
```

CHART TITLE - SUBROUTINE - GEN

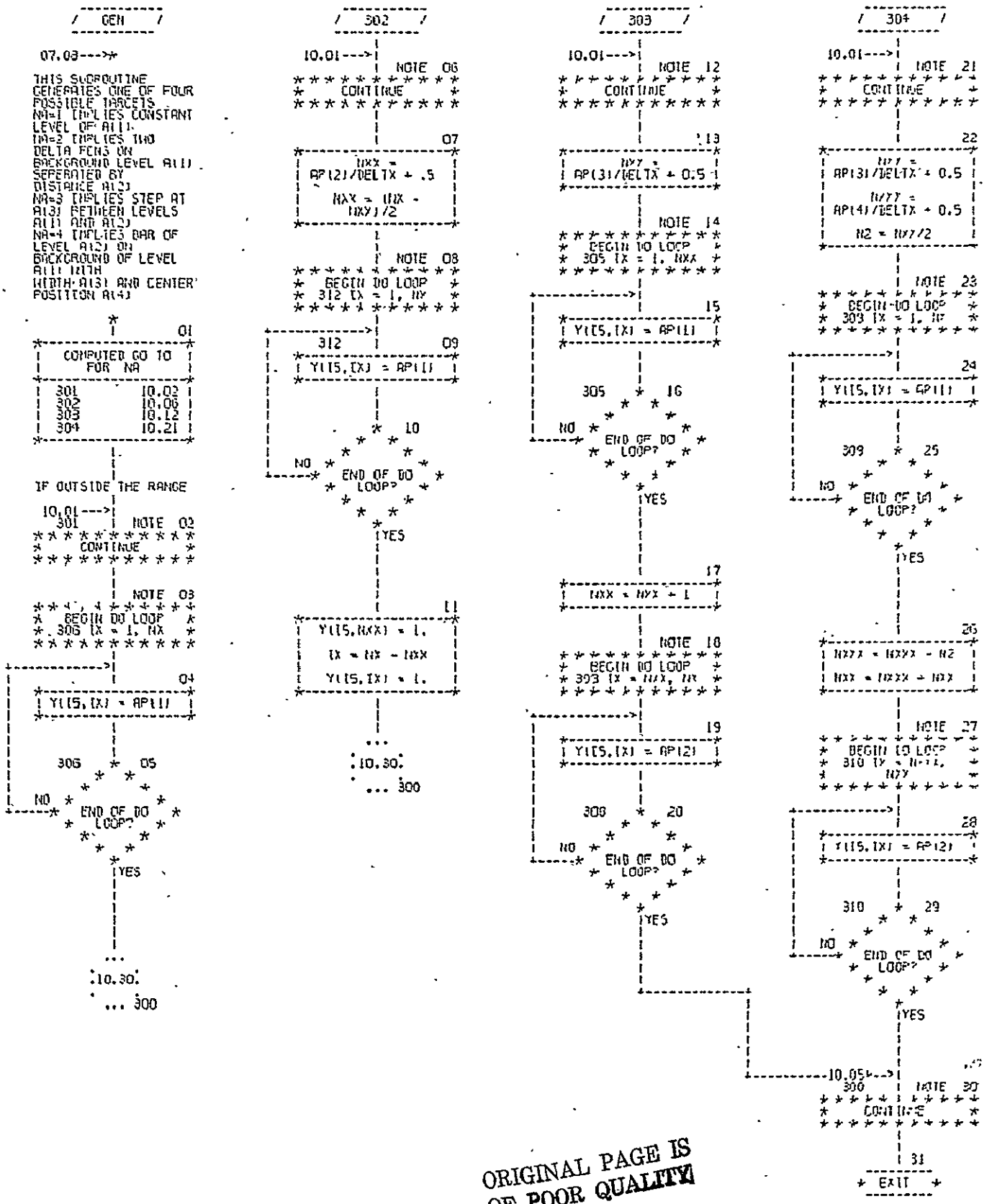

CHART TITLE - NON-PROCEDURAL STATEMENTS

```
COMMON NA,NX,NBLOCK,I5,IRUN,I8,DIFA,DELTX,OP(20,3),ICON(20,20),ILE
V(20,20),INDIS(20,20),A(4),AP(4),Y(20,999),DYDA(4,999),SIG(4,4),SF
CN(20,200),SIGMA(20),NODE,IERR,CLEV(20,4),MONTE,
DIN(20,30),DOUT(20,30),ND(20),NS
```

CHART TITLE - SUBROUTINE SYSTEM(NPUNCH)

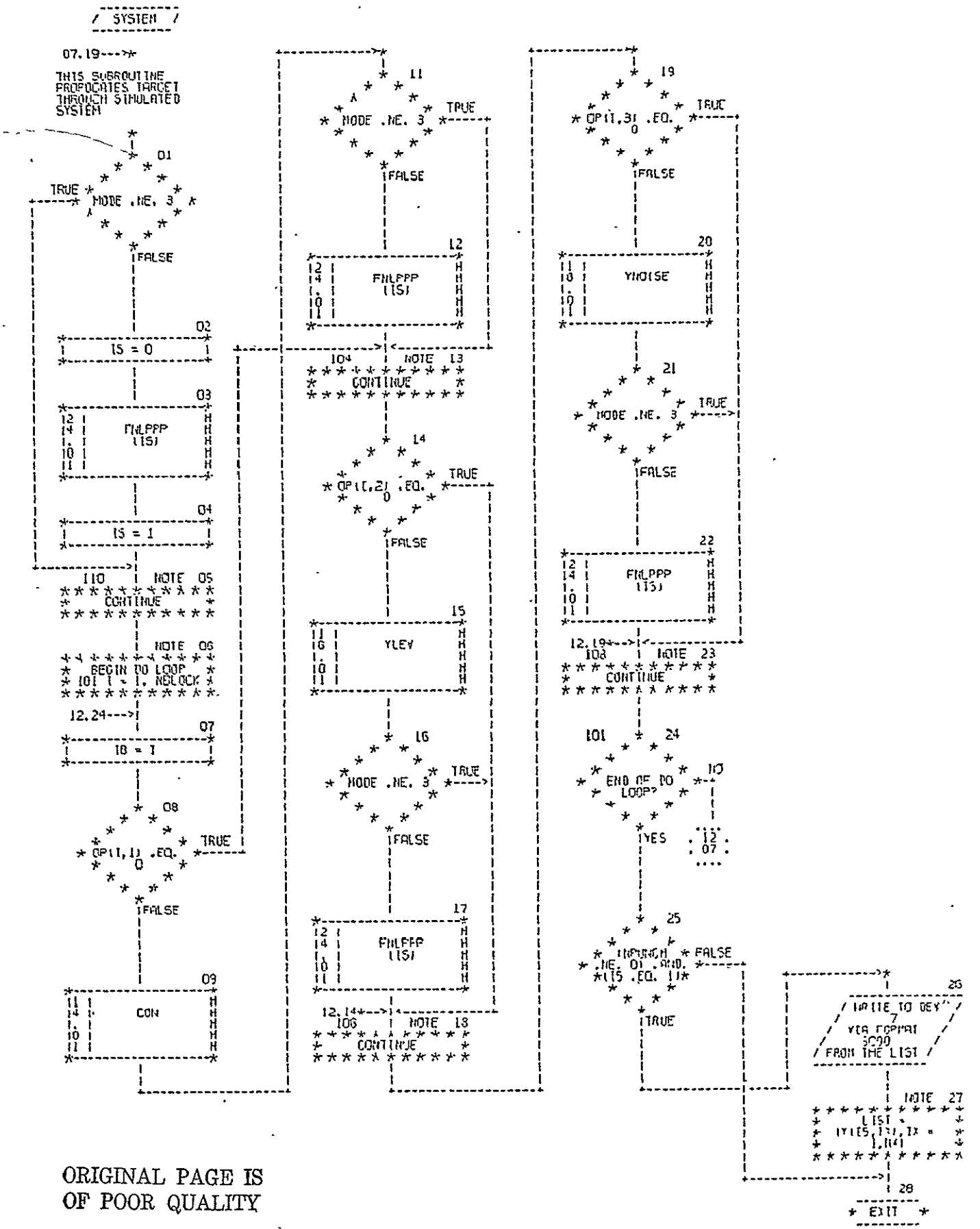

ORIGINAL PAGE IS
OF POOR QUALITY

CHART TITLE - NON-PROCEDURAL STATEMENTS

```
      COMMON NA,NX,NBLOCK,IS,IRUN,IB,DIFA,DELTX,OP(20,3),ICON(20,20),ILE
      Y(20,20),INDIS(20,20),A(4),AP(4),Y(20,999),DYDA(4,999),SIG(4,4),SF
      CN(20,200),SIGMA(20),NODE,TERR,CLEV(20,4),MONTE,
      DIN(20,30),DOUT(20,30),ND(20),NS
3000  FORMAT(10F8.5)
```

CHART TITLE - SUBROUTINE CON

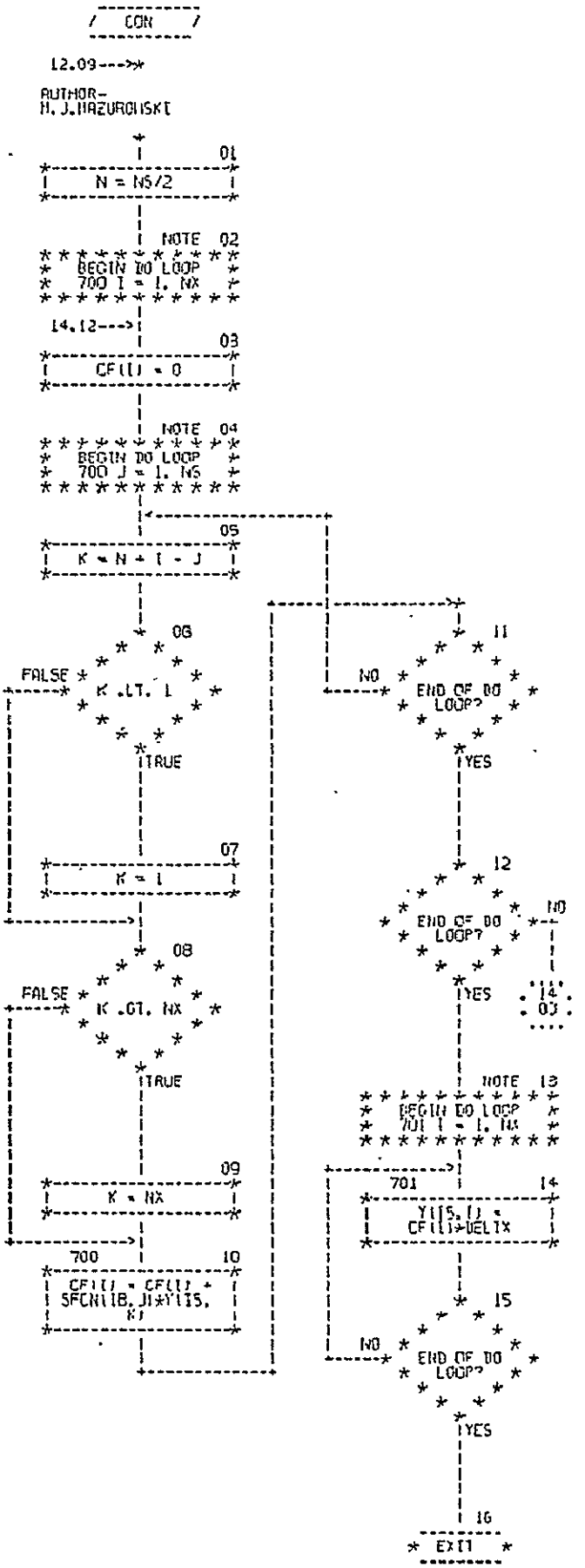

CHART TITLE - NON-PROCEDURAL STATEMENTS

```
      DIMENSION CF(999)
      COMMON NA,NX,NBLOCK,I5,IRUN,I6,DIFA,DELTX,OP(20,3),ICON(20,20),ILE
     V(20,20),INOIS(20,20),A(4),AP(4),Y(20,999),DYDA(4,999),SIG(4,4),SF
     CN(20,200),SIGMA(20),MODE,IERR,CLEV(20,4),MONTE,
     DIN(20,30),DOUT(20,30),ND(20),NS
```

CHART TITLE - SUBROUTINE YLEV

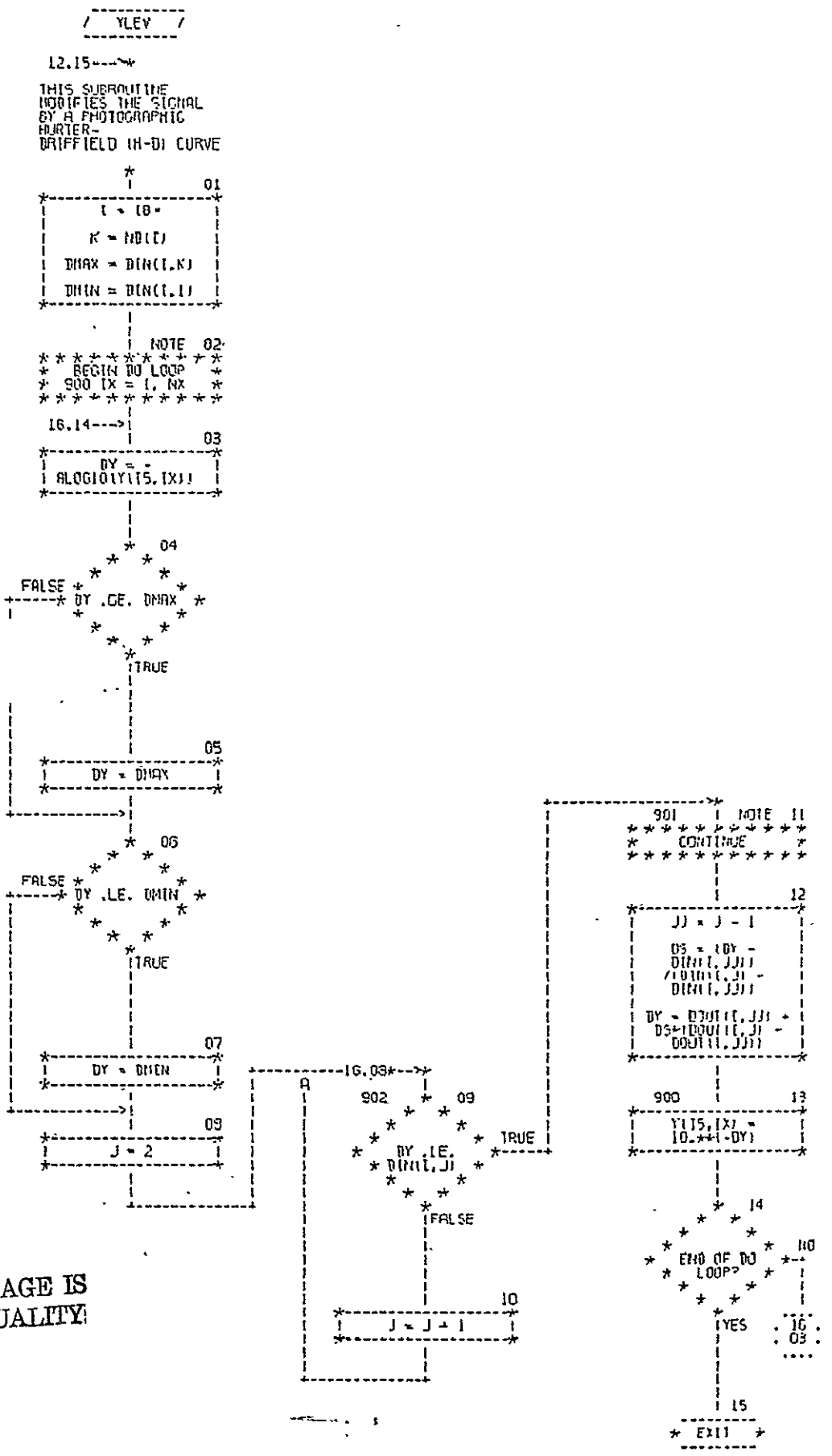

ORIGINAL PAGE IS
OF POOR QUALITY

CHART TITLE - NON-PROCEDURAL STATEMENTS

```
      COMMON NA,NX,NBLOCK,I5,CRUN,IB,DIFA,DELTX,OP(20,3),ICON(20,20),ILE
     V(20,20),INOIS(20,20),A(4),AP(4),Y(20,999),DYDA(4,999),SIG(4,4),SF
     CN(20,200),SIGNA(20),NODE,IERR,CLEV(20;4);MONTE,
     *DIN(20,30),DOUT(20,30),NB(20),NS
```

CHART TITLE - SUBROUTINE YNOISE

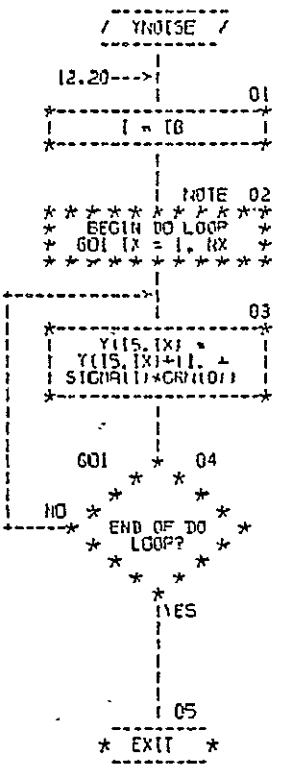

CHART TITLE - NON-PROCEDURAL STATEMENTS

```
COMMON NA,NX,NBLOCK,15,IRUN,18,DIFA,DELTX,OP(20,3),ICON(20,20),ILE
V(20,20),INDIS(20,20),A(4),AP(4),Y(20,999),DYDA(4,999),SIG(4,4),SF
CN(20,200),SIGNAL(20),NODE,IERR,CLEV(20,4),MONTE,
DIN(20,30),DOUT(20,30),ND(20),NS
```

CHART TITLE - SUBROUTINE DIF

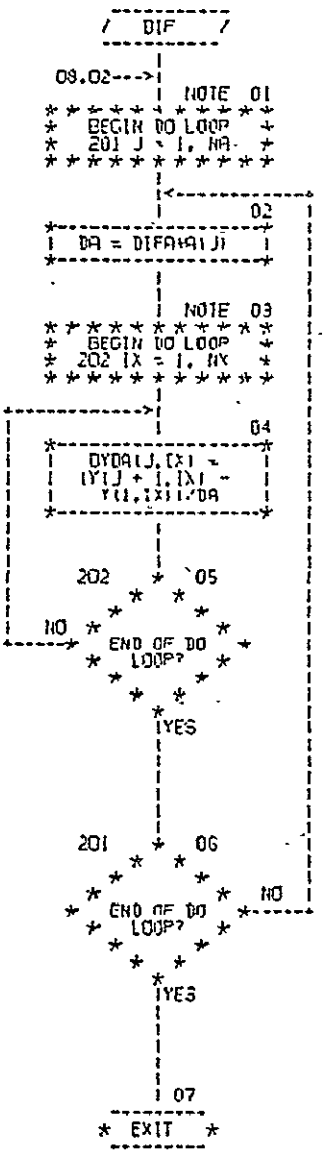

CHART TITLE - NON-PROCEDURAL STATEMENTS

```
      COMMON NA,NX,NBLOCK,IS,IRUN,IB,DIFA,DELTX,QP(20,3),ICON(20,20),TLE
     V(20,20),INOIS(20,20),A(4),AP(4),Y(20,999),D(DA(4,999),SIG(4,4),SF
     CN(20,200),SIGNA(20),NODE,IERR,CLEV(20,4),MONTE,
     DIN(20,30),DOUT(20,30),ND(20),NS
```

CHART TITLE - SUBROUTINE INT

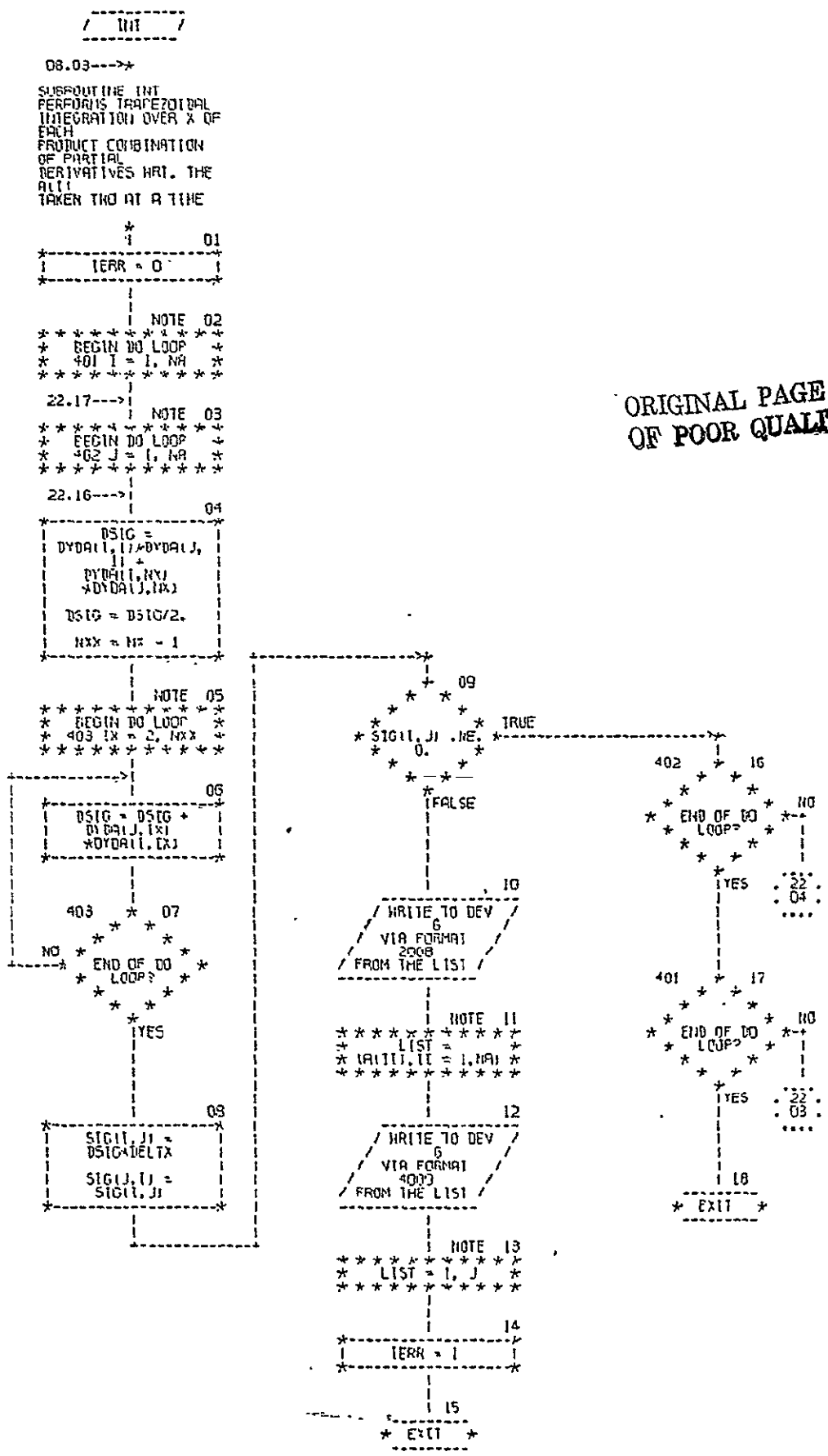

CHART TITLE - NON-PROCEDURAL STATEMENTS

```
      COMMON NA,NX,NBLOCK,I5,IRUN,I6,DIFA,DELTX,OP(20,3),ICON(20,20),ILE
     *V(20,20),INDIS(20,20),A(4),AP(4),Y(20,999),DYDA(4,999),SIG(4,4),SF
     *CN(20,200),SIGNAL(20),NODE,IERR,CLEY(20,4),MONTE,
     *DIN(20,30),DOUT(20,30),ND(20),NS
2098  FORMAT(1H ,4E10.3)
4000  FORMAT(1H+,40X,'SIG(',I2,I2,')=0. CALCULATION TERMINATED').
```

CHART TITLE - SUBROUTINE FNLPPP(IS)

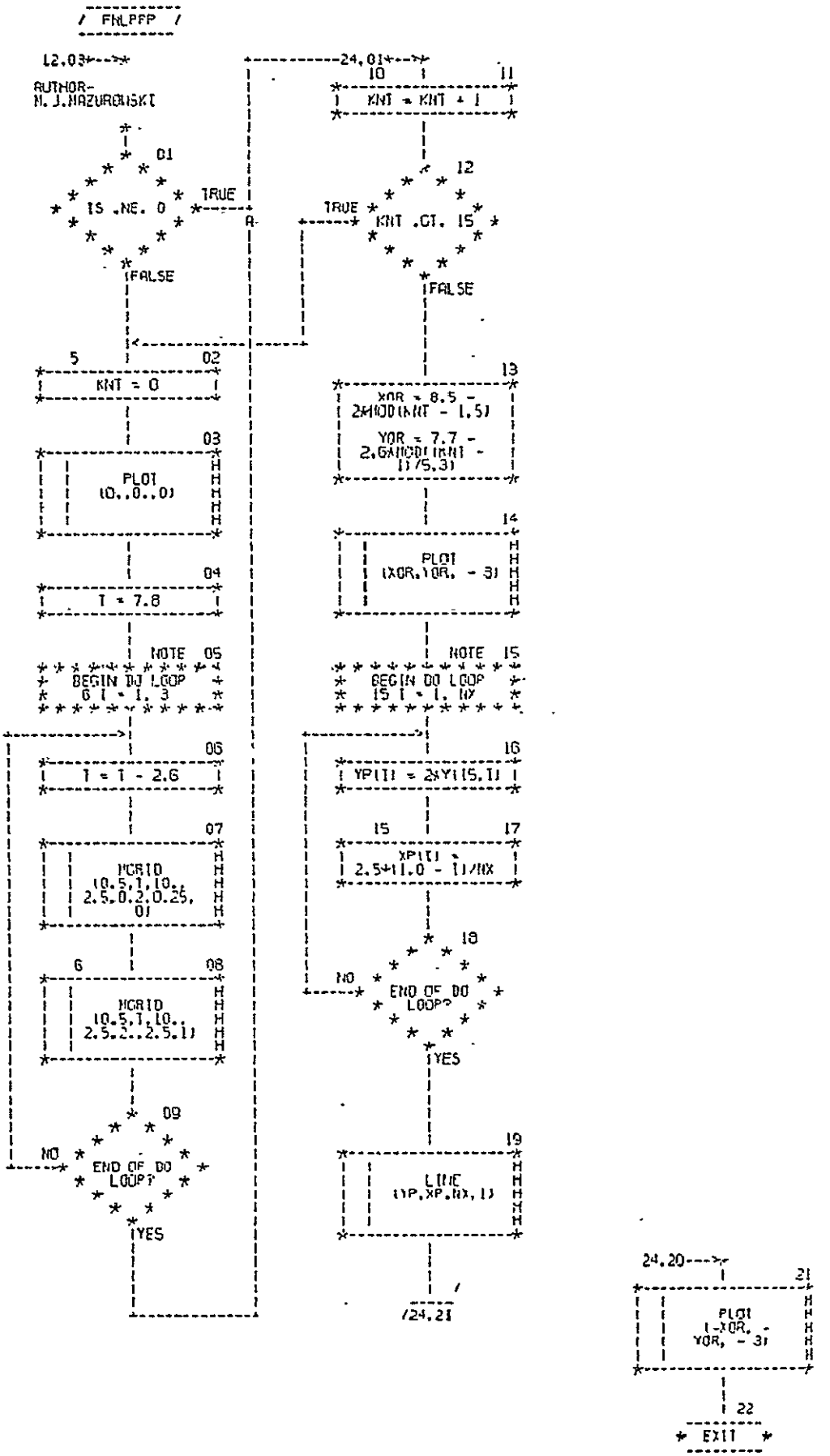

ORIGINAL PAGE IS
OF POOR QUALITY

CHART TITLE - SUBROUTINE POSPEC

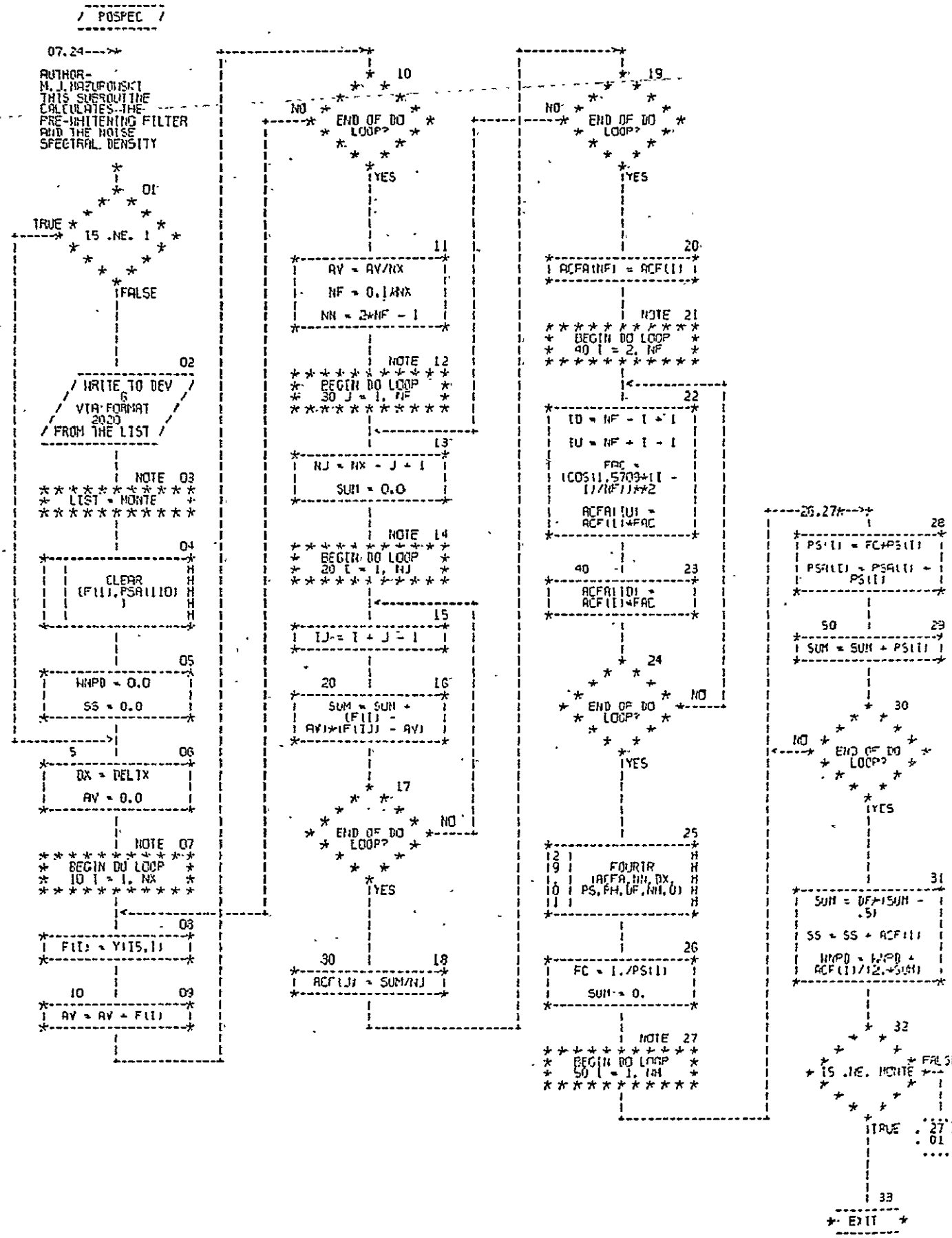

CHART TITLE - SUBROUTINE POSPEC

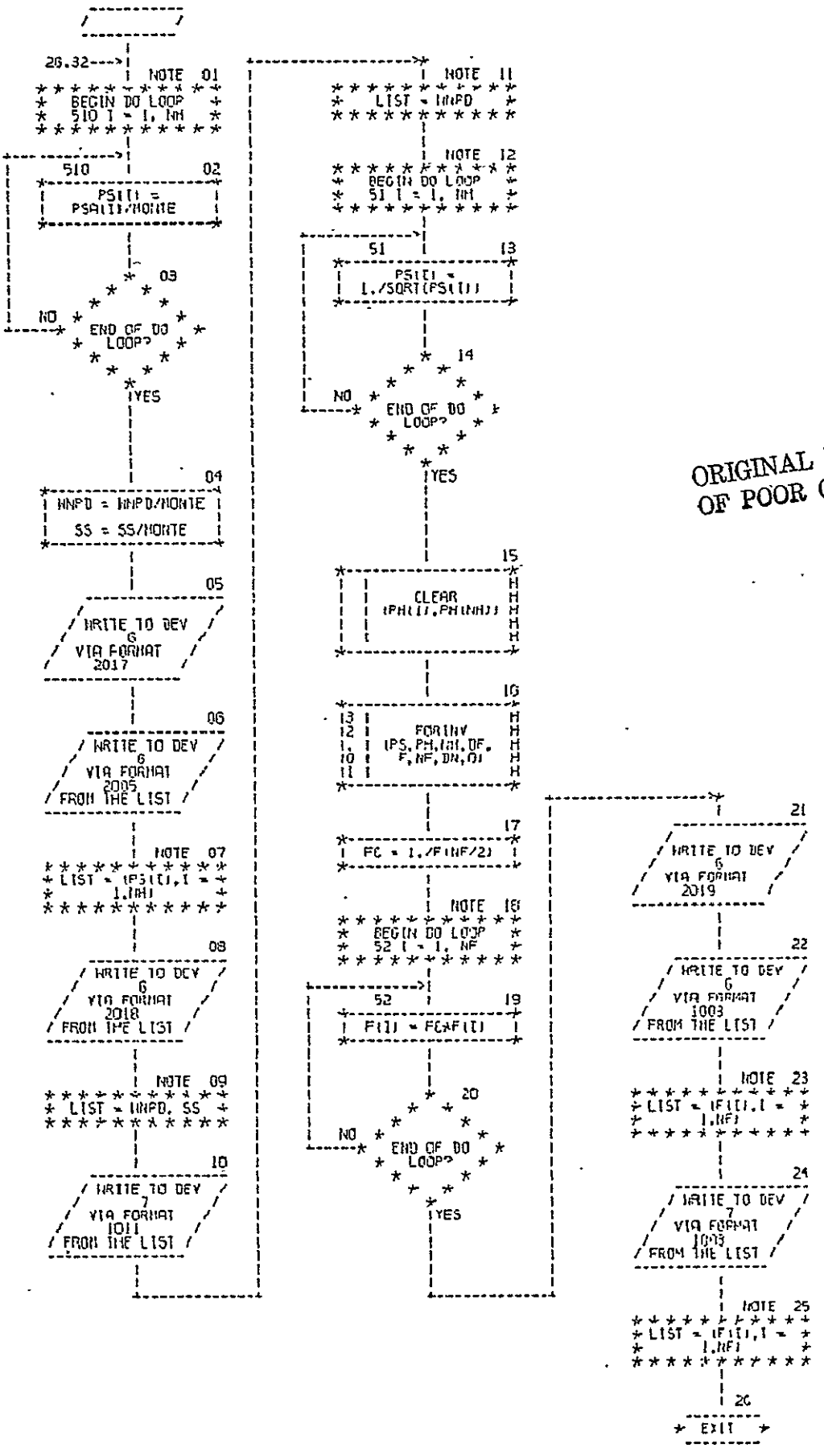

CHART TITLE - NON-PROCEDURAL STATEMENTS

```
      . DIMENSION F(200),PSI(101),PHI(101),ACF(101),ACFA(220),PSA(101)
        COMMON NA,NX,NBLOCK,I5,CRUN,I8,DIFA,DELTX,OP(20,3),ICON(20,20),ILE
        V(20,20),INOIS(20,20),A(4),AP(4),Y(20,9999),DYDA(4,9999),SIG(4,4),SF
        CN(20,200),SIGMA(20),NODE,IERR,CLEV(20,4),MONTE,
        DIN(20,30),DOUT(20,30),ND(20),NS
 2020   FORMAT(1H0,'MONTE=',I4)
 1003   FORMAT(10F8.3)
 1011   FORMAT(F10.3)
 2005   FORMAT(1H ,10F8.5)
 2017   FORMAT(1H0,'NORMALIZED POWER SPECTRUM')
 2018   FORMAT(1H0,'XNPO=',E16.5,2X,'SIGMA SQUARED=',E16.5)
 2019   FORMAT(1H0,'PRE-WHITENING SPREAD FUNCTION').
```

CHART TITLE - SUBROUTINE FOURTR(DATA,NDATA,DX,TAU,PHI,DELNU,NHARM,NOPT)

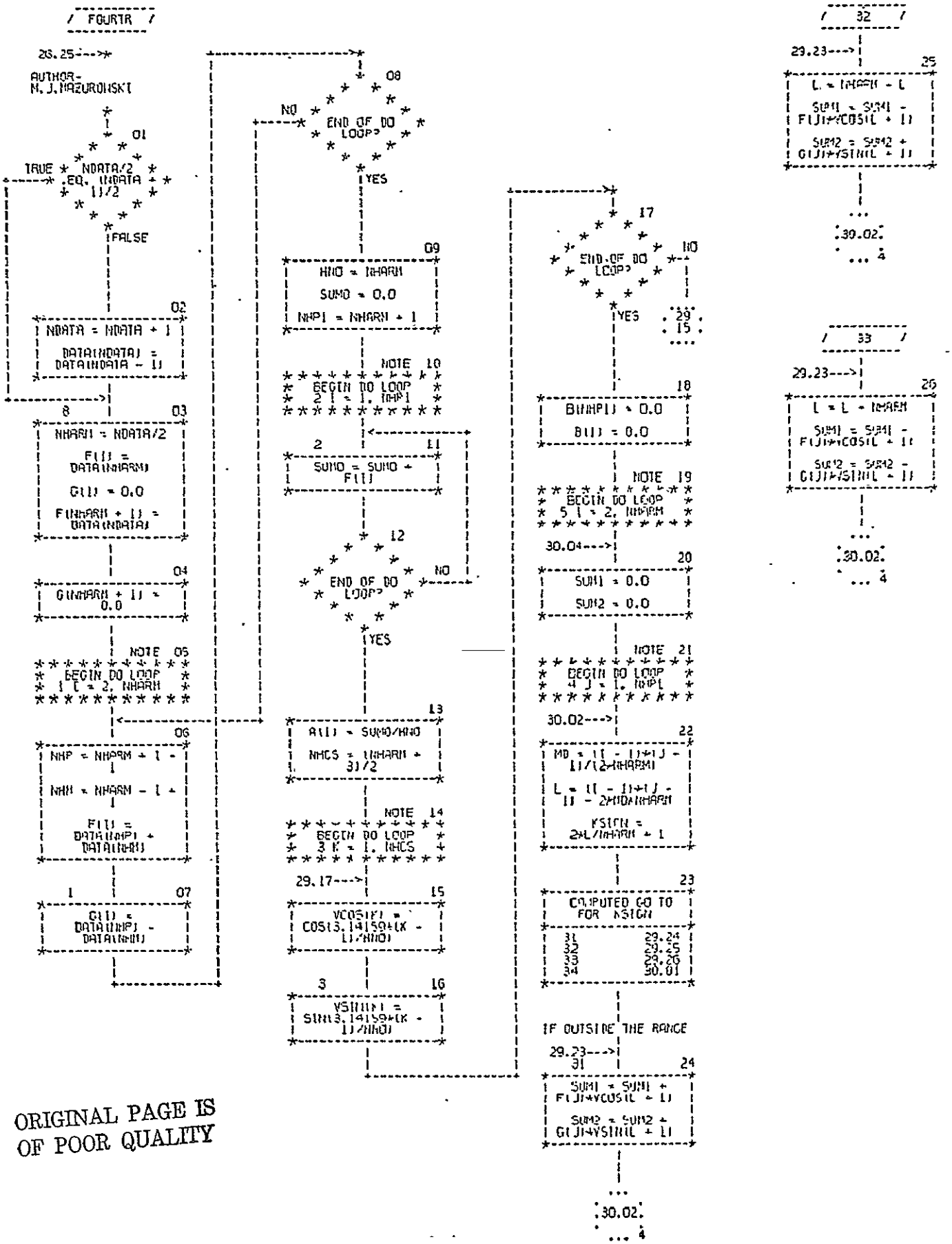

ORIGINAL PAGE IS
OF POOR QUALITY

CHART TITLE - SUBROUTINE FOURTR(DATA,NDATA,DX,TAU,PHI,DELNU,NHARM,NOPT)

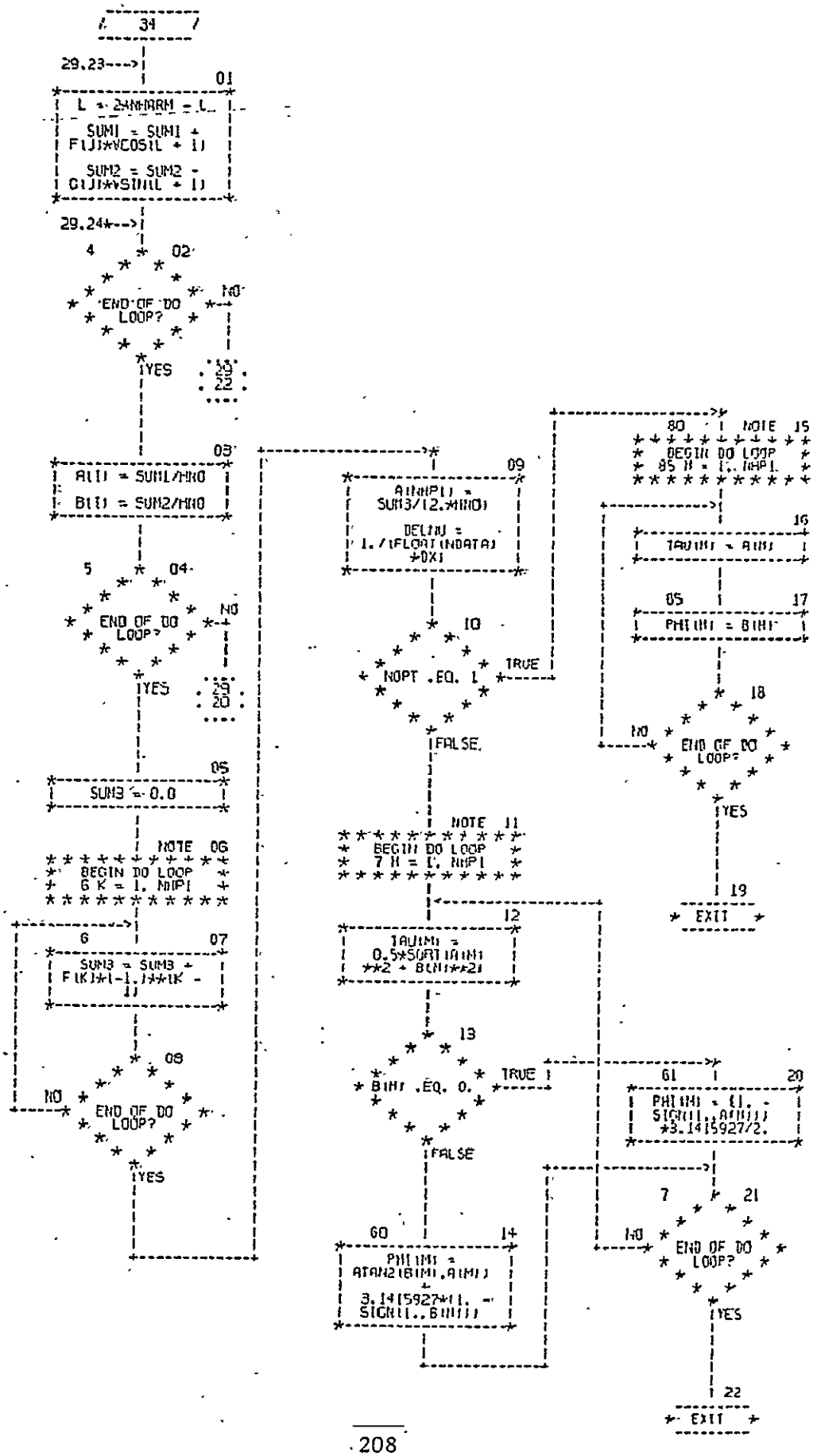

CHART TITLE - NON-PROCEDURAL STATEMENTS

```
      DIMENSION DATA(1),TAU(1),PHI(1),F(950),G(950),A(950),B(950),
     VCOS(576),VSIN(576)
```

CHART TITLE - SUBROUTINE FORINV(TAU,PHI,NHARM,DELNU,FUNC,NFUN,DELF,KLIP)

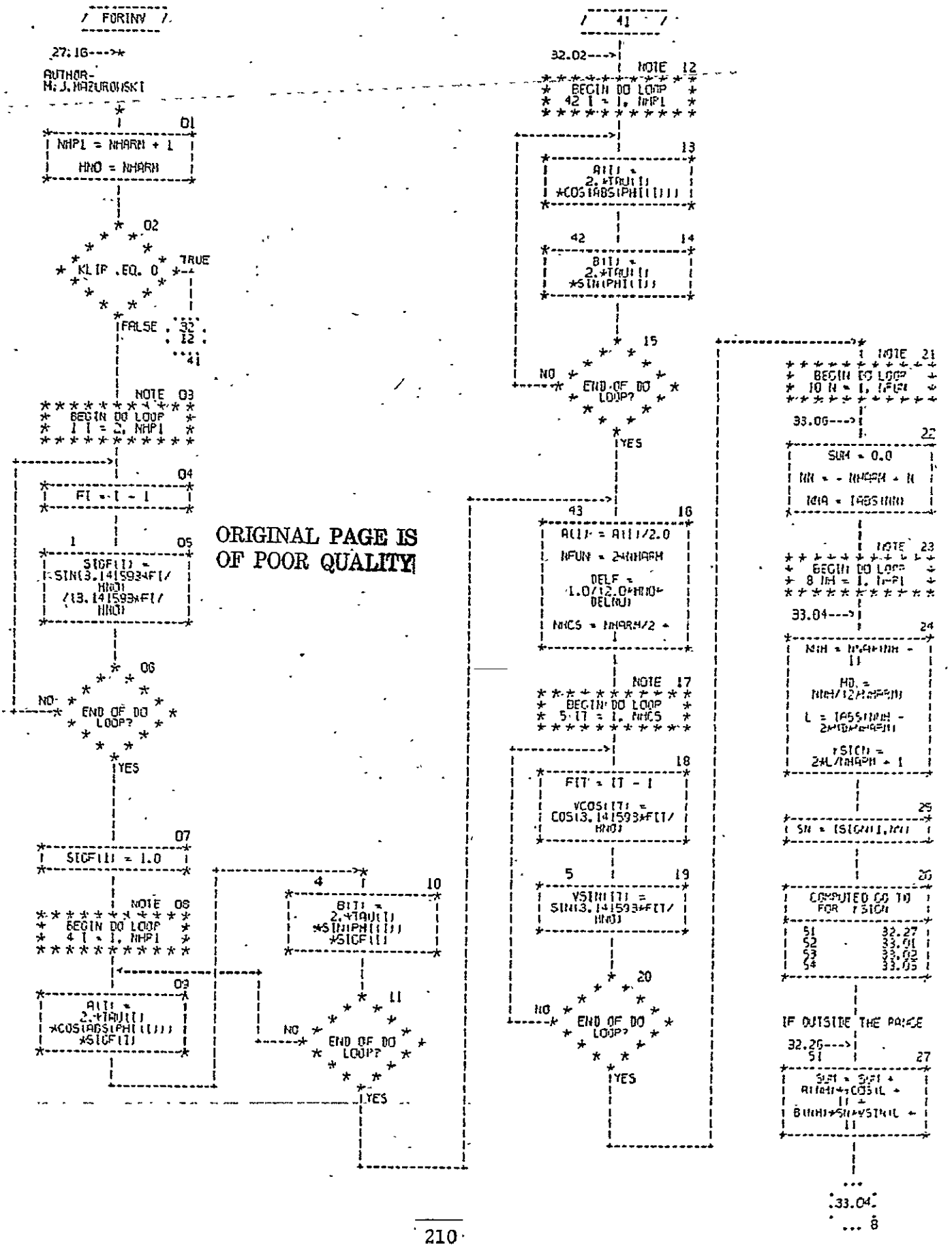

ORIGINAL PAGE IS OF POOR QUALITY

CHART TITLE - SUBROUTINE FORINVITAU,PHI,NHARM,DELNU,FUNC,NFUN,DELF,KLIP1

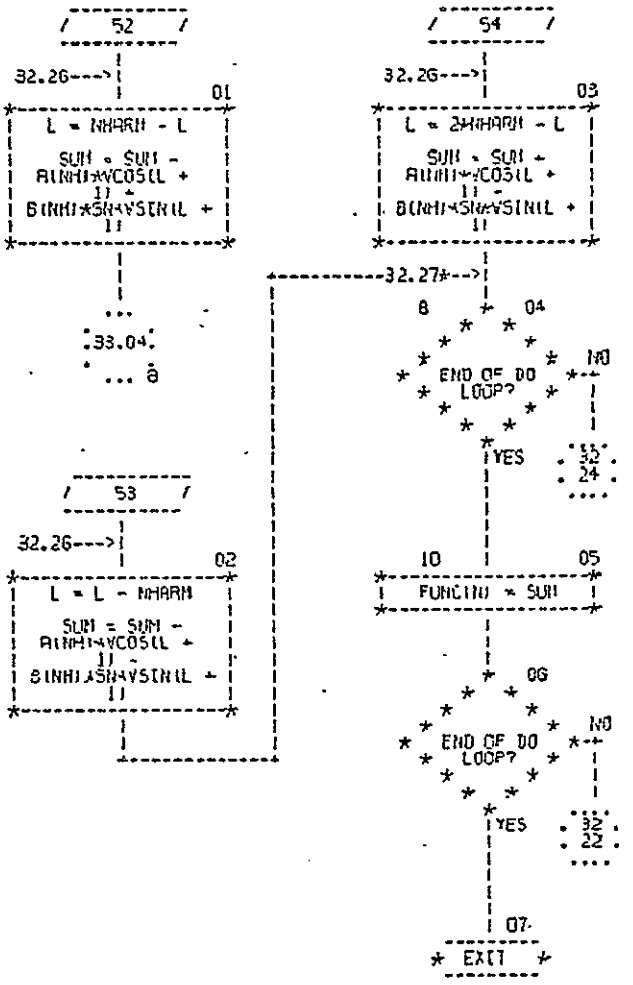

CHART TITLE - NON-PROCEDURAL STATEMENTS

```
      DIMENSION TAU(500),PHI(500),FUNC(1000),A(500),B(500),YCOS(255),
     YSIN(255),SIGF(501)
```

APPENDIX C

SIGNAL TRACE DATA

Notes on data in this Appendix:

(1) Progression of target through system is down consecutive columns, the input target signal being shown as the upper left-hand corner plot.

(2) All ordinates are calibrated from 0 to 1 arbitrary full scale radiance unit, R_m

(3) All abscissas are calibrated in units of length, the size/division being given before each set of data.

(4) The plots show the effect of each ERTS image processing system element (excluding noise) in the MSS nominal configuration defined in Section 7.1.

The plots on pages 214 through 233 are for three parameter edge targets. Record length is 100. micrometers and abscissa calibration is 10. micrometer/box.

The plots on pages 234 through 278 are for the four parameter square pulse target. Record length is 150. micrometers and abscissa calibration is 15. micrometers/box. Note that the record length is a bit short to see the entire blur of the widest (105. mm) target.

The plots on pages 279 through 283 are for the two parameter pseudo delta function or "resolution" target. Record length is 150. micrometers and abscissa calibration is 15. micrometers/box.

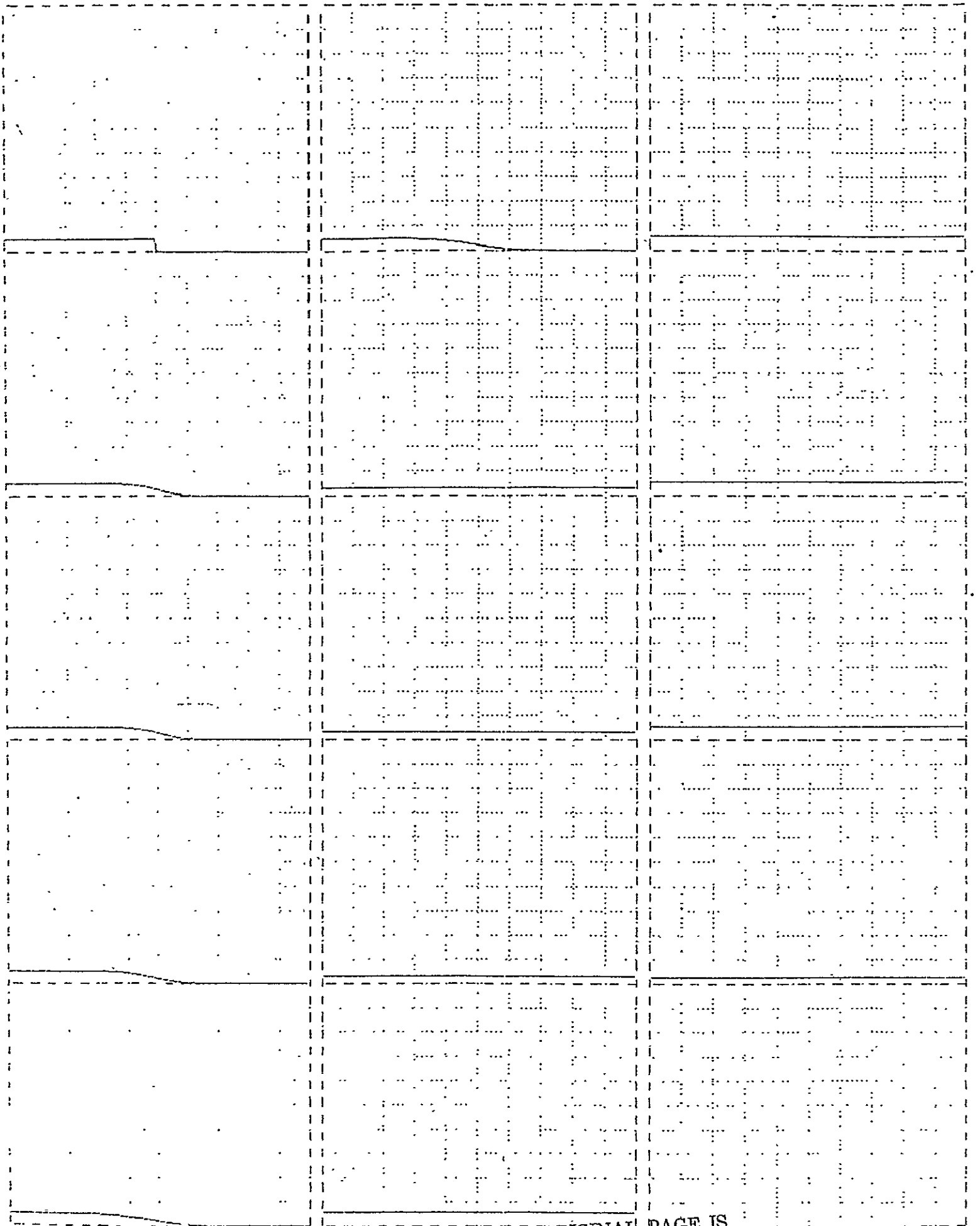

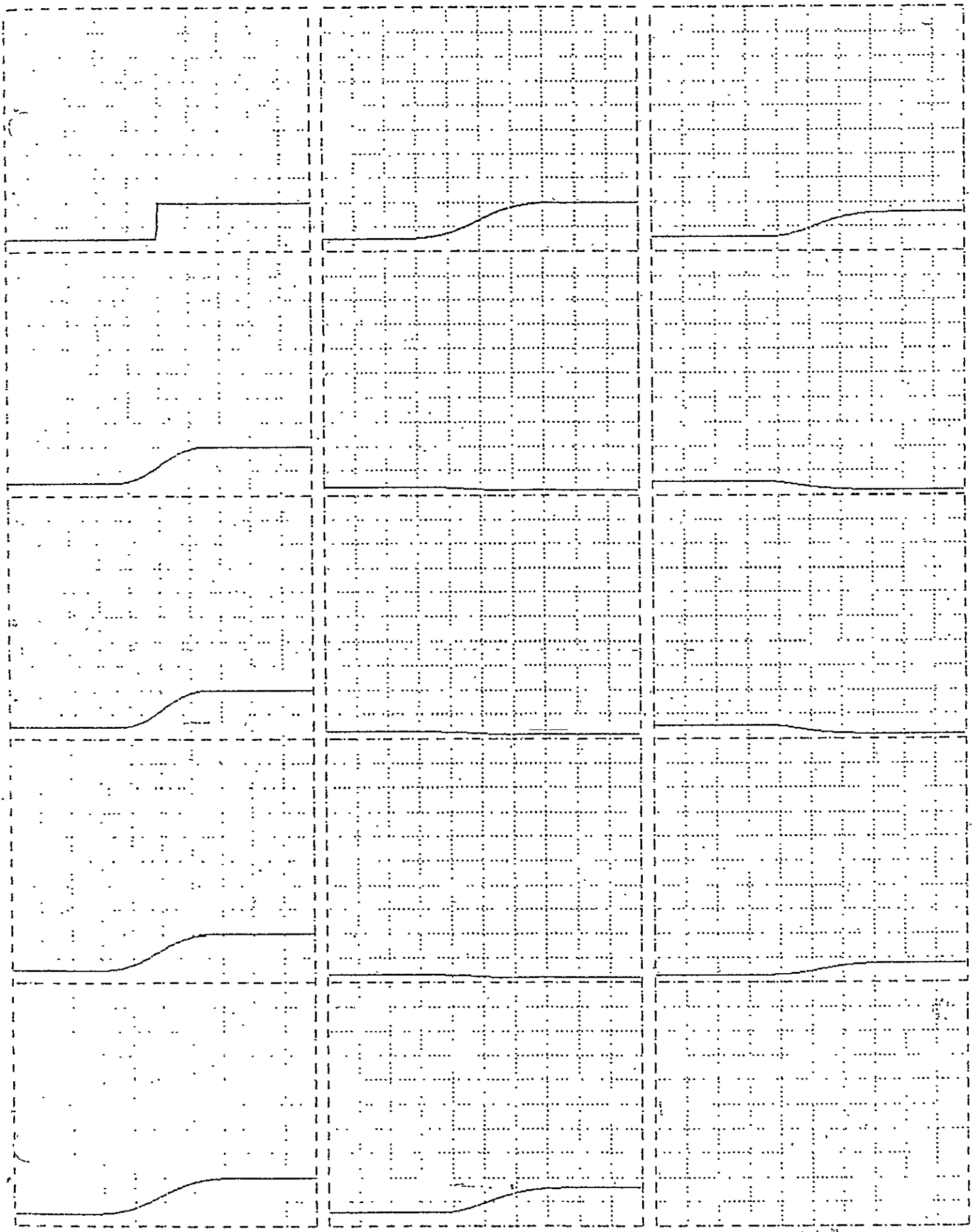

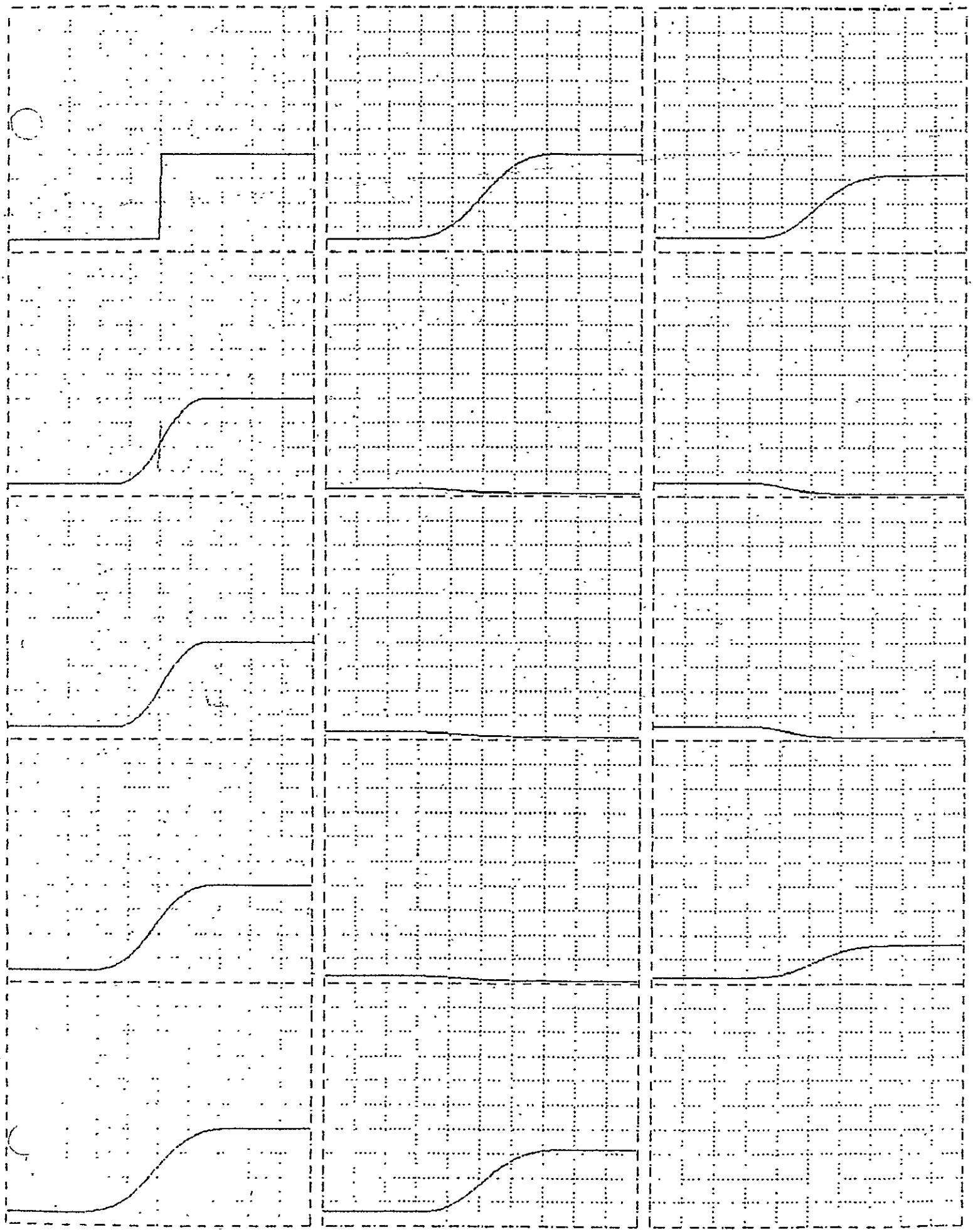

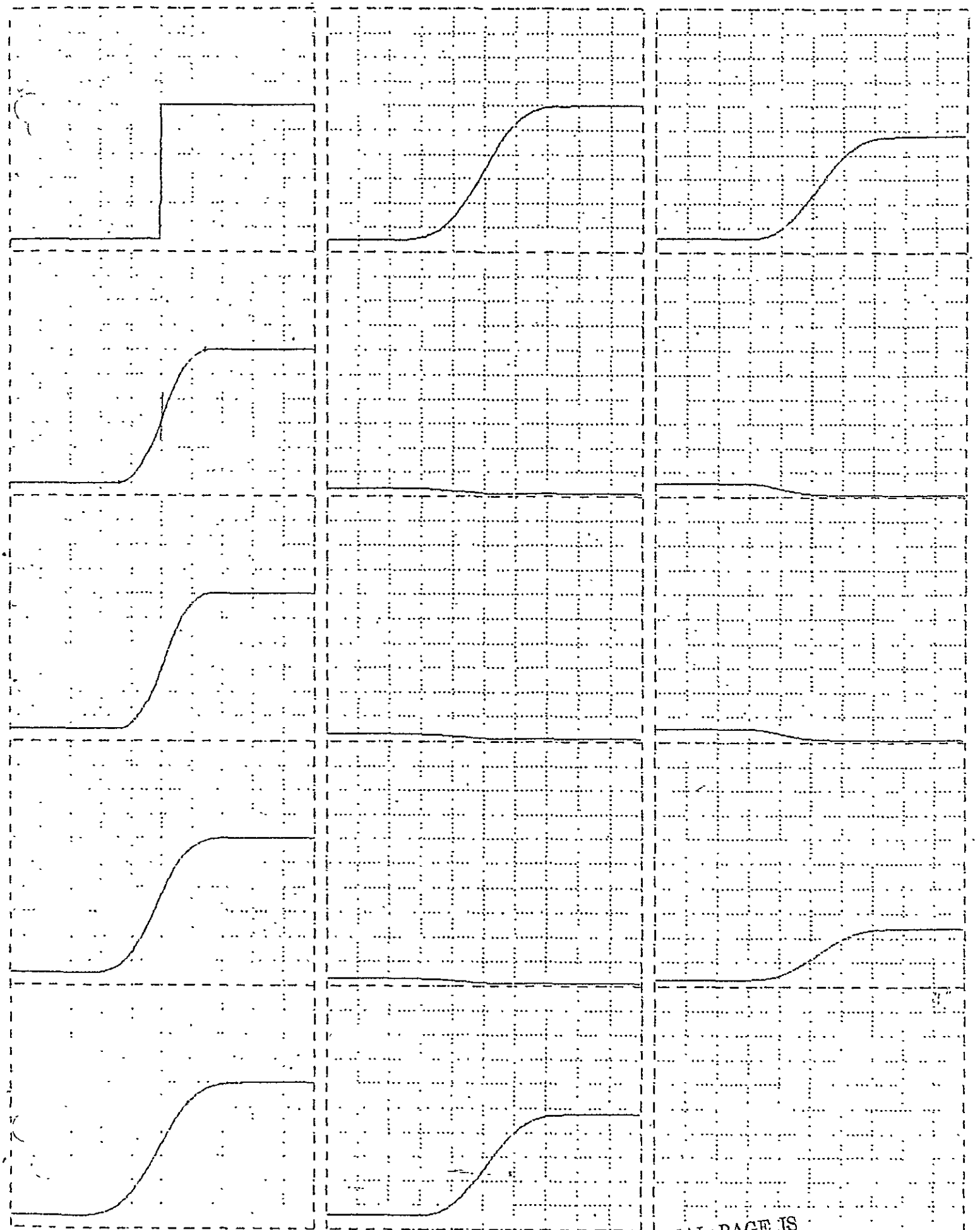

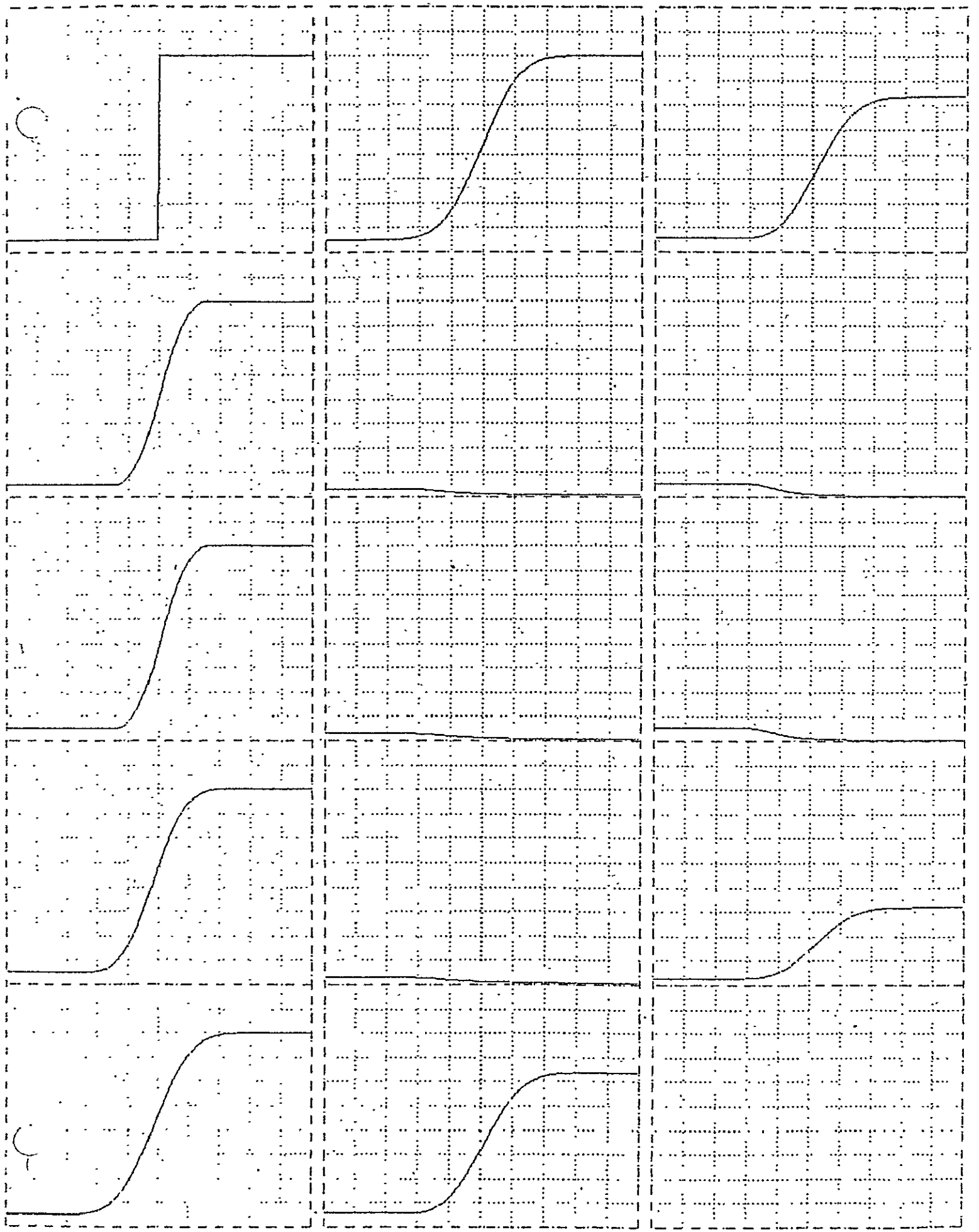

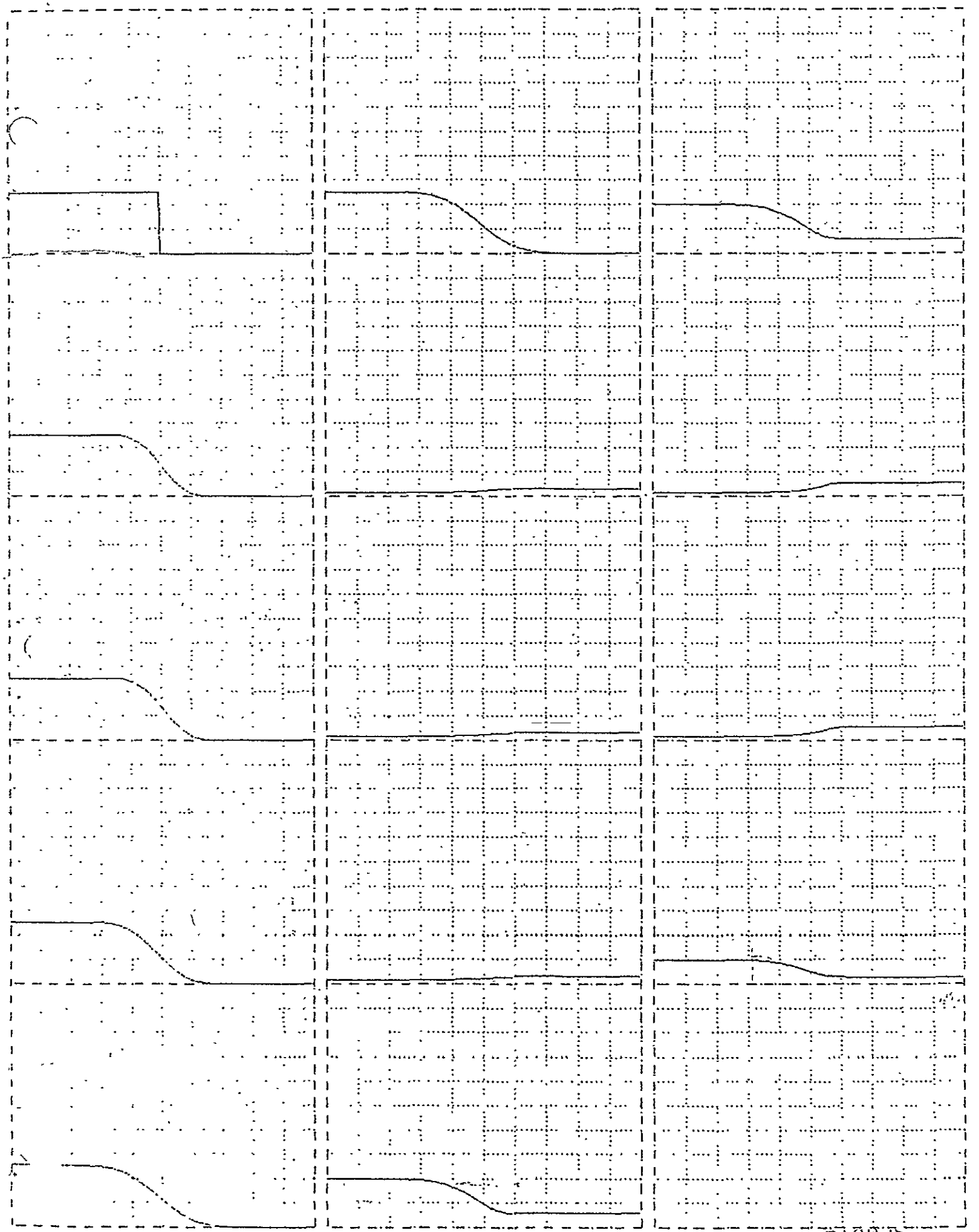

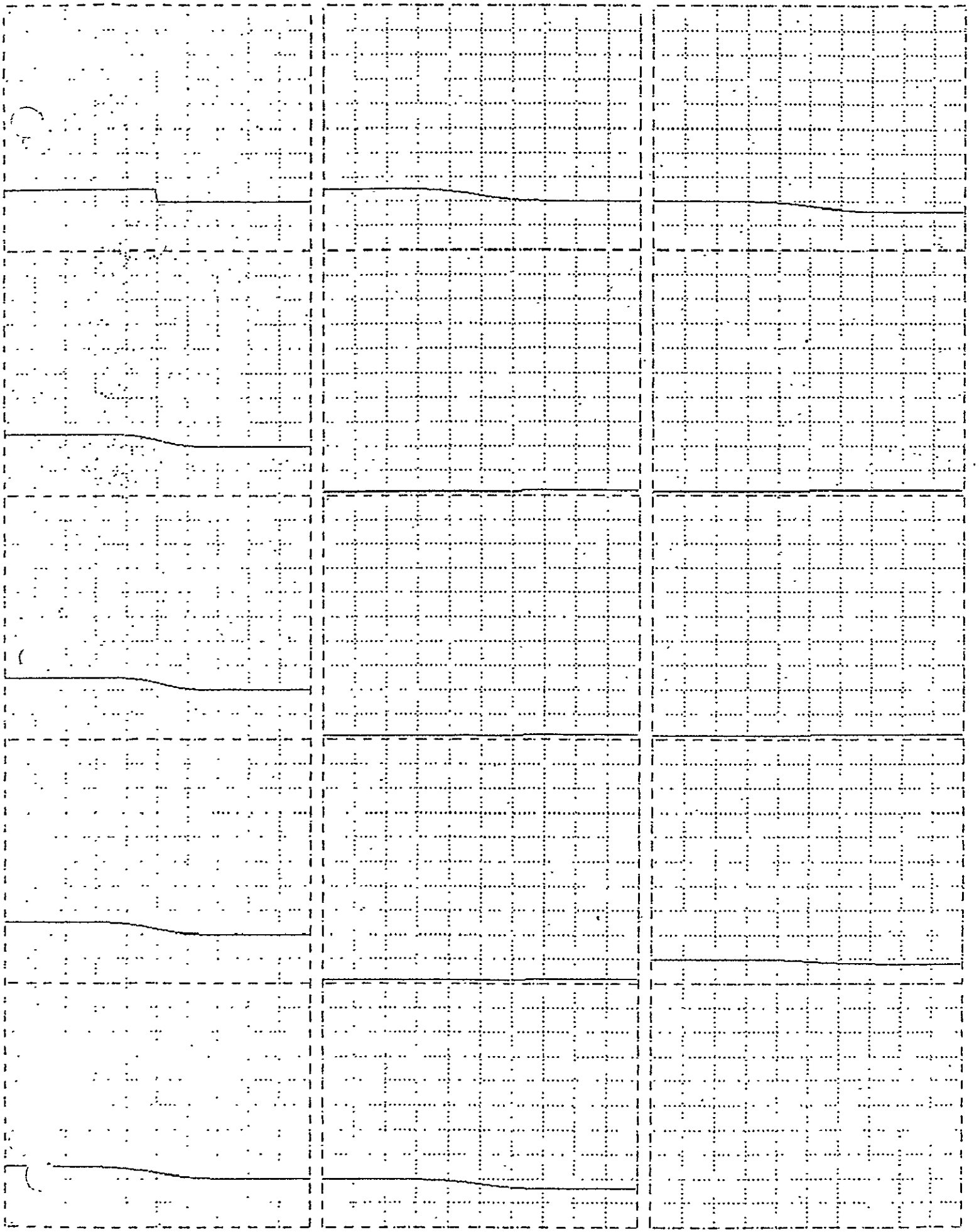

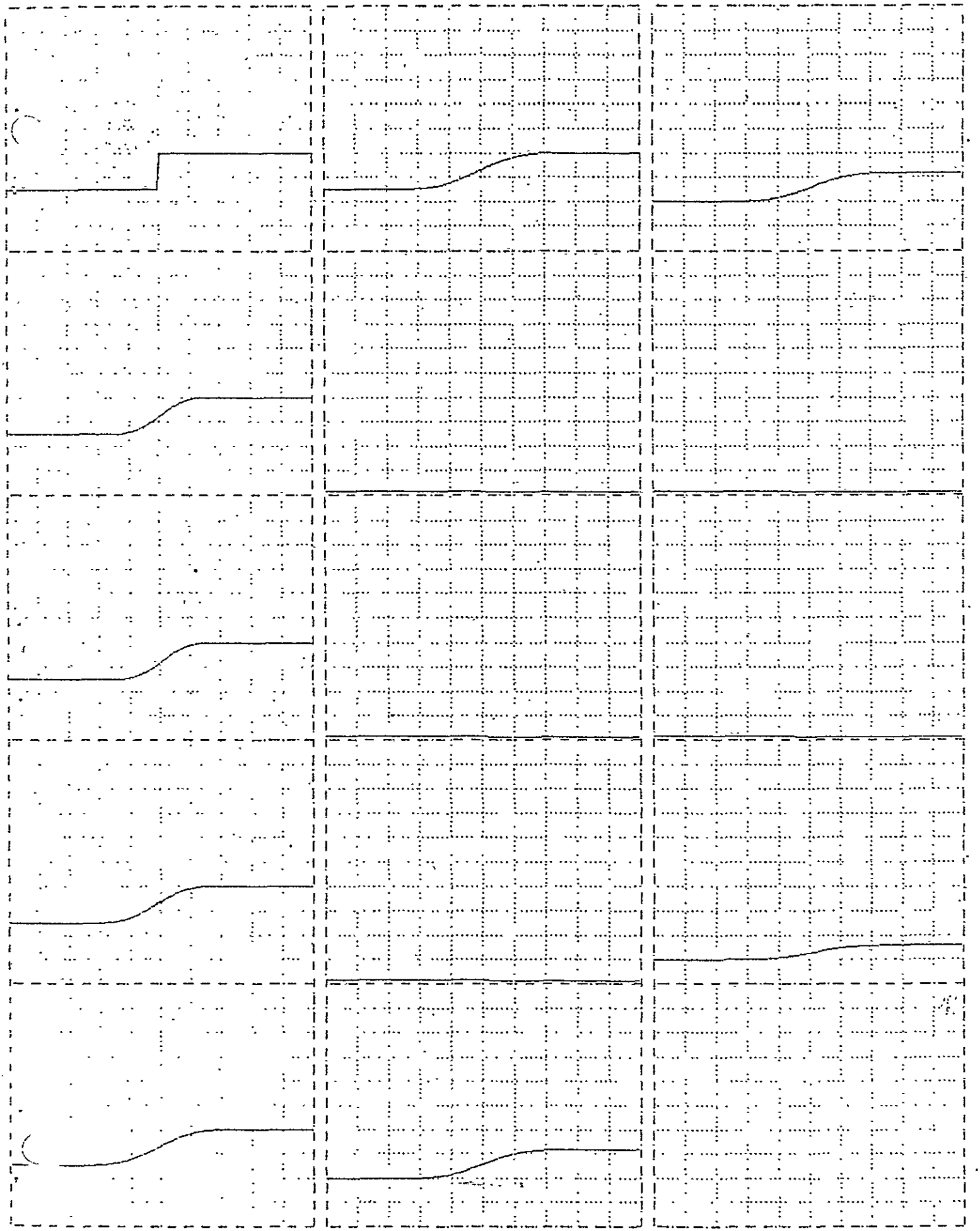

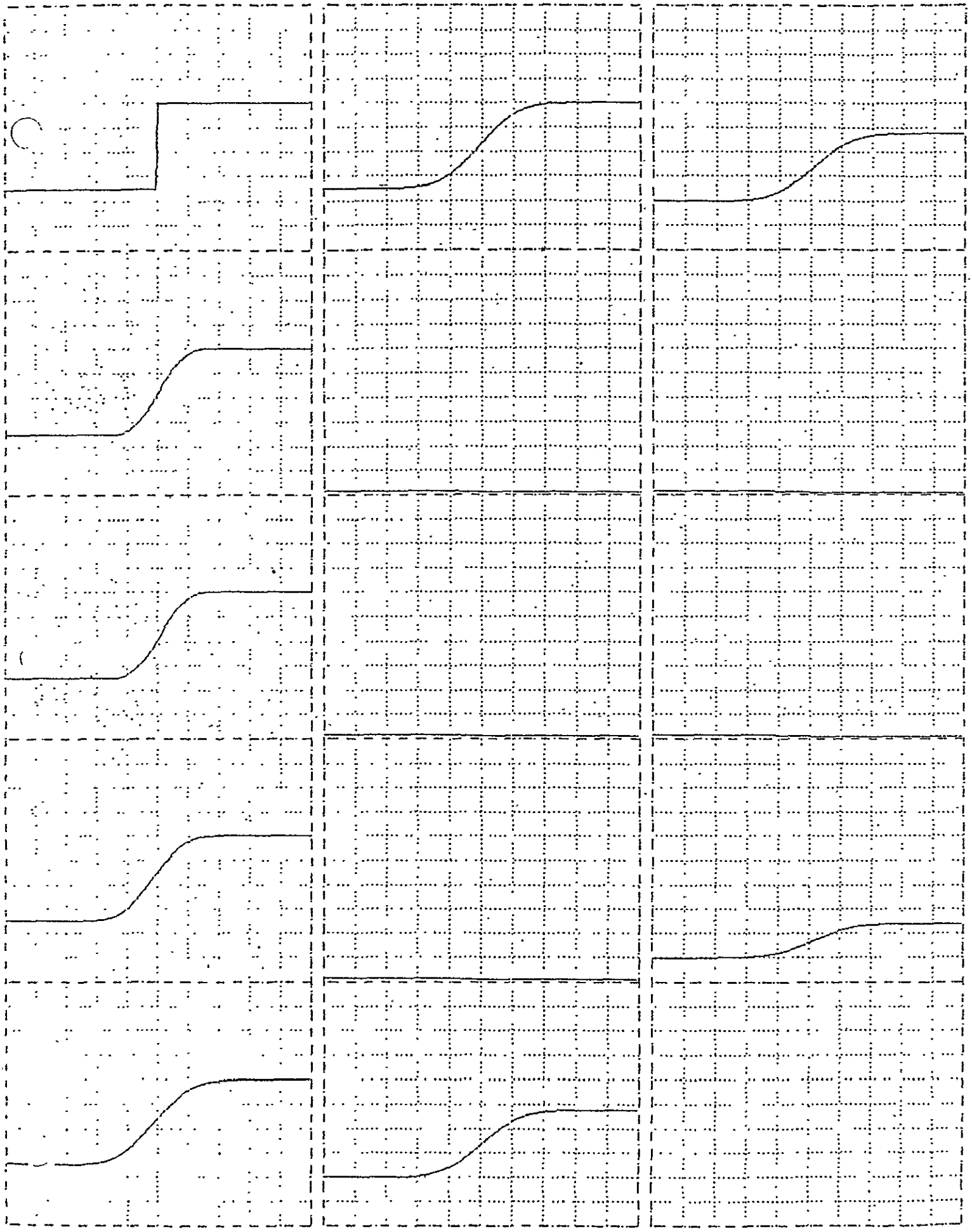

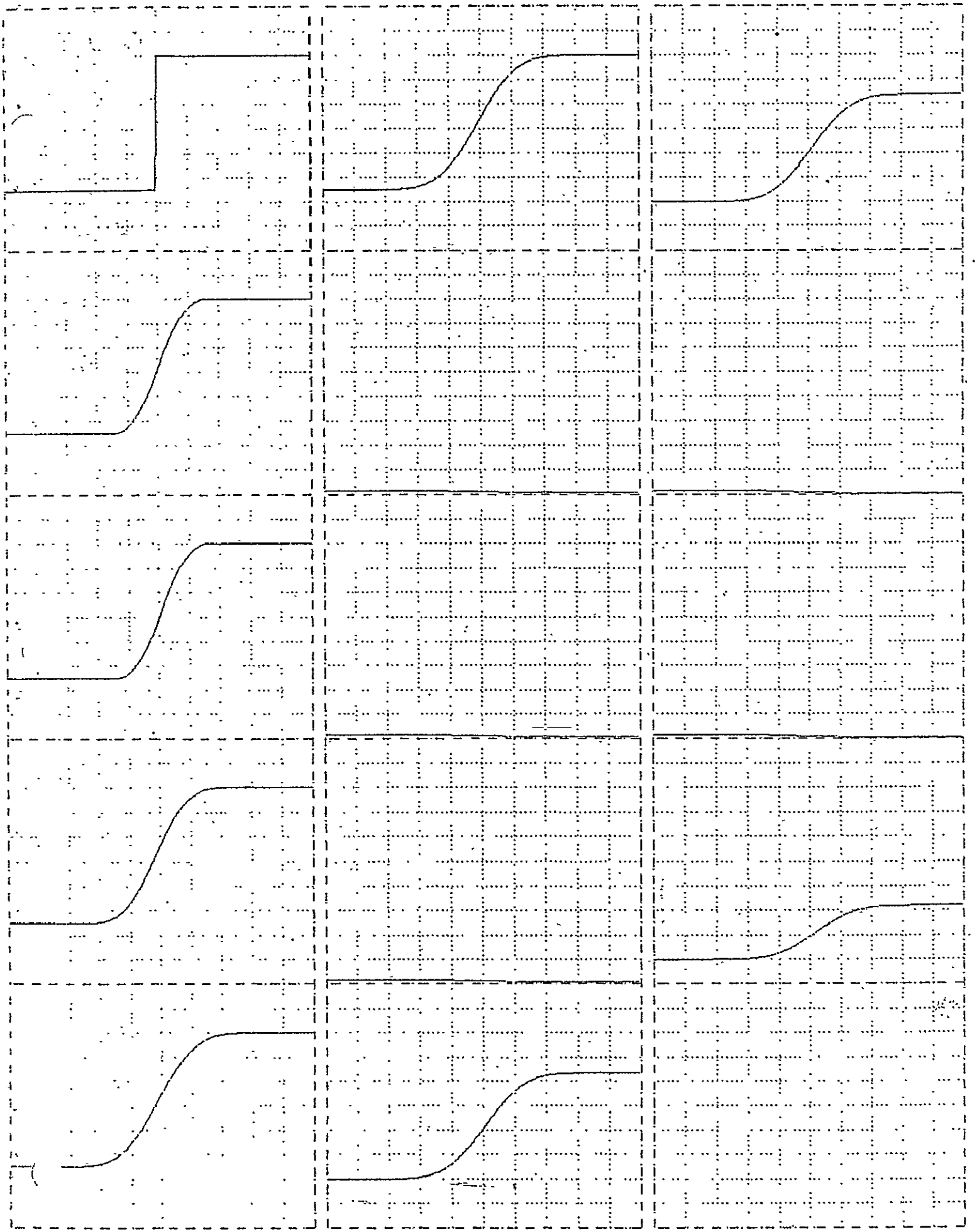

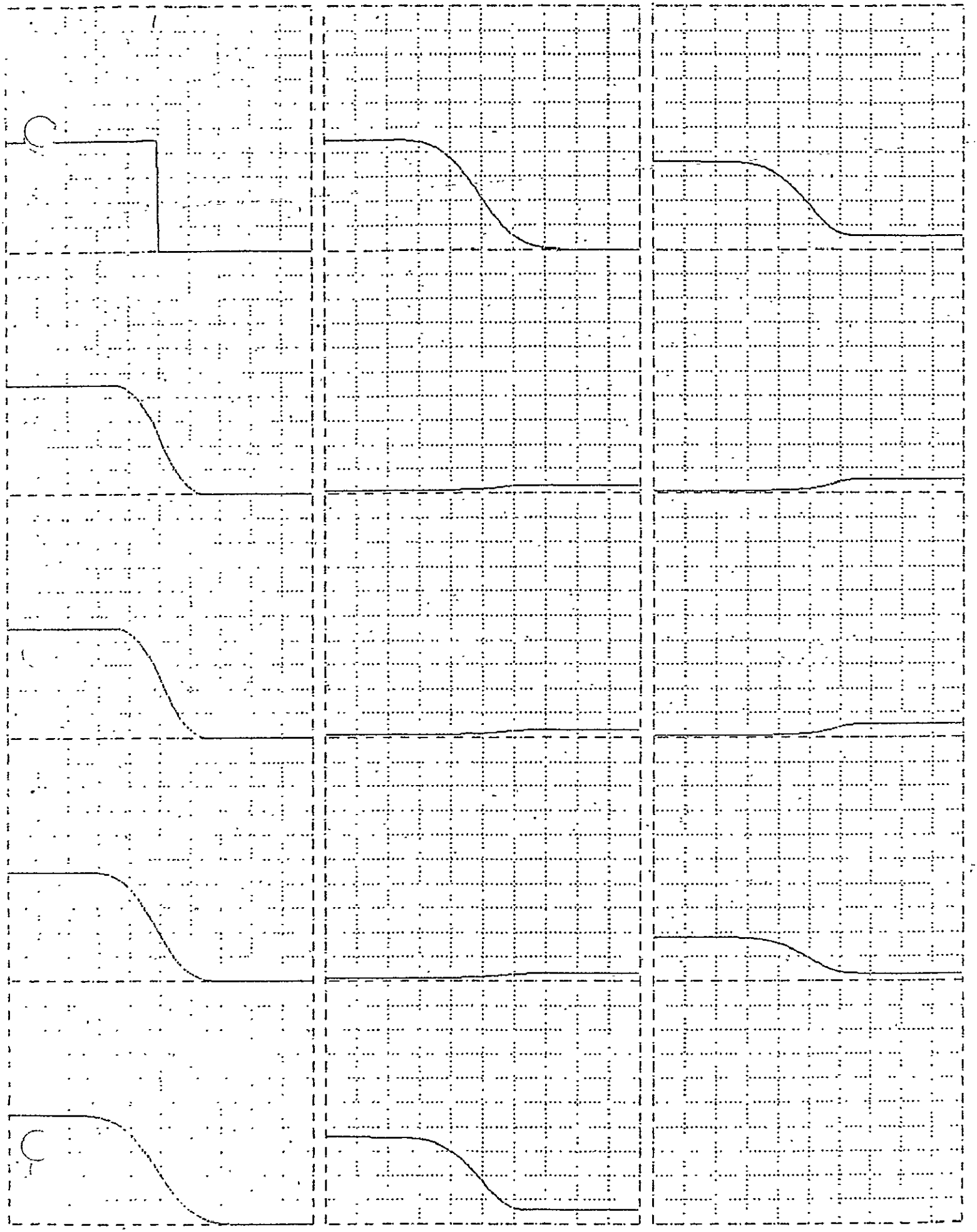

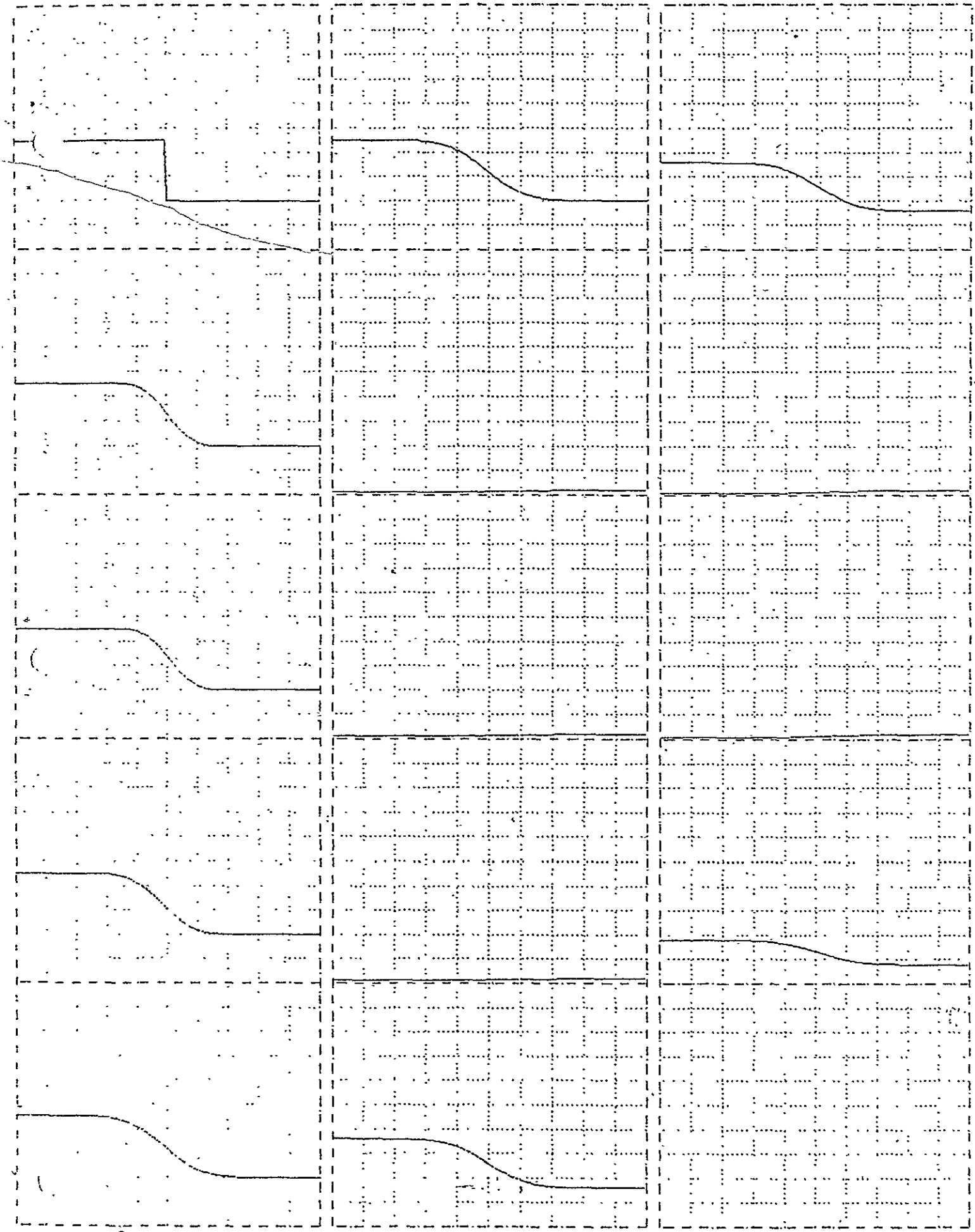

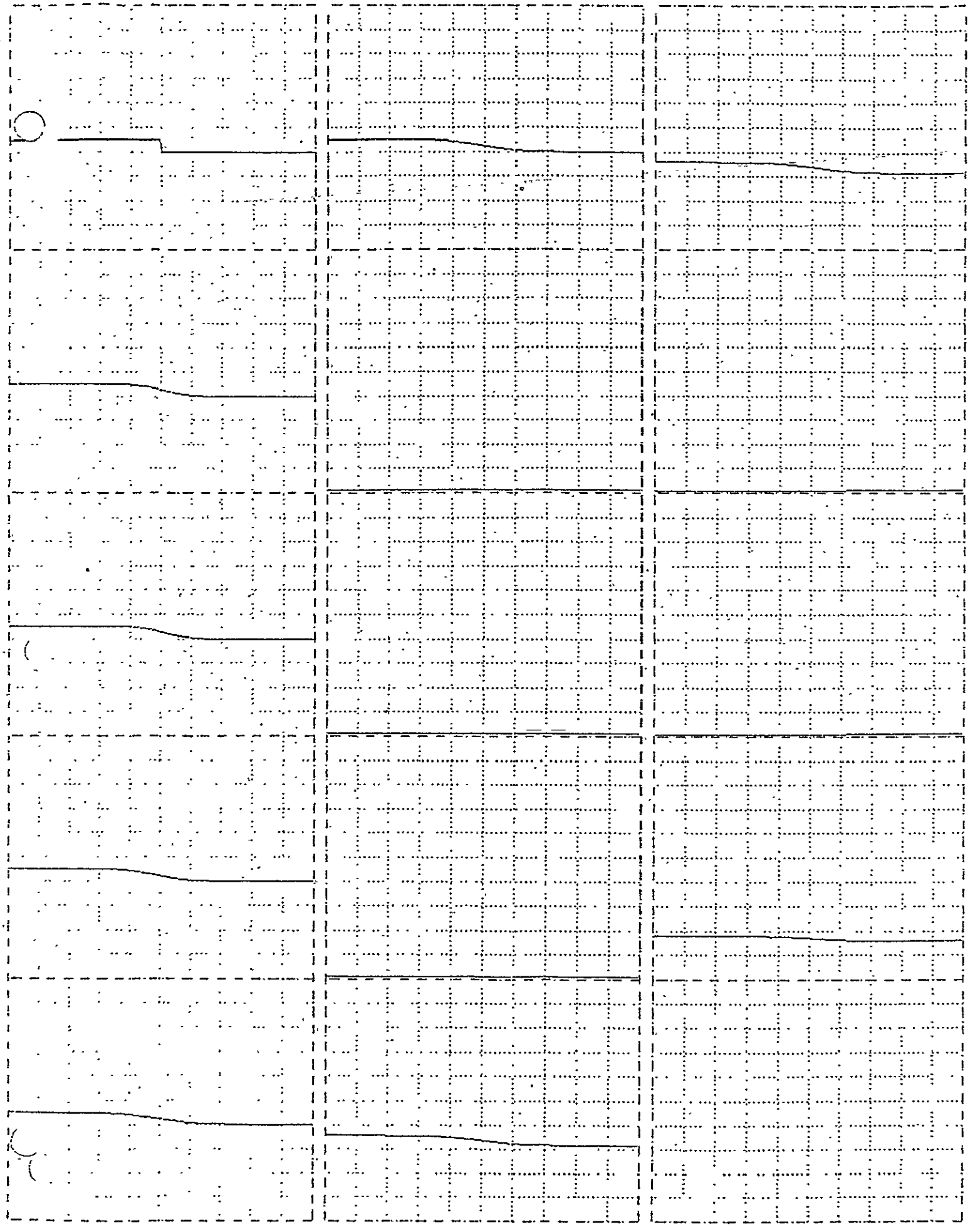

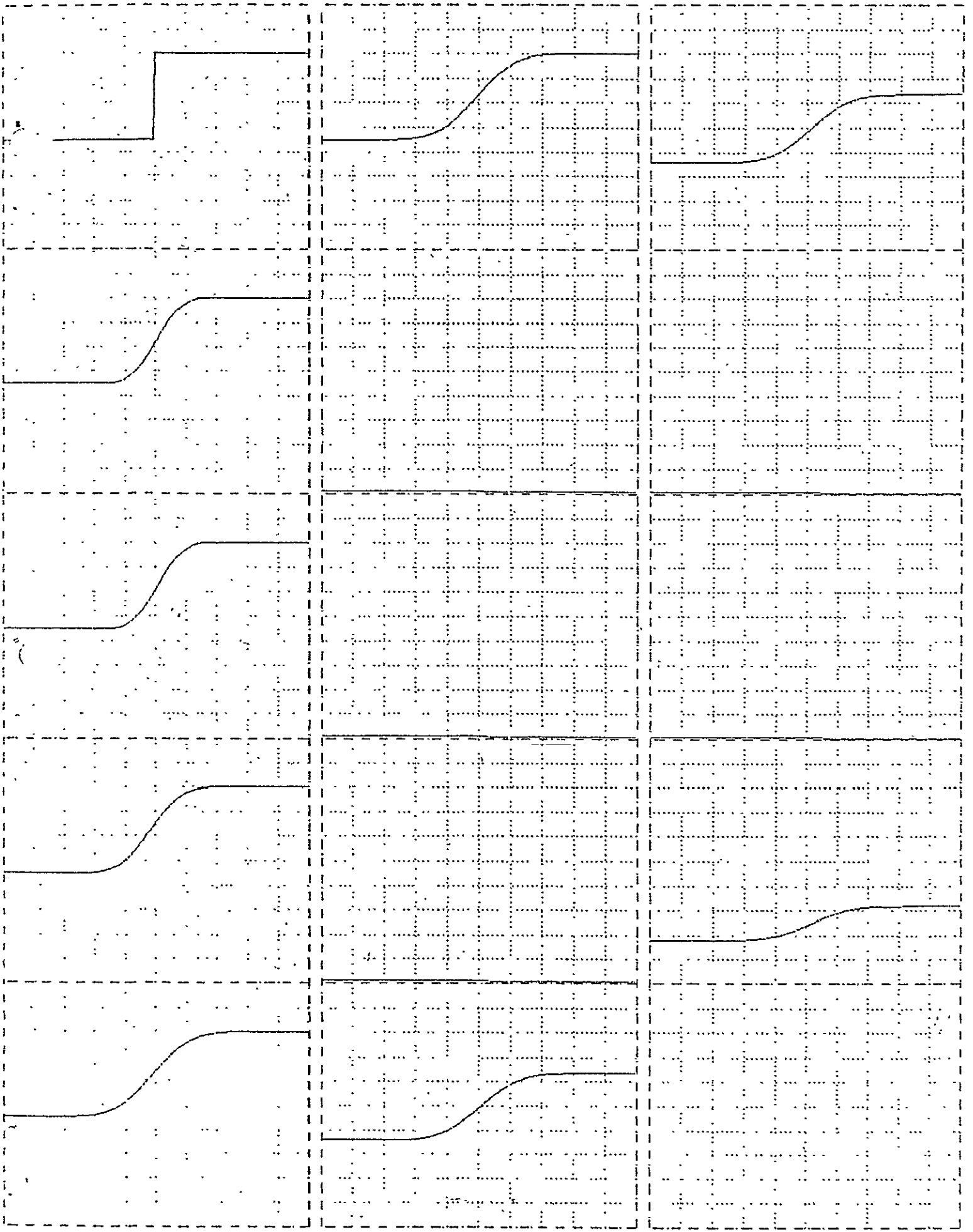

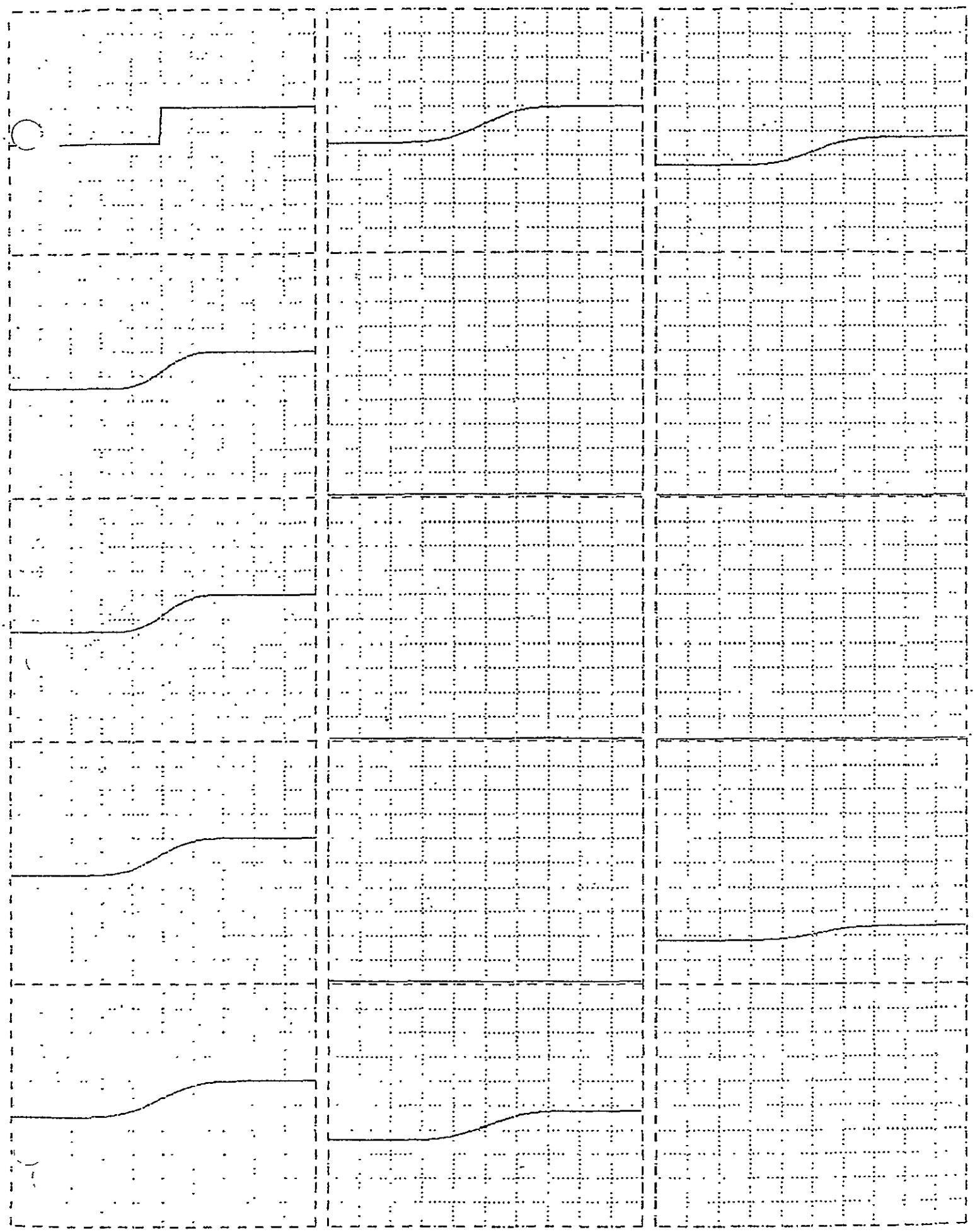

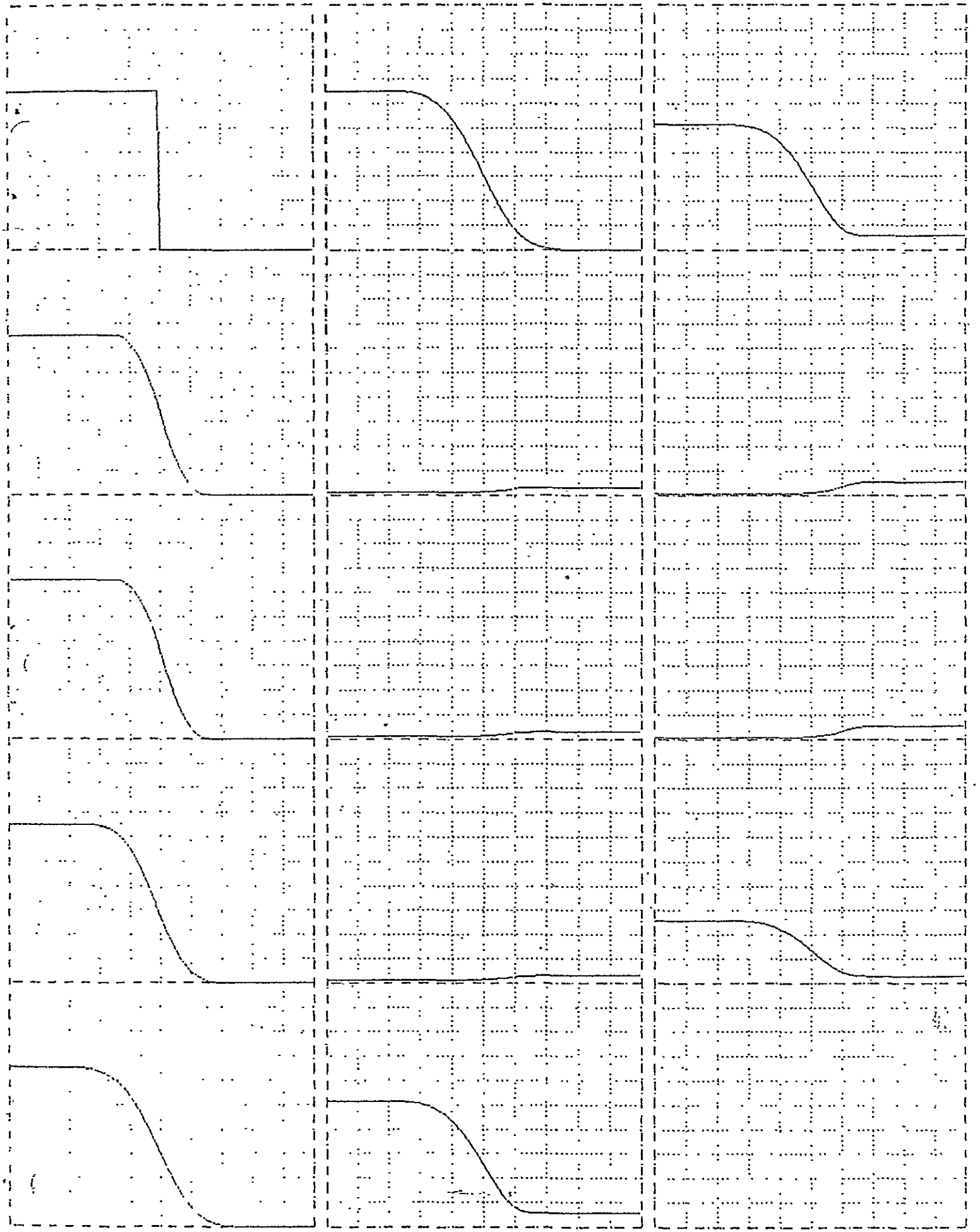

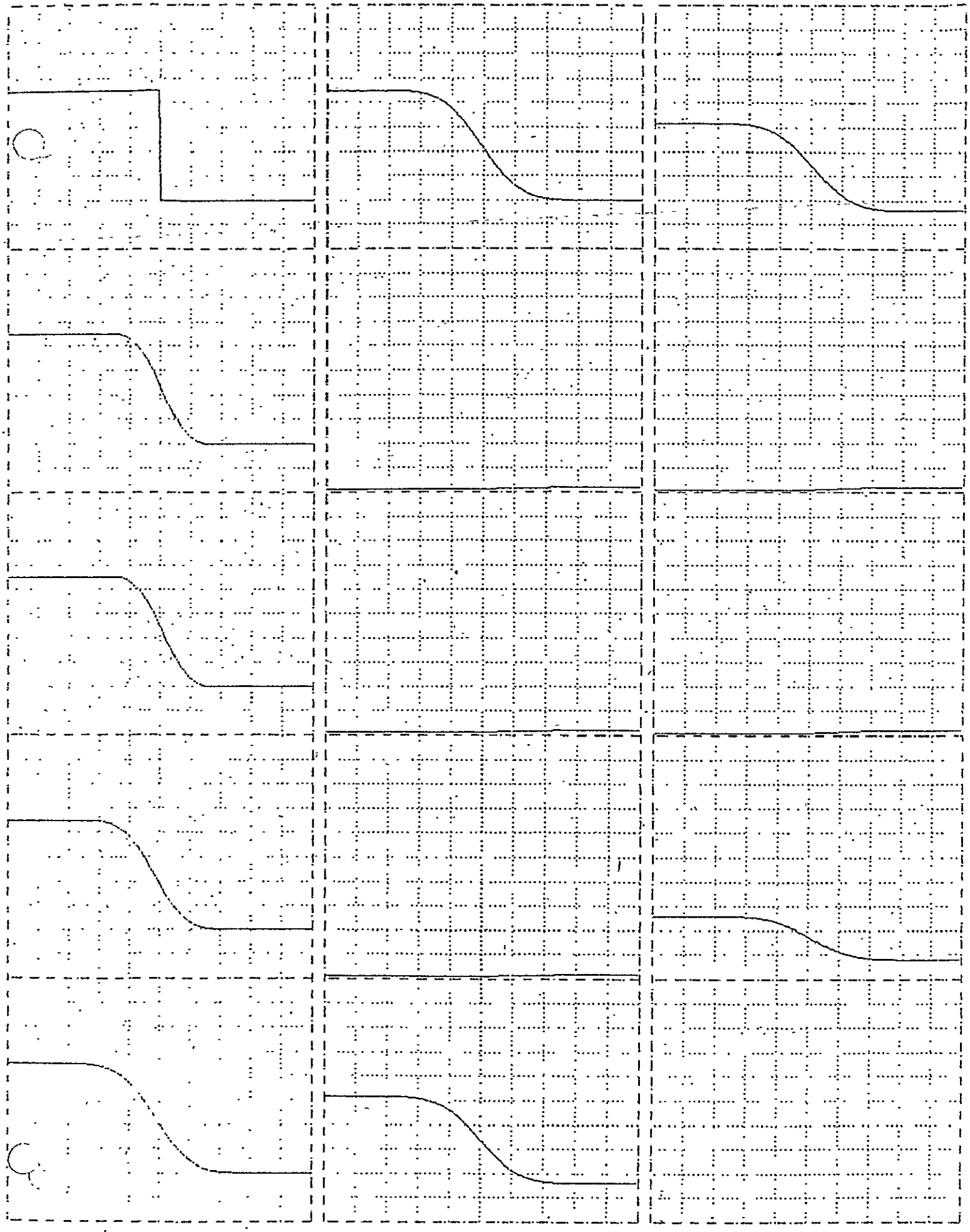

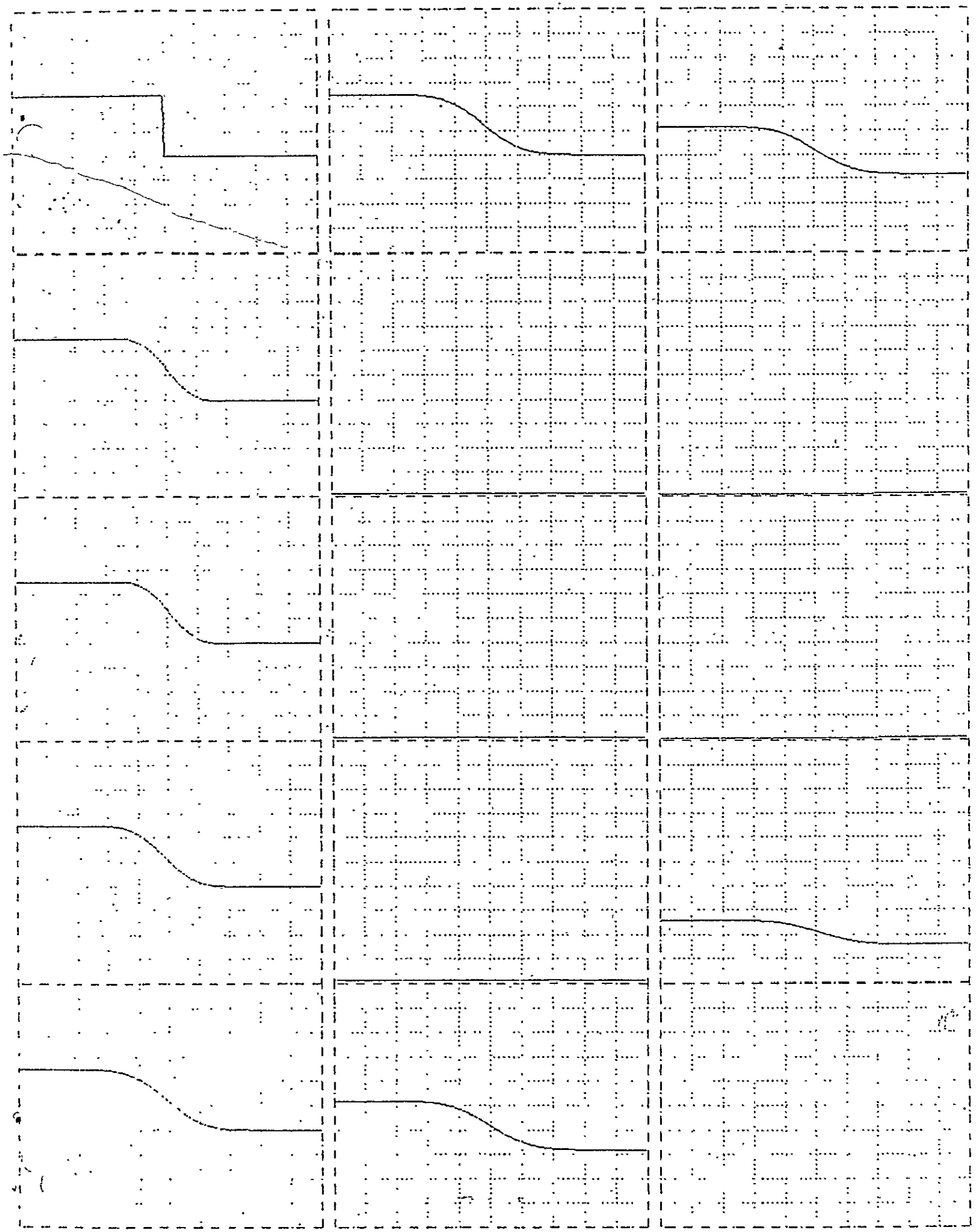

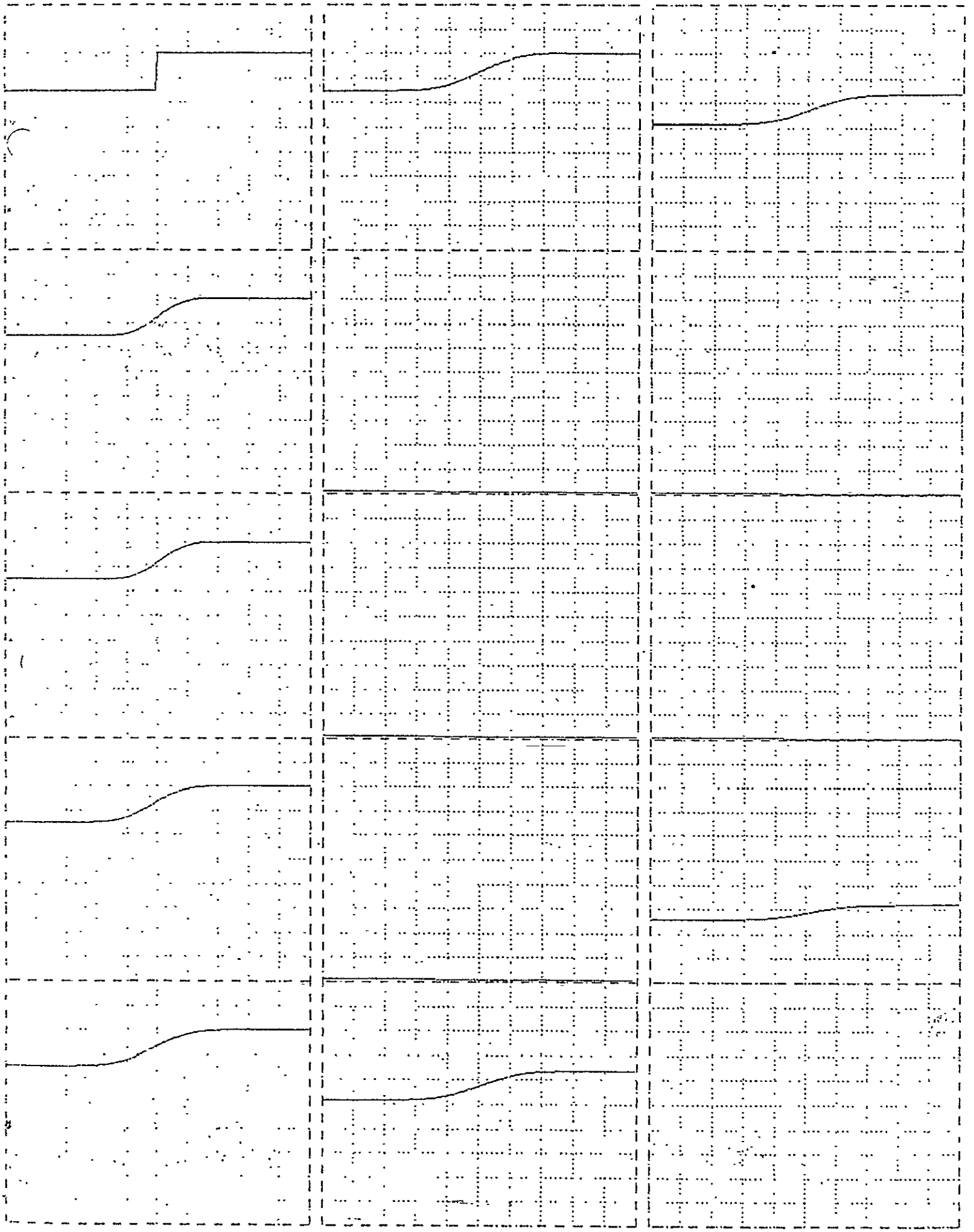

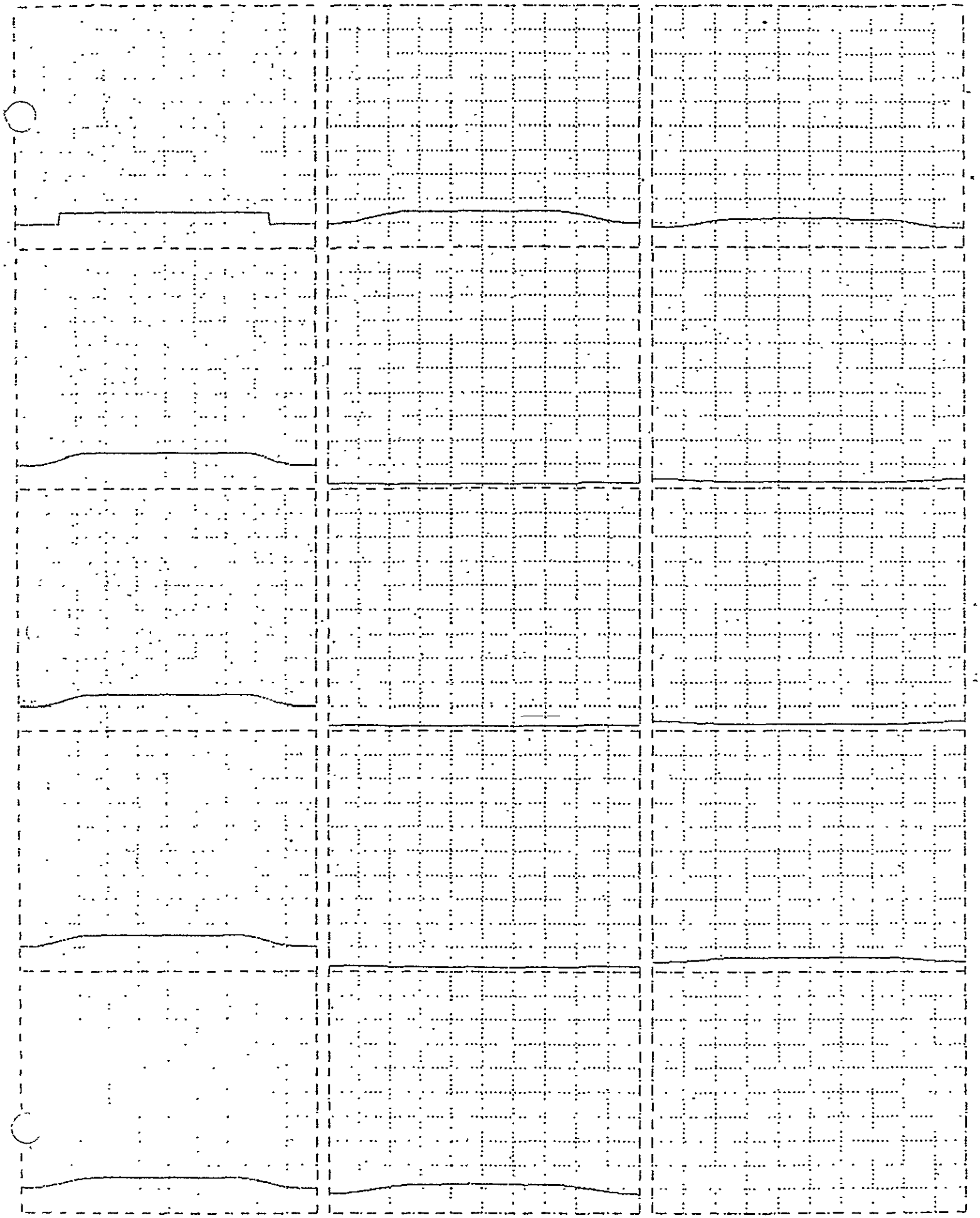

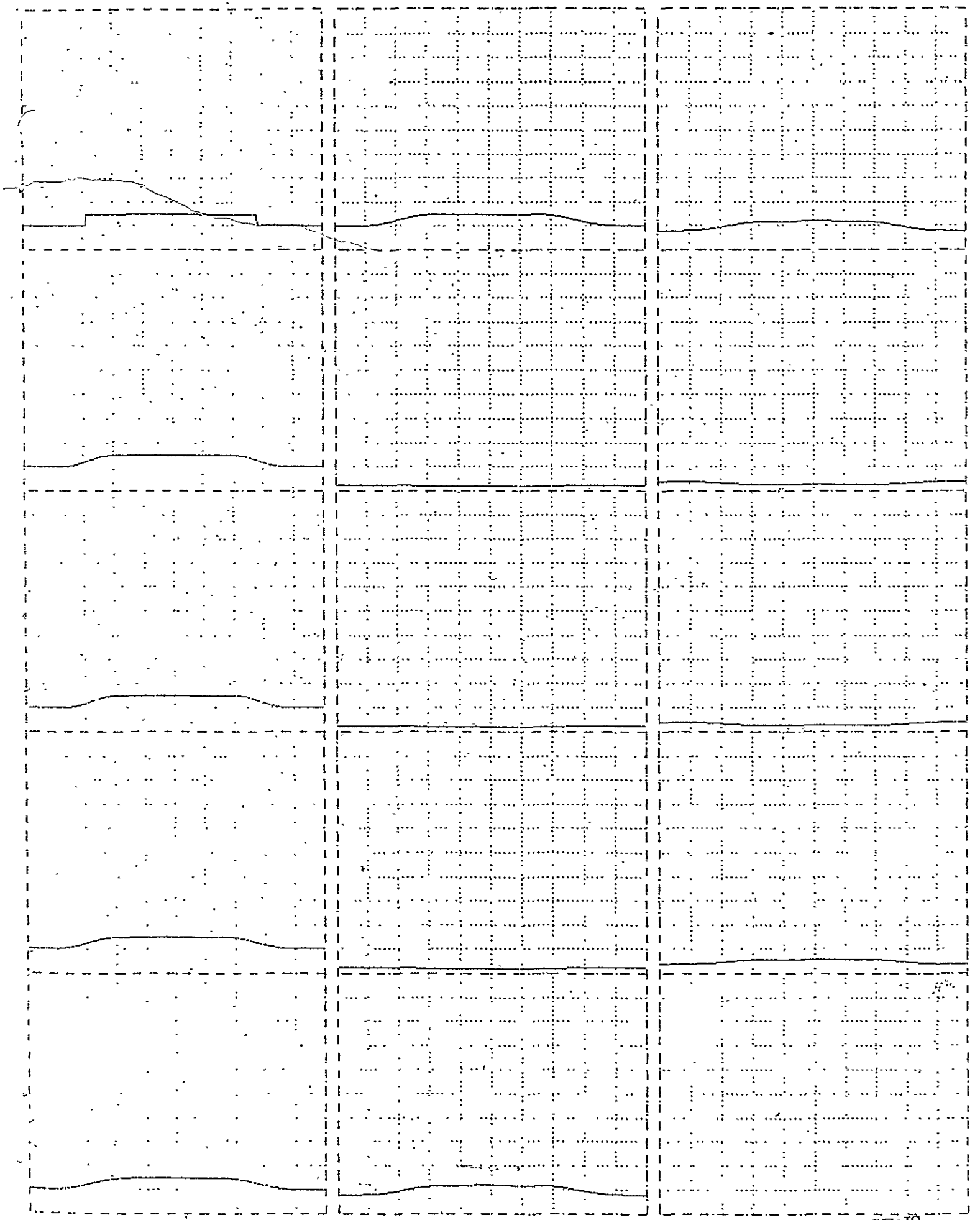

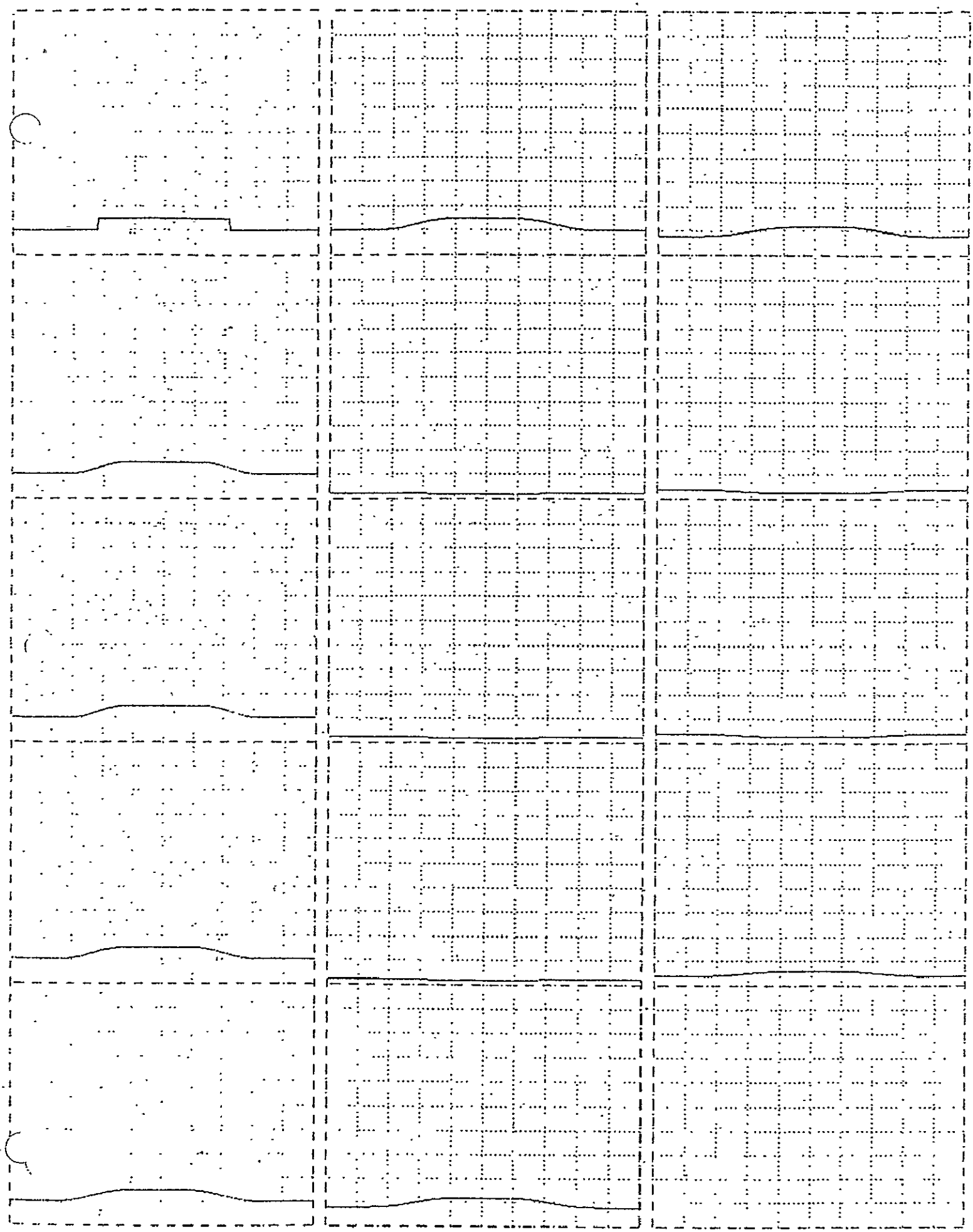

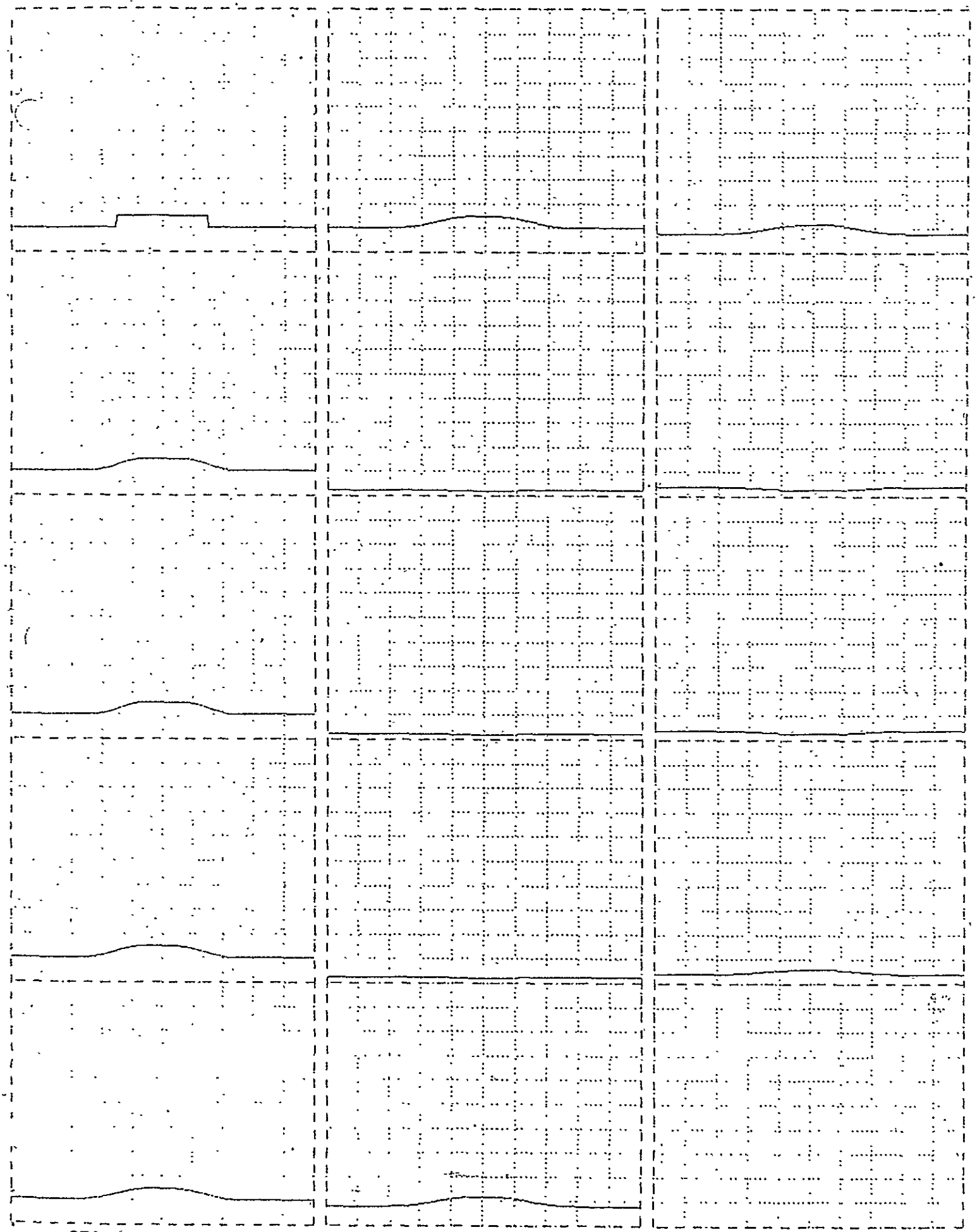

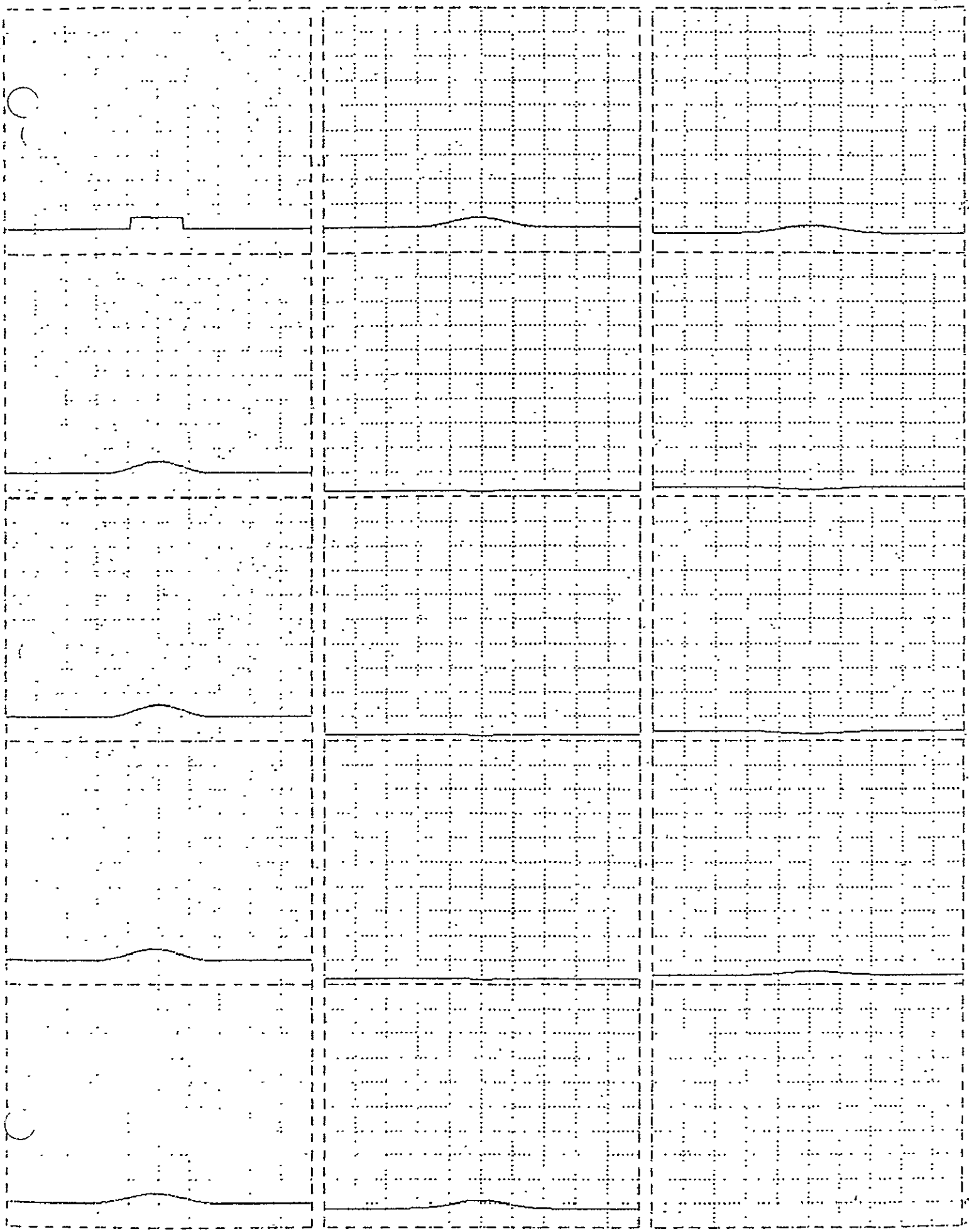

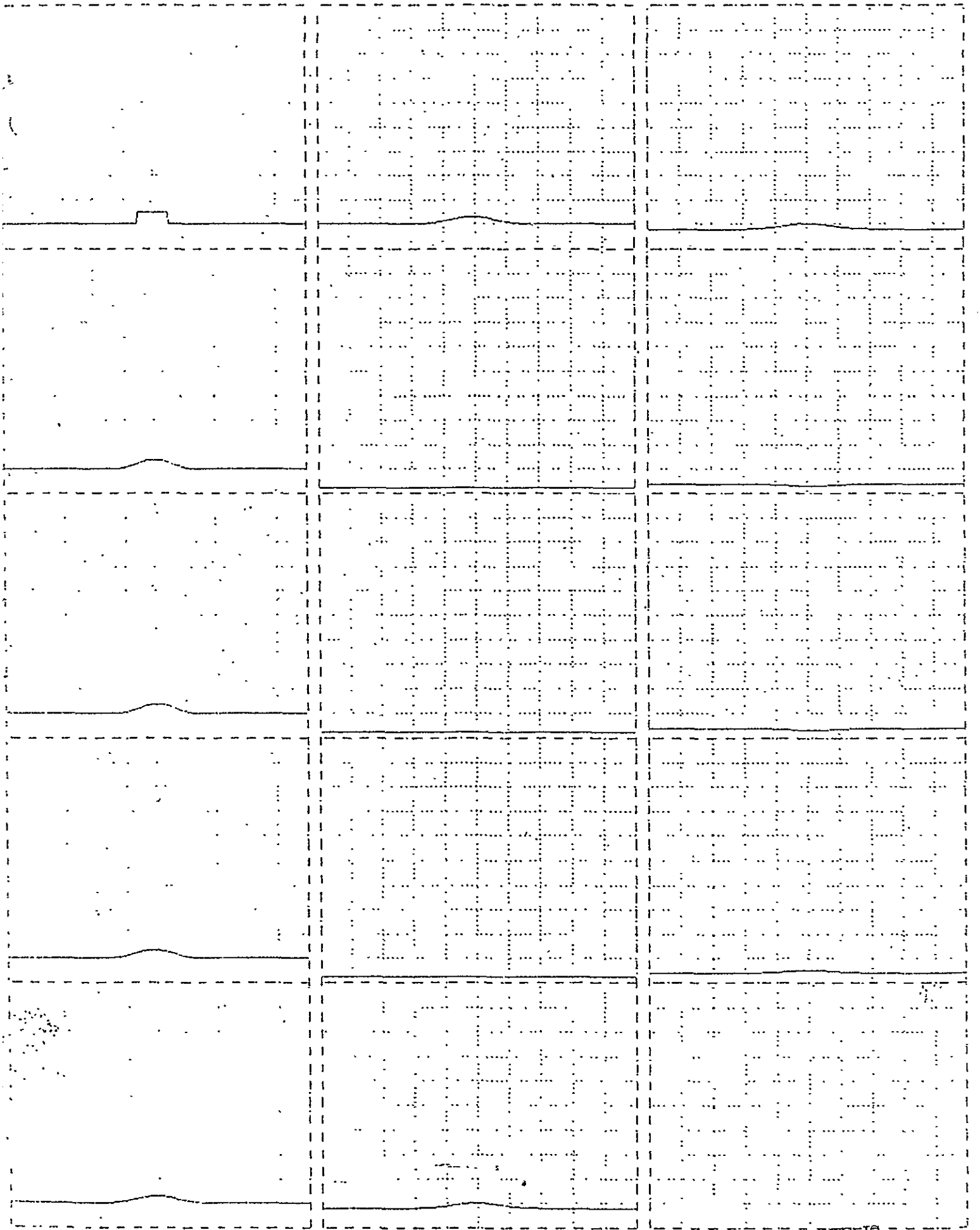

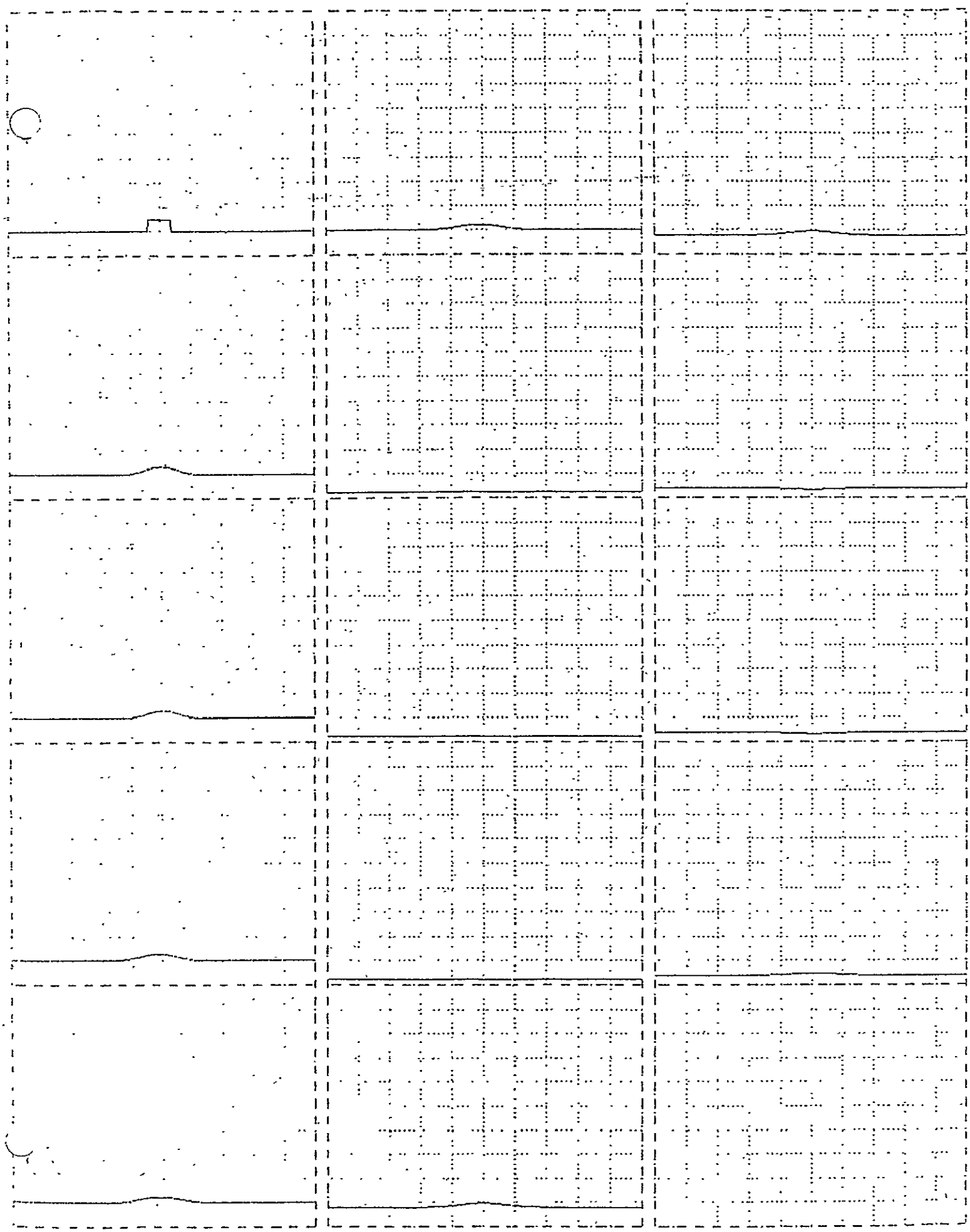

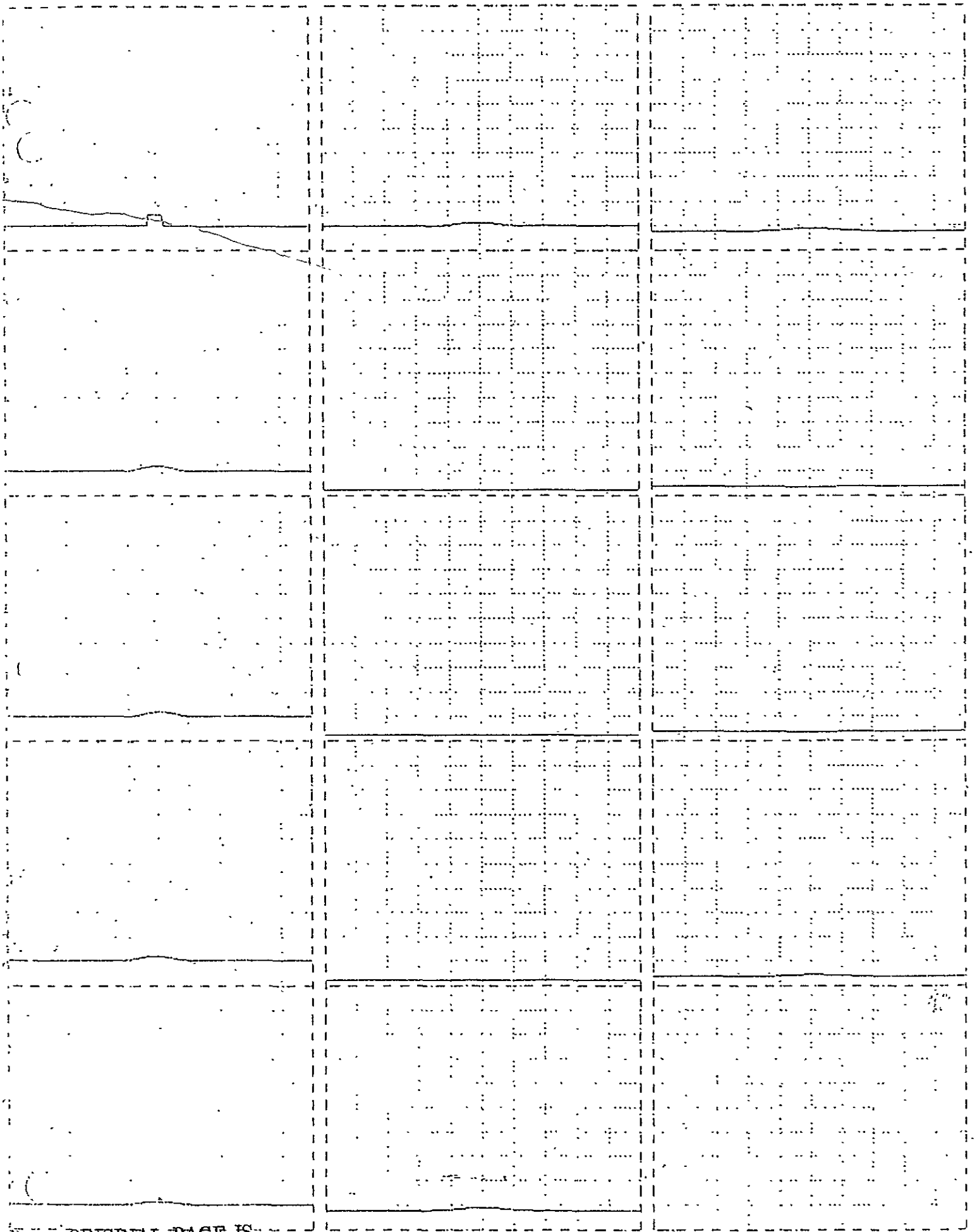

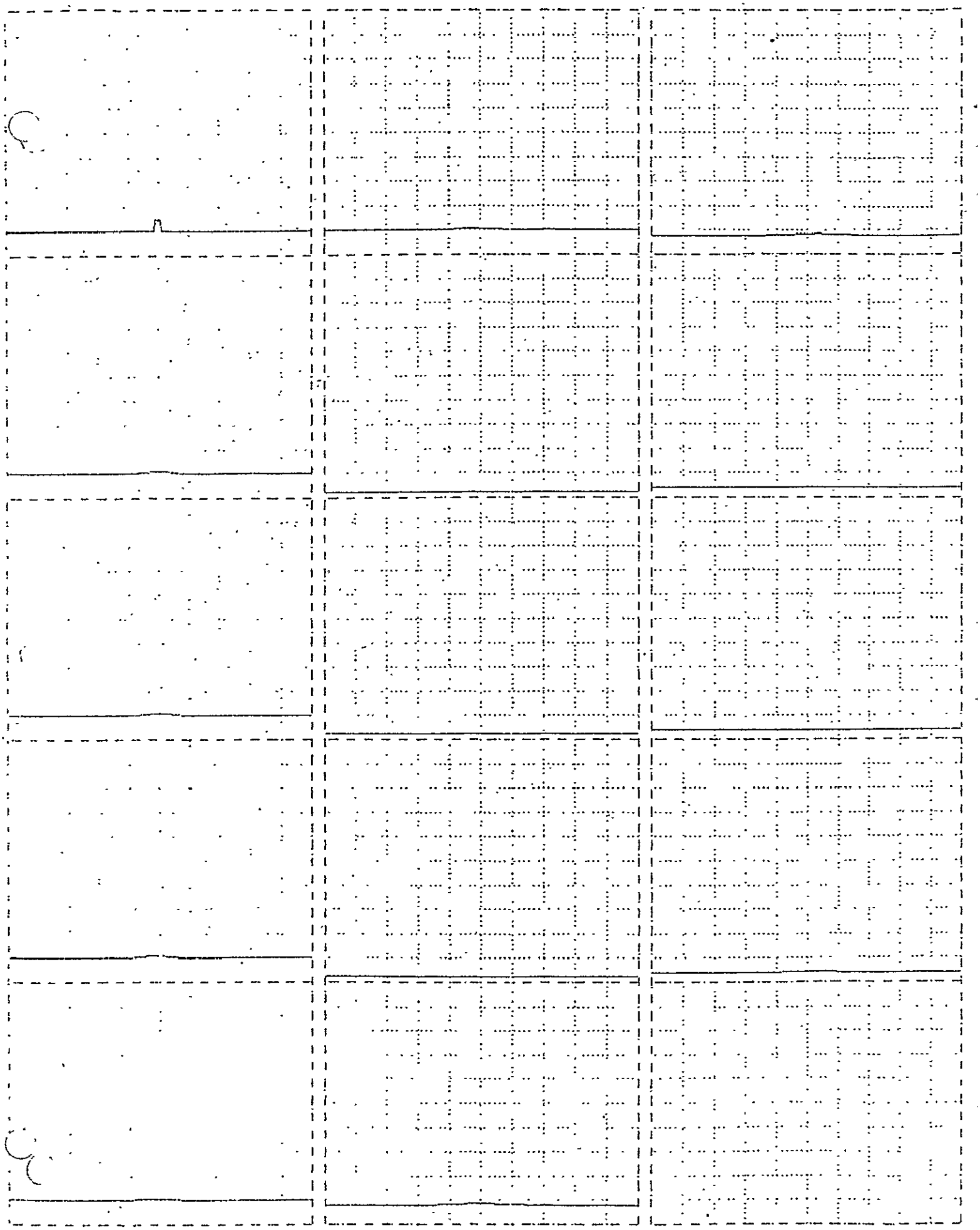

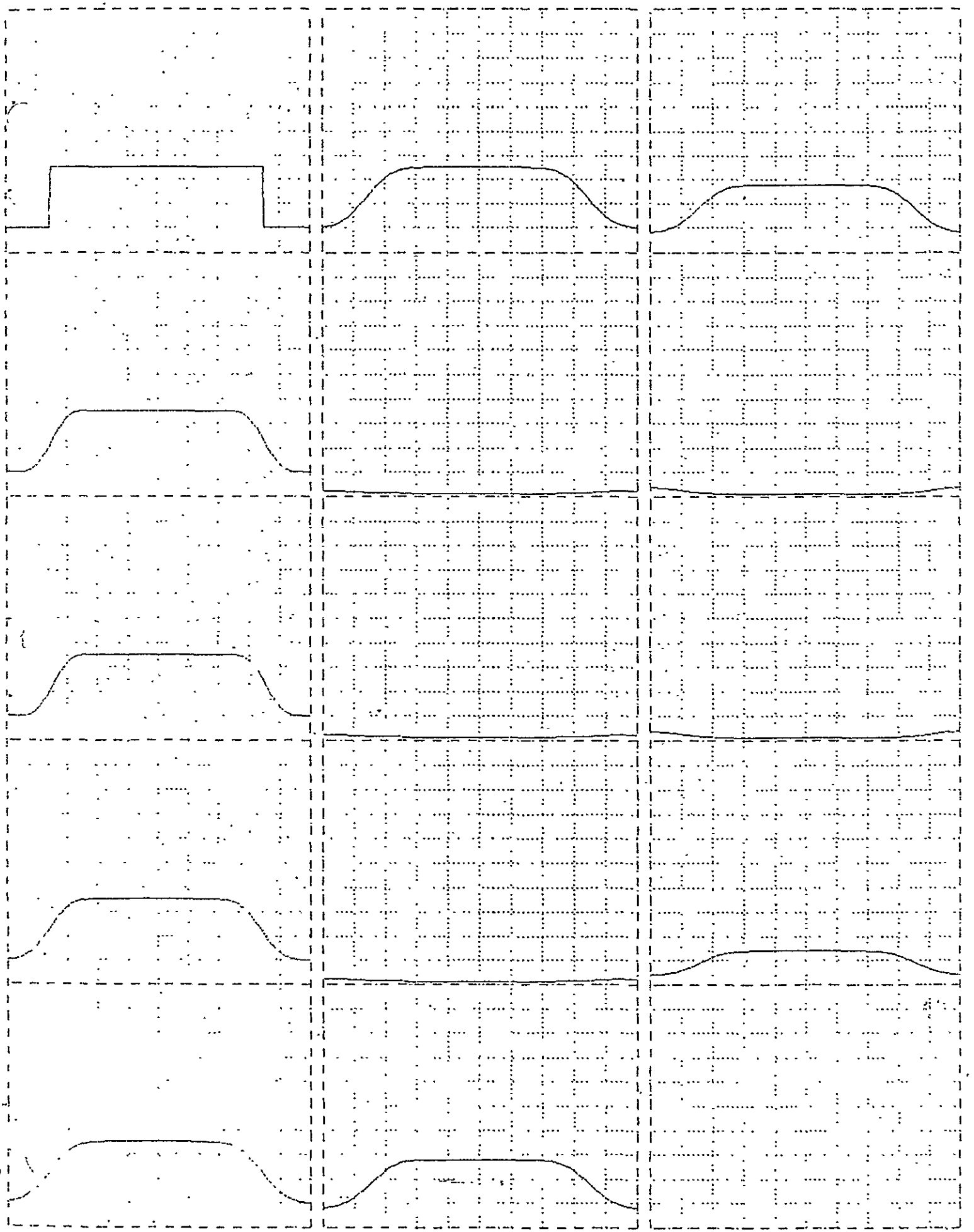

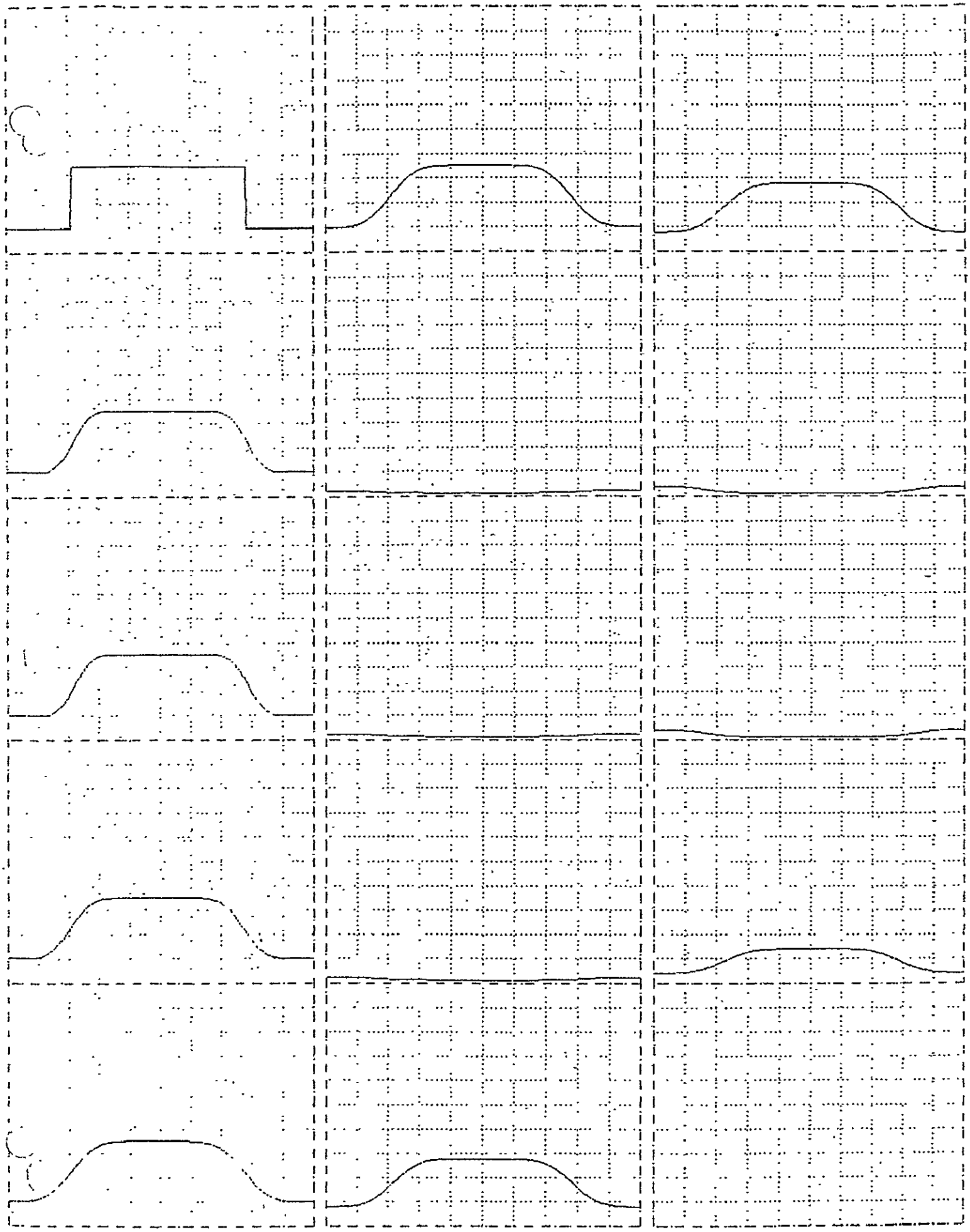

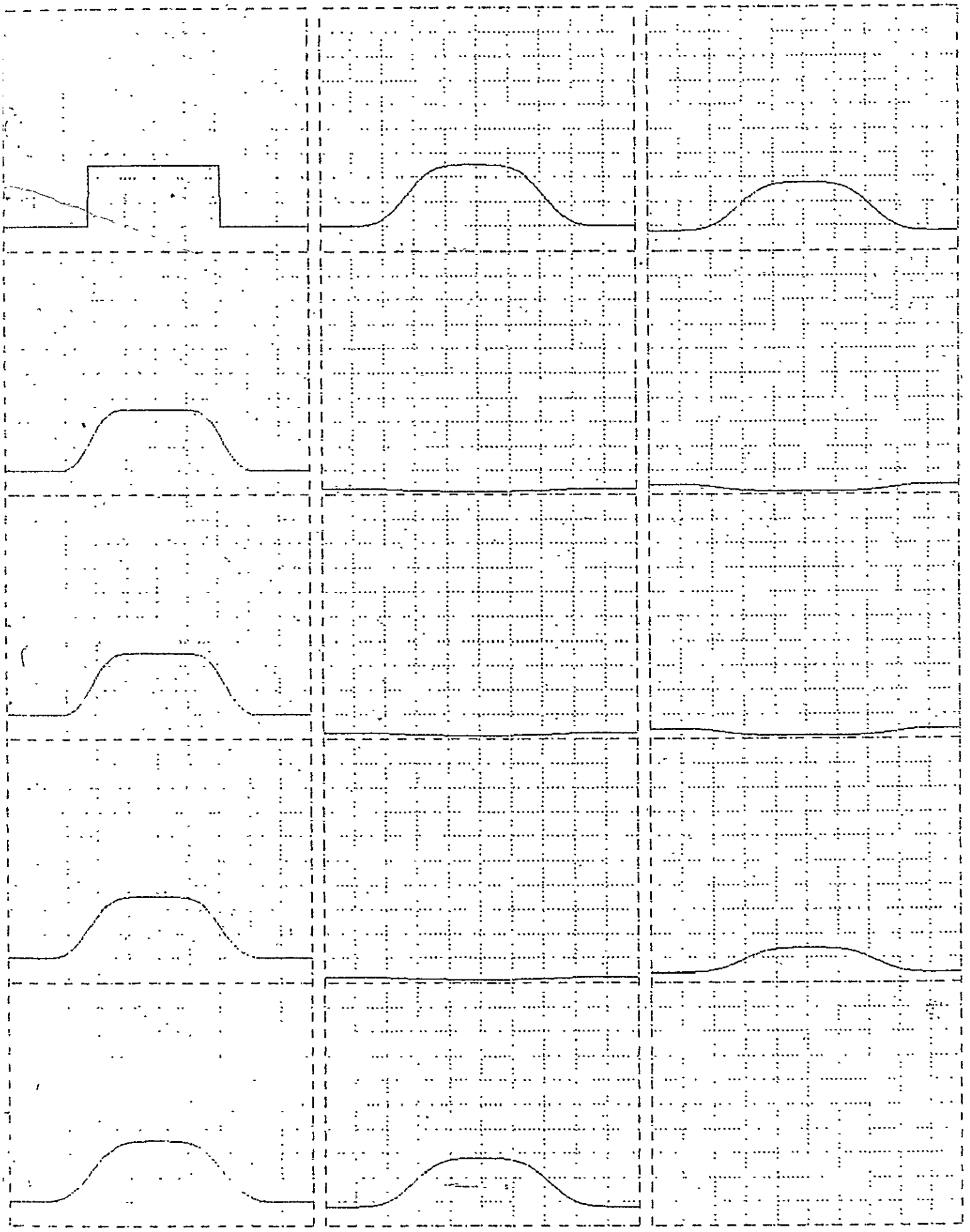

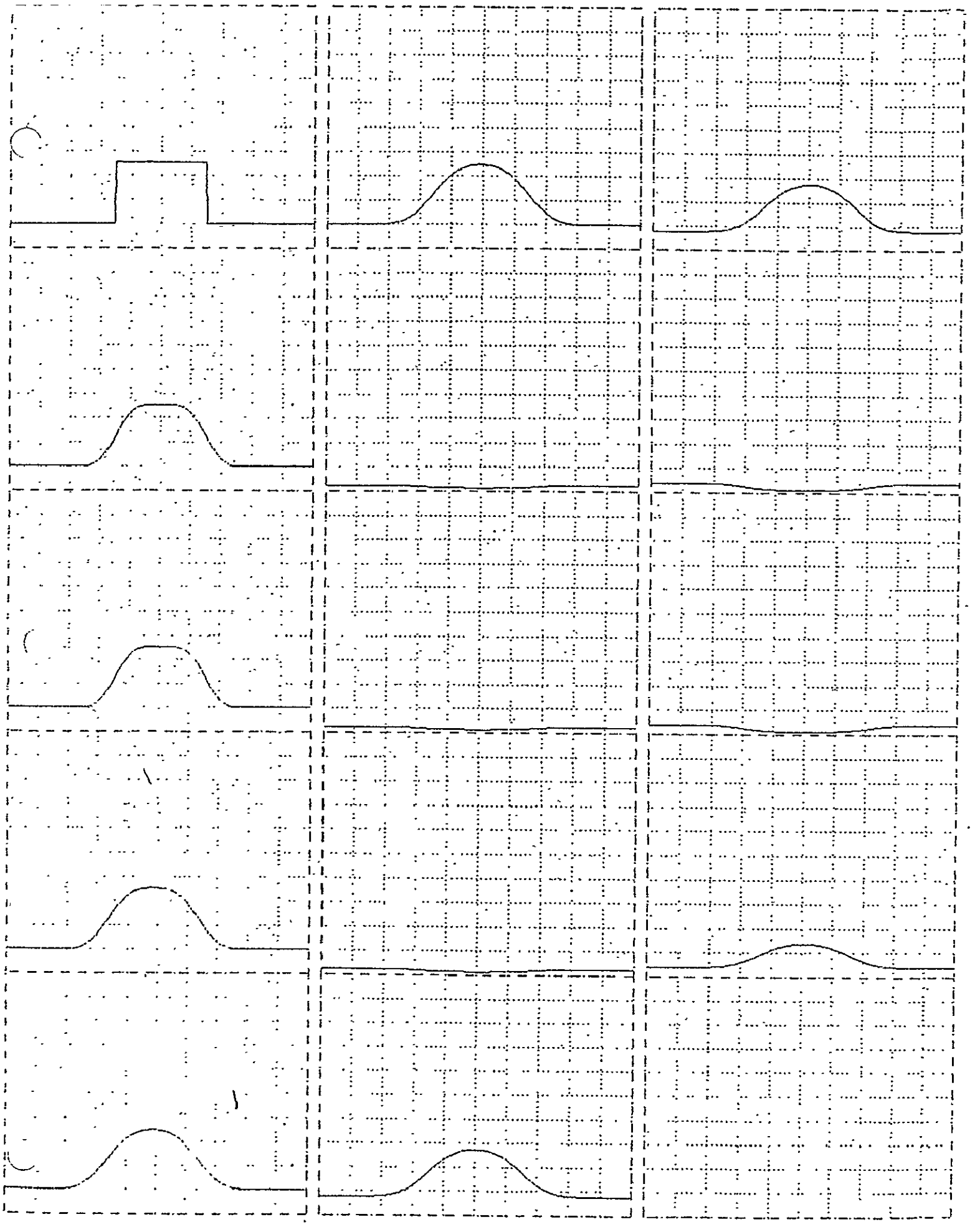

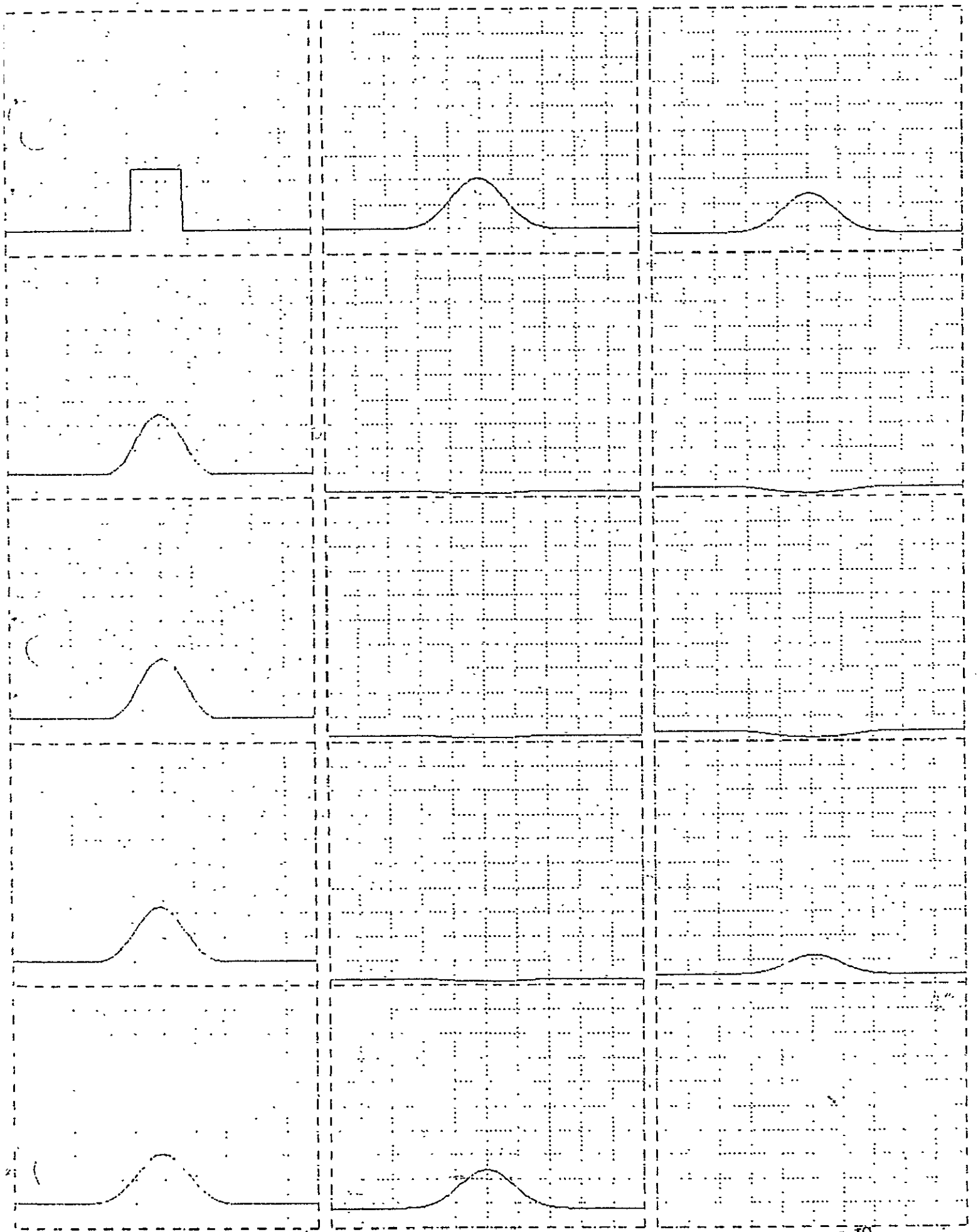

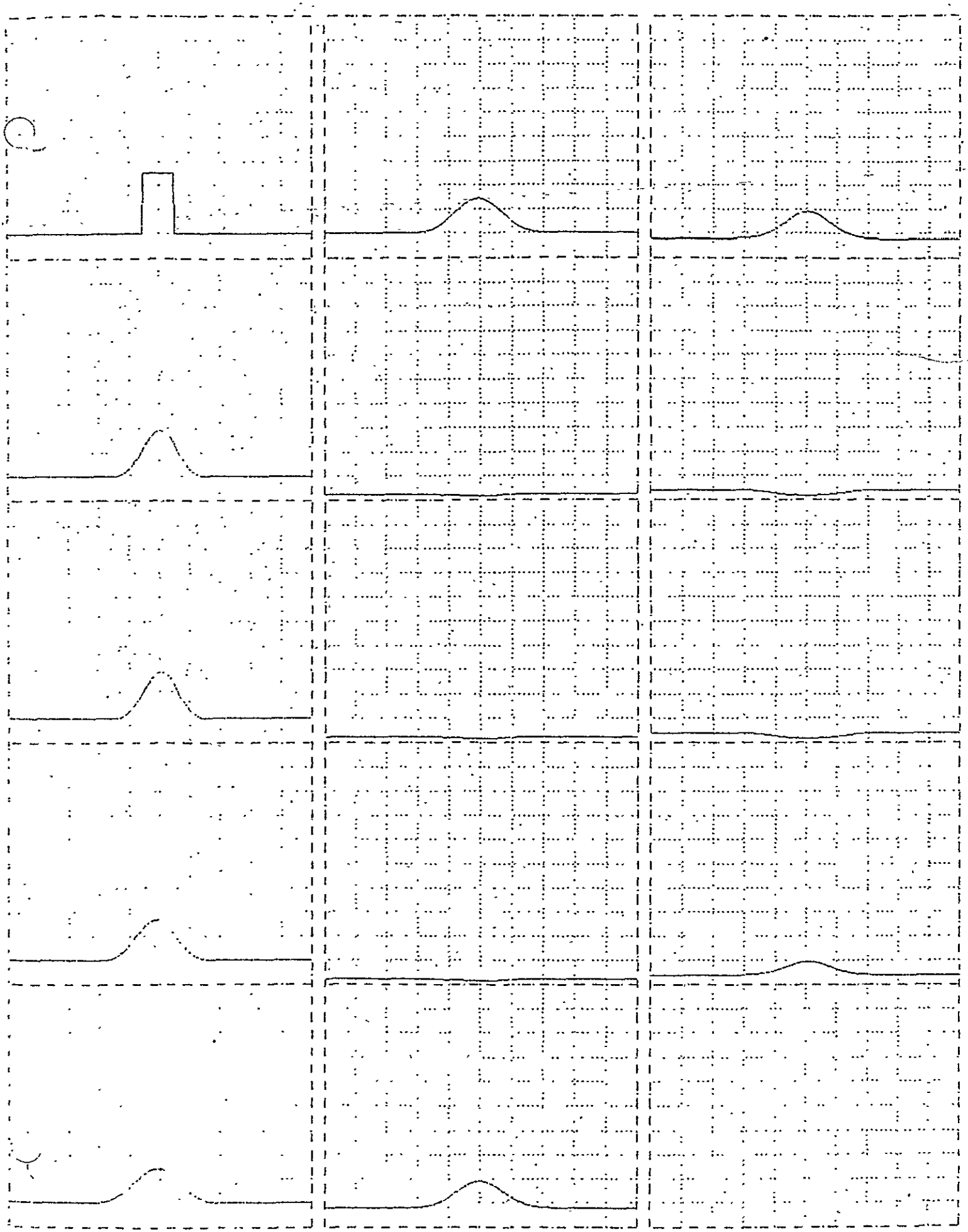

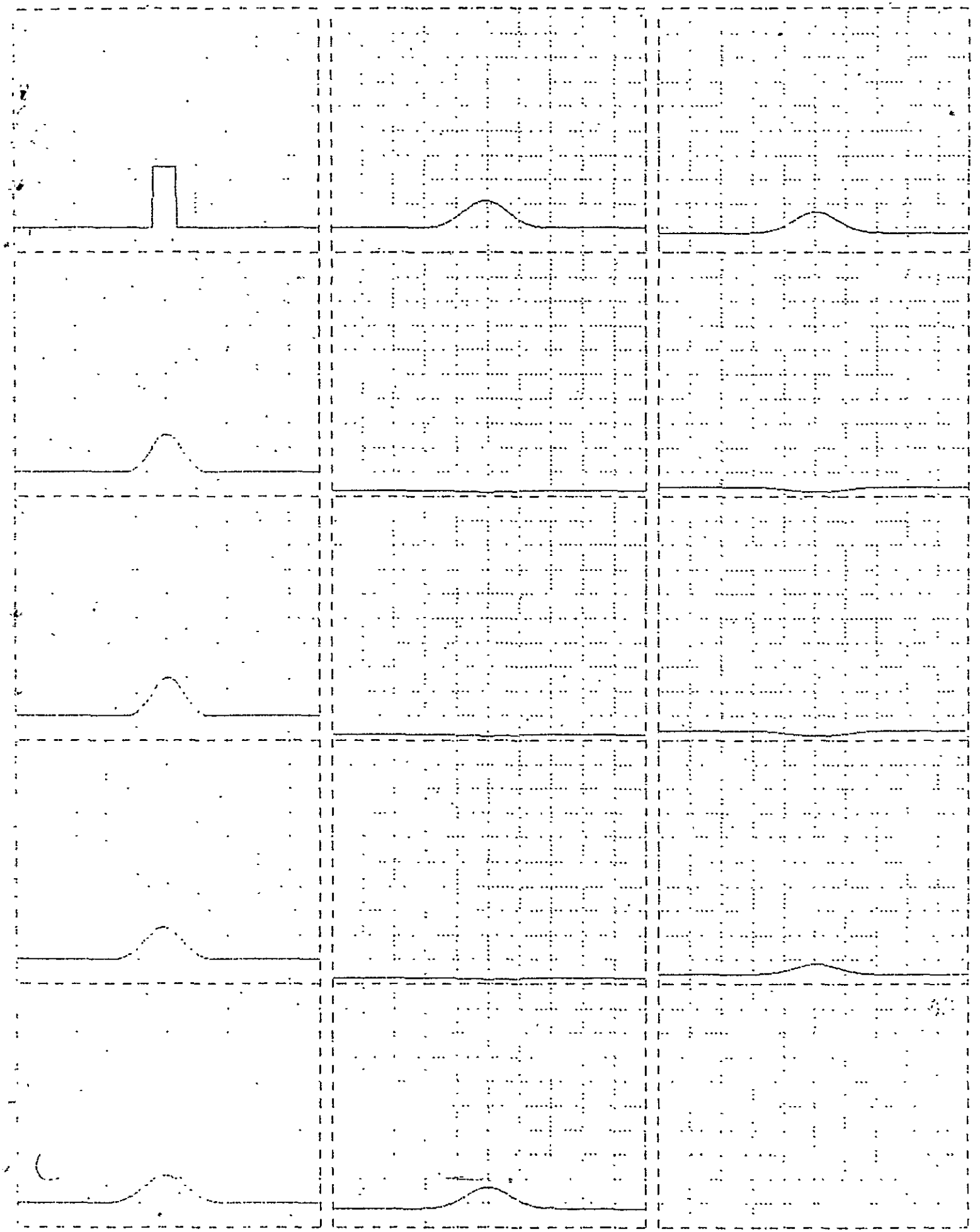

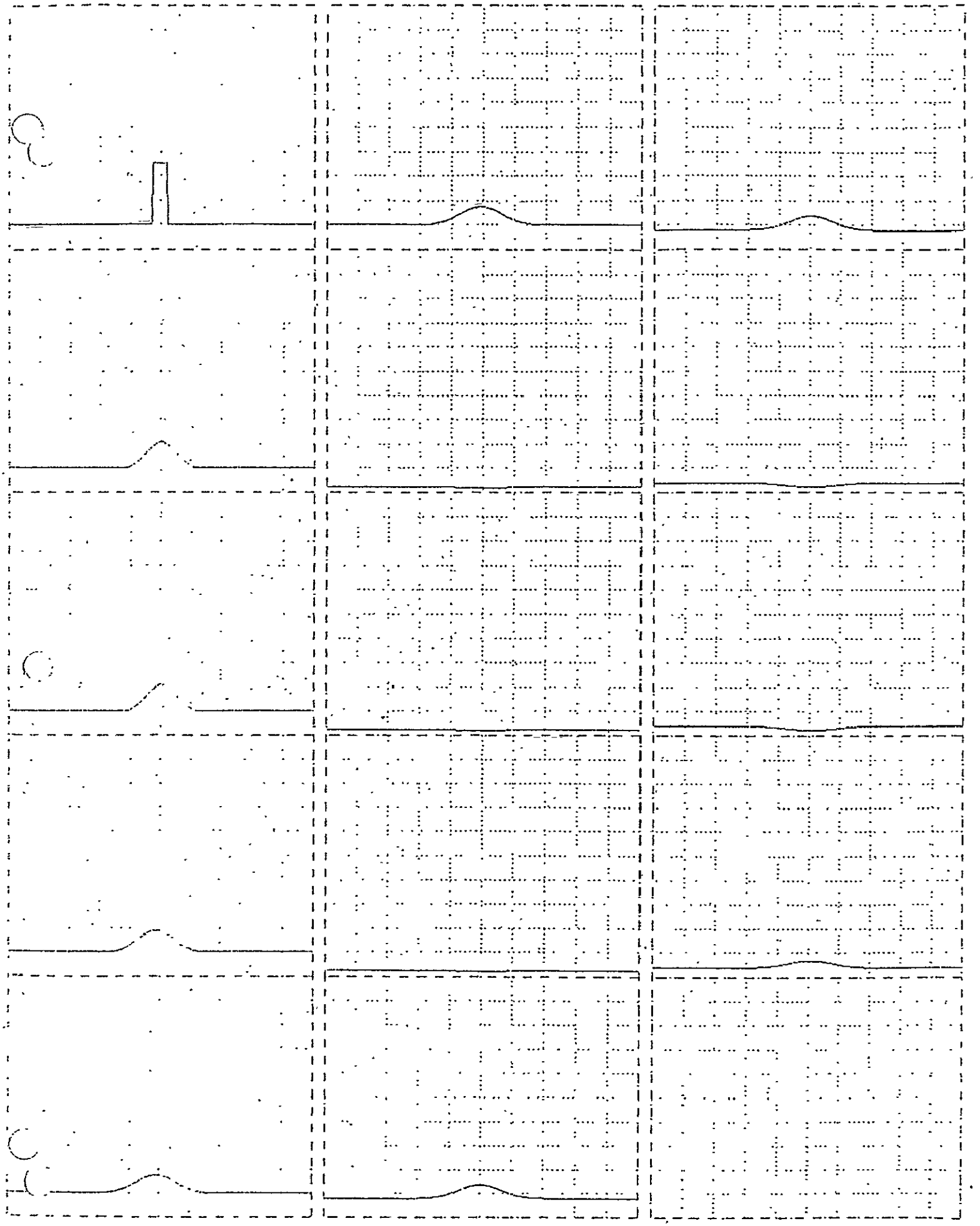

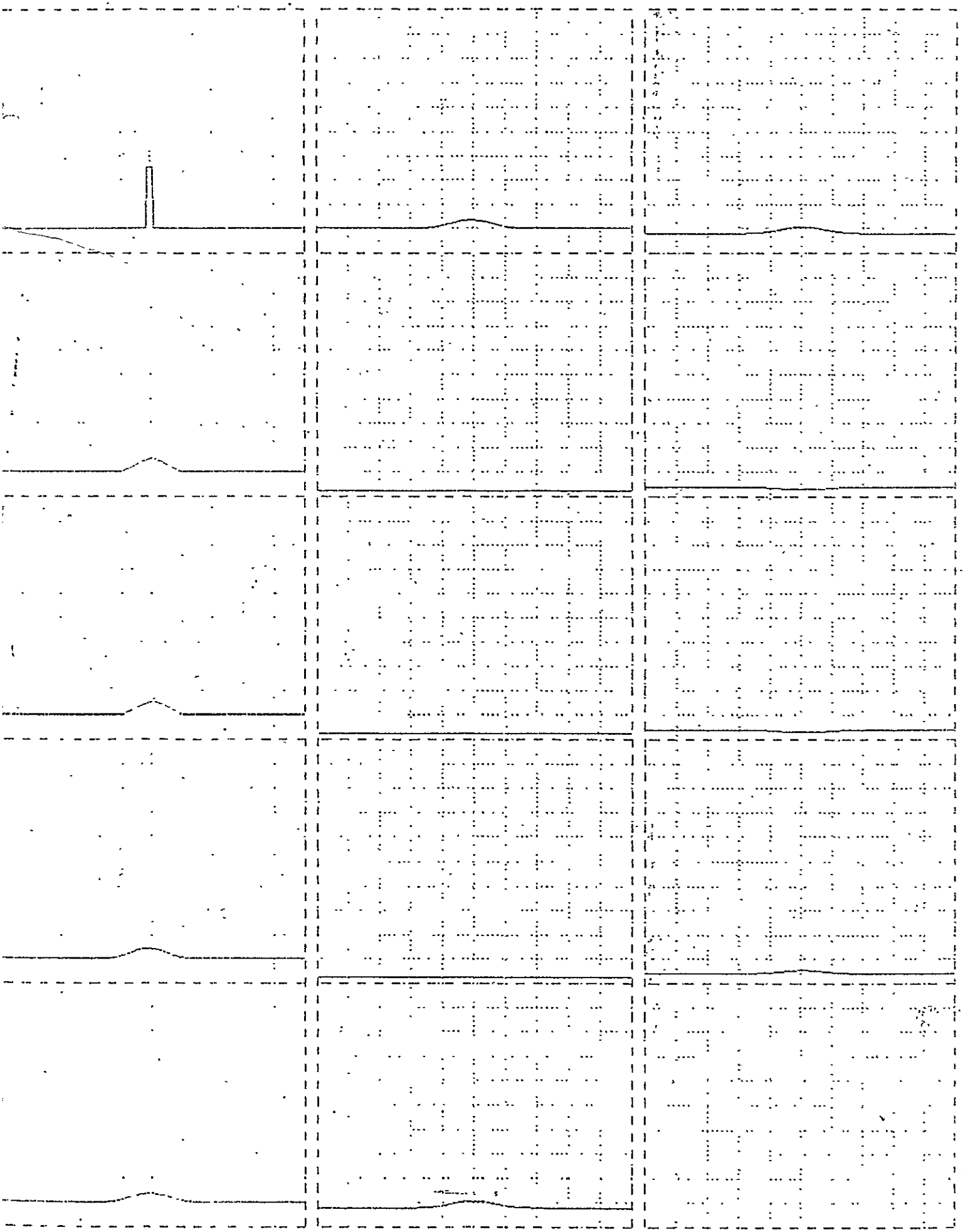

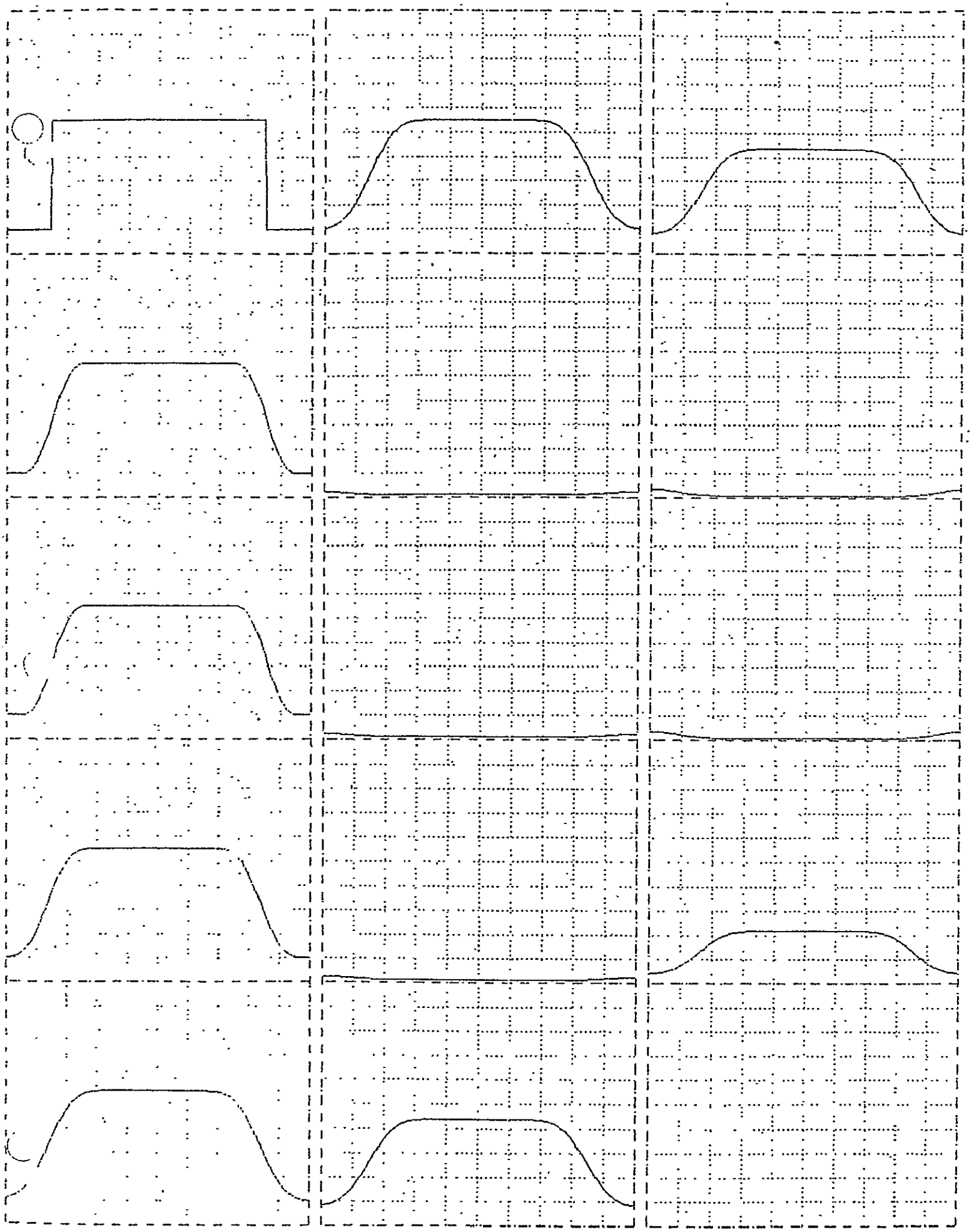

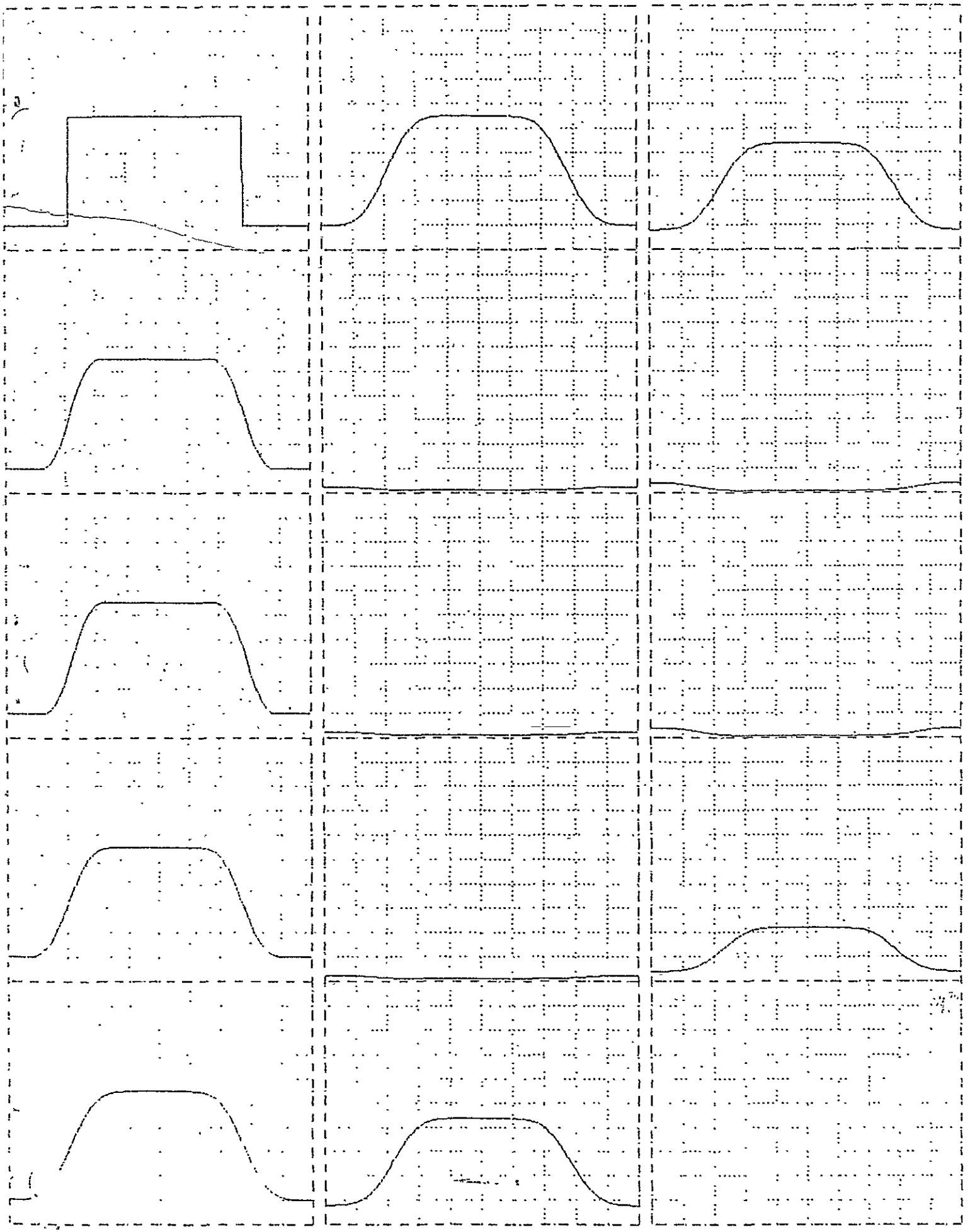

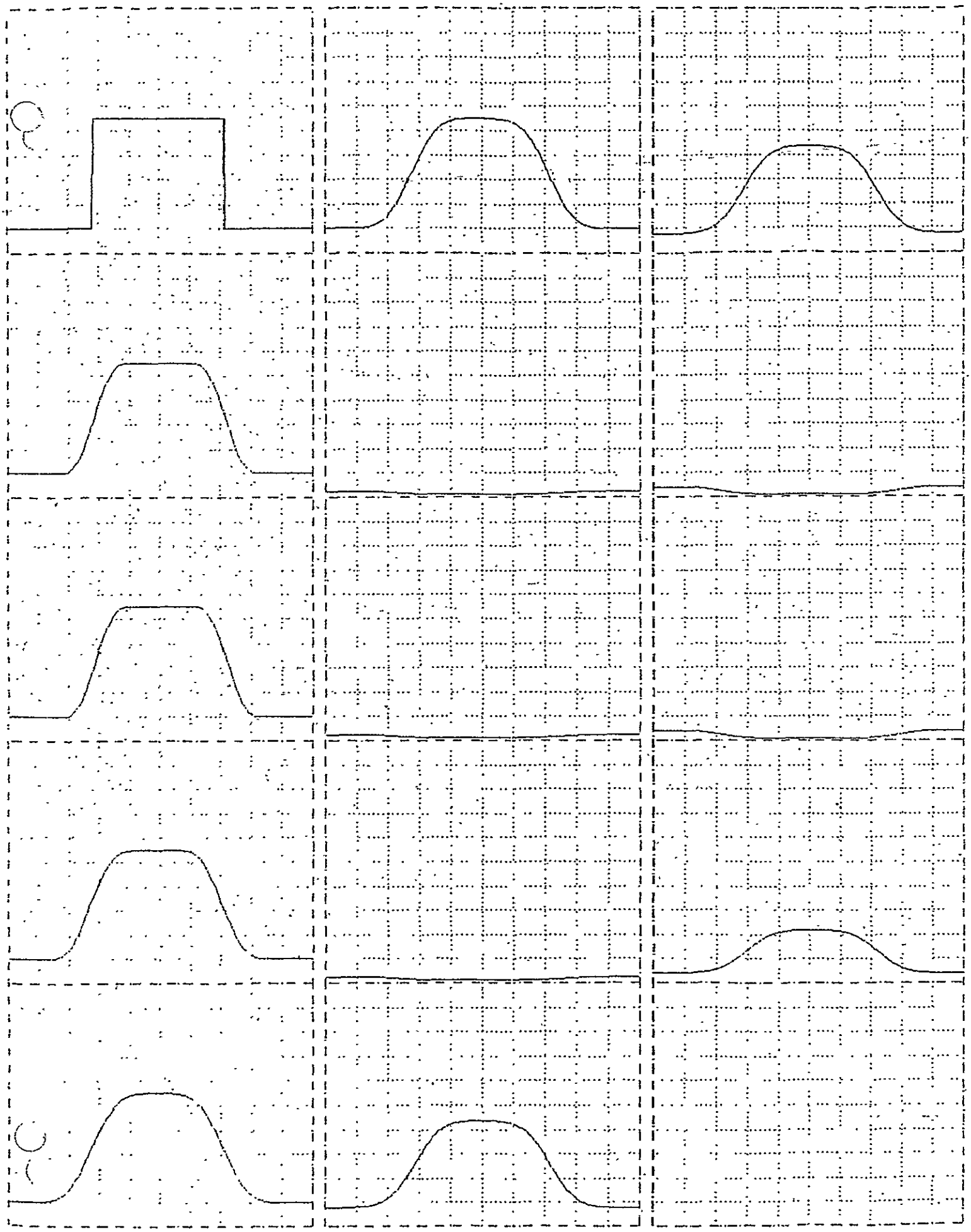

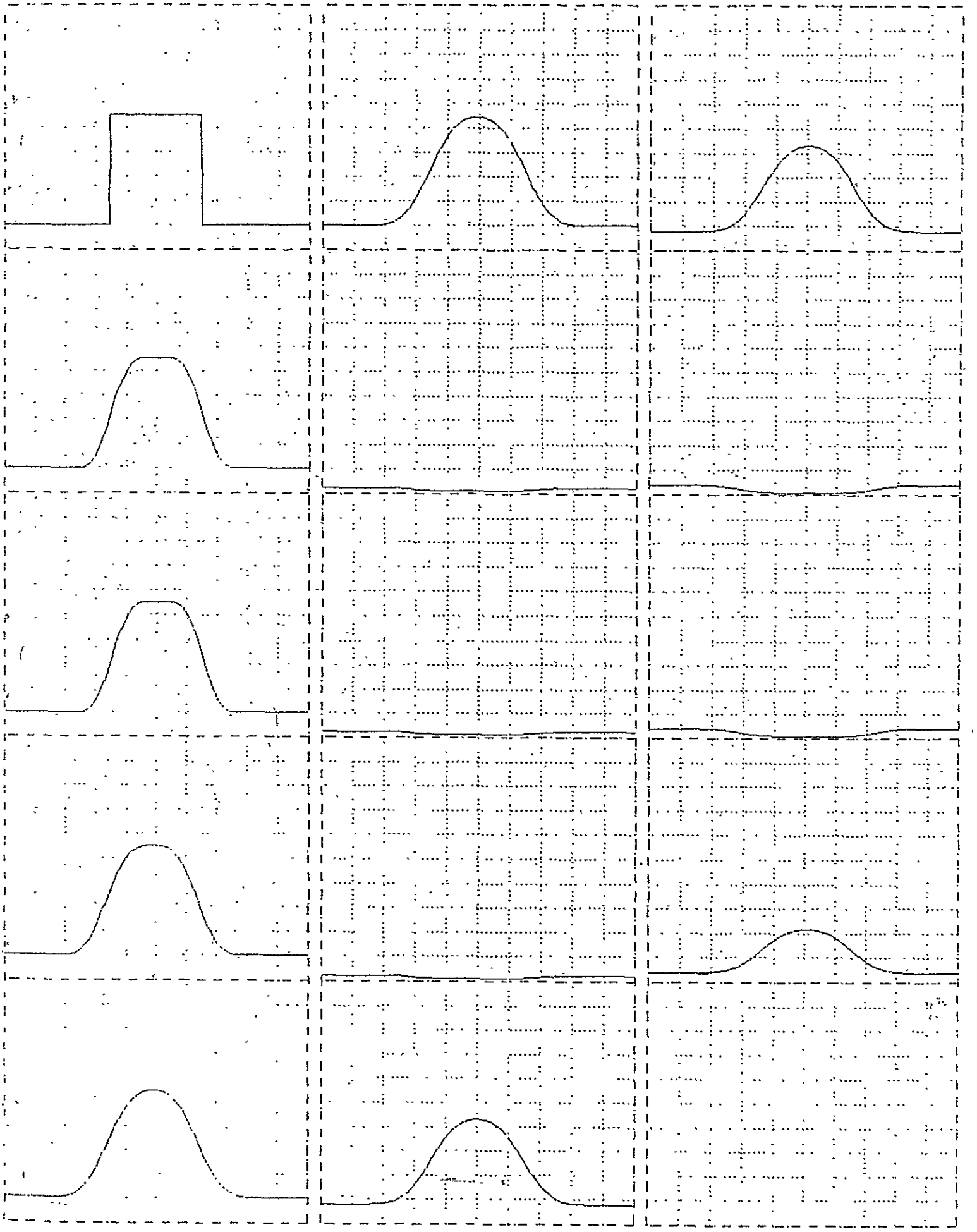

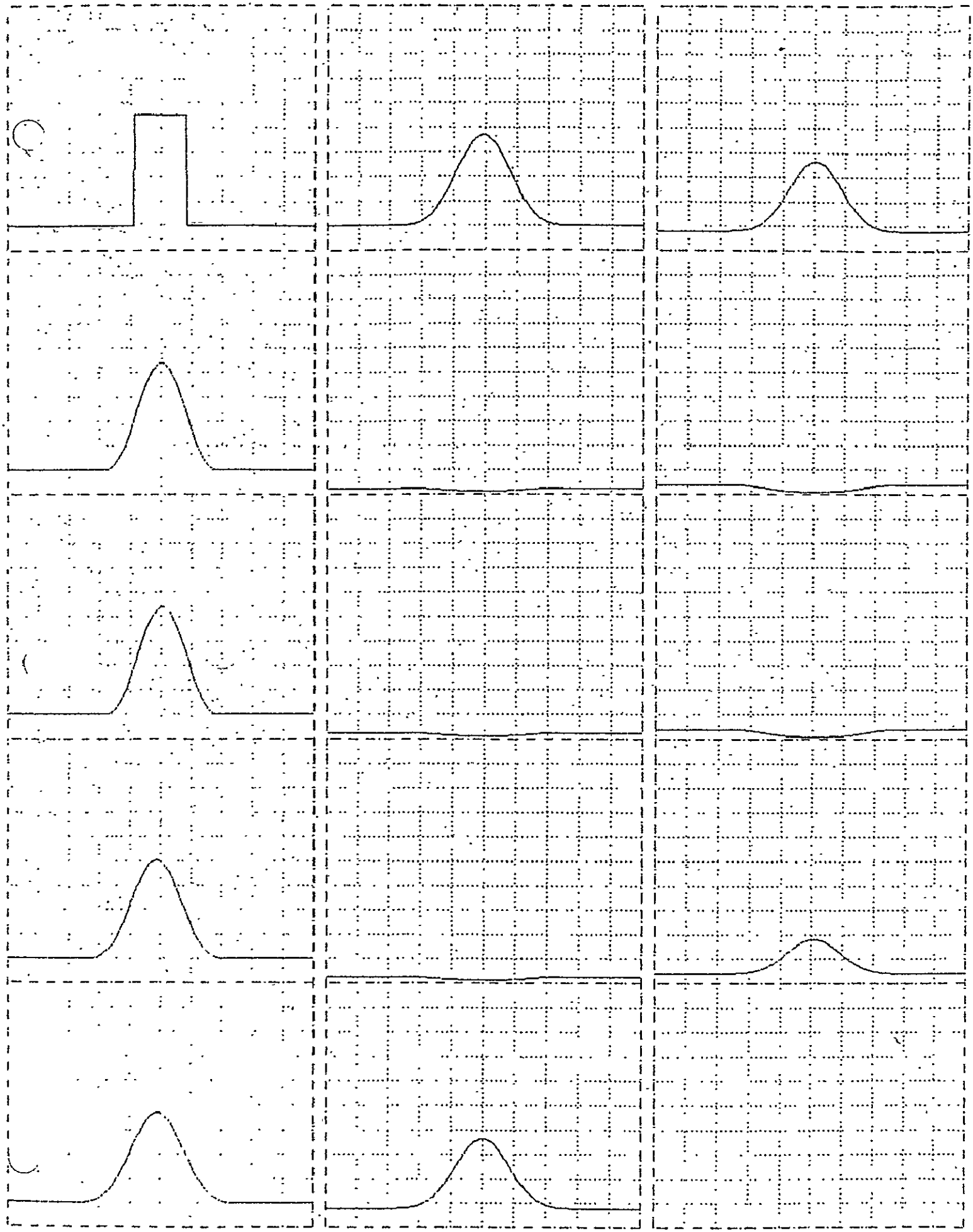

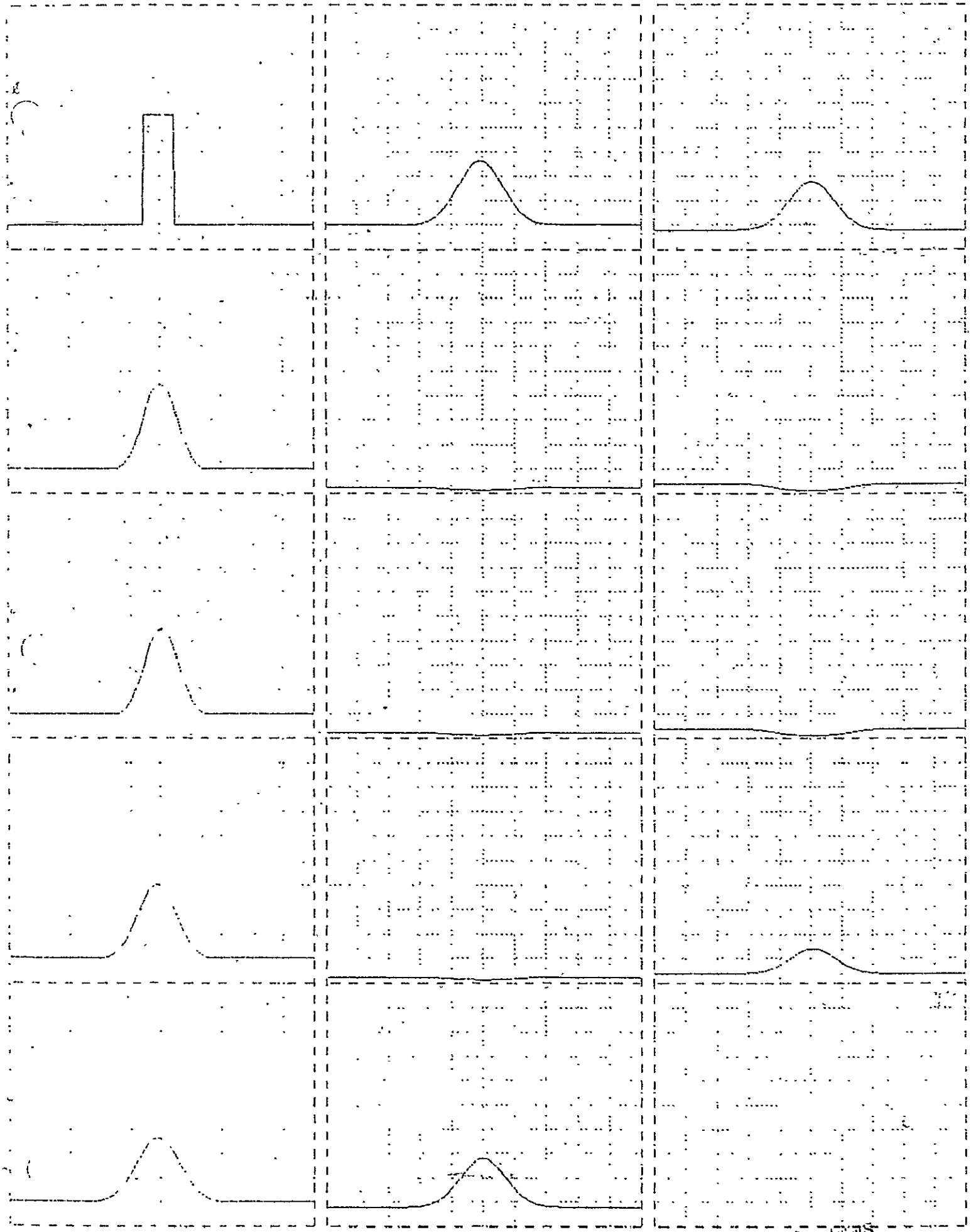

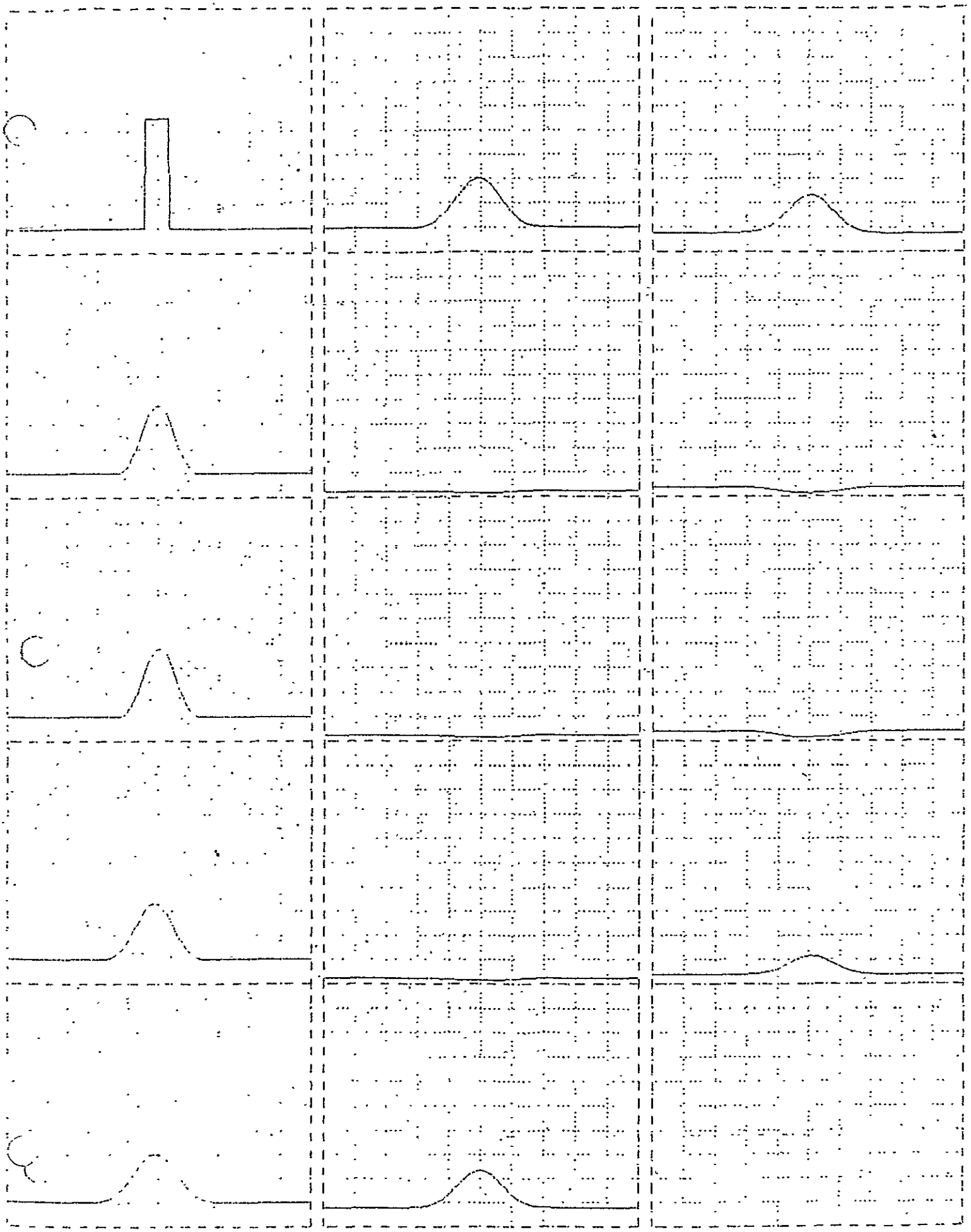

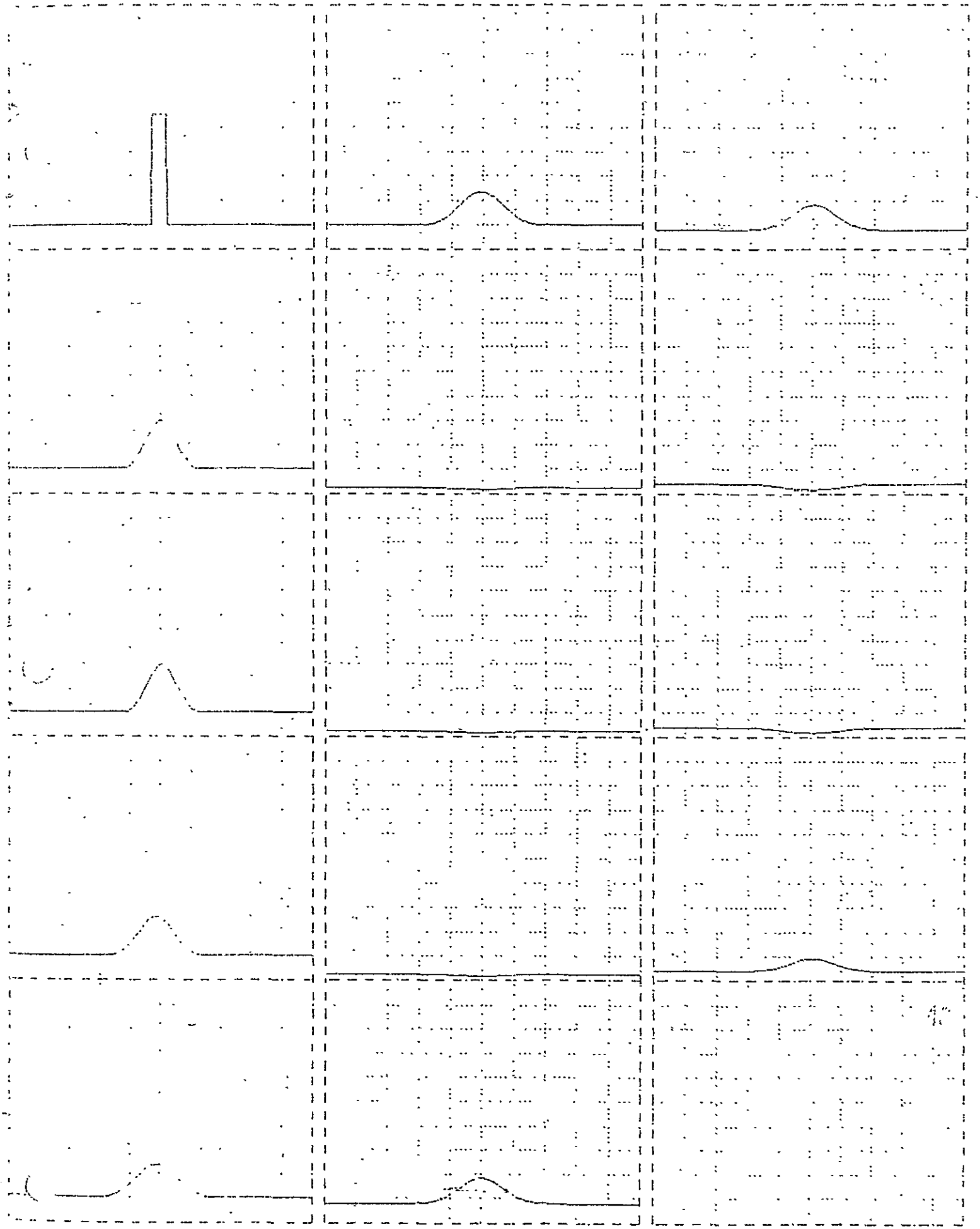

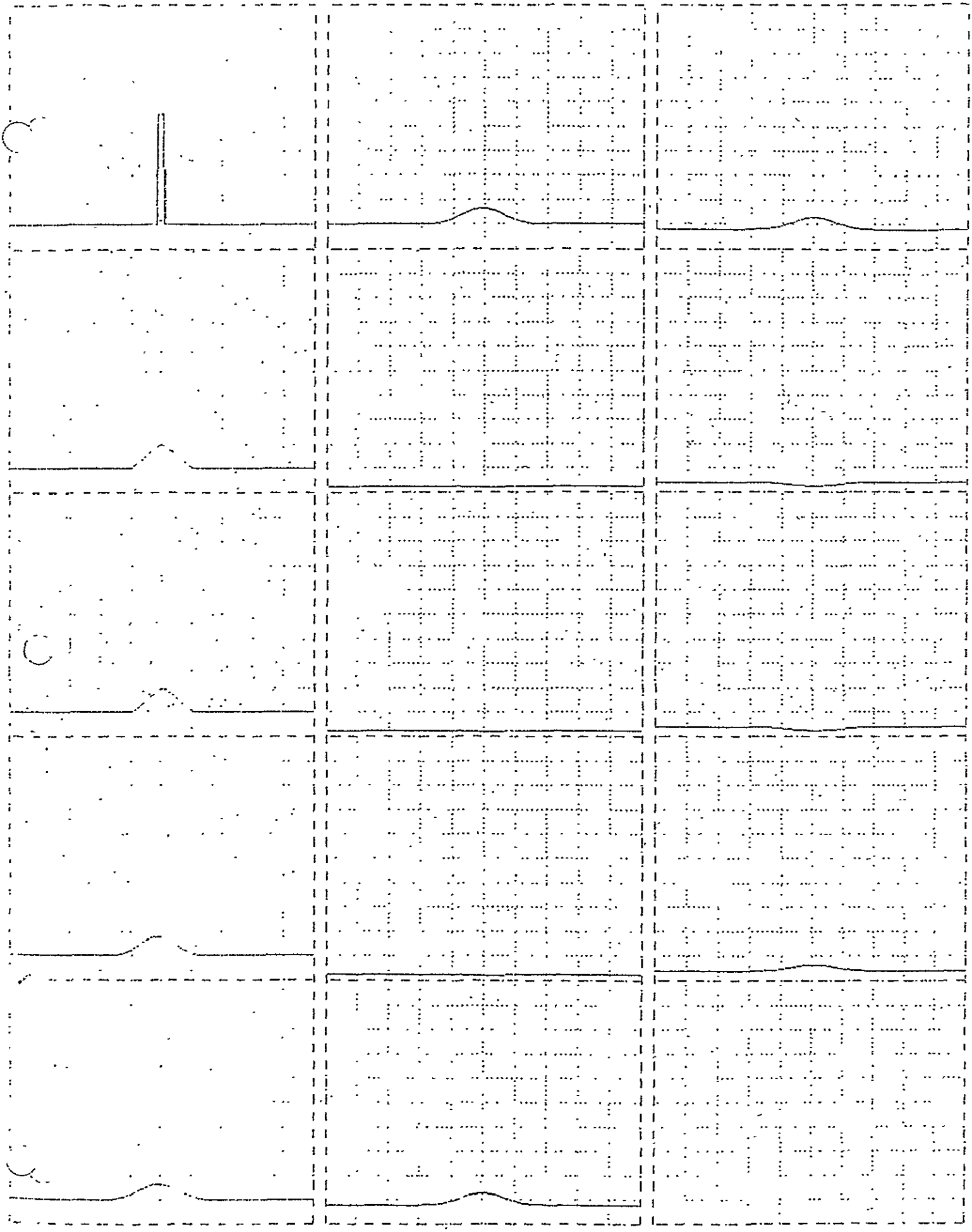

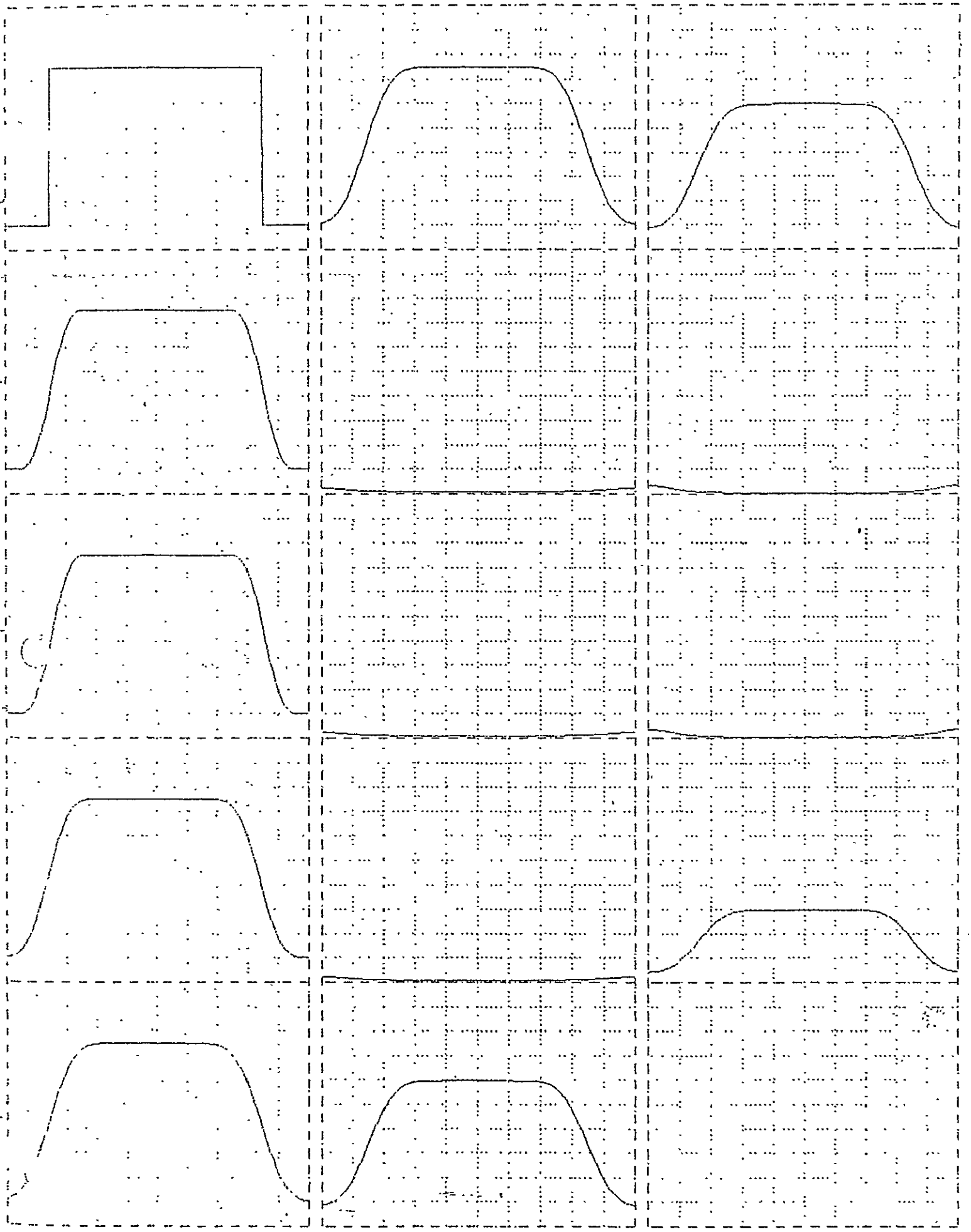

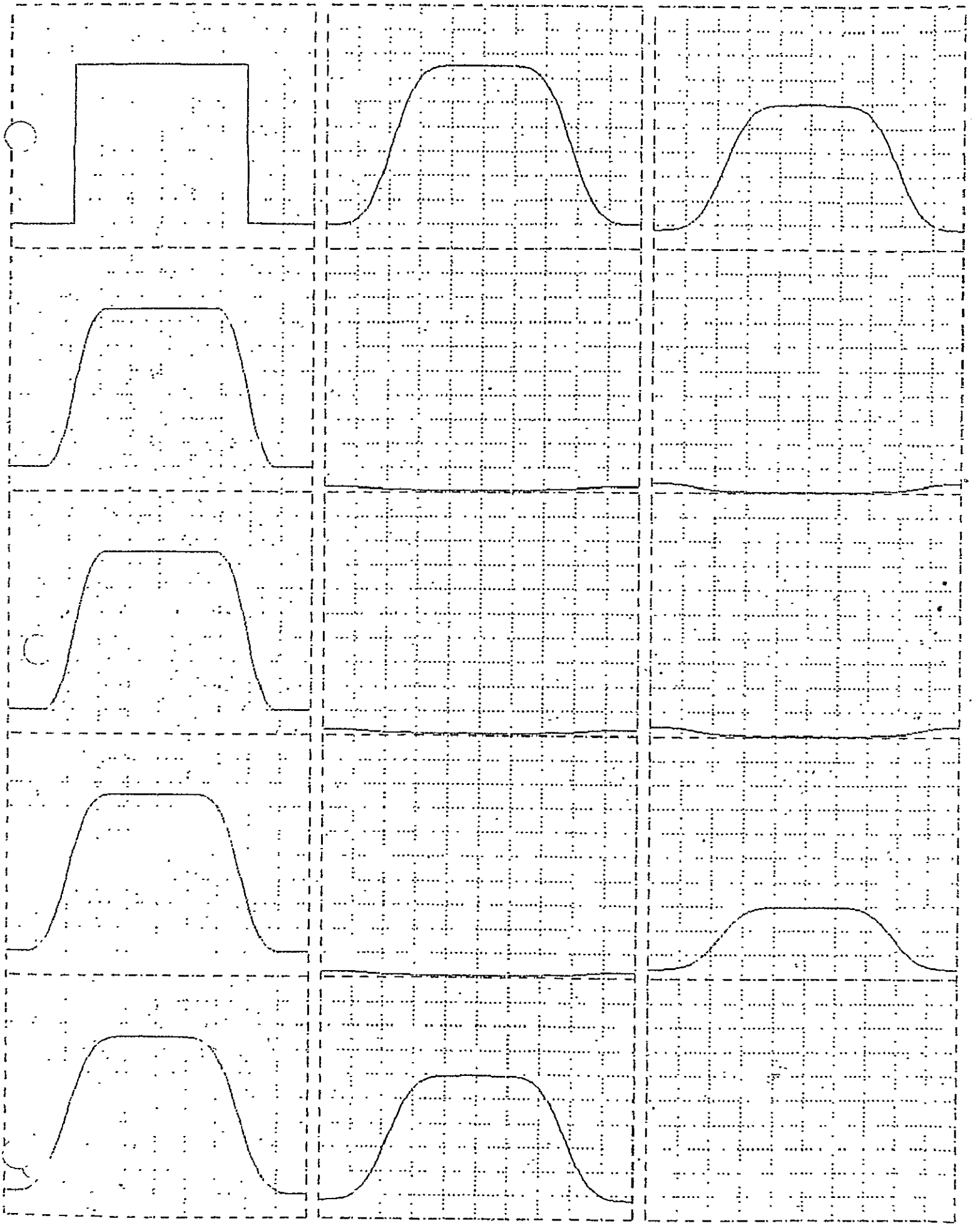

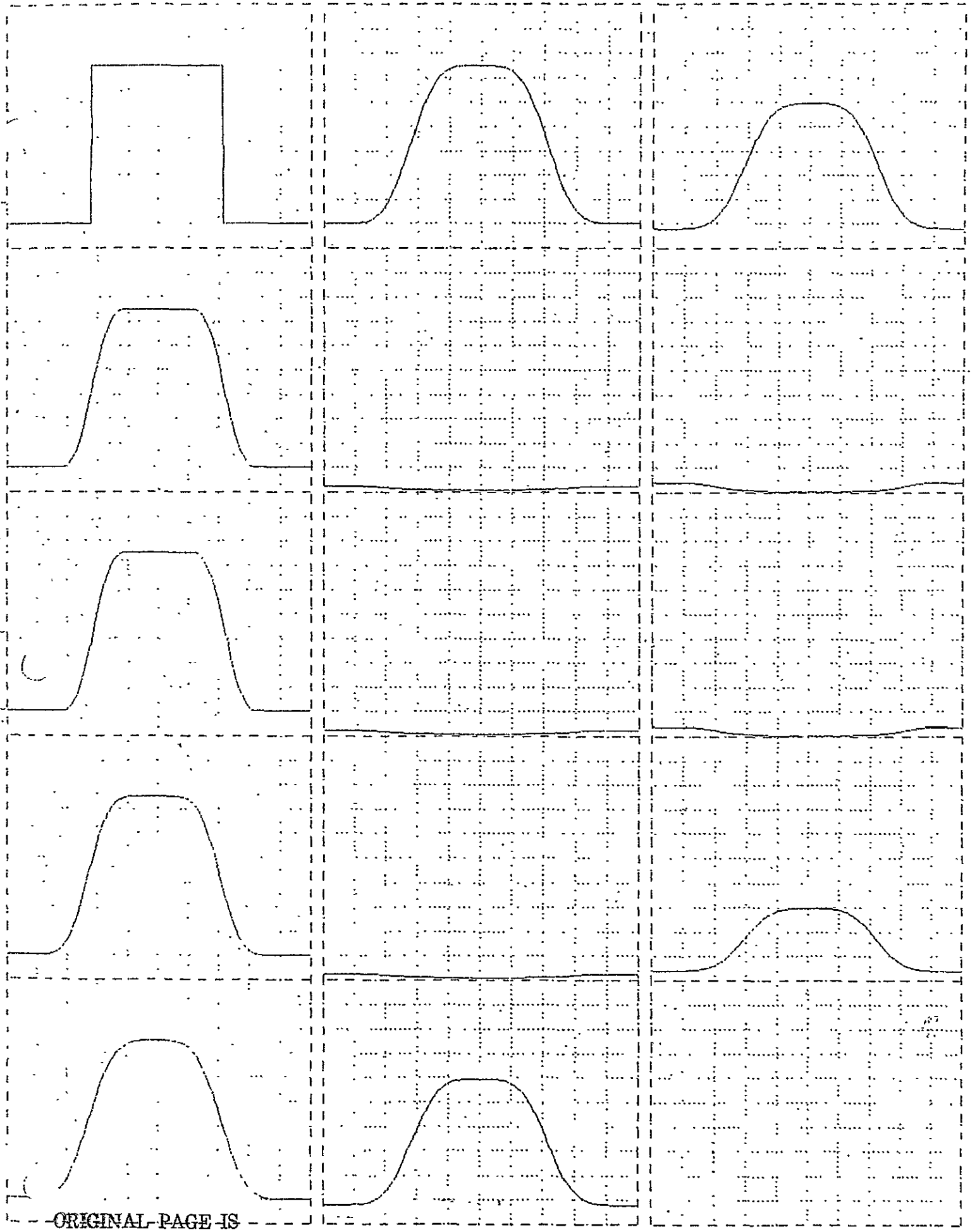

ORIGINAL PAGE IS
OF POOR QUALITY

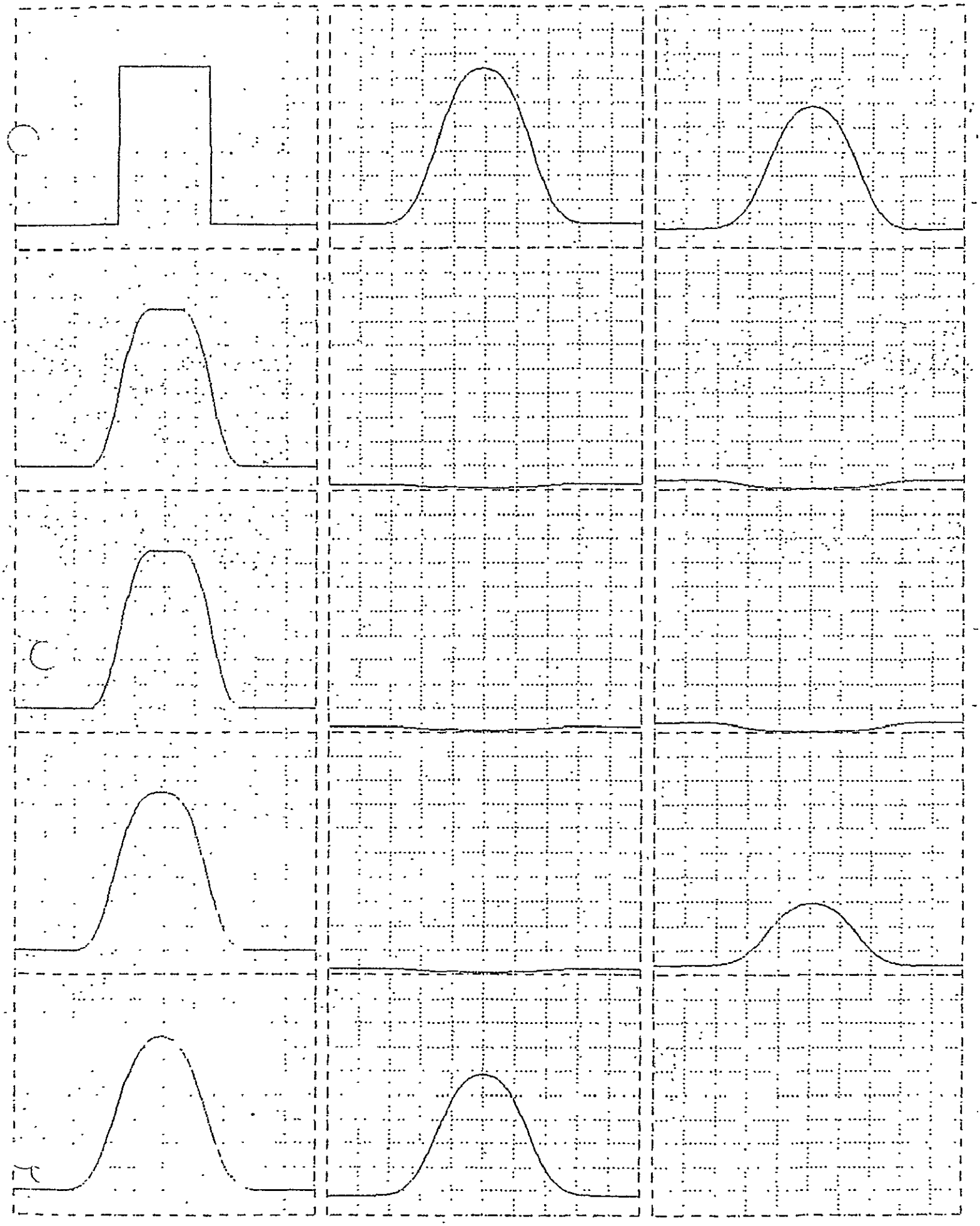

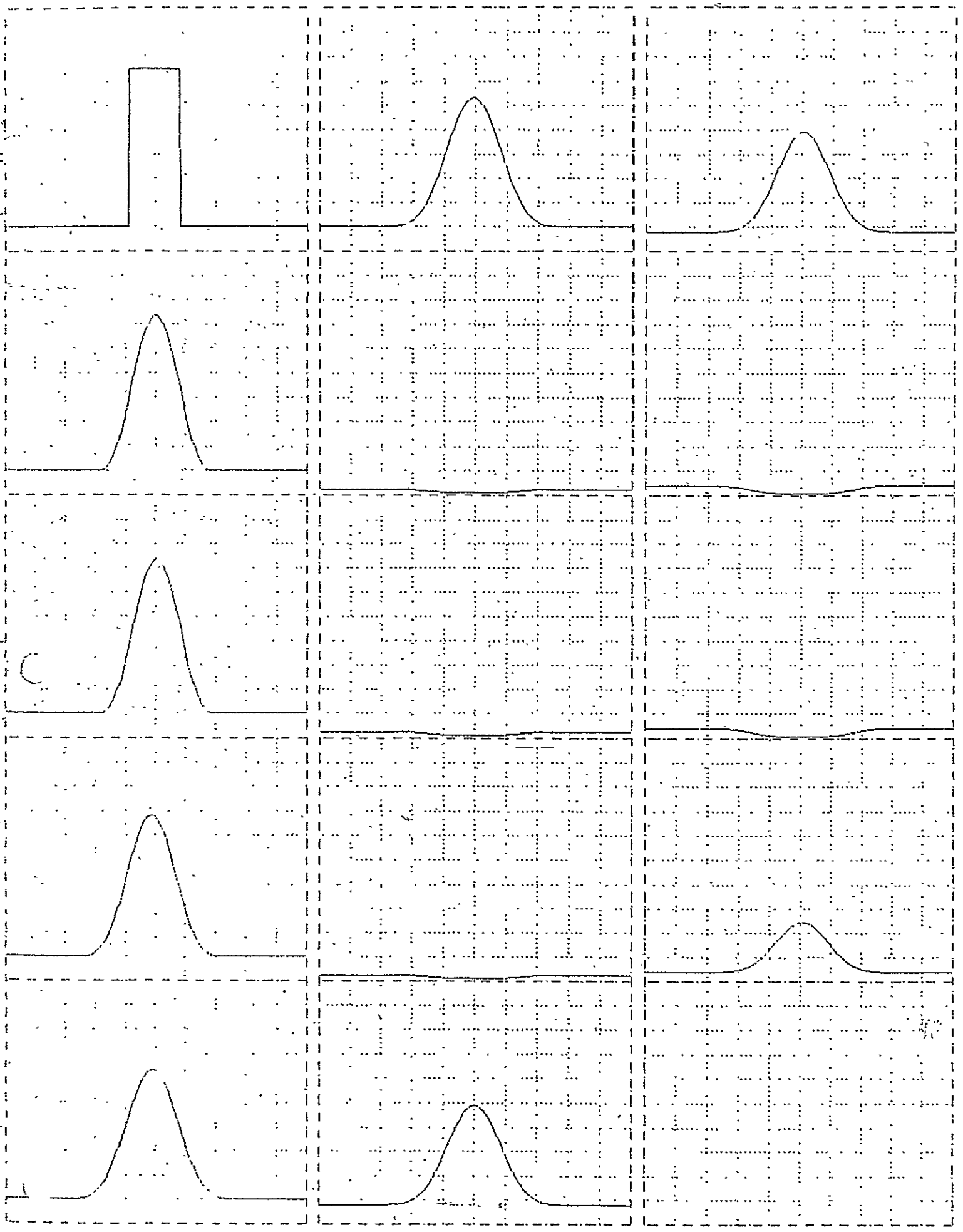

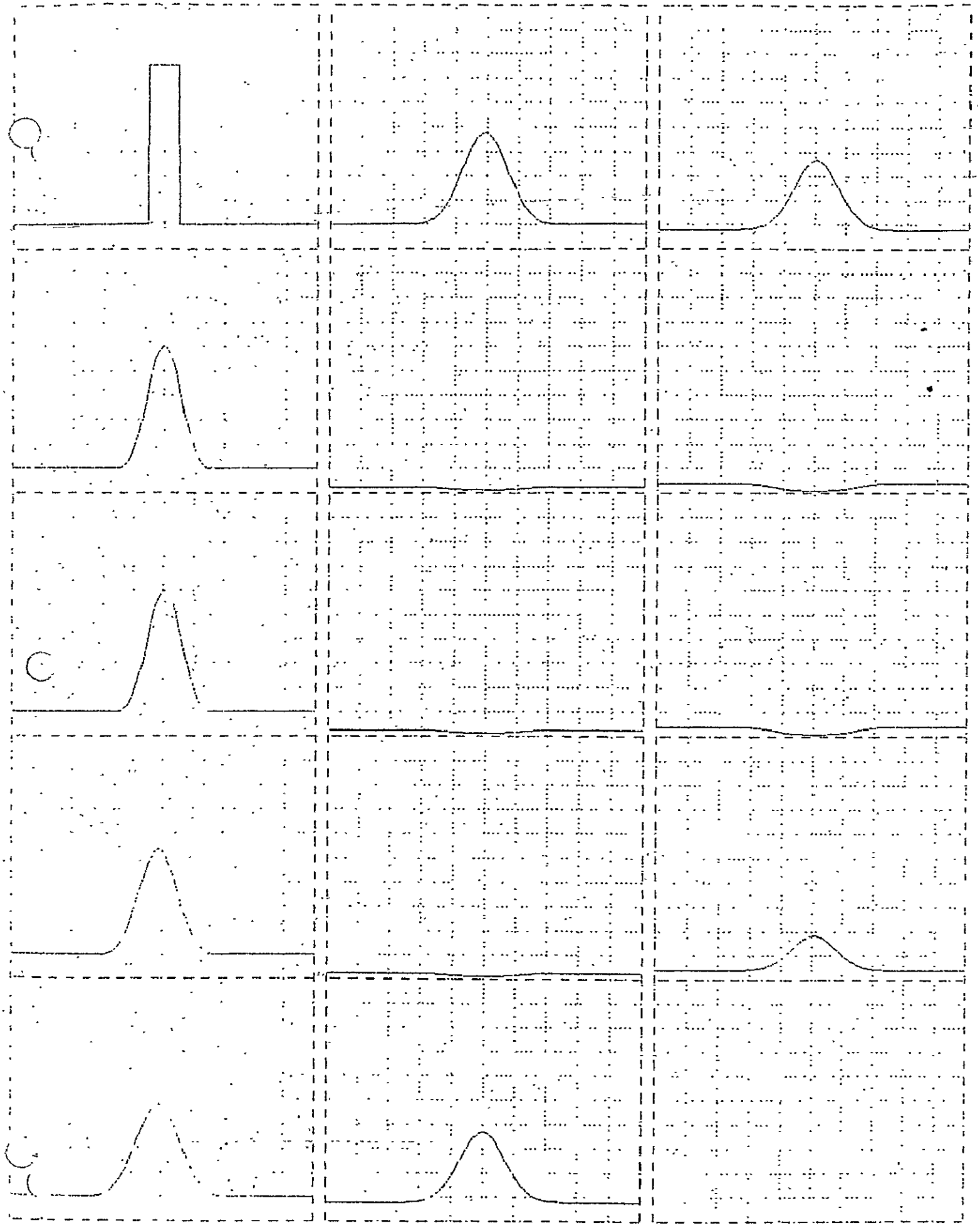

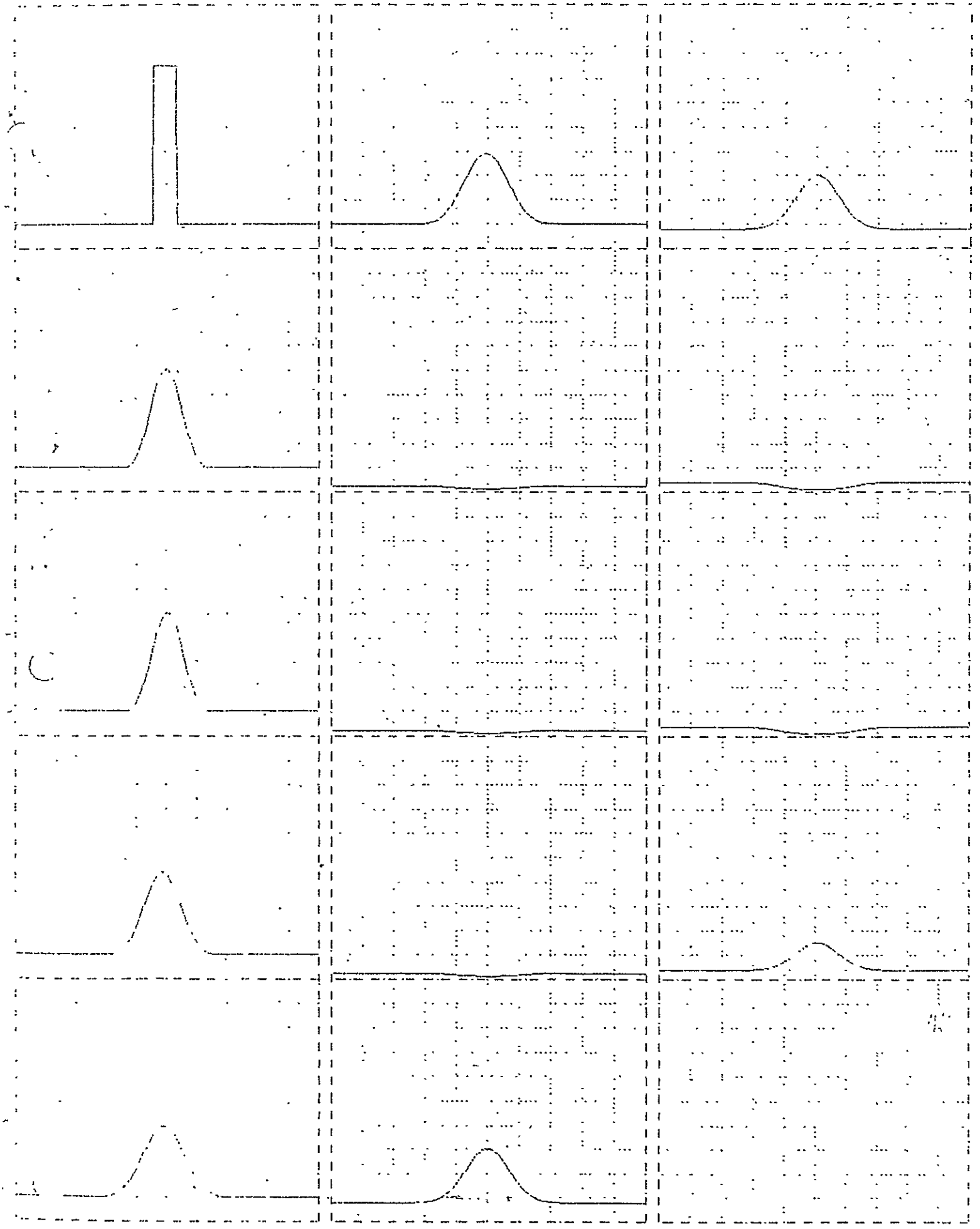

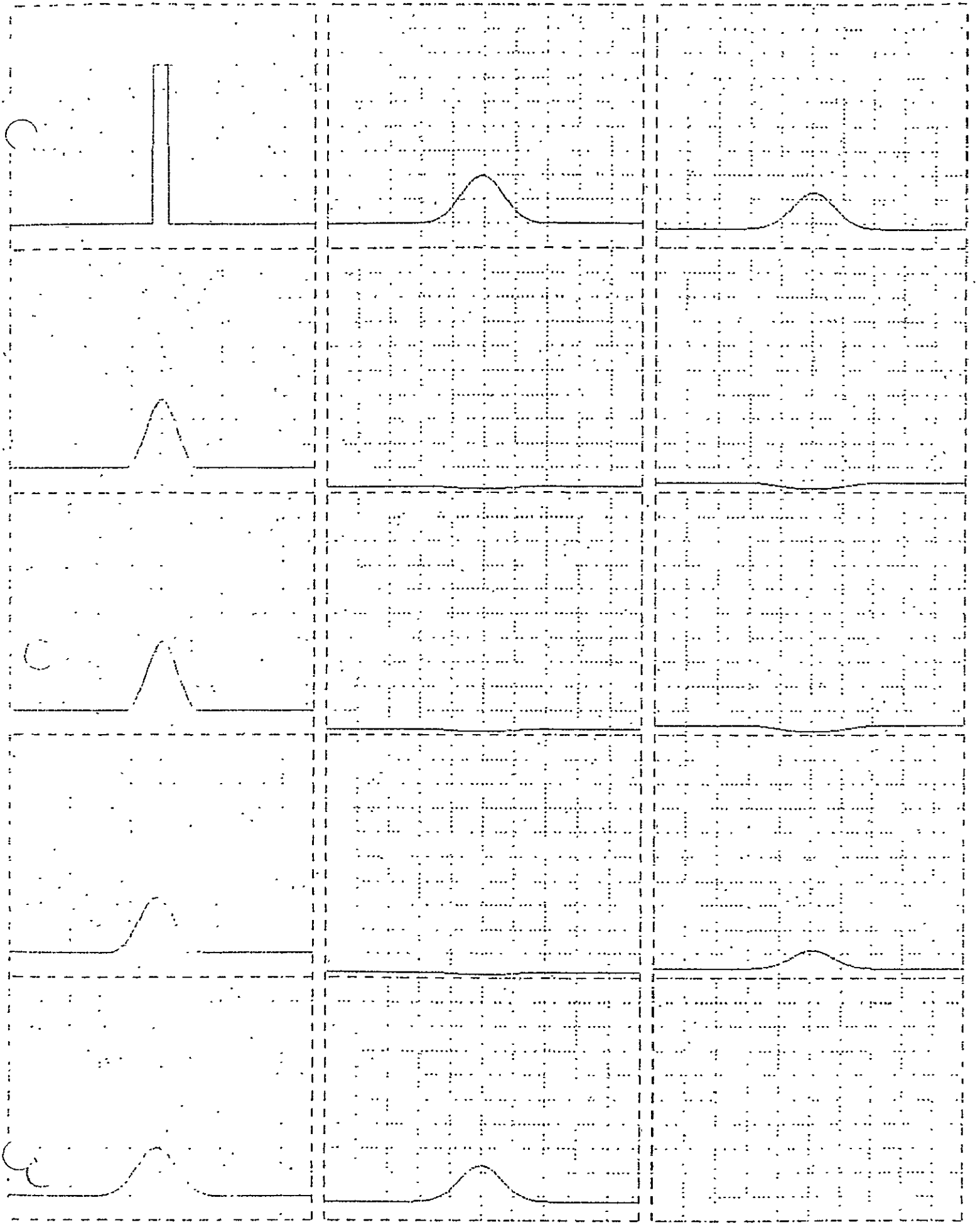

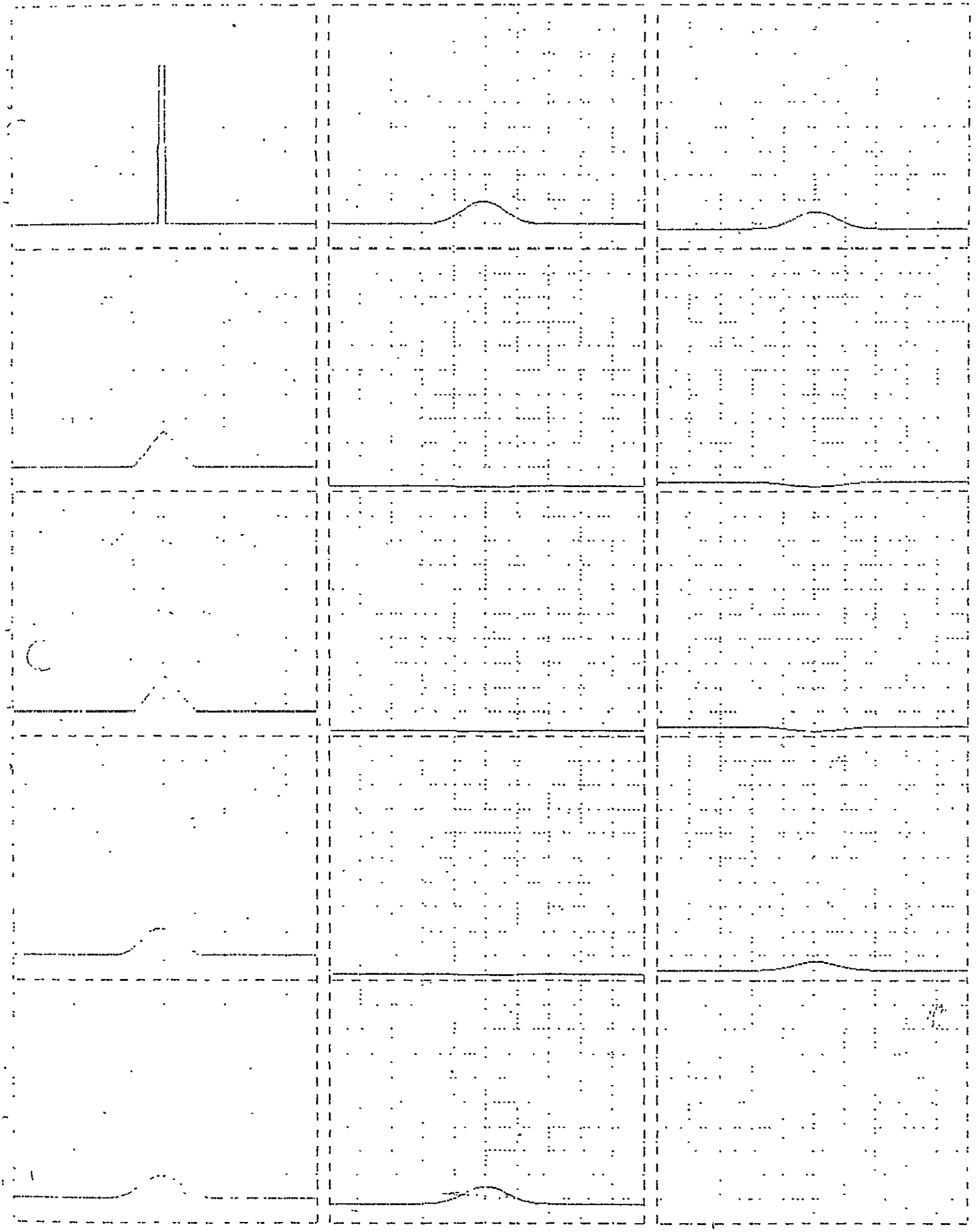

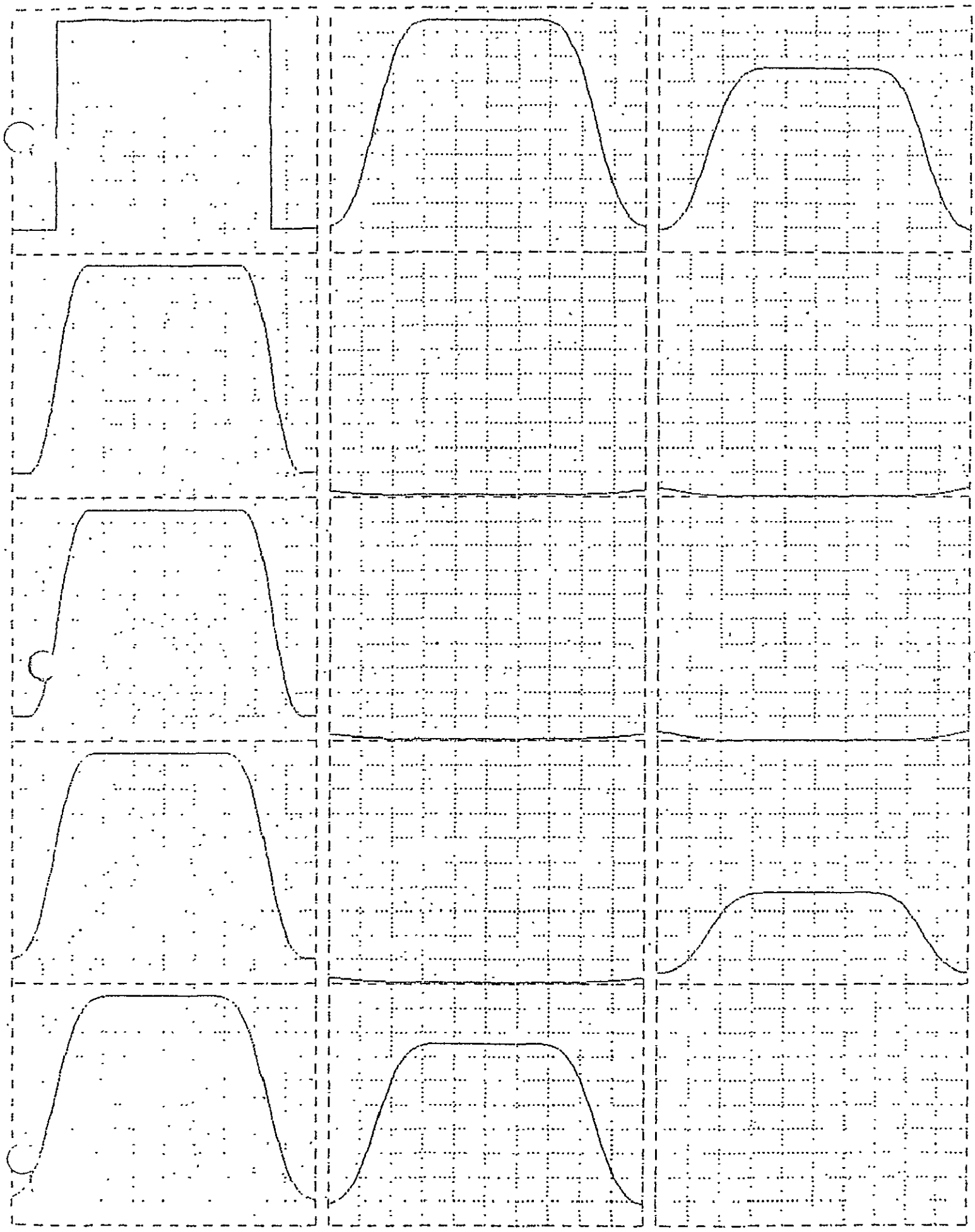

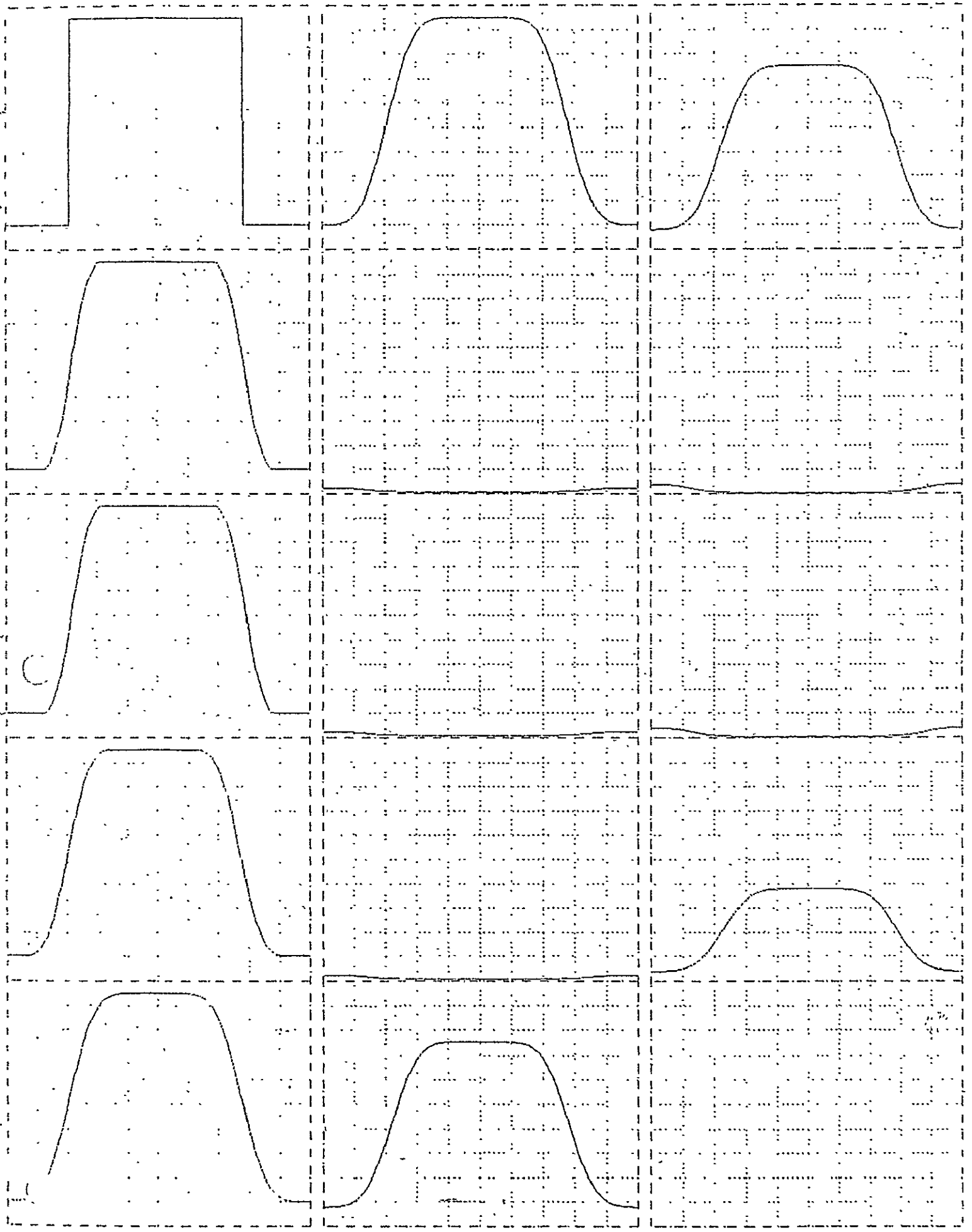

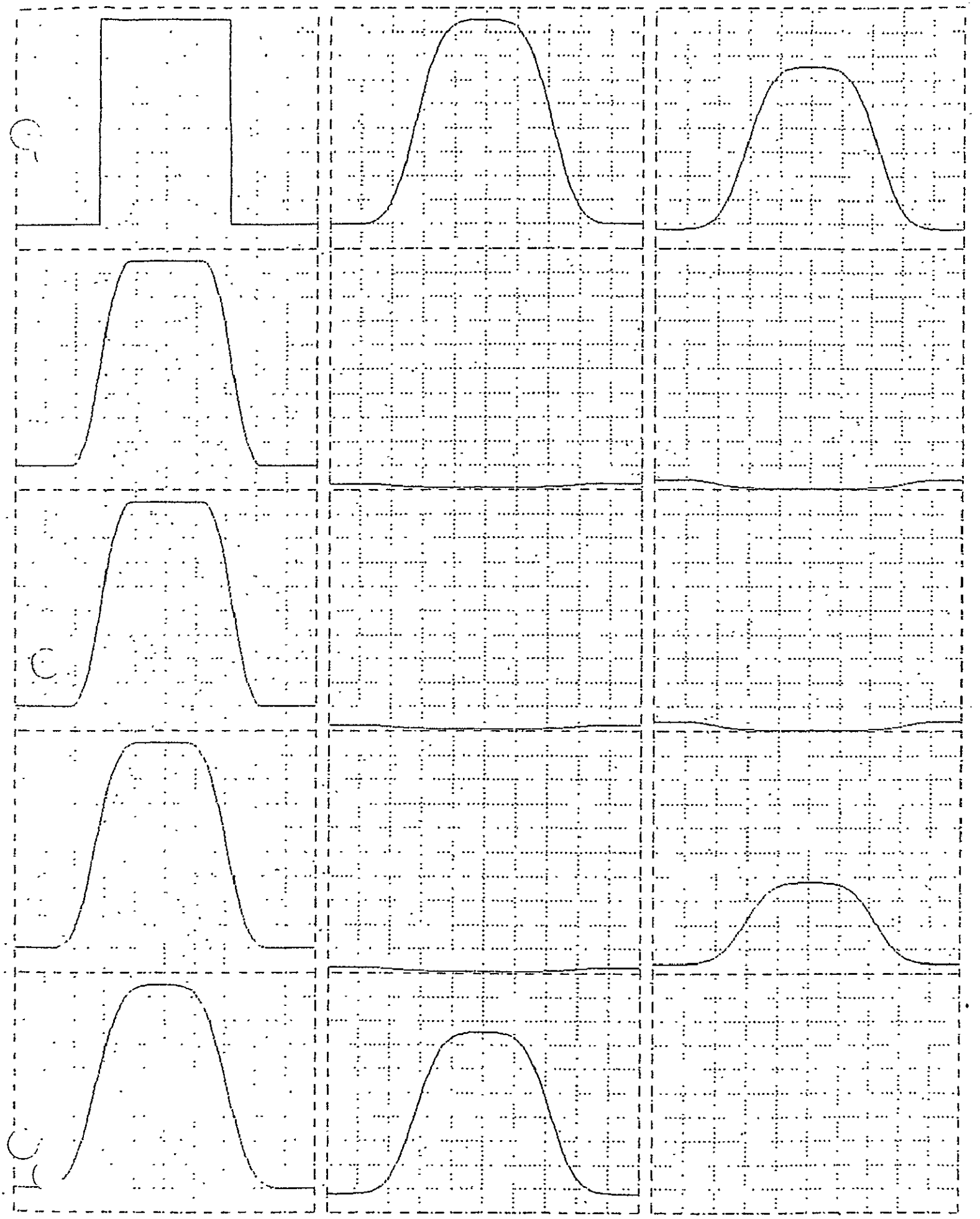

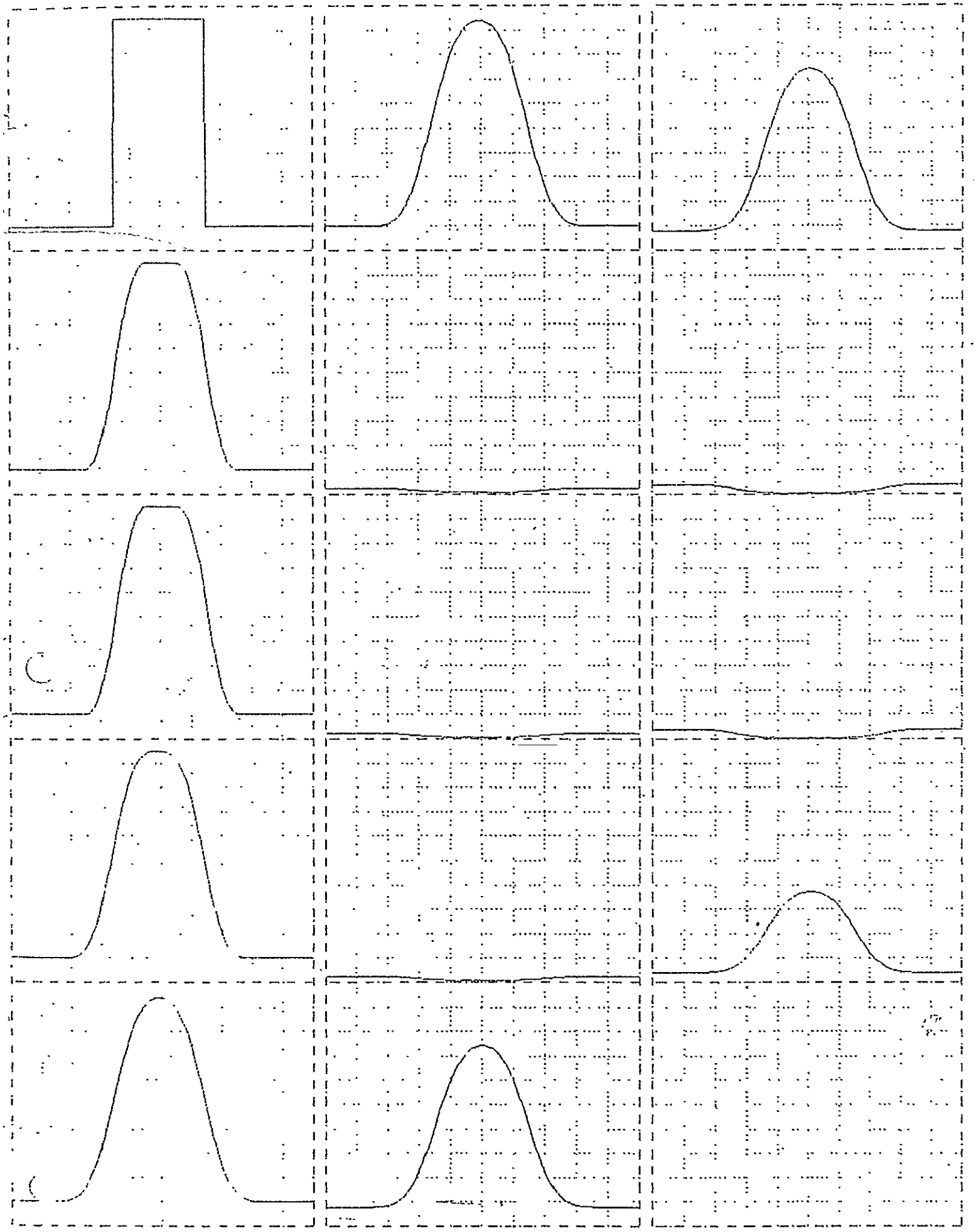

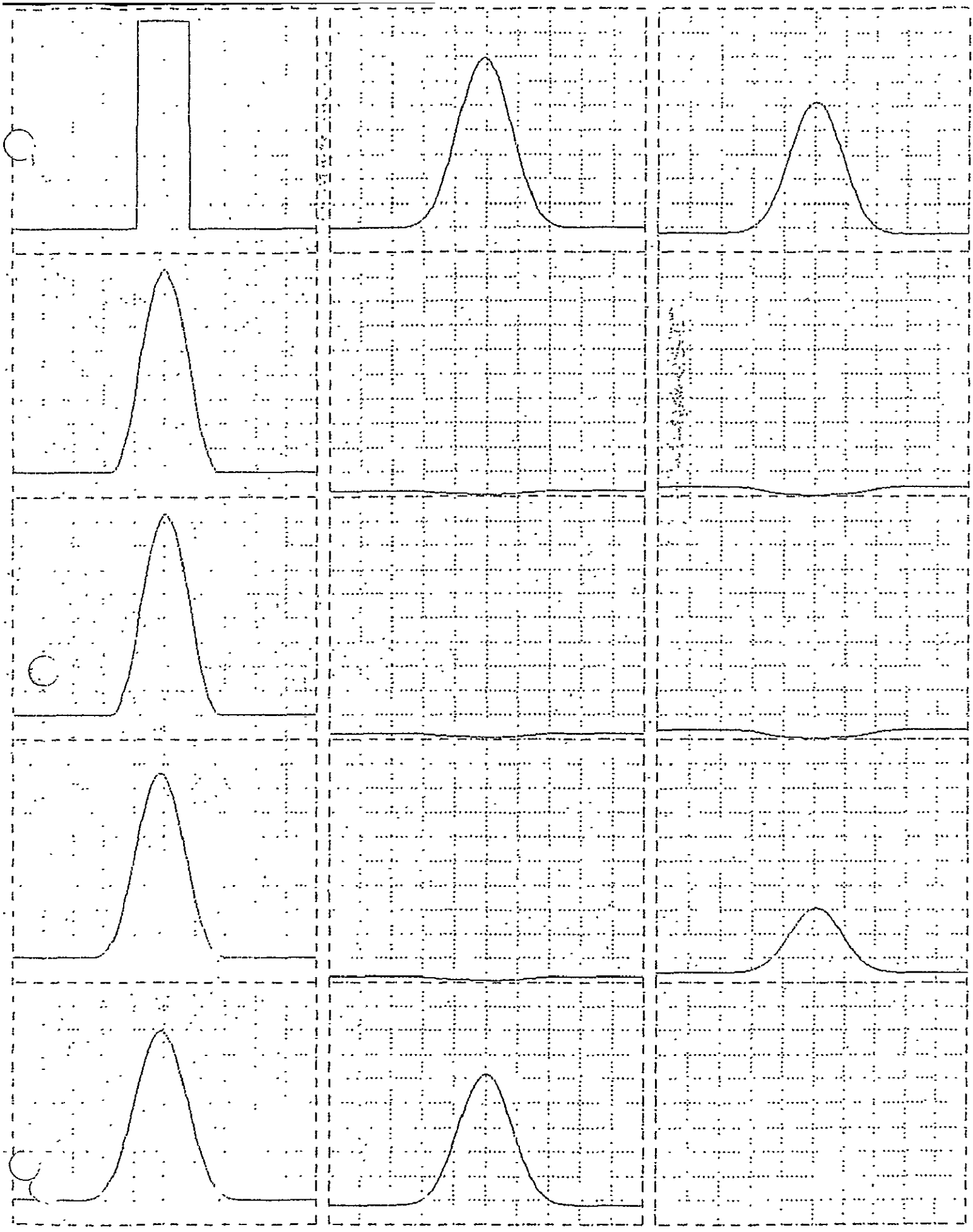

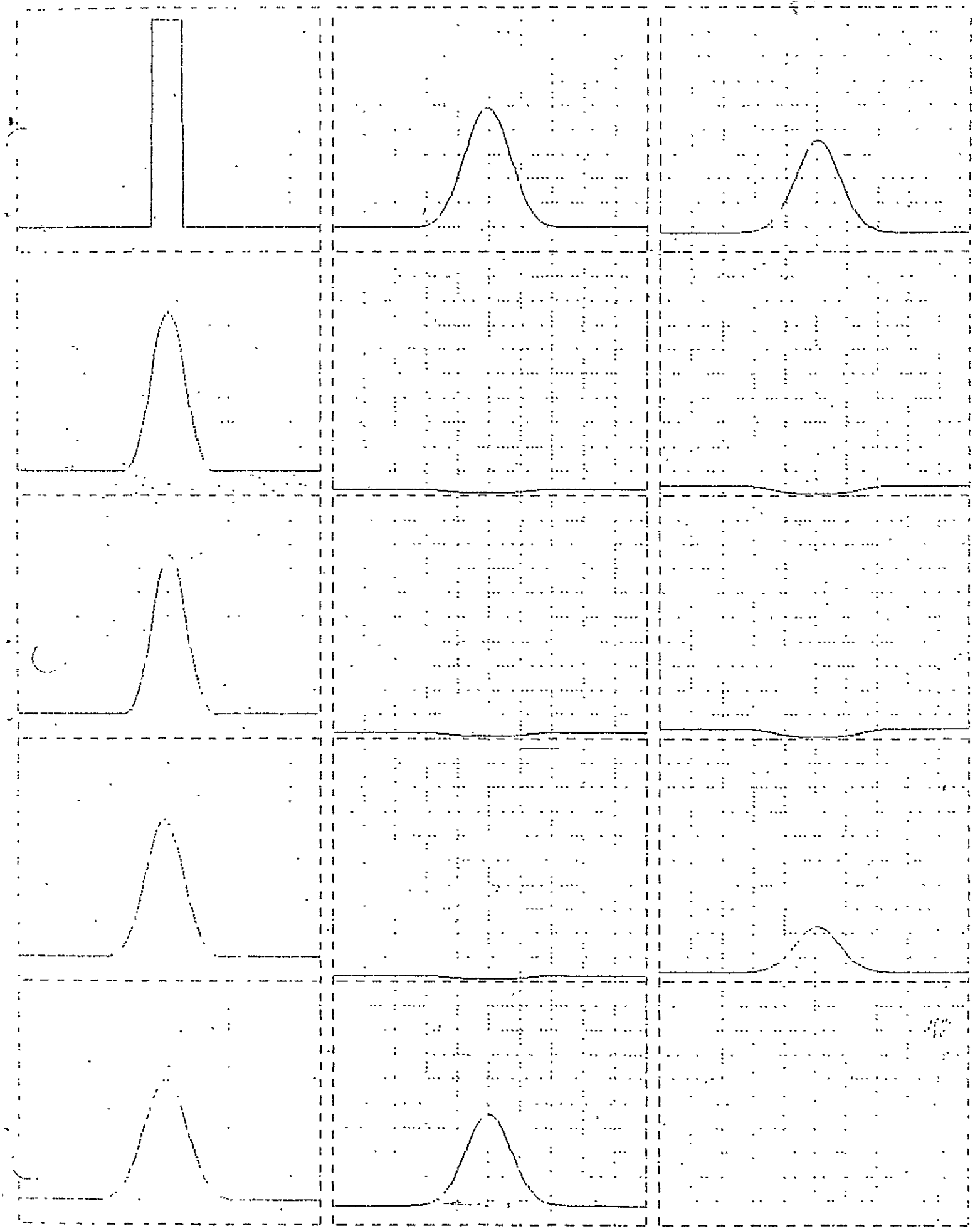

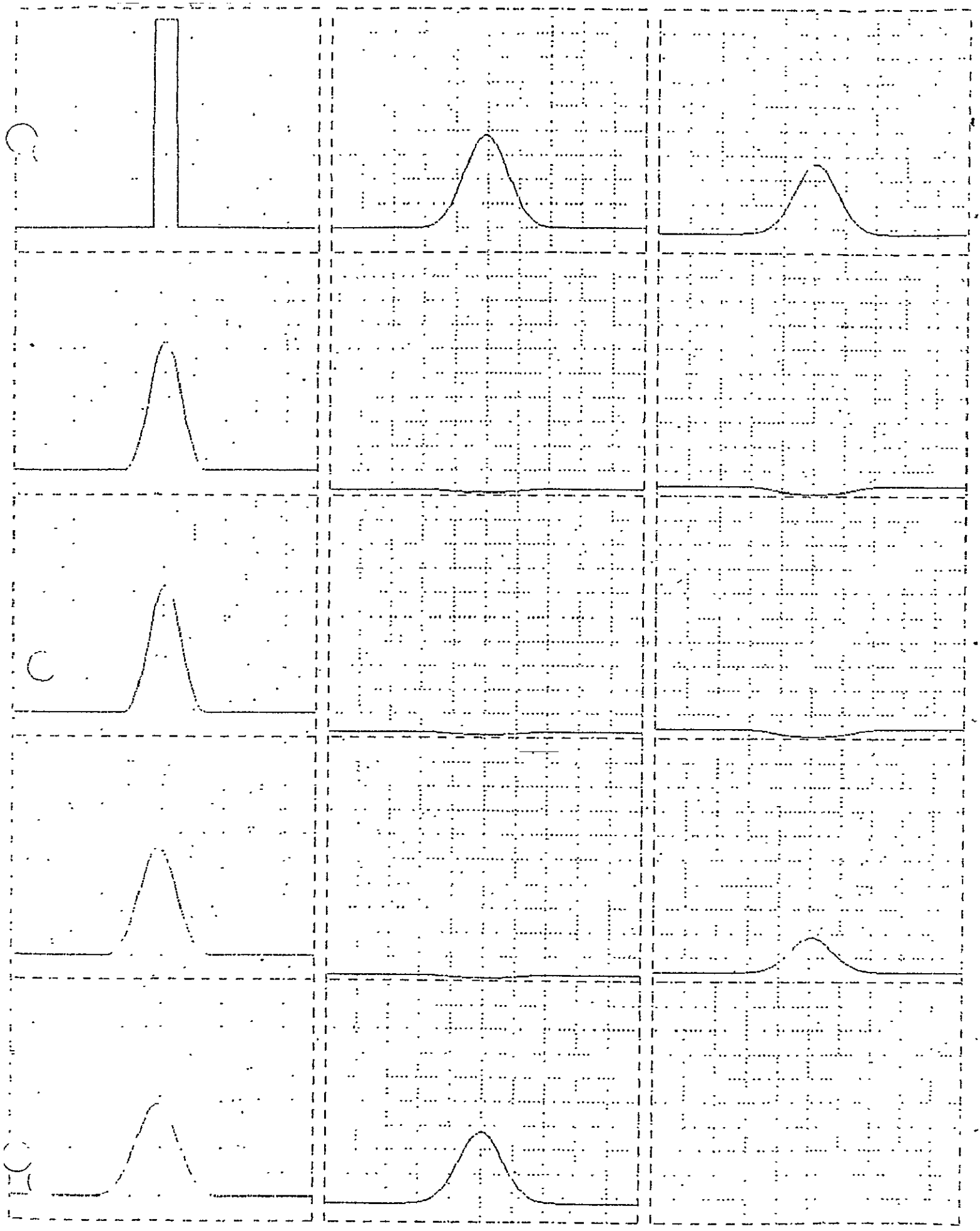

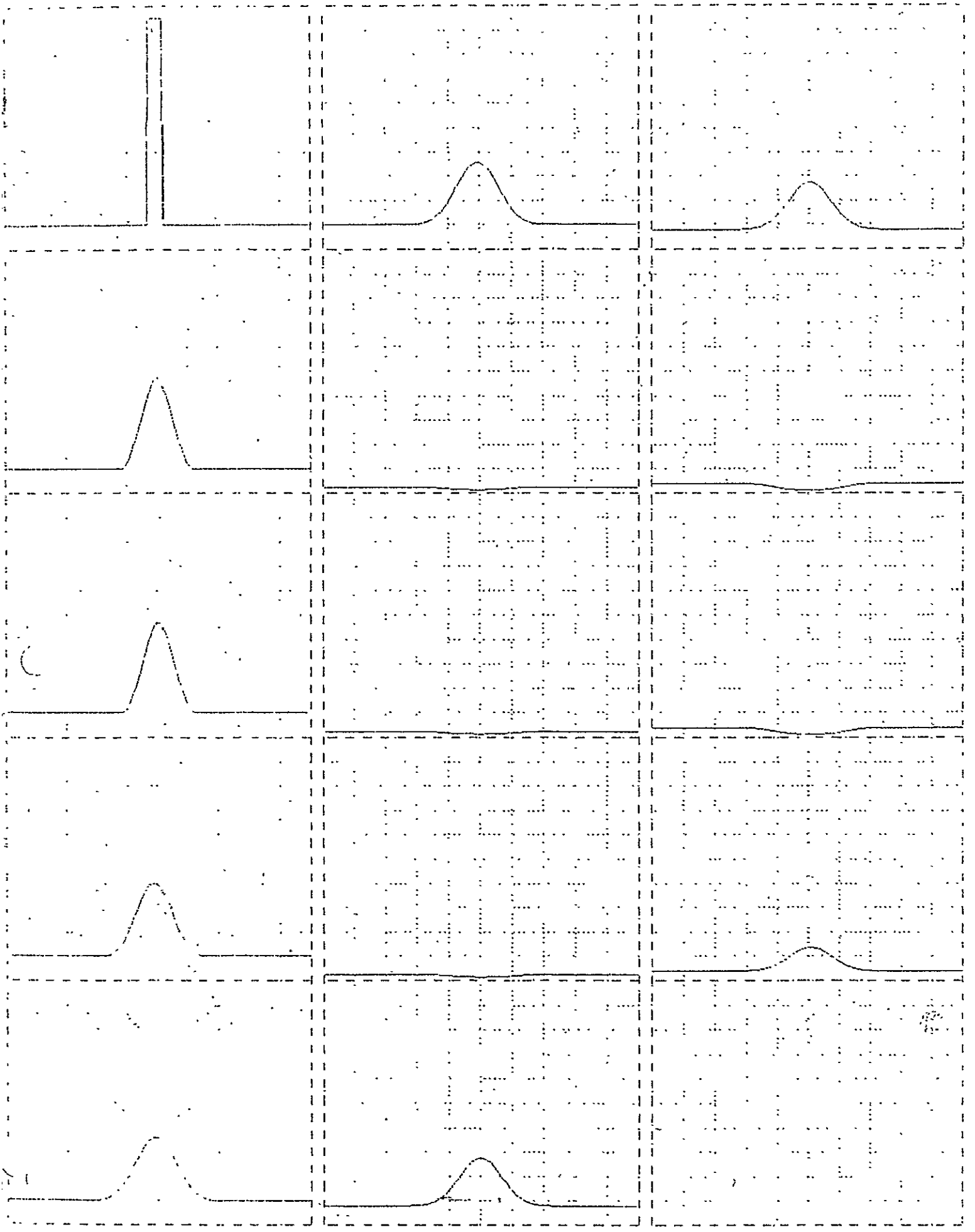

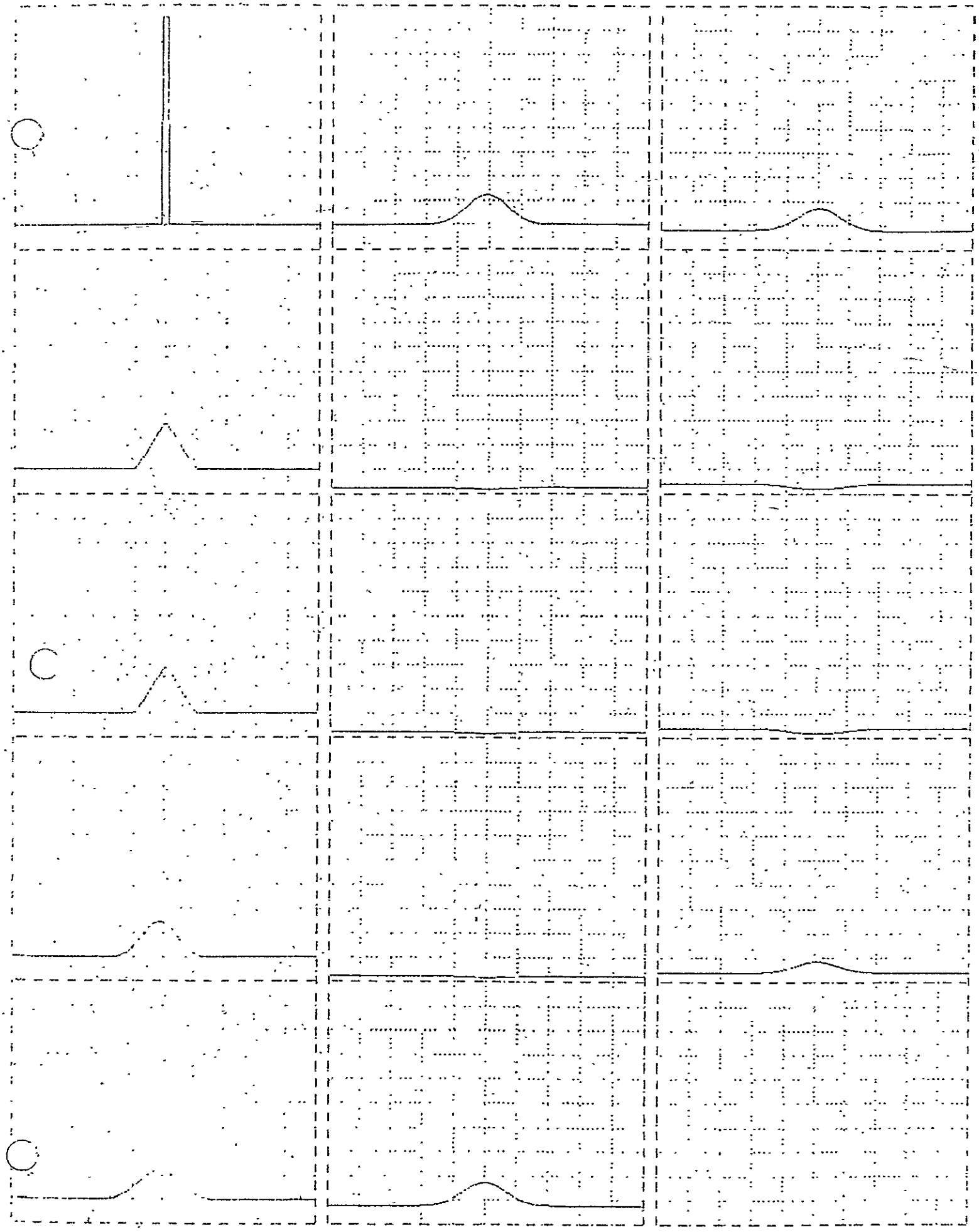

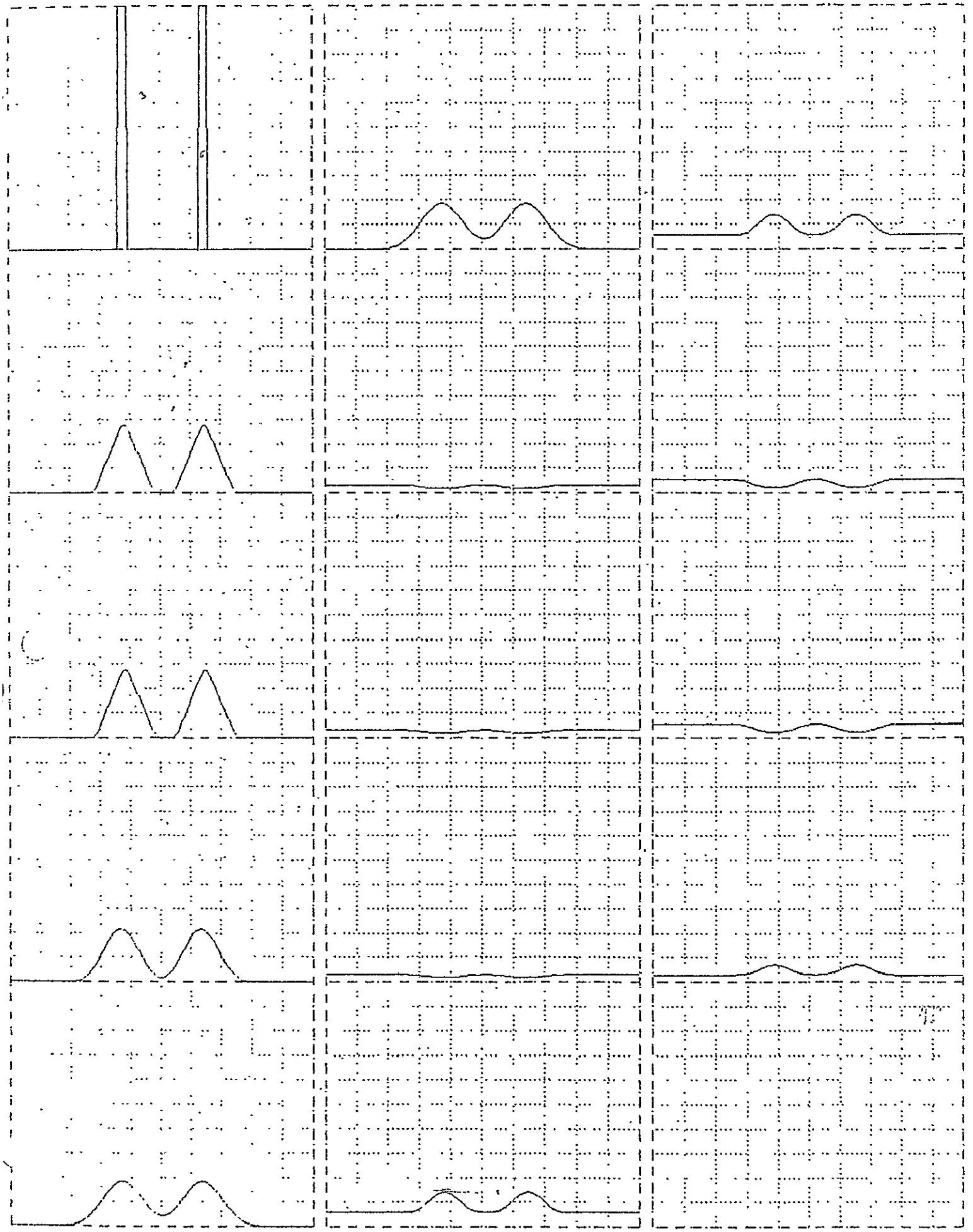

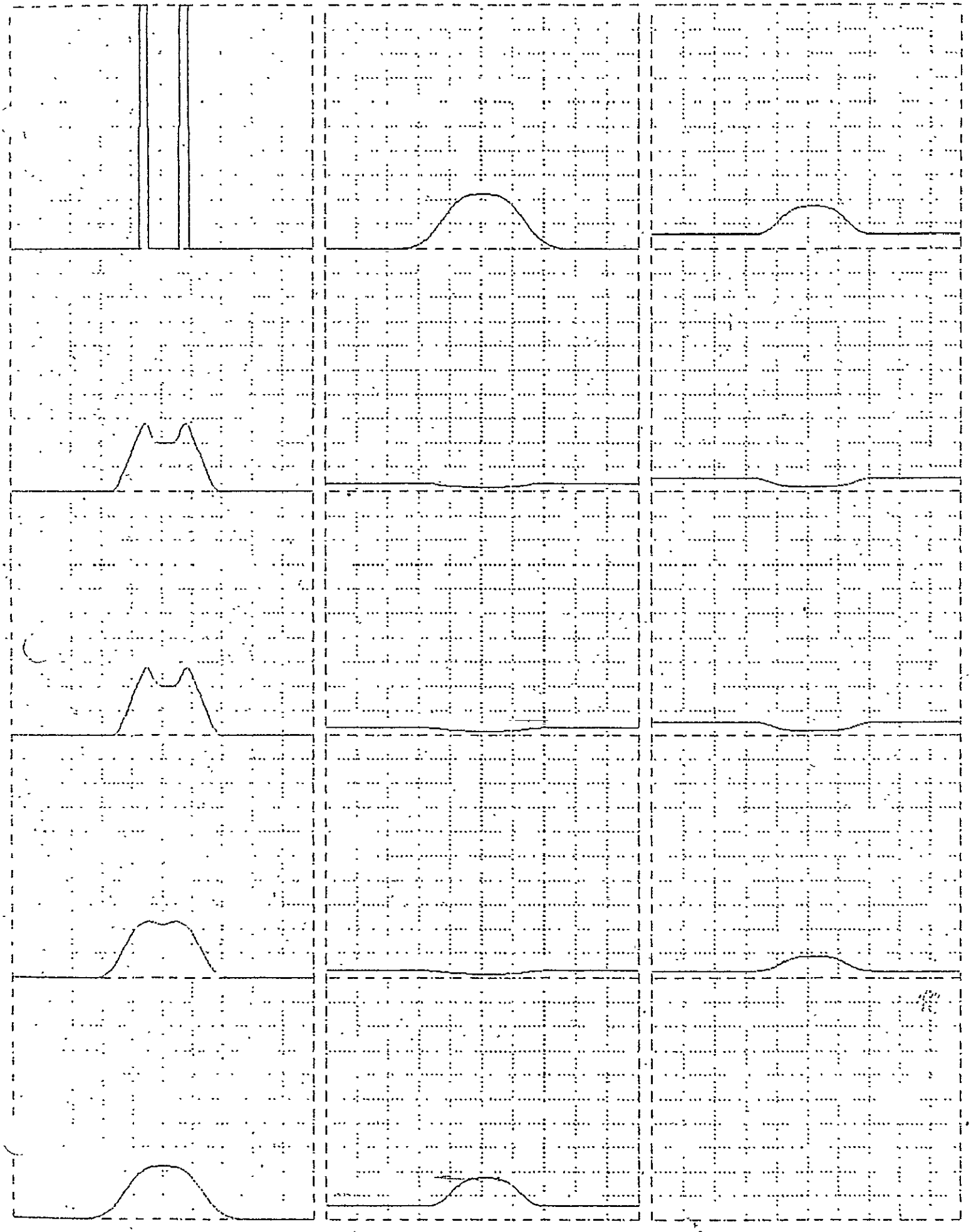

APPENDIX D

EDGE GRADIANT SPECTRUM PROGRAM

C-4

The Fortran computer program EGA determines the line spread and transfer function of an optical system using a digital representation (in density, transmission or exposure) of an edge. An edge is taken to be two adjacent regions each of constant density.

The program works in exposure space; thus, if the input edge array is in transmission or density space the program first converts the array to exposure space, and the H-D curve must also be inputted. The next major portion of the program is the input array smoothing. This step is optional and the effective frequency cutoff of the smoothing is controlled by an input constant. The smoothing is performed by convolving a triangle with the input record. (This is equivalent to multiplying the input power spectrum by a sinc squared function.

The next step is the computation of the line spread function; first according to:

$$S(x) = \left(\frac{dE}{dx}\right) \Big/ \Delta E$$

where. ΔE is the exposure difference between the two sides of the edge.

Then the optical transfer function, its modulus and phase are calculated as:

$$FTM(\nu_\eta) = \left(CO_\eta^2 + SI_\eta^2\right)^{1/2}$$

$$PHI(\nu_\eta) = \arctan\left(SI_\eta / CO_\eta\right)$$

where

$$SI_\eta = \sum_{k=1}^{N} s(xk) \sin\left[\frac{2\pi\eta}{N}(k-1)\right]$$

$$CO_\eta = \sum_{k=1}^{N} s(xk) \cos\left[\frac{2\pi\eta}{N}(k-1)\right]$$

Finally, the line spread function is normalized by the distance increment:

$$S(x) = s(x) / \Delta x$$

The following table is a list, with definitions, of the fortran variables used in the program. In addition, a list of the fortran coding and an "autoflow" flow chart of the program are included.

N	number of points in the input edge array
DX	spacing (in distance) of the points in the input edge array
L	filter control; integer; the smaller the number, the lesser the smoothing; L = 1 implies no smoothing
IND	controls preliminary processing of input array; integer; IND < 0 implies transmission input to be converted first to density, then exposure = 0 implies density input to be converted to exposure > 0 implies exposure input
ID	integer label for the input edge
E	input edge data array; may be exposure, density, or transmission as a function of distance
ES	the E array after smoothing
S	spread function array
DC, EC	density, exposure for the film used; inputted if density to exposure conversion is required
FTM	modulation transfer function array
PHI	phase (of the transfer function) array
WF	weighting factor used in smoothing operation

FORTRAN MODULE (LIST)

CARD NO	**** CONTENTS ****
1	DIMENSION E(1000),ES(1000),S(1000),DC(25),EC(25),FTH(1000),
2	1PHI(1000),NF(1000)
3	5 READ (5,100,END=99) N,DX,L,IND,ID
4	READ (5,101) (E(I),I=1,N)
5	IF(IND) 9,15,31
6	9 DO 10 I=1,N
7	10 E(I)=ALOG10(1./E(I))
8	15 READ (5,103) NC
9	READ (5,102) (EC(I),I=1,NC)
10	READ (5,102) (DC(I),I=1,NC)
11	DO 30 I=1,N
12	J=2
13	20 IF(E(I).LE.DC(J)) GO TO 30
14	25 J=J+1
15	IF(J.LT.NC) GO TO 20
16	30 E(I)=(E(I)-DC(J-1))*(EC(J)-EC(J-1))/(DC(J)-DC(J-1))+EC(J-1)
17	31 K=N-L+1
18	IF (L.EQ.1) GO TO 46
19	DENN=FLOAT((L/2+1)**2)
20	INUM=(L/2)+1
21	DO 40 I=1,L
22	IF (I.GE.INUM) GO TO 35
23	NF(I)=FLOAT(I)/DENN
24	GO TO 40
25	35 NF(I)=FLOAT(L-I+1)/DENN
26	40 CONTINUE
27	DO 45 I=1,K
28	ES(I)=0.
29	DO 45 J=1,L
30	45 ES(I)=ES(I)+(NF(J)*E(I+J-1))
31	GO TO 48
32	46 DO 47 I=1,N
33	47 ES(I)=E(I)
34	48 NN=N/5
35	ES1=0.
36	ESN=0.
37	DO 49 I=1,NN
38	ES1=ES1+ES(I)
39	49 ESN=ESN+ES(K-I+1)
40	DE=(ESN-ES1)/NN
41	S(K)=0.
42	M=K-1
43	DO 50 I=1,M
44	50 S(I)=(ES(I+1)-ES(I))/DE
45	FTH(1)=1.
46	PHI(1)=0.
47	MM=K+1
48	Z1=3.141593/FLOAT(K)
49	DO 60 J=2,MM
50	Z2=Z1*FLOAT(J-1)
51	C0=0.
52	S1=0.
53	DO 55 I=1,K
54	Z3=Z2*FLOAT(I)

CARD NO **** CONTENTS ****

```
      CO=CO+S(I)*COS(Z3)
   55 SI=SI+S(I)*SIN(Z3)
      FTM(J)=SQRT(CO**2+SI**2)
   60 PHI(J)=ATAN(SI/CO)
      DO 65 I=1,K
   65 S(I)=S(I)/DX
      WRITE (6,200)
      WRITE (6,110) N,DX,L,IND,ID
      WRITE (6,201)
      WRITE (6,111) (E(I),I=1,N)
      IF (L.EQ.1) GO TO 70
      WRITE (6,203)
      WRITE (6,111) (ES(I),I=1,K)
   70 WRITE (6,204)
      WRITE (6,112) (S(I),I=1,K)
      WRITE (6,205)
      WRITE (6,111) (FTM(I),I=1,M1)
      WRITE (6,206)
      WRITE (6,111) (PHI(I),I=1,M1)
      GO TO 5
   99 STOP
  100 FORMAT (I10,F10.5,I10,I10,I10)
  101 FORMAT (10F8.5)
  102 FORMAT (8F10.5)
  103 FORMAT (I10)
  110 FORMAT (' ',I10,F10.5,3I10)
  111 FORMAT (' ',10F8.5)
  112 FORMAT (' ',8F10.5)
  200 FORMAT ('1   NO OF PTS DELTA X      FILTER   INDICATOR    ID')
  201 FORMAT ('0    INPUT EDGE DATA')
  202 FORMAT ('0    D LOG(E) DATA')
  203 FORMAT ('0    SMOOTHED EDGE DATA')
  204 FORMAT ('0    SPREAD FUNCTION')
  205 FORMAT ('0    MODULATION TRANSFER FUNCTION')
  206 FORMAT ('0    PHASE FUNCTION')
      END
```

CHART TITLE - PROCEDURES

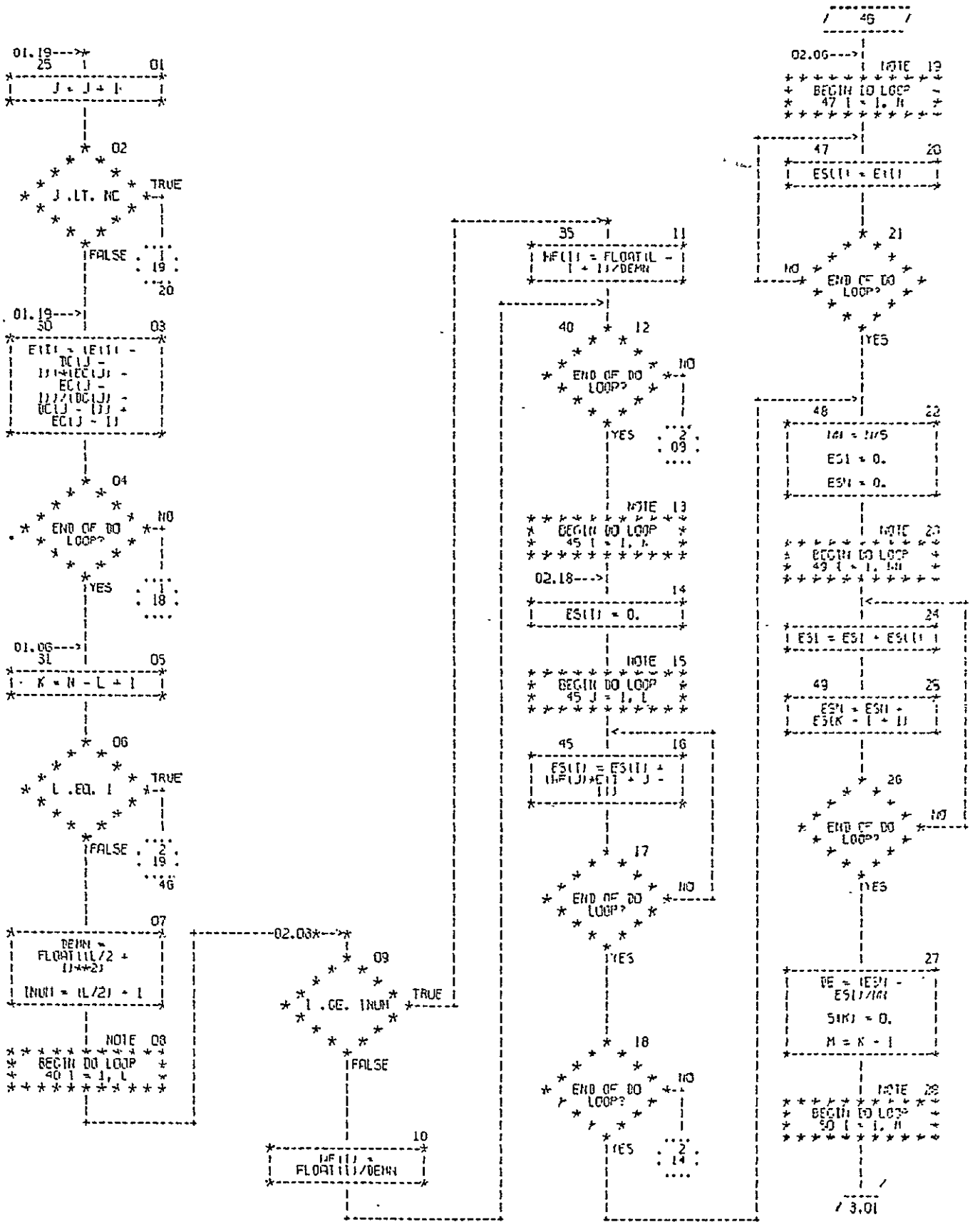

CHART TITLE - PROCEDURES

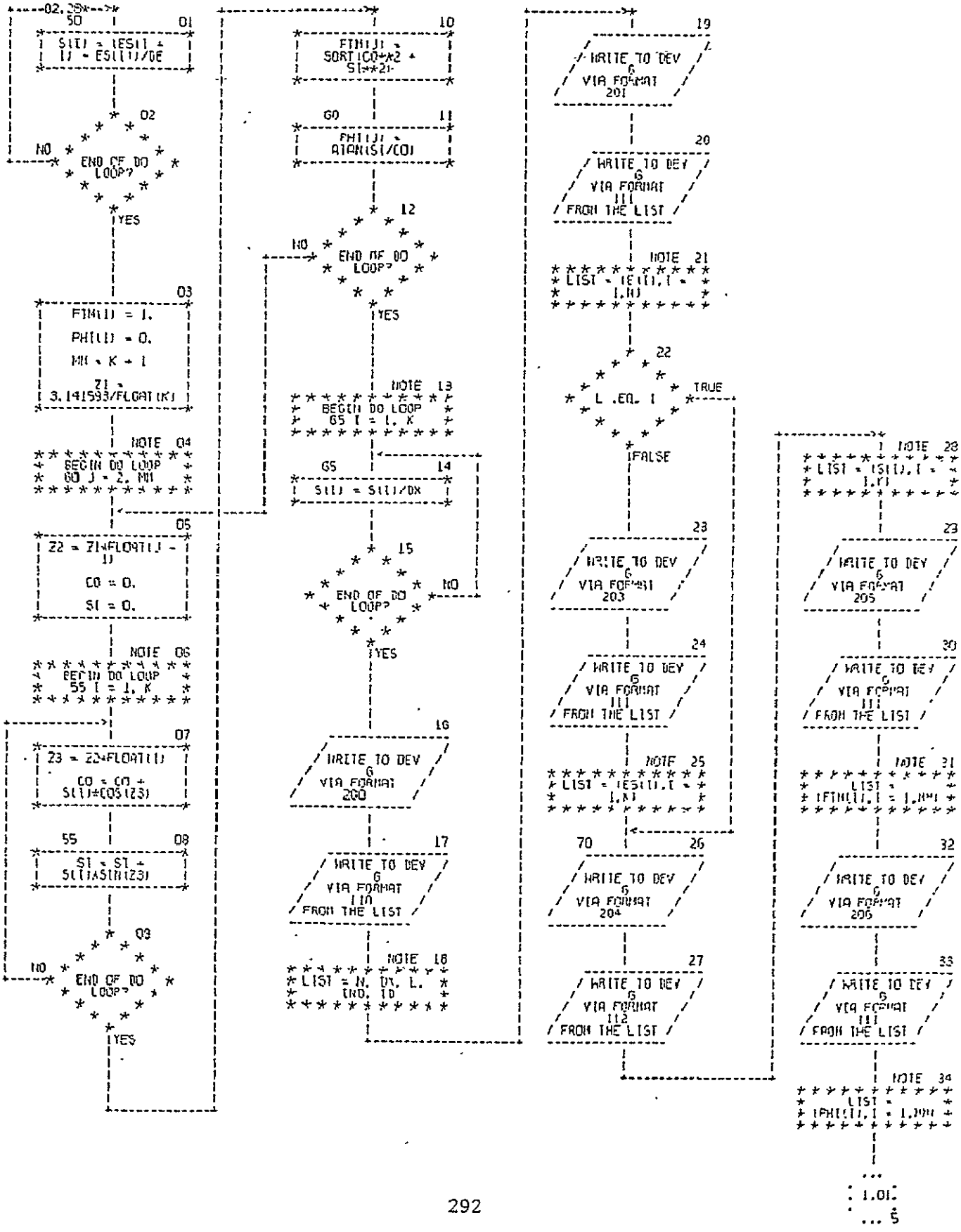

CARD ID PAGE/BOX NAME REFERENCES (SOURCE SEQUENCE NO. AND PAGE/BOX)

FORTRAN MODULE ECA

CHART TITLE - PROCEDURES

CHART TITLE - NON-PROCEDURAL STATEMENTS

CHART TITLE - PROCEDURES

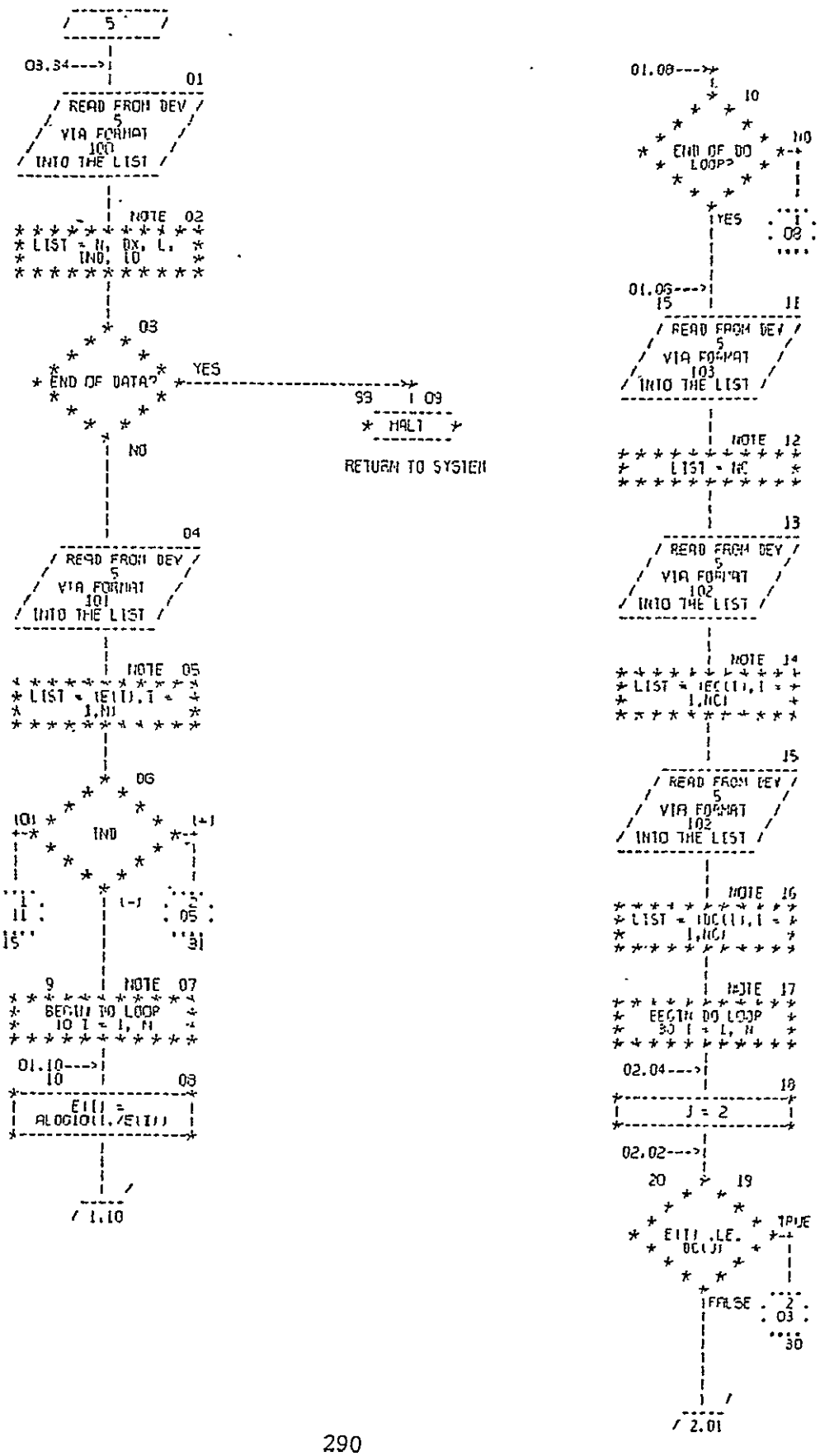

CHART TITLE - NON-PROCEDURAL STATEMENTS

```
      DIMENSION E(1000),ES(1000),S(1000),DC(25),EC(25),FTH(1000),
      PHI(1000),MF(1000)
100   FORMAT (I10,F10.5,I10,I10,I10)
101   FORMAT (10F8.5)
102   FORMAT (8F10.5)
103   FORMAT (I10)
110   FORMAT (' ',I10,F10.5,3I10)
111   FORMAT (' ',10F8.5)
112   FORMAT (' ',8F10.5)
200   FORMAT ('1   NO OF PTS DELTA X      FILTER   INDICATOR    ID')
201   FORMAT ('0    INPUT EDGE DATA')
202   FORMAT ('0    D LOG(E) DATA')
203   FORMAT ('0    SMOOTHED EDGE DATA')
204   FORMAT ('0    SPREAD FUNCTION')
205   FORMAT ('0    MODULATION TRANSFER FUNCTION')
206   FORMAT ('0    PHASE FUNCTION')
```